Development of an Aircraft Landing Database and Models to Estimate Aircraft Runway Occupancy Times

Navid Mirmohammadsadeghi

Dissertation submitted to the faculty of the Virginia Polytechnic Institute and State University in partial fulfillment of the requirements for the degree of

Doctor of Philosophy

In

Civil Engineering

Antonio A. Trani, Chair

Susan Hotle, Co-Chair

Montasir M. Abbas

Kevin Heaslip

August 6, 2020

Blacksburg, Virginia

Keywords: Airport, Aircraft, Runway, Simulation, ASDE-X, Machine Learning, Database, Monte Carlo Simulation, Clustering, Classification, Analytics, Landing Behavior

Development of an Aircraft Landing Database and Models to Estimate Aircraft Runway Occupancy Times

Navid Mirmohammadsadeghi

ABSTRACT

This dissertation represents the methodologies used to develop an aircraft landing database and predictive models for estimating arrival flight runway occupancy times. In the second chapter, all the algorithms developed for analyzing the airport surface radar data are explained, and detailed statistical information about various airports in the United States in terms of landing behavior is studied. In the third chapter a novel data-driven approach for modeling aircraft landing behavior is represented. The outputs of the developed approach are runway occupancy time distributions and runway exit utilizations. The represented hybrid approach in the third chapter is a combination of machine learning and Monte Carlo simulation methods. This novel approach was calibrated based on two years of airport radar data. The study's output is a computer application, which is currently being used by the Federal Aviation Administration and various airport consulting firms for analyzing and designing optimum runway exits to optimize runway occupancy times at airports. In the fourth chapter, four real-world case scenarios were analyzed to show the power of the developed model in solving real-world challenges in airport capacity. In the fifth chapter, pilot motivational behaviors were introduced, and three methodologies were used to replicate motivated pilot behaviors on the runway. Finally, in the sixth chapter, a neural network approach was used as an alternative model for estimating runway occupancy time distributions.

Development of an Aircraft Landing Database and Models to Estimate Aircraft Runway Occupancy Times

Navid Mirmohammadsadeghi

ABSTRACT (General Audience)

The federal aviation administration predicts ongoing growth in the aviation industry over the following 20 years. Therefore, the airports will be more crowded, and a higher number of operations will occur at those facilities. An accurate prediction of airports' capacities can help the authorities to improve the airports appropriately. Due to significant reductions in in-trail aircraft separations, runway occupancy times will become more significant in airport arrival procedures. In this study, a landing event database was developed to represent the accurate distributions of runway occupancy times. Also, it is essential to have computer applications capable of replicating runway occupancy time distributions. In this dissertation, a novel approach was developed to replicate aircraft runway occupancy times. A massive amount of airport surface radar data was utilized to create all the mentioned computer applications. The results of the final products were validated against real data. Real-world case scenarios were discussed as part of this study to showcase the strengths of the final developed product in solving challenging problems related to airport capacity. Finally, extreme cases of motivated landing behavior from airline pilots were studied, and multiple methodologies were introduced to replicate pilot motivational behavior while landing on runway.

Contents

Table of Figures

Chapter1. Introduction

1.1 Research Motivation

Runway occupancy time is the amount of time that an aircraft spends on the runway. For arrival flights, it is measured from the moment that the aircraft nose passes the runway threshold to the time when its fuselage completely clears the runway. For departure flights, it is estimated between the time that the aircraft enters runway polygon until the moment when it has wheels-off. In this study, arrival runway occupancy times are investigated by various methods. In recent years due to many improvements in air traffic control technologies, the separation between arrival flights has been reduced. Federal Aviation Administration (FAA) has started a new era where new separation rules are applied at many airports around the country. Based on the recently published separation criteria between each pair of airplanes, many times the runway occupancy times for the leader planes are considered as the minimum separation between an arrival pair. Therefore, understating the actual distributions of runway occupancy times for each aircraft type under various environmental and geometrical conditions on different runways is critical for having smooth arrival and departure operations at airports. Since nowadays there are systems implemented at the airports to monitor the movement of airplanes, we can analyze the collected data in two ways:

First, create useful databases for potential users and help them explore the behavior at various facilities for different aircraft types.

Second, to develop predictive and simulation models to help analysts and airport designers designing runway exits or improving the performance of current facilities in terms of runway occupancy time.

This dissertation focuses on analyzing runway occupancy times for arrival flights. For this matter, Airport Surface Detection Equipment Model X (ASDE-X) data was analyzed and then collected in forms of an interactive database for further usages. The landing behavior of airplanes was studied and critical landing moments were extracted from the surveillance data to understand the required input data for the study.

Finally, various approaches were proposed and evaluated for predicting runway occupancy times and runway exit distances. Modeling runway occupancy time and individual aircraft landing performance will help airport designers improve current and future airport facilities.

1.2 Research Contributions

The organization of this dissertation is as follows:

- Chapter 2 provides information about the input data for this study, the algorithms that were developed to analyze the data and extract useful engineered features. Moreover, in this chapter, lots of information are provided about the developed landing database as one of the major deliverables of this study. 37 Terabytes of Airport Surface Equipment Detection Model –X (ASDE-X) data was collected, cleaned, and converted into a relational database with 134 features. The author explains the methodology about MATLAB scripts, which were used to tabulate, perform quality control, and visualize the data. The developed database is used by the FAA, airport designers and planners, and airline analysts.
- Chapter 3 provides information about the new proposed hybrid data-driven approach used to predict runway occupancy times and runway exit utilizations. In this chapter, all the improvements to the old Runway Exit Design Interactive Model (REDIM) are explained and the methodology behind the newly developed simulation model is described. A novel

approach was developed by combining machine learning and Monte Carlo simulations to solve the runway assignment and runway occupancy time problems. A clustering methodology was developed to identify runway exit groupings based on their geometry features and to estimate stochastic runway exit performance for 274 unique aircraft types. Also, a clustering methodology was developed to model individual landing performance based on 20 generated runway clusters. The methodology developed in this chapter can have applications in ground transportation studies such as modeling vehicle behavior in highway ramps. The model developed is being used by FAA and industry practitioners.

- Chapter 4 presents four case studies that the new simulation model was used to analyze the potential improvements in runway occupancy times (ROT) at four airports in the united states. This chapter defines the current performance of those facilities and proposes different alternatives as solutions for improving the ROT values. In this chapter the author applied the model developed to four case studies suggested by the FAA sponsor. Also, practical runway exit improvements were identified to five runways currently considered for future infrastructure improvements (Airport Improvement Program).
- Chapter 5 provides information about motivational factors that pilots can show while landing on different runways. These factors can be related to the gate or terminal location at the airport or based on the commands of the air traffic controllers on faster runway evacuation. Three methods were developed to model pilot motivational factors. The methods developed replicate the real data successfully. The findings in this chapter can be used by airline analysts and airport planners to understand the impact of gate location on runway exit behavior. There have been very few previous attempts to replicate such behavior in simulation models.

- Chapter 6 represents a machine learning approach for predicting runway occupancy times and distances by utilizing artificial neural networks. In this chapter, the author attempted to estimate runway occupancy times and runway exiting distances from a different approach than the one suggested in chapter three. A neural network approach was developed to predict runway occupancy times and exiting distance distributions. The neural network model can be used to construct runway occupancy time cumulative density plots and exit distances which are useful for design purposes. The approach represented in this chapter is complementary to the model presented in chapter three. The neural network models can predict the runway occupancy time and exit distances, but cannot estimate runway exit utilization.
- Chapter 7 concludes this dissertation.

Chapter 2. Landing Database and ASDE-X Parser

Federal Aviation Administration (FAA) implemented a system called Airport Surface Detection Equipment Model X (ASDE-X) at 37 airports in the United States since 2003 to help air traffic controllers in monitoring the movements at the airports up to 60 nautical miles in a more efficient and secured way [1]. This system visualizes flights while their operations are on screens in front of the controllers and can avoid runway and taxiway incursions [2].

This equipment includes a combination of tracking systems such as surface movement radar installed at the top of air traffic control tower in the airport, multilateral sensors, ADS-B (Automatic Dependent Surveillance-Broadcast) sensors, terminal radars, terminal automation systems, and aircraft transponders [3]. The following table represents the names, airport codes, and locating states of all the 37 airports in the United States that are equipped with this system.

Table 1. All the 37 Airports in the United States Equipped with ASDE-X.

ICAO Code	IATA Code	Airport Name	City, State
KATL	ATL	Hartsfield–Jackson Atlanta International Airport	Atlanta, GA
KBDL	BDL	Bradley International Airport	Windsor Locks, CT
KBOS	BOS	Logan International Airport	Boston, MA
KBWI	BWI	Baltimore/Washington International Thurgood Marshall Airport	Baltimore, MD
KCLE	CLE	Cleveland Hopkins International Airport	Cleveland, OH

KCLT	CLT	Charlotte Douglas International Airport	Charlotte, NC
KDCA	DCA	Ronald Reagan Washington National Airport	Arlington County, VA
KDEN	DEN	Denver International Airport	Denver, CO
KDFW	DFW	Dallas/Fort Worth International Airport	Dallas–Fort Worth, TX
KDTW	DTW	Detroit Metropolitan Airport	Detroit, MI
KEWR	EWR	Newark Liberty International Airport	Newark, NJ
KFLL	FLL	Fort Lauderdale–Hollywood International Airport	Fort Lauderdale, FL
KHNL	HNL	Daniel K. Inouye International Airport	Honolulu, HI
KHOU	HOU	William P. Hobby Airport	Houston, TX
KIAD	IAD	Washington Dulles International Airport	Dulles, VA
KIAH	IAH	George Bush Intercontinental Airport	Houston, TX
KJFK	JFK	John F. Kennedy International Airport	Queens, NY
KLAS	LAS	McCarran International Airport	Las Vegas, NV
KLAX	LAX	Los Angeles International Airport	Los Angeles, CA
KLGA	LGA	LaGuardia Airport	Queens, NY

KMCO	MCO	Orlando International Airport	Orlando, FL
KMDW	MDW	Chicago Midway International Airport	Chicago, IL
KMEM	MEM	Memphis International Airport	Memphis, TN
KMIA	MIA	Miami International Airport	Miami, FL
KMKE	MKE	Milwaukee Mitchell International Airport	Milwaukee, WI
KMSP	MSP	Minneapolis–Saint Paul International Airport	Hennepin County, MN
KORD	ORD	O'Hare International Airport	Chicago, IL
KPHL	PHL	Philadelphia International Airport	Philadelphia, PA
KPHX	PHX	Phoenix Sky Harbor International Airport	Phoenix, AZ
KPVD	PVD	Theodore Francis Green Memorial State Airport	Warwick, RI
KSAN	SAN	San Diego International Airport	San Diego, CA
KSDF	SDF	Louisville Muhammad Ali International Airport	Louisville, KY
KSEA	SEA	Seattle–Tacoma International Airport	Seattle, WA
KSFO	SFO	San Francisco International Airport	San Francisco, CA
KSLC	SLC	Salt Lake City International Airport	Salt Lake City, UT

KSNA	SNA	John Wayne Airport	Santa Ana, CA
KSTL	STL	St. Louis Lambert International Airport	St. Louis, MO

Figure 1 also represents the location of each of the airports mentioned in Table 1 that are equipped with the ASDE-X system over the United States map. As shown in Figure 1, some areas have many big airports that are equipped with ASDE-X, while many states just have one airport which has ASDE-X technology.

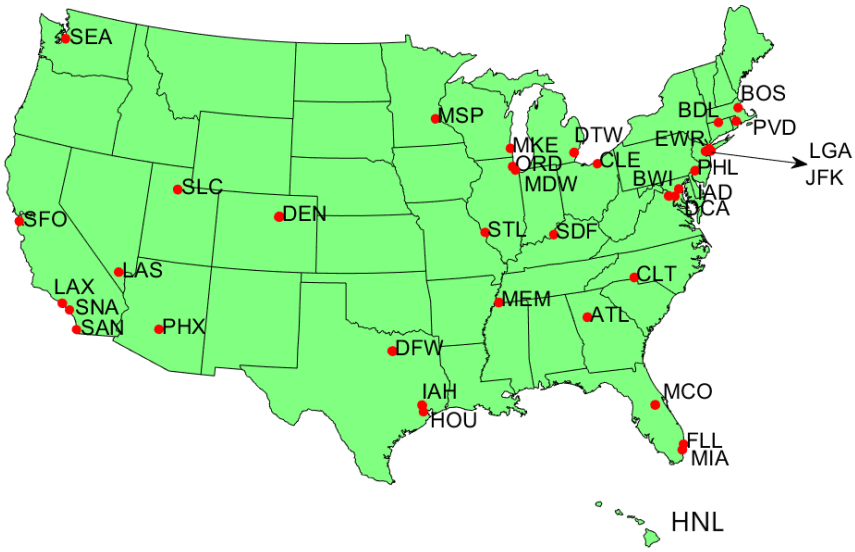

Figure 1. ASDE-X Supported Airports in United States.

There were other studies that analyzed the ASDE-X data for different purposes. Spencer used this data to develop Bayesian models for predicting runway occupancy times for arrival and departure flights [4]. Hu used the analyzed ASDE-X data from six airports in the final approach segment to calculate the buffer times in the real world which are applied by controllers for each arrival pair

and evaluated the sensitivity of those buffer times in airports' arrival throughput [5][6]. Mirmohammadsadeghi used ASDE-X data from six airports in the US and proposed a new method for estimating the unimpeded taxi times based on the calculated taxiing speeds which he calculated from the surveillance data [7][8]. In another study ASDE-X data was used to improve the predictions of departure taxi times [9][42].

For this study two years of ASDE-X data was provided by FAA. The data is for years 2015 and 2016 and is extracted from all the 37 airports which are equipped with this system. Raw ASDE-X data is in text format and the files consist of data records for periods of 30 minutes.

ASDE-X data includes many useful information about every aircraft within the limitations of the surveillance system. This tracking system identifies every vehicle with enabled transponders which is within 60 nautical miles from the airport. Some of the major fields in the ASDE-X raw data are as follows: Data Source Identifier, Message type, Time of Track, Position in WGS 84 (World Geodetic System 84) coordinates including Latitude and Longitude, Position in Cartesian Coordinates, Measured Flight Level, Track Number, Track Status, Flight Plan Related Data like Call Sign, Aircraft Type, Wake Turbulence Category, etc. Upon request of FAA, we were tasked to develop a landing database by using the given ASDE-X data for 37 airports. Figure 2 shows an example of collected arrival tracks at Atlanta International Airport (ATL) on December 31st 2016. As shown in Figure 2 there is a distance limit in ASDE-X data collection and data recording starts from defined distance thresholds from the airport. In the following figure, arrival tracks from each direction on various runways are shown.

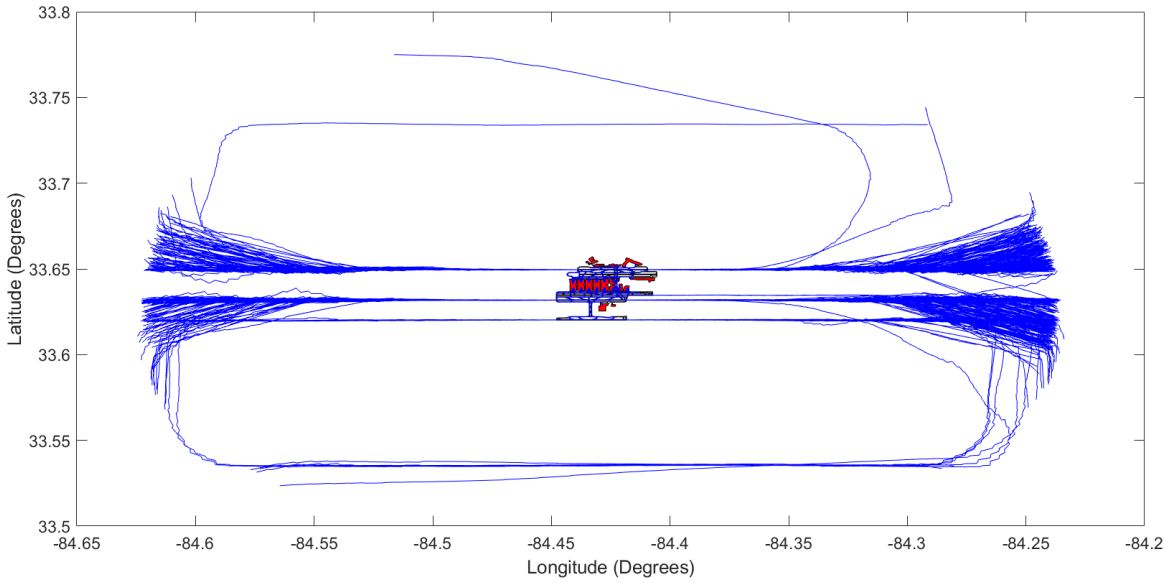

Figure 2. ATL Arrival Tracks Based on ASDE-X Data on December 31st 2016.

ASDE-X system was primarily implemented at airports to report x-y coordinates accurately on the runways and taxiways. This of course needs the pilot to turn on the transponder in the cockpit to enable the radars to locate the aircraft. At some facilities depending on the precision of the terminal surveillance, the coverage is very high at the apron (terminal) areas, while at some other airports most of the tracks end close to the terminal area. Figure 3 represents a sample of ASDE-X tracks at LaGuardia Airport on July 15th of year 2015.

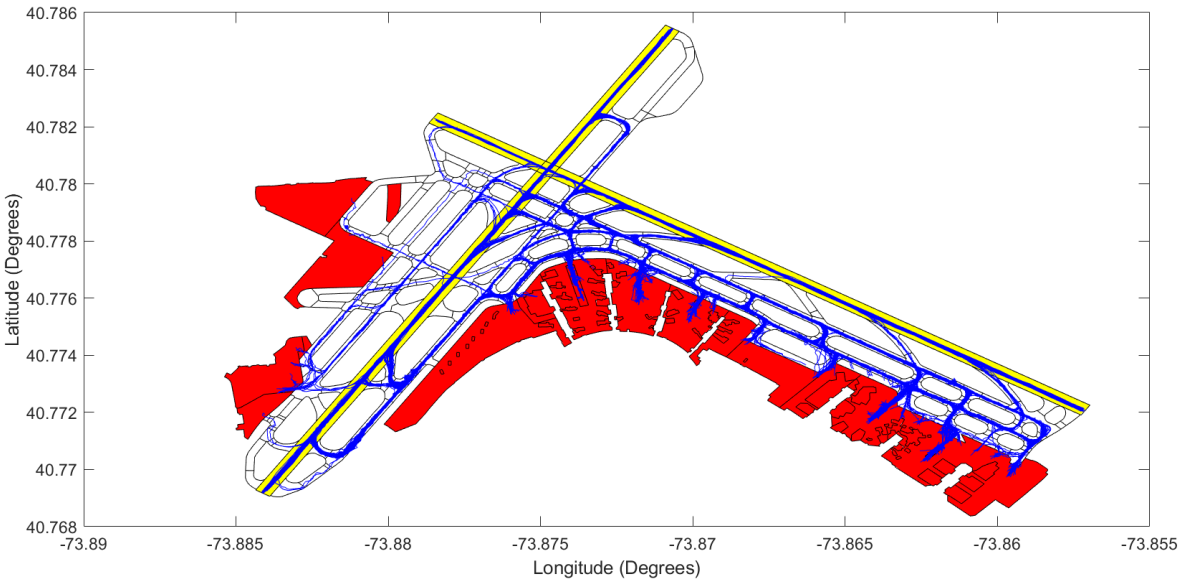

Figure 3. LGA Arrival Tracks on July 15th 2015 Based on ASDE-X Data.

Figure 3 represents the analyzed ASDE-X tracks for arrival flights from the point that airplanes passed the runway thresholds to the final recorded location for each flight on July 15th 2015 at LGA airport. As it is shown in Figure 3, some of the arrival tracks enter the apron area (shown with red color in the map) and they continue up to some of the gate locations, but most of the arrival tracks end after entering the apron area and we can't see which gate they took. In this study even though the developed algorithm for parsing ASDE-X data tries to find the finishing point and extracts the label for the apron area, we were mostly focused on the critical landing parameters on the runway until the nose of the airplane touched the hold-bar of the runway exit.

For analyzing the raw ASDE-X data, initially a parser was developed in MATLAB programming language to parse all the text files for each airport. Since each file was named properly at the time of creation, we could combine all the files belonging to the same day. After concatenating all parsed text files for each day, we had to separate individual unique flight track and data based on flight ID and flight unique identifier that the system assigned to each transponder record. After finding all the unique flight IDs and collecting all the recorded latitude and longitudes in addition

to the time stamps, the first set of output files were saved in structure format. From this point on there are two different sets of input files which are required to analyze the spatial data and extract the critical landing moments from the ASDE-X tracks.

The required separate input files for the analysis are:

1- A database for runway geometry information which includes accurate location of runway end thresholds' latitude and longitude in addition to other critical geometry parameters such as elevation, width, and displaced threshold.
2- A database for runway exit geometry information which includes runway exits of the 37 ASDE-X supported facilities and their geometry parameters such as radius of the arc, the path length of the runway exit, and the angle the runway exit has with the runway centerline. Also, the location of the runway exits and their distance from the runway threshold are critical parameter for our analysis.

Not only we need the databases which we mentioned above, but we also need more accurate data and information regarding the aircraft altitude changes during the final approach segment all the way to the approximate moment of landing gear touchdown. ASDE-X data provides precise latitude and longitude information, however its precision in reporting altitude is not acceptable. The reported values for altitude have very noisy trends that we couldn't find any proper smoothing algorithms to find the approximate moment of touchdown. Therefore, we collected some video data from airplanes landing at three facilities: Chicago O'Hare International Airport (ORD), Charlotte Douglas International Airport (CLT), and Ronald Reagan Washington National Airport (DCA) in order to find a mathematical logic to find the approximate touchdown moment of airplanes by analyzing their speed profiles.

After understating the required databases and information for extracting critical landing parameters we represent each mandatory information through the subsections of this chapter. We initially review some of the collected video data and explain the analysis procedure in addition to the conclusions and we review some of the collected distributions. Then we explain the runway geometry database and the algorithms used to create runway polygons in addition to some primary statistical reviews of runway geometry parameters in the US. The third required database is runway exit geometry information and we review the procedures for creating them in addition to some primary statistical overview of runway exits used in our database. Finally, we summarize the chapter by representing the final product which was delivered to the FAA as Landing Events Database and detailed explanations of the functionalities and user interface capabilities.

2.1 Video Data

As mentioned earlier in this chapter, ASDE-X technology was initially implemented at busy airports in the United States to locate every moving vehicle with transponder and avoid potential runway and taxiway incursions under low visibility conditions. Therefore, the accuracy in reporting the latitude and longitude for this system must be high and reliable for controllers in air traffic control tower making critical decisions. However, the accuracy of the reported altitude values for each flight is not as much as the accuracy for reported x-y coordinates. Figure 4 shows an example of an altitude profile from the ASDE-X data and the reported elevation for the runway in which the sample flight landed on [7]. As it is shown in Figure 4, the reported altitude from ASDE-X has values below the runway elevation and also the trend for the time series of reported altitudes is not in a way that by smoothing the profile we would get more reasonable values. Also, by smoothing such profiles we might move the values further than what happened in the real world, which might cause a considerable error in estimating the approximate touchdown location.

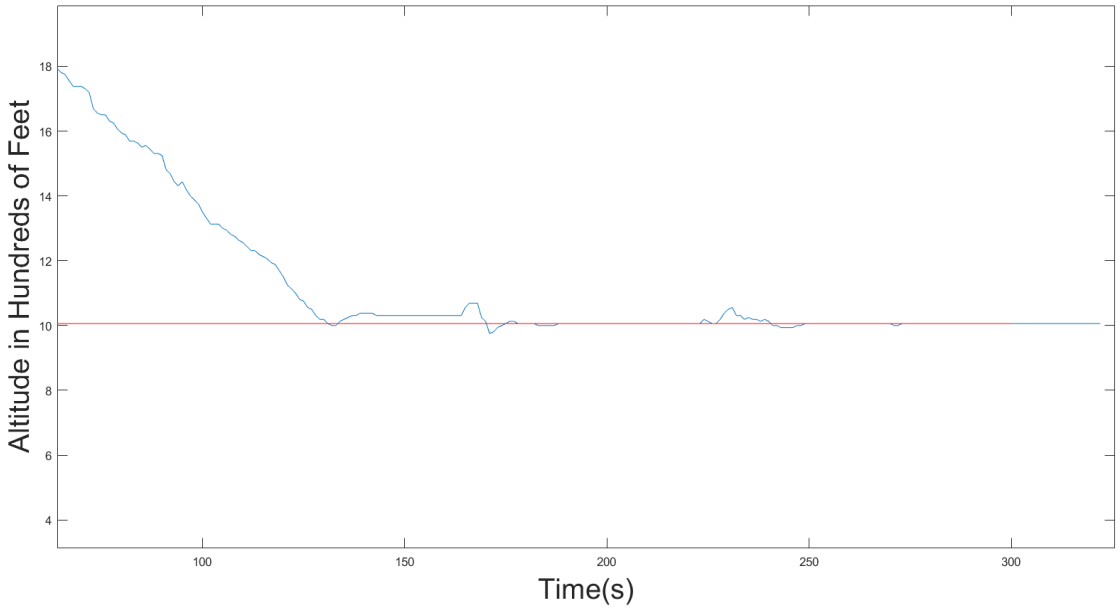

Figure 4. Sample of a Fuzzy Altitude Profile. (Red Line Shows the Referenced Altitude of the Arrival Runway.)

The importance of the altitude profiles for each arrival flight is in estimating the approximate location and time for the touchdown. Touchdown location and time measured from the runway threshold are critical parameter for every landing flight and they can have an impact on the amount of time that the aircraft spends on runway. For finding out a mathematical logic for estimating not only accurate touchdown locations, but also validating other algorithms in finding runway occupancy times we went to the following three facilities and collected some video data from arrival flights on various runways. The visited airports were: Chicago O'Hare International Airport (ORD), Charlotte Douglas International Airport (CLT), and Ronald Reagan Washington National Airport (DCA).

Figure 5. Recording Landings on Runway 10C at Chicago O'Hare International Airport (ORD).

The recorded videos from the three airports that we visited were then analyzed by an application called Visual Studio to recreate the speed profiles for each collected video [10]. For this purpose, we chose some reference points on each runway and tried to measure our angle and distance to those reference points then we could capture the distance of occurrence for each recorded critical parameter. Basically, the following parameters were extracted from each video if the video was clear and we could read the following events:

1- The moment of passing runway threshold

2- The moment of landing gear touchdown

3- The moment of nose gear touchdown

4- The moment of activating the thrust reversers

5- The moment of activating the wing spoilers

Not all the mentioned parameters were used in either extracting critical landing moments from ASDE-X data or in simulating the landings in the new version of the REDIM model, however the video data helped us to derive a mathematical logic to estimate the approximate touchdown location based on the calculated speed profiles from ASDE-X data. Figure 6 represents a re-generated landing profile based on a real collected video data from runway 28C at Chicago O'Hare International Airport. Because the number of aircraft types operating in the National Airspace System (NAS) is more diverse than the video data collected, we assigned landing roll distributions to all aircraft using the Airplane Design Group (ADG) categories developed by the FAA.

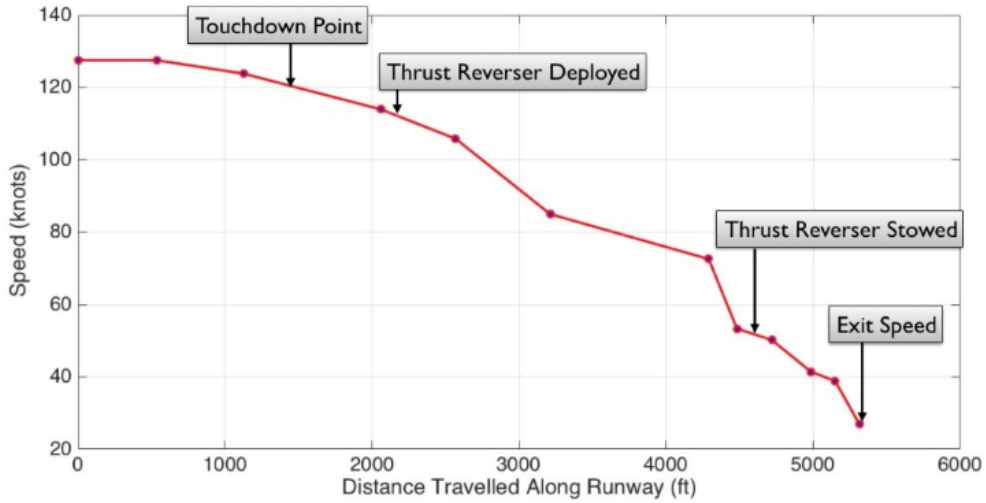

Figure 6. Sample Landing Roll Data Collected Using Video Equipment at ORD.

After analyzing video data and the generated speed profiles, we noticed that touchdown location is approximately where the landing aircraft losses 5% of its threshold crossing speed. Therefore, in analyzing every ASDE-X speed profile we find the first moment where the speed is 95% of the threshold crossing speed and the deceleration values after that moment have a monotonic decreasing trend.

Moreover, for having a better understanding of the distribution of the timing for applying different braking systems on the runway after the main gear touchdown, we studied the time difference distributions between the main and nose gear touchdowns in addition with main gear and thrust reverser activations. Figure 7 represents the values generated from a truncated normal distribution assigned to the collected values for the time differences between main gear and nose gear touchdowns. The mean for this truncated distribution is 4.5 seconds and the standard deviation is 2.0 seconds. The values represented in Figure 7 are for all the aircraft types we observed in the video data, however further categorizing was done to extract the distributions for different ADG aircraft groups.

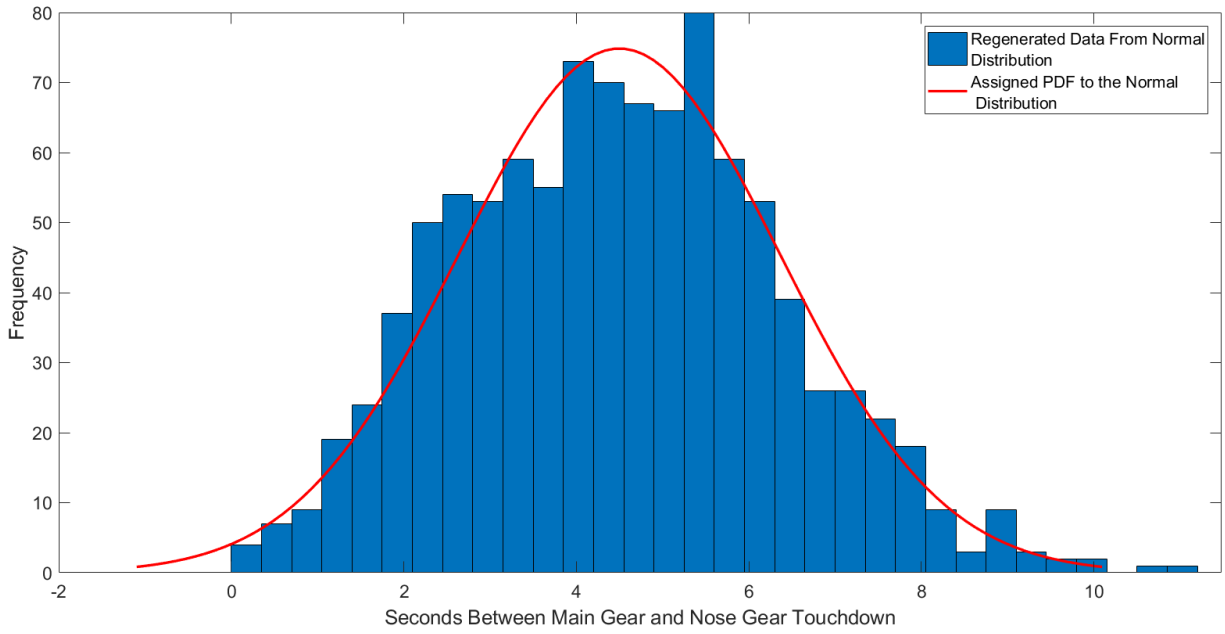

Figure 7. Assigned Normal Distribution to the Collected Values for Main Gear, Nose Gear Touchdown Time Difference.

2.2 Runway Geometry Database

A critical input data for analyzing ASDE-X and creating a useful landing database is a runway geometry database. We should know on which runway end each of our landing flights landed. This will result in getting beneficial insights in runway usage at airports for arrival traffic, airport arrival fleet mix, statistics on runway occupancy times on each unique runway end, and eventually extracting meaningful patterns and relations between runway geometry and aircraft landing behavior. For this purpose, the FAA database for geometry information of airports' runway ends was used [11]. The files from the FAA source are in text format and they report the following information for every registered runway end around the country:

1- Latitude of the center point of runway threshold
2- Longitude of the center point of runway threshold
3- Elevation of the center point of runway threshold
4- Width of runway
5- Length of runway
6- Location of displaced threshold and the displacement distance

After parsing the files with their latest update in 2016 (since our ASDE-X data was for years 2015 and 2016) the 37 ASDE-X supported facilities with all of their runway ends were extracted and based on mapping toolbox features in MATLAB, runway polygons were created for each airport. Therefore, each of the airports in our data was assigned to a runway geometry database where we could identify any intersection of flight track points with any of their runway polygons. Figure 8 represents an example of created runway exit polygons at Dallas Fort Worth International Airport (DFW). As shown in Figure 8 based on the available geographic data, a database for runway

polygons was made for all the 37 airports similar to the represented runway polygons of DFW in the figure.

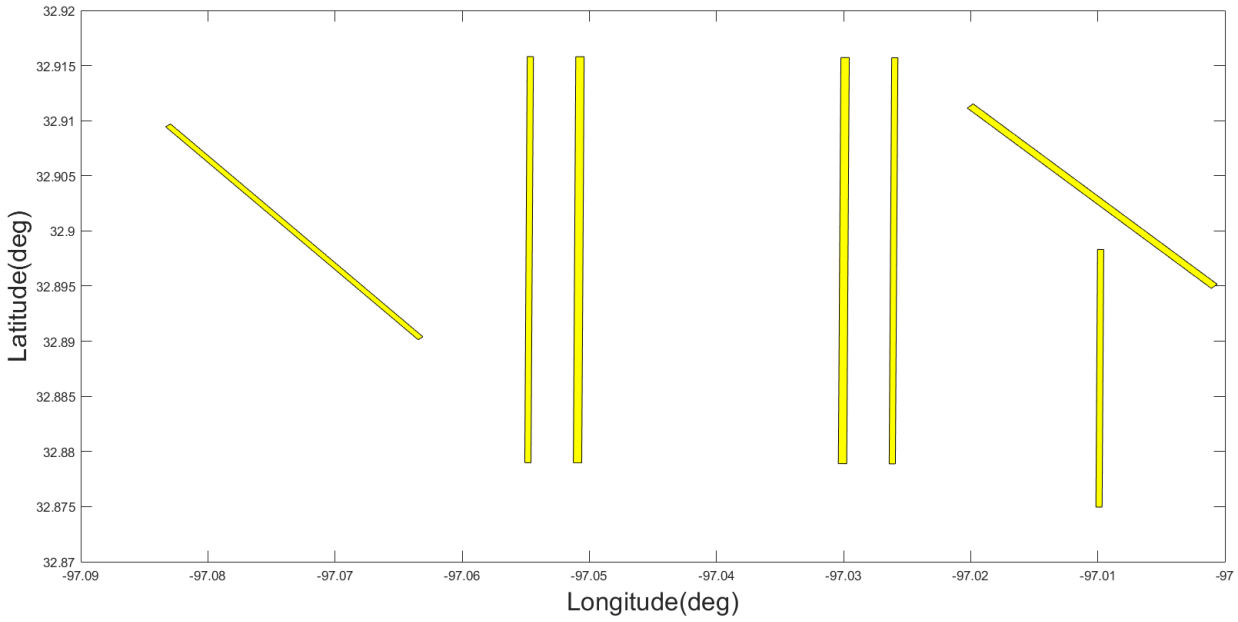

Figure 8. Created Runway Polygons Based on FAA Geometry Data for DFW.

Understanding the geometry features of runways in the analysis of aircraft landing behavior is crucial. There are 290 runway ends and 145 runways in the runway geometry database for the 37 ASDE-X supported airports. Those runways have a wide range of lengths from 2'555 (ft.) which is at BOS runway 15L-33R to the longest one at DEN which is runway 16R-34L with a length of 16'020 (ft.). Among the 37 airports in the database, DEN airport has the highest average runway length with 12'666 (ft.) and SNA has the lowest average runway length with 4'299 (ft.). The highest standard deviation of runway lengths is for SLC with 3'112 (ft.) and the lowest standard deviation of runway lengths is for SAN with 0 (ft.) as it is the only single runway airport in our runway database. The following box plot represents the variability of runway lengths at each of the airport members of our runway database. As shown in Figure 9 while some facilities have many similar runways in terms of the available landing length, a few of them have runways with

different ranges of length. For the latter condition the fleet mix of the arrival aircraft would vary on each runway due to the length limitations.

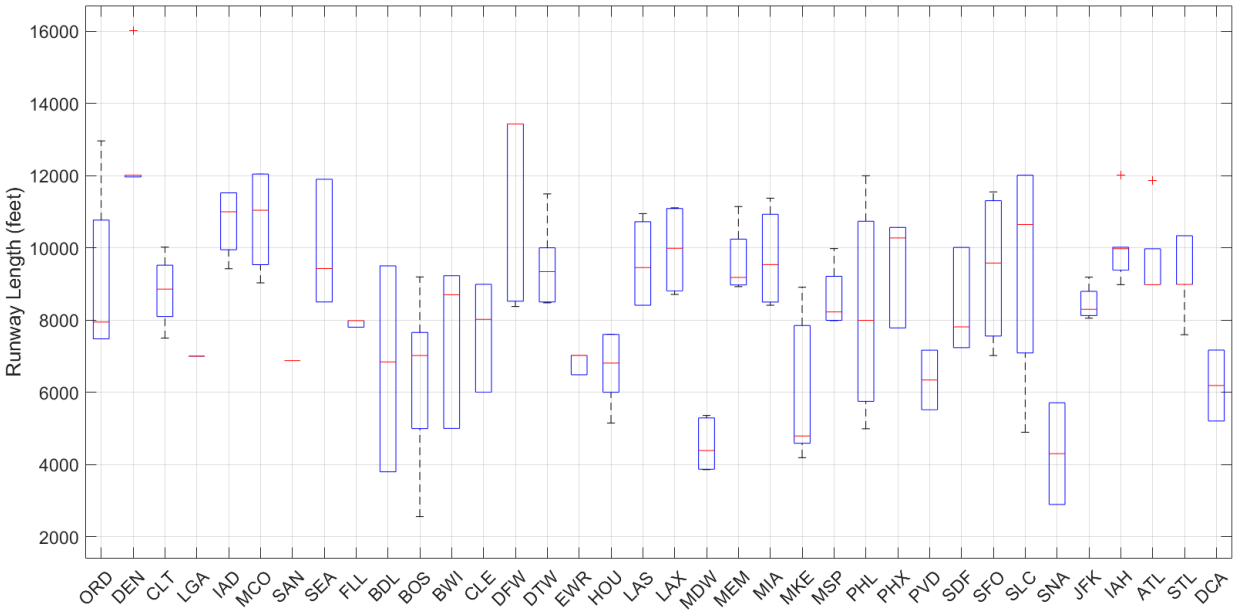

Figure 9. Variability of Runway Lengths Among the Airports in the Runway Geometry Database.

While we took a look at the variability of runway lengths at the ASDE-X supported airports, we can always see how many runways are at each of our studied airports, since that can be a very useful information for assigning the arrival traffic and analyzing the count of operations on each runway based on the available data for years 2015 and 2016. Figure 10 represents the number of runways at each airport based on the runway geometry database. As shown in the figure both ORD and DFW are at the top of the list with 7 runways at their facilities while SAN is the only single runway ASDE-X supported airport.

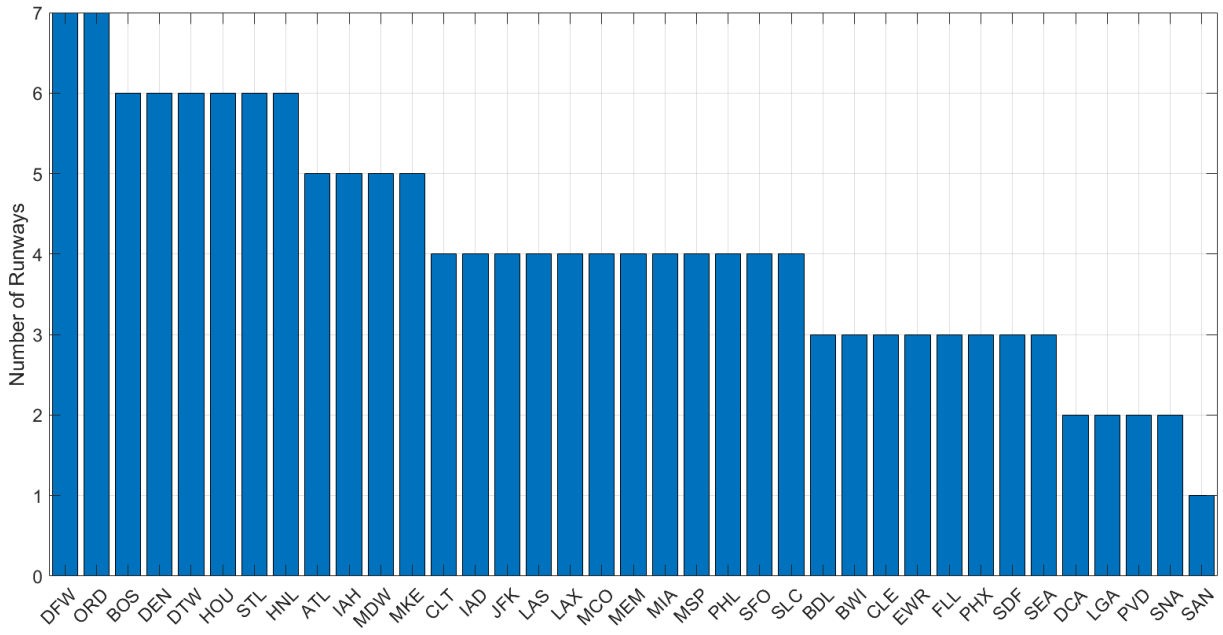

Figure 10. Number of Runways at Each ASDE-X Supported Airport in the Runway Geometry Database.

In Appendix. B, the complete tabular format of the created runway geometry database is provided.

2.3 Runway Exit Geometry Database

The second required input database is the runway exit geometry database. Since the primary goal of this study is to analyze the runway occupancy times and runway exit utilizations, we should know how long does it take for each aircraft to entirely vacate the runway by using exit ramps or so-called runway exits. The geometry parameters of the runway exits, along with their location on the runways, can help us deriving relations with arrival flight runway occupancy time. For this purpose, Google Earth was used since there is no official data source for reporting the geographical parameters of runway exits at airports [4]. For each runway exit at the 37 ASDE-X supported airports the following parameters were calculated by using Google Earth application:

1- Runway exit path length from the point of the curvature at the beginning of the arc all the way to the exit hold-bar

2- Runway exit radius of the arc

3- Runway exit angle with the runway centerline

4- Runway exit width

5- Runway exit distance from the operational runway threshold

Figure 11 shows an example of the drawn runway exit arcs with their proper labeling for one of the runways at DFW airport. Each measurement from the Google Earth files were stored in a spread sheet with the same label for both exit name and runway id [4]. The final runway exit geometry database is a combination of collected numerical measurements and geographical information for each runway exit arc and hold-bar.

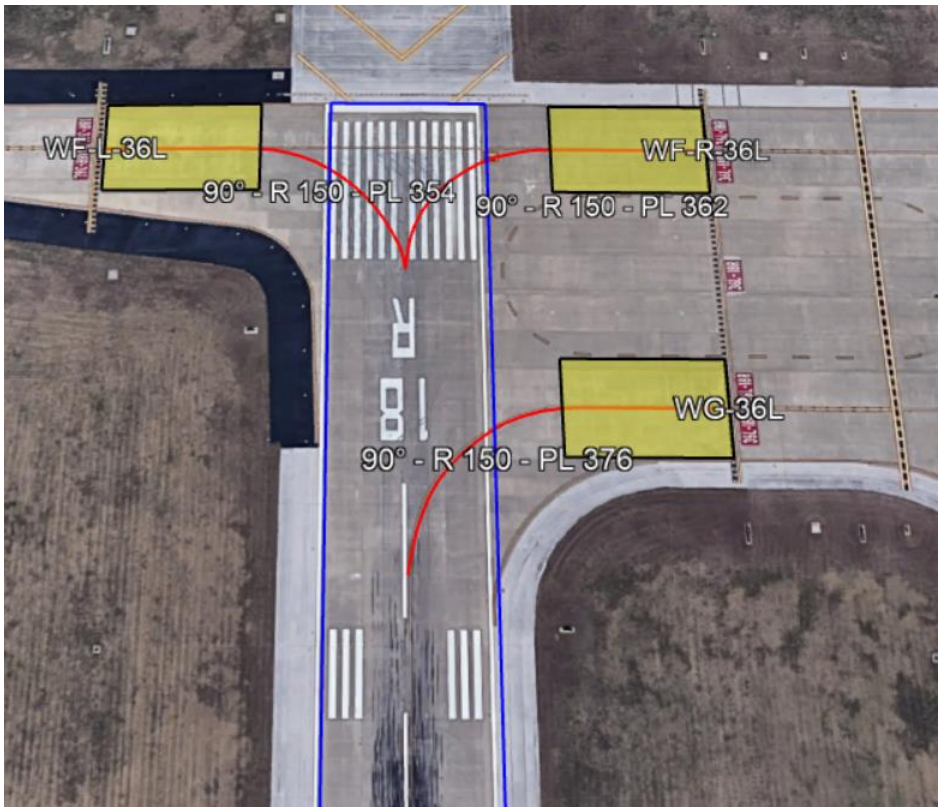

Figure 11. Example of Drawn Arcs from the Point of Curvature to the Runway Exit Hold-Bar for Some Exits at DFW.

Since we have to identify the utilized runway exit for each arrival flight in the ASDE-X data, based on the collected arcs from the Google Earth files for each airport, runway exit polygons were generated to identify the exact moment of entrance for each track point. The way that each of those polygons were made is as following: based on the last point on the arc, the location of exit hold-bar is identified. Since we have collected the runway exit width, we can reckon two more points based on the identified location for the exit hold-bar. From the new generated points, we create a rectangle with a length of 200 (ft.) in the heading of the exit angle to cover for possible maneuverings in the radar data or biased smoothed path based on heavy fuzzy reported locations. We noticed that for some runways due to the short distance between the runway exit hold-bar and runway centerline, the runway exit polygons length should've changed to 150 (ft.) to avoid confusion in recognizing the exact exit polygon intervention. Figure 12 represents the processed runway exit polygons for DFW and all of its collected runway exits.

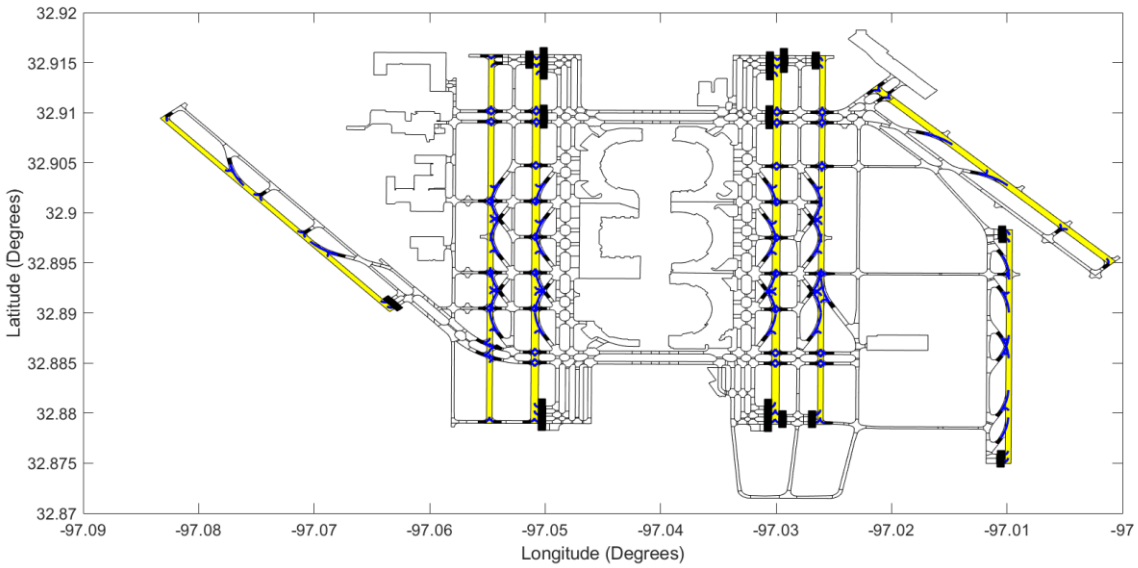

Figure 12. Generated Runway Exit Polygons and Exit Arcs at DFW from the Google Earth Files.

After collecting all the runway exit geometry information we noticed that there are 3'385 runway exits totally at the 37 ASDE-X supported facilities. Analyzing the geometry features of the runway

exits and trying to find relations with aircraft exit speeds is one of the critical aspects of this study. Therefore, it is valuable to review the statistics of the measured parameters for each runway exit. The following figure represents three histograms that show the distribution of runway exit angle, radius, and path lengths. As it is shown in Figure 13, 48% of the runway exits in the country are right angle exits with radius values lower than 500 (ft.), and only 8% of the runway exits have angles between 30 and 40 degrees with radius values more than 1000 (ft.). The remaining exits are either low angle, back-turn, or non-standard exits.

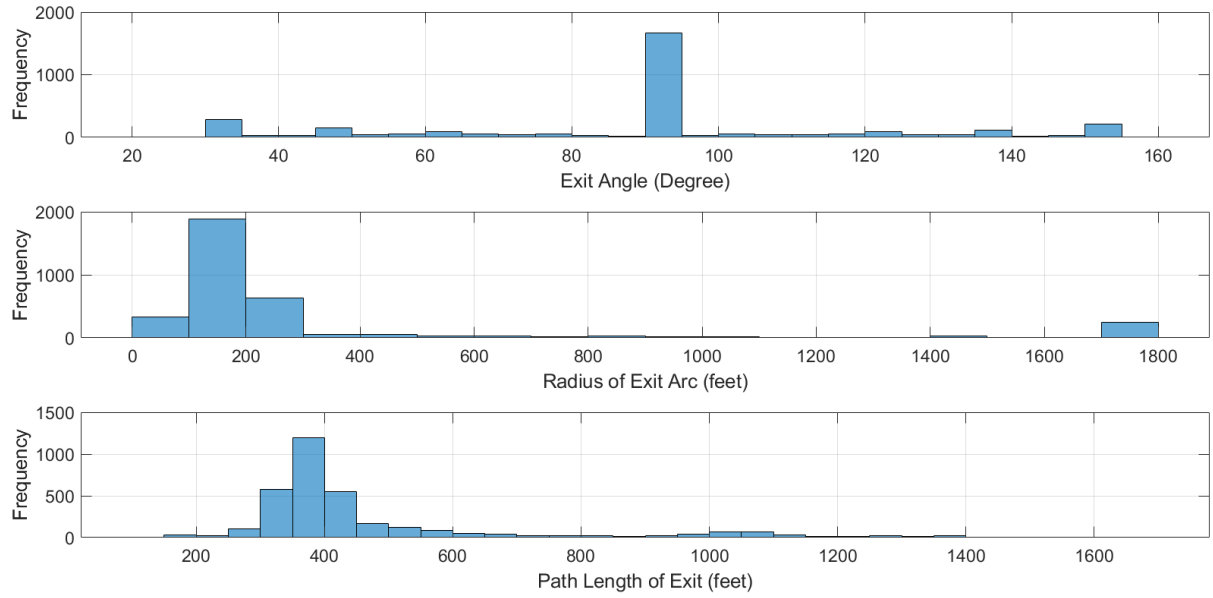

Figure 13. Runway Exits Angle, Radius, and Path Lengths for the 3'385 exits at the 37 ASDE-X Supported Facilities.

Another important parameter in analyzing the runway occupancy time is understanding the configuration of runway exits along the runway. Depending on the location of exits and their geometry features, airplanes can take them at various speeds unless they're poorly located. By looking at the distribution of exit locations on the 290 runways that we have in our database we can learn more about the current state of runway exit locations that in later chapters we can evaluate whether they are located at desirable distances from runway thresholds for pilots, or they are at

non-efficient distances. As shown in Figure 14, 50% of the runway exits in the database are located before 5’200 (ft.) which is around 60% of the median of runway lengths for ASDE-X supported airports. Moreover, the fact that almost 90% of the runway exits are located before 10’000 (ft.) tells us that by that distance most of the airport designers think that airplanes can easily evacuate the runways. According to the plot there are very few runway exits which are located beyond 12’000 (ft.) which are right angle exits at DEN airport.

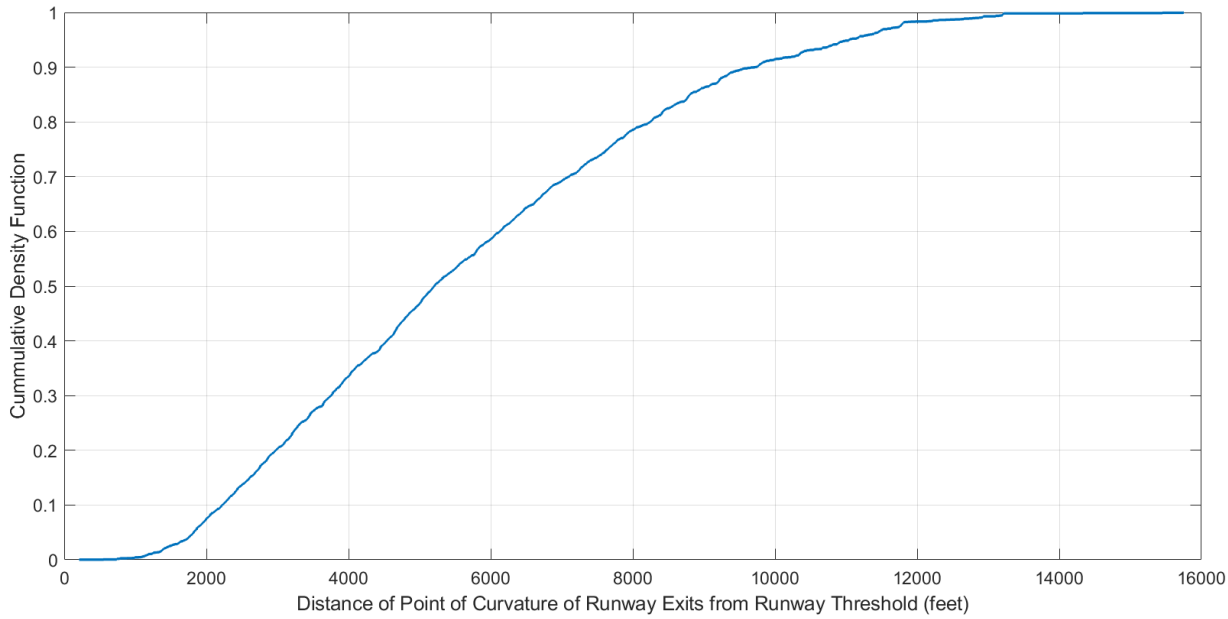

Figure 14. CDF Plot for Exit Locations at all the 37 ASDE-X Supported Airports.

The following figure represents the variability of exit geometry features among all the 37 airports that we collected in the database. As we can see in Figure 15, IAH has the lowest exit angle average among all the 37 airports with 66.6 degrees while ATL has the highest exit angle average with 94.7 degrees. Most of the facilities have a median of runway exit angles around 90 degree which supports the fact that right angle exits are very popular around the country. IAH has the highest average exit radius with 796.9 (ft.) and after that IAD has the second highest average exit radius while MDW has the lowest in the country with only 142.2 (ft.). This observation for IAH supports

the lowest exit angle average and tells us that this facility has many low (acute angle) exits. Moreover, low values for average exit radius are mostly because of having too many right angle or non-standard exits. The ranking changes when comparing the average path lengths and DEN becomes the top airport with an average of 691.6 (ft.) for path length and this tells us that at that airport the runway exits are located further from the runway centerline due to sufficient available land.

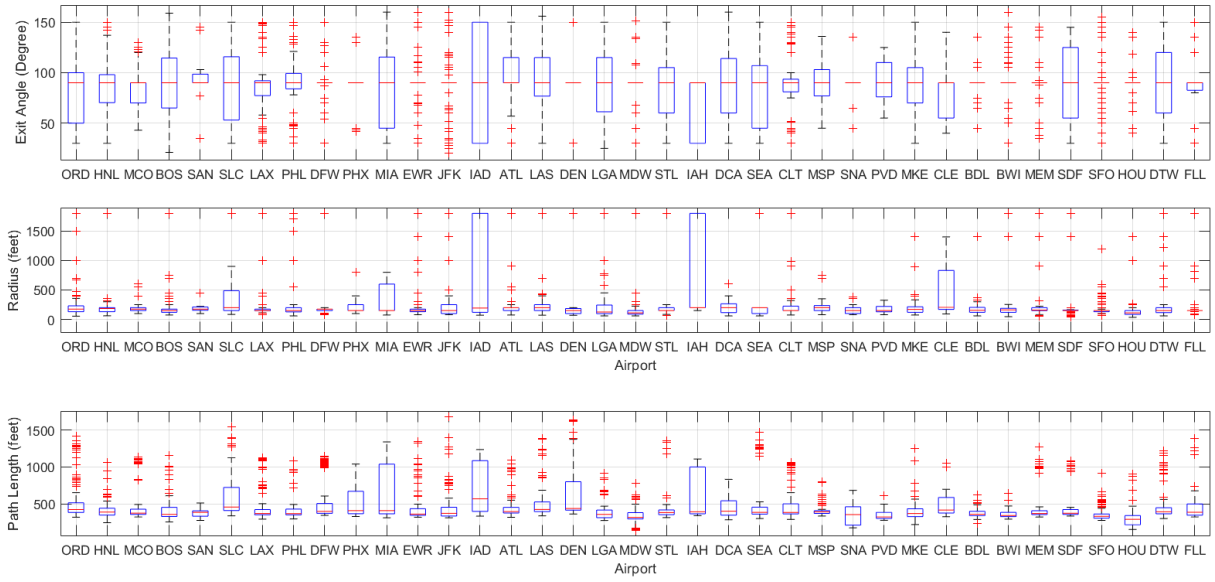

Figure 15. Variability of Runway Exit Geometry Features at all the 37 ASDE-X Supported Airports.

2.4 Aircraft Dimension Database

Since we are trying to extract the runway occupancy time for each individual flight, it is very important to identify the moment when the entire fuselage of the airplane evacuated the runway and was not on the runway polygon anymore. Because we have the latitude and longitude of the track points we can identify the exact moment of runway evacuation if we know which part of the fuselage is reported by the ASDE-X data. After reviewing many video data from the three airports

and animating the track data from ASDE-X, we noticed that with an acceptable approximation for various classes of aircraft, ASDE-X tracking data reports the location of the nose gear. Therefore, by knowing the dimensions of every individual aircraft from the data, we can replicate the imaginary fuselage of each arrival aircraft and check the critical points of the fuselage which are the tail and wingtips, to monitor the movement of the aircraft along the runway exit and capture the exact moment when the entire fuselage vacated the runway. For this, a database of aircraft dimensions was collected to report the following parameters for each of the 274 individual aircraft types in the data [10]:

1- The distance between aircraft nose gear and main gear
2- The distance between aircraft nose gear and tail tip
3- The wing span of the aircraft

By having the above parameters, we can check for every reported location in the radar data, whether any parts of the aircraft fuselage were still on the runway or not.

Figure 16 compares the dimensions of two different aircraft as an example to show the collected parameters in the database. By referencing every point to (0,0) point in the x-y space, you can compare the approximate size difference between Airbus A319 and Airbus A388 by looking at the size of the imaginary circle passing their wing tips and the approximate location of nose and tail of the airplanes if we imagine the point (0,0) as the center point of the fuselages.

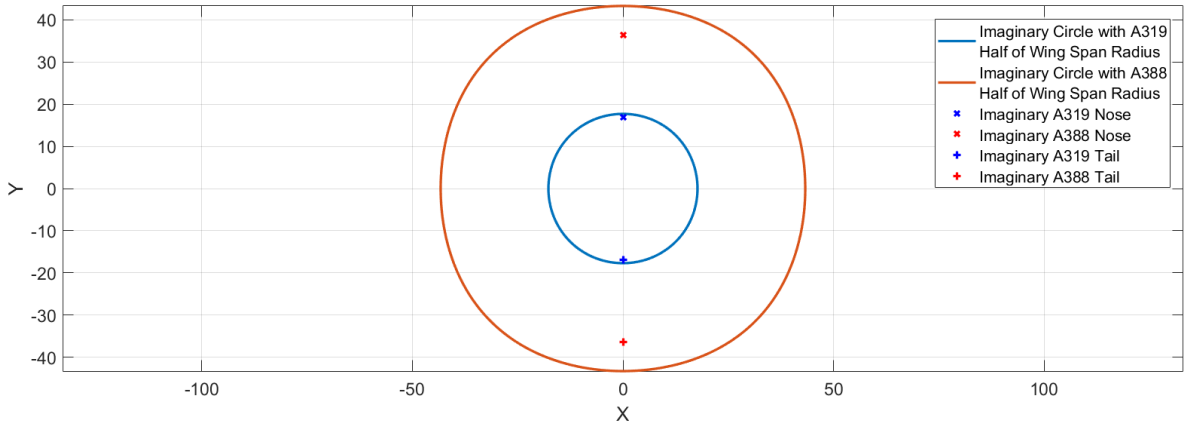

Figure 16. Comparing the Dimensions of A319 and A388 Based on the Parameters in the Aircraft Dimension Database.

2.5 Landing Events Database and Computer Tool

After preparing the required input databases for analyzing the ASDE-X data, we can start parsing the ASDE-X raw files and concatenate them to extract the critical landing parameters for each landing flight. For identifying the operational runway, we have to find that which runway polygon the flight track points showed up. Since we already have the exact boundaries for each of our runway polygons, this task can be easily done by any mapping toolbox library. The other important feature for assigning the operational runway is the heading of the track. We know that runways are labeled based on their azimuth heading, therefore we can calculate the azimuth heading of the arrival track and based on the absolute difference with the azimuth headings of either of the runway ends, we can choose between the runway threshold which yielded smaller absolute difference value. Since we might not be lucky to capture the exact tracking point above the assigned runway threshold, the next move is to interpolate the speed when the nose of the aircraft passes over the assigned runway threshold. We consider that value as the threshold crossing speed. The next critical point is touchdown location and time. For extracting the touchdown location as we explained earlier in this chapter, we look for the first speed value after threshold crossing that has

95% or less speed compare to the threshold crossing speed. Note that because of the noise in reported location and small time gaps between each reported point, we had to smooth the speed profiles for each landing to have a better reading of the speed trends. Figure 17 depicts the calculated speed profile from the latitude and longitudes and reported time stamps. As it is shown in Figure 17 the smoothed values for the speed are more reliable for any of our critical parameters. The smoothing algorithm used was moving average with a neighborhood of 5 nearby neighbors. This way we could remove the noise from the calculated speed values clearly.

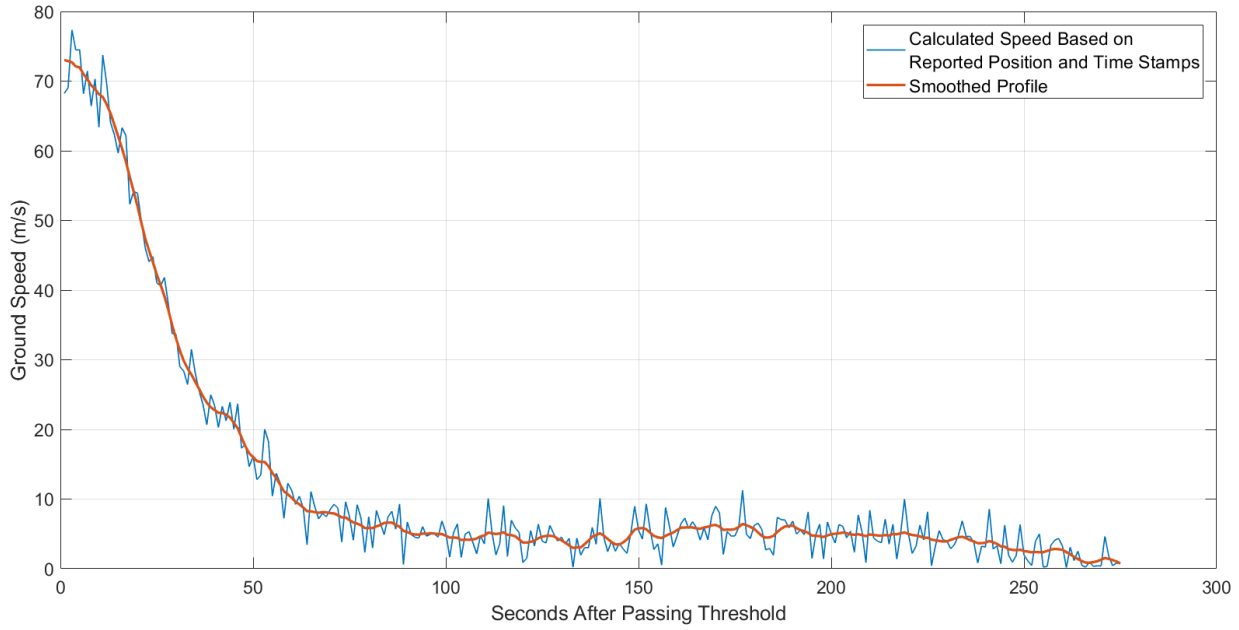

Figure 17. A321 Landing on Runway 10L in ORD, Speed Profile Example vs. Smoothed Speed Profile.

The touchdown moment is the first time when the speed profile gets to 95% of threshold crossing speed or lower than that. We store the touchdown moment and its distance from the runway threshold. From that point on, we store the average deceleration all the way to the point of curvature of the runway exit that the pilot took. We also capture the deceleration from the touchdown point all the way to a moment that we call nominal speed on the runway, which is considered as 70 knots for narrow bodies and heavy jets, and is 70% of threshold crossing speed

for small aircraft class. The reason for capturing this deceleration is to have an understanding of the braking behavior for each aircraft until the moment that pilots are comfortable to start making decisions about selecting a runway exit ahead of them for evacuating the runway. The moment that pilots start the maneuvering for taking the runway exits is what we call the moment at the PC point. For capturing that moment, we keep a record of cumulative distances of the aircraft from the operational runway threshold and when that distance is equal or bigger than the recorded PC distances of the runway exits retrieved from the runway exit database, we capture the first moment that passed the criteria and store its index and speed at that moment. The path that airplanes take over the arc of the runway exit can be a zigzag move if we just rely on the pure reported radar locations, therefore we smoothed the path of maneuvering over the exit arc with a polynomial of second degree in regards to the retrieved information of the associated runway exits' arcs. When the nose of the aircraft (or the ASDE-X track point) touches the runway polygon, we store that moment with its speed and index from the threshold. From that point on we refer to the airplane dimension database and check the imaginary circles passing both wingtips of the aircraft and imaginary location of aircraft's tail tip to capture the first moment that the entire fuselage was observed outside of the runway polygon. This moment is the true moment of runway evacuation and even though it is hard to capture it in the real-world from far located ATC towers, we consider this value as true ROT. From that point on we continue monitoring the track until the nose of the aircraft touches the recorded hold-bar location for the associated runway exit. The ROT to that moment is called ROT to the hold-bar. In the original parser we monitor the flight track all the way to the last reported location and we try to find the label of the apron area based on the published GIS layouts for airports from FAA. We also capture the taxi time, taxi distance, average taxiing speed and deceleration, and unimpeded taxi times. However, in the final version of the

published landing events database we report the information just until the runway exit hold-bar and we don't report any of the taxing parameters. Figure 18 summarizes all the explained points about the critical landing parameters for a sample flight which operated at LAX on 15th of April 2015. This landing belongs to a popular landing runway called 24R and is for a Boeing B772. As it is shown in Figure 18, we could capture the runway id, touchdown moment, PC moment, the moment when the aircraft nose touched the edge of the runway, the fuselage out moment, and finally the moment when the aircraft was at the hold-bar. This landing had a touchdown distance of 713.2 meters and it took 9.5 seconds to have the landing gear touchdown. The threshold crossing speed was 149 knots and it landed with a speed of 139.3 knots while it took the PC point of runway exit "AA" with 51 knots. The ROT edge for this flight was 46.7 seconds while the true ROT was 59.7 seconds and it touched the hold-bar after 61 seconds. For achieving that ROT, the aircraft had a nominal deceleration of -1.84 m/s^2. These are very valuable information which the parser extracts with high resolution for every input arrival flight from every available airport. Figure 19 represents the speed-time diagram of the same landing with the associated critical moments.

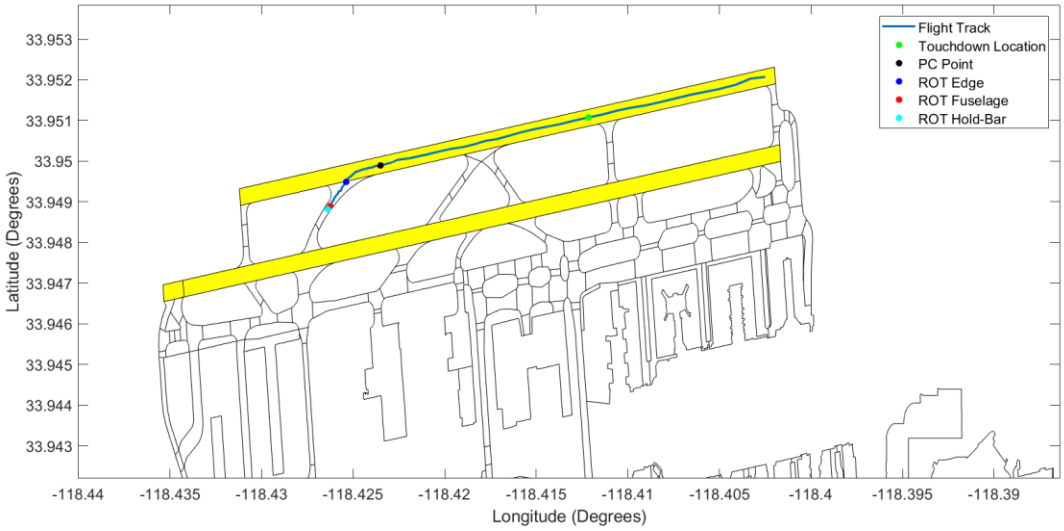

Figure 18. An Example for an Arrival Flight at LAX with its Extracted Critical Landing Moments.

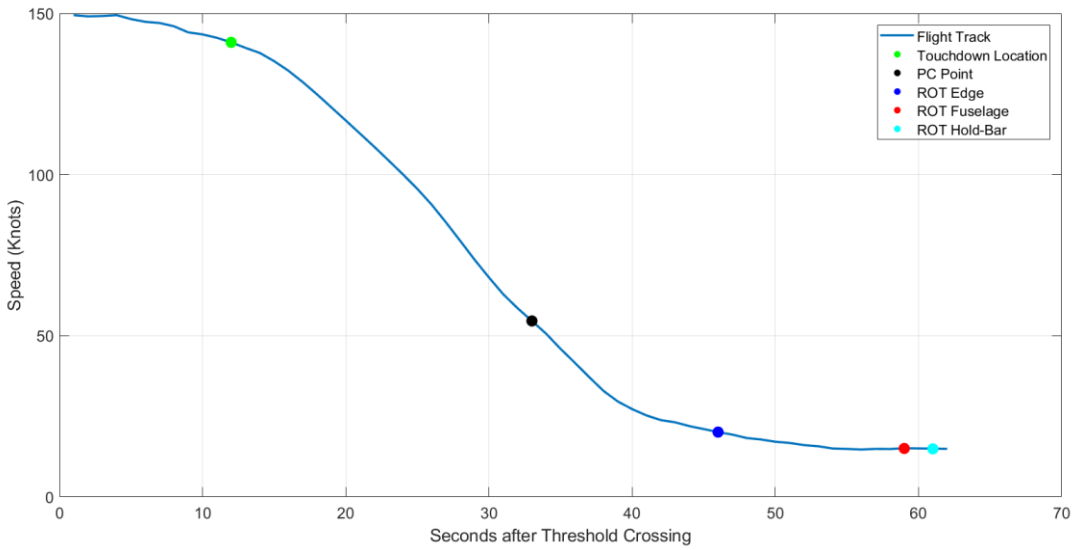

Figure 19. An Example for an Arrival Flight at LAX with its Speed Profile.

Around 12 million flights were analyzed for two years at 37 airports which the accurate statistics of the parsed flights with their critical parameters will be presented in the next section of this chapter. The data was gathered into a SQL database and access was given to FAA and many consulting companies [10]. An interactive user interface was designed to extract lots of meaningful statistical queries from the data [10]. For each airport the raw radar data, aircraft fleet mix data, aircraft runway occupancy times, runway exit utilizations, touchdown locations, deceleration profiles, approach speeds, and exiting speeds are available through different windows from the database. Figure 20 represents an example of the aircraft fleet mix for the ATL airport.

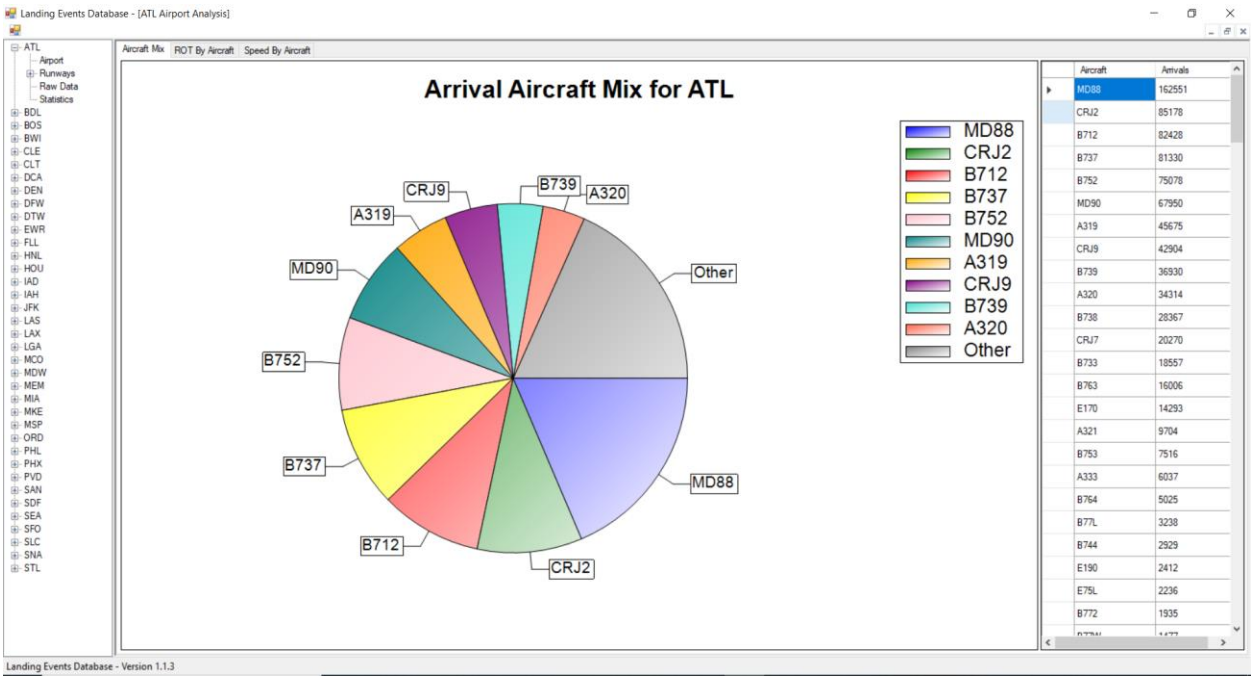

Figure 20. Aircraft Fleet Mix for ATL Based on Two Years of Ground Radar Data.

Figure 21 shows an example of average runway occupancy times for various aircraft types at ATL airport. These box plots can provide useful insight for the potential user of this database to analyze the aircraft behavior at different air fields in terms of runway occupancy measures. For designing purposes, the percentiles of popular fleet at commercial airports can be extremely helpful for future modifications on runway exits or potential changes in operational procedures while evacuating the runways.

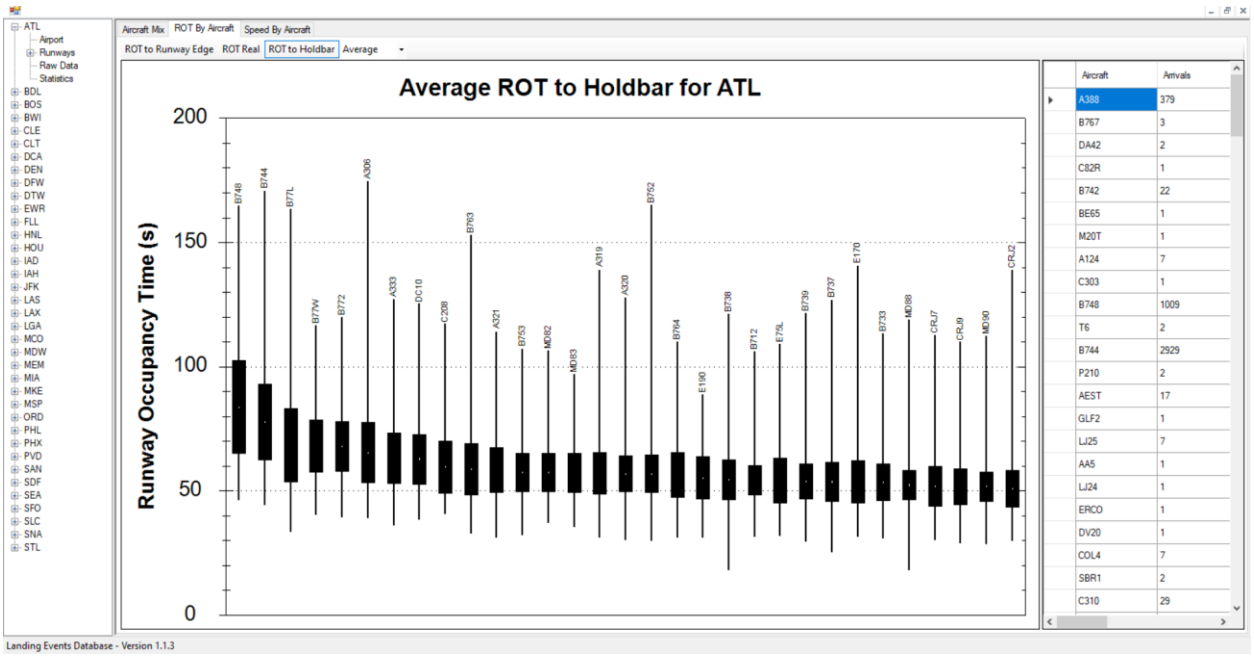

Figure 21. Average Runway Occupancy Times for ATL for Various Aircraft Types.

Not only for internal validation of the correctness of extracted critical points, and the goodness of assigning runways and exits to each landing operation, but also for helping the users to track each individual cleaned arrival track from the ASDE-X data, we enabled a visualization mode over the real airport layout with highlighted critical moments on the runway. This way any user can validate individual flight tracks on runways and they can filter for a specific airport, aircraft class, runway, or even unique exits. For example, Figure 22 represents all the track information and critical moments of Airbus A321 flights on runway 08L at ATL airport which used exit B11 for vacating the runway. As you can see in the figure, the first point in the runway, touchdown location, the moment at the point of curvature for the runway exit, the moment of touching the runway polygon, and the full fuselage out moments are all shown with pinpoints over the flight track.

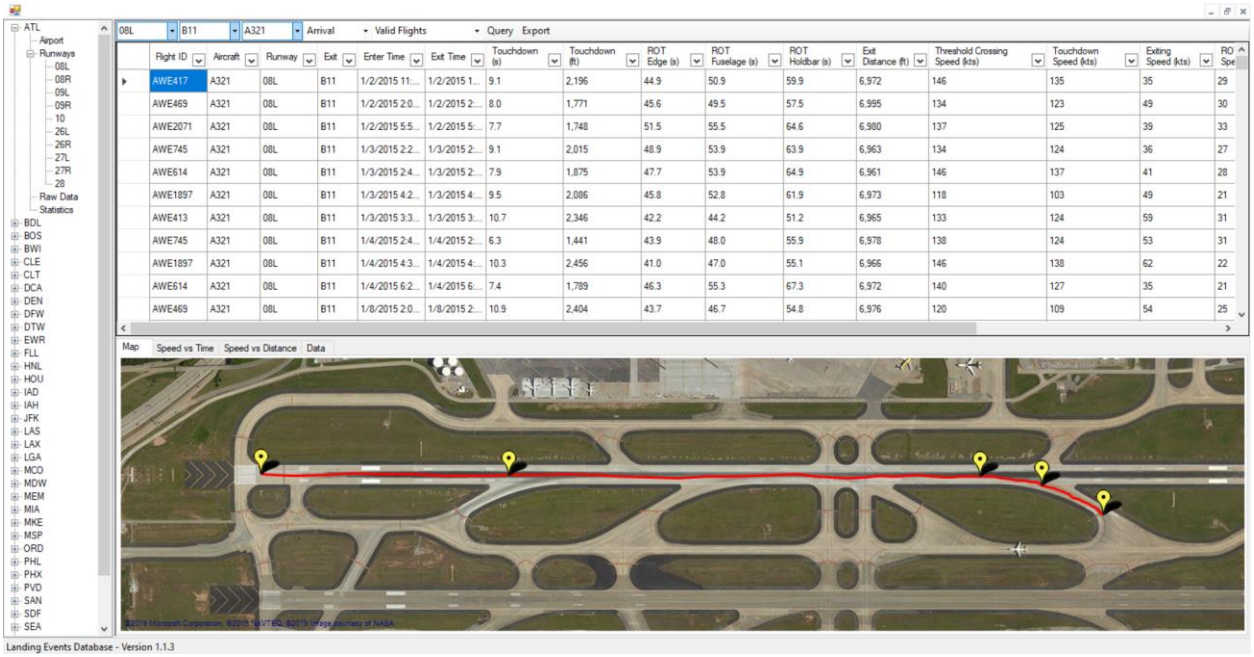

Figure 22. An Example of an Arrival Flight Track at ATL on Runway 08L.

The landing database is a helpful tool for analyzing the exit utilizations at big airports in the United States and it is currently being used by many consulting companies for analyzing the landing behavior and exit utilizations of different classes of airplanes.

2.6 Statistical Analysis on Extracted Parameters

After analyzing the entire dataset which in the raw text format it approximately takes 37 terabytes of hard disk, we could collect the detailed information for more than 12 million landing flights at 37 ASDE-X supported facilities for years 2015 and 2016. Table 2 represents the accurate number of landings retrieved for each of the studied airports. As it is shown in Table 2 ATL had the highest number of arrivals for the time period that we had data for, while BDL had the lowest number of operations among the ASDE-X supported facilities.

Table 2. Number of Retrieved Operations from ASDE-X Data for Each Airport.

Airport	Number of Operations in The Landing Database	Airport	Number of Operations in The Landing Database
'ATL'	874,526	'LGA'	343,969
'BDL'	82,497	'MCO'	310,180
'BOS'	368,074	'MDW'	229,451
'BWI'	234,907	'MEM'	201,326
'CLE'	53,754	'MIA'	394,041
'CLT'	528,058	'MKE'	99,304
'DCA'	279,723	'MSP'	396,443
'DEN'	539,212	'ORD'	850,169
'DFW'	663,368	'PHL'	376,822
'DTW'	362,791	'PHX'	416,403
'EWR'	408,134	'PVD'	45,172
'FLL'	264,995	'SAN'	180,997
'HNL'	188,486	'SDF'	136,543
'HOU'	178,913	'SEA'	381,260
'IAD'	279,648	'SFO'	395,447
'IAH'	468,800	'SLC'	269,703
'JFK'	432,568	'SNA'	124,989
'LAS'	408,560	'STL'	171,359
'LAX'	649,347		
Total			12,589,939

After analyzing all the input flights, we can take a look at the primary statistics of critical landing parameters at each airport for each aircraft type. Having a deep understanding of ROT distributions, speed distributions, deceleration distributions, touchdown locations, and exiting distances for various aircraft types at different facilities is very important for analyzing the arrival behavior and also for planning purposes. Since many big airports are moving towards new separation rules that will reduce the in-trail separation between arrival pairs, for avoiding potential conflicts and go-arounds on arrival runways, understanding the status of runway occupancy times around the country is essential [12]. Figure 23 represents the variability of true runway occupancy times at each of the studied airports. As it is shown in Figure 23 all the airports in the database have ROT outliers that exceed 75 seconds, however most of the facilities have a centrality of ROT

data between 50 and 60 seconds. The overall arithmetic mean of ROT fuselage among all the samples in our dataset is 50.75 seconds, while the standard deviation among all the samples is 11.6 seconds. If we consider the median of a dataset as a better representative for the population since median values are not affected by the outliers, we notice that overall the ROT fuselage had a median of 48.9 seconds during years 2015 and 2016. Table 3 Represents the summary of ROT average, standard deviation, and median for each of the 37 airports.

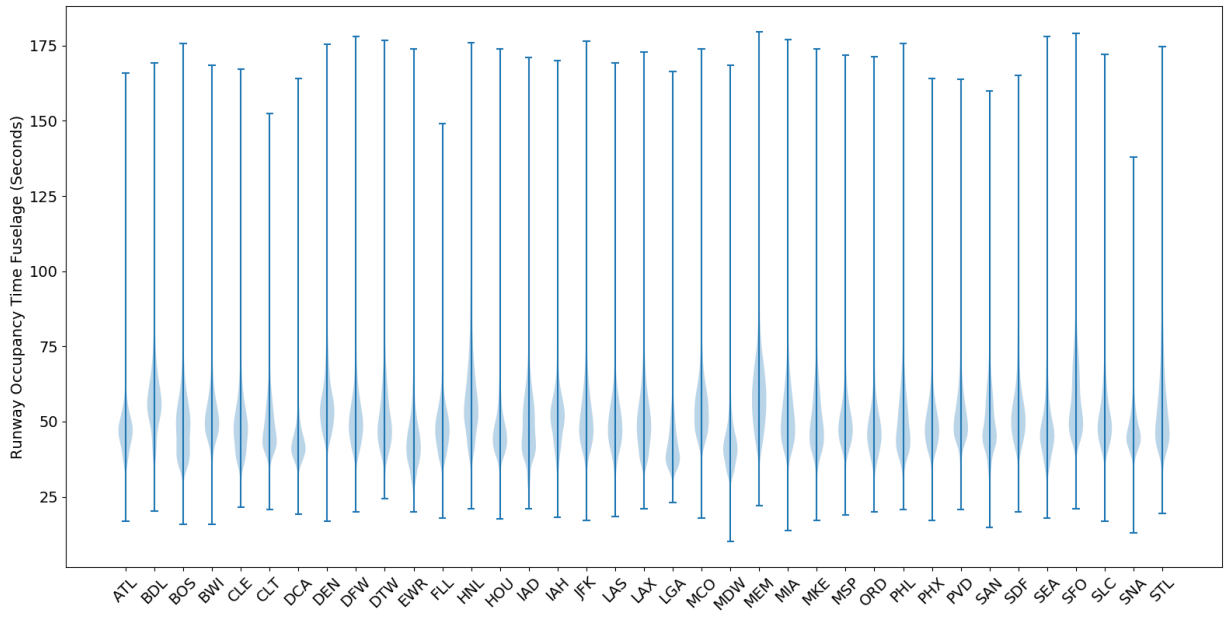

Figure 23. Variability of ROT Fuselage for all the 37 ASDE-X Supported Airports.

Based on the information shown in Table 3, LGA airport had the lowest ROT median with a value of 41 seconds which sounds very reasonable for this facility with two relatively short runways and multiple available exiting options for pilots. The highest ROT median was for MEM airport which might be because of the higher percentage of heavy class aircraft share in the airport fleet mix. Moreover, HNL showed the highest standard deviation of ROT with a value of 16 seconds which might be because of poorly located runway exits that causes many planes spending more time on the runway.

Table 3. Summary of ROT Fuselage Statistics for all the 37 Airports.

Airport Code	Average ROT Fuselage (Seconds)	Standard Deviation for ROT Fuselage (Seconds)	Median ROT Fuselage (Seconds)
ATL	47.3	7.4	46.9
BDL	57.7	11.9	56.7
BOS	49.6	12.1	48.2
BWI	52.9	10.3	51.2
CLE	50.9	13.2	48.4
CLT	48.7	8.5	47.0
DCA	43.0	5.9	42.0
DEN	58.1	13.9	55.0
DFW	52.1	11.3	50.0
DTW	51.9	12.1	49.6
EWR	44.0	9.6	42.7
FLL	48.3	8.5	47.6
HNL	59.7	16.0	56.4
HOU	47.2	8.4	45.7
IAD	50.0	12.6	48.4
IAH	53.5	11.9	52.1
JFK	52.4	11.4	50.3
LAS	49.9	9.5	48.9
LAX	51.4	11.5	49.8
LGA	42.6	7.5	41.0
MCO	55.9	11.3	54.0
MDW	42.6	7.8	41.6

MEM	59.6	13.1	58.2
MIA	53.4	12.9	51.1
MKE	51.8	13.3	49.1
MSP	50.3	8.4	49.0
ORD	48.2	9.5	46.9
PHL	50.1	10.5	48.3
PHX	49.6	8.8	48.5
PVD	52.9	12.2	50.6
SAN	49.9	10.1	48.4
SDF	55.2	13.2	52.3
SEA	49.6	12.9	47.0
SFO	58.9	13.7	55.8
SLC	52.0	11.0	50.0
SNA	47.2	7.8	46.0
STL	55.4	14.6	51.8

One of the great benefits of the landing database is that users can not only review the statistics for landing parameters at the airport level, but also they can analyze each individual aircraft type. There are 274 unique aircraft types that for each of them we retrieved various landing parameters from different airports. Not all the airports have the same fleet mix and number of operations for each aircraft type, therefore having an understanding of the operational fleet at each facility can help in analyzing runway occupancy times in a more sophisticated way. The following pie chart shows the percentage of appearance for every aircraft type in the database. This chart tells us that the dominant aircraft in the ASDE-X supported facilities during years 2015 and 2016 was Boeing

B737-800 with 10.1% of the entire operations. This chart also tells us that 77.1% of the entire fleet mix of those 37 airports is shared among only 17 distinct aircraft types and the remaining 257 airplanes have a total share of 22.9% of the entire operations.

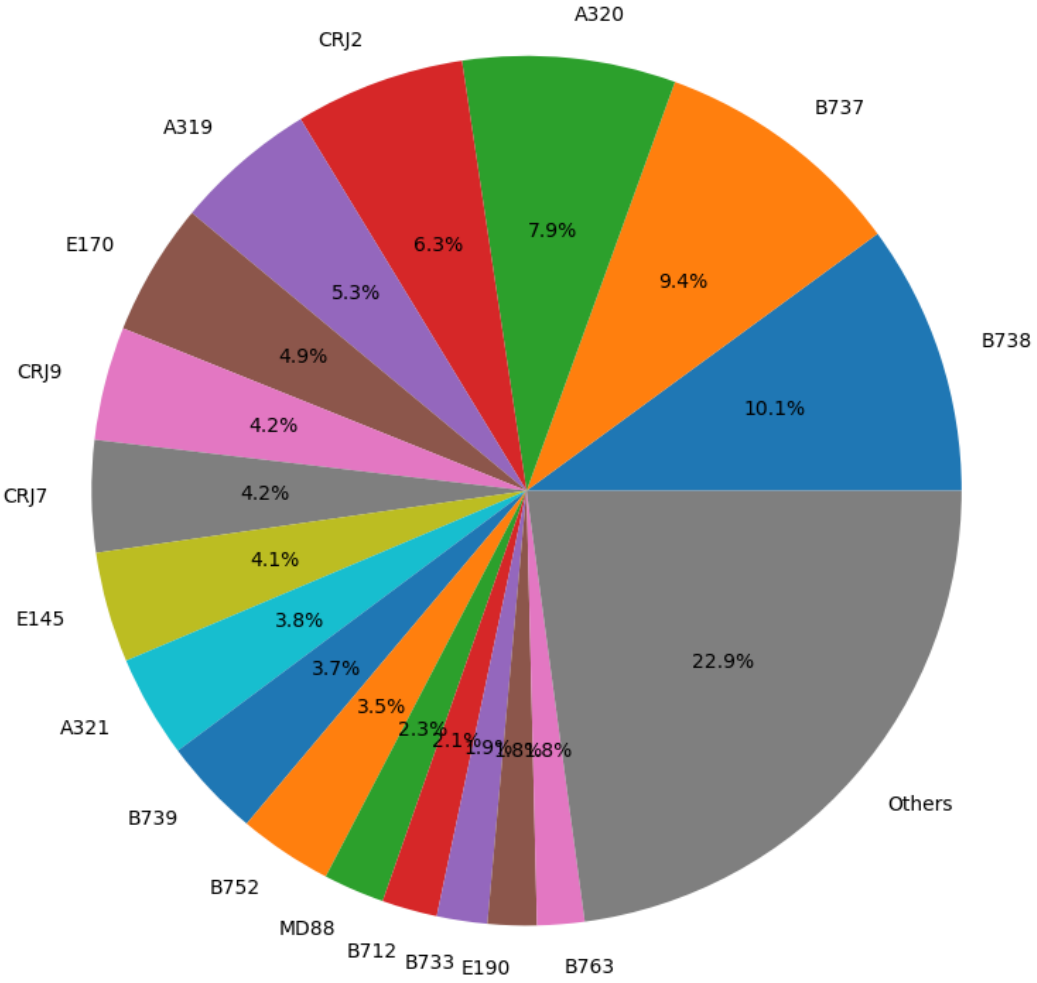

Figure 24. Share of Fleet for Distinct Aircraft Types During Years 2015 and 2016 at all 37 ASDE-X Supported Airports.

An interesting observation that we made across all the data, was that the lowest and the highest true ROT medians belong to airplanes of Cessna family. C320 or Cessna Executive Sky knight which is a twin-pistol aircraft had the lowest ROT fuselage compare to any other aircraft with a median value of 35.9 seconds. While we expected an aircraft of class heavy or super-heavy would

have the first rank, C162 or Cessna 162 Sky catcher had the highest median of ROT with a value of 84 seconds. The potential reason behind this value is that the studied airports in our database are mostly used by commercial flights and many time small engine planes land on long runways that they can coast on the runway for a long time and take very far away runway exits. Therefore, many times we observed high values of runway occupancy times for small engine airplanes in ASDE-X data which makes the modelling process for that class of aircraft more challenging. We will explain more about the challenges of modelling ROT behavior of small airplanes in the next chapter of this dissertation. However, if we take a look at the following ranked planes in terms of ROT median values we can see more expected results. The second highest median ROT was for Antonov An-124 with a ROT median of 83.6 seconds and the third rank was for Boeing B744-200 with 82.4 seconds of median ROT. A complete table for median values of true ROT for all the distinct aircraft types in the database is provided in Appendix. C.

While analyzing the runway occupancy time, we have to consider many parameters simultaneously. From the threshold crossing speed to the touchdown location, then braking rate and finally the exiting speed, there can be various dependencies and relations that make the modelling of the entire process very challenging. So far we analyzed some primary statistics about the runway occupancy times and fleet mixes at different airports. We now take a look at some other extracted parameters such as touchdown distributions and exiting speed distributions to have a deeper understanding of the behaviors before stepping into next chapter where we start modeling and regenerating the observed behaviors.

Figure 25 represents the variability of touchdown locations at all the 37 airports. Figure 25 depicts that MDW had the lowest average touchdown location with a value of 322 (meter) from the threshold. Considering the fact that this airport has relatively short runways that we could check

from Figure 9, having short landing locations is rational for this facility. As expected due to high elevation and long runways, the highest average touchdown location observed in the data belongs to DEN airport with a value of 551 (meter) from the threshold. The trends shown in Figure 25 and Figure 26 are really helpful in understanding the relation between runway lengths and touchdown locations. For example, based on the standard deviation values shown in Figure 26, most of the airports with relatively short runways such as DCA, LGA, MDW, SNA had lower deviation in touchdown locations compare to other facilities with longer primary arrival runways. The potential reason for this observation is that when pilots land on short runways, they know that there is not extensive available runway length for landing, therefore that reduces the variability of their landing locations.

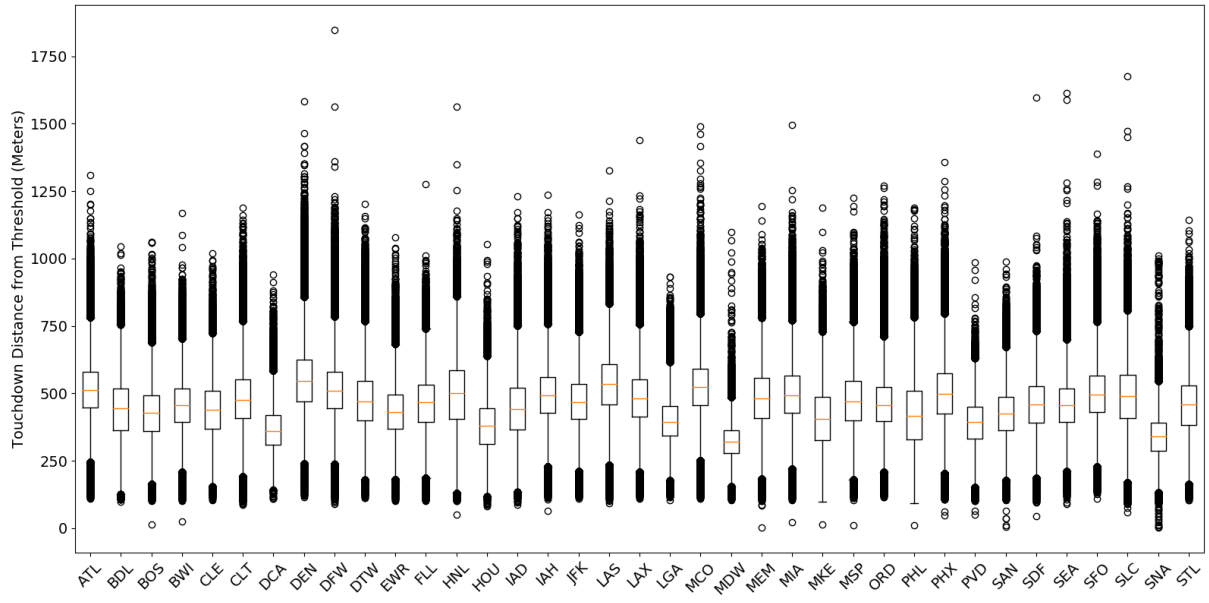

Figure 25. Variability of Touchdown Locations at all the 37 Airports.

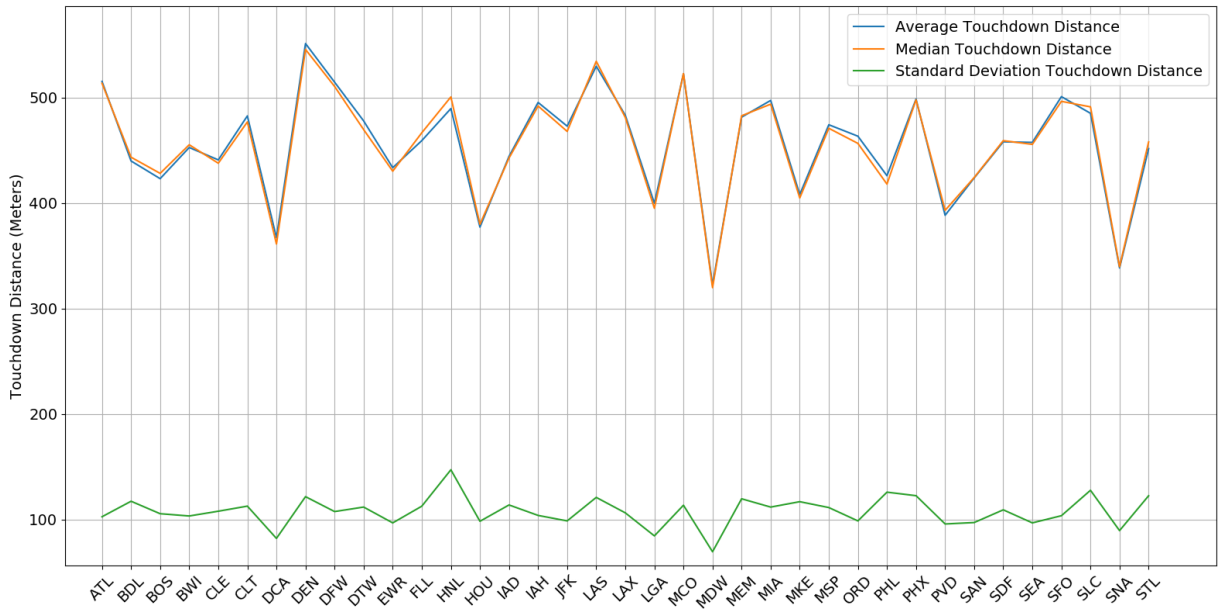

Figure 26. Average, Median, and Standard Deviation of Touchdown Locations at Different Airports.

Finally, before concluding this chapter and moving on to the simulation and modeling chapter, we briefly review the distributions of exiting speeds at all the 37 ASDE-X supported airports. Figure 27 represents the violin plots for exiting speeds at PC points for all the retrieved operations in the landing database. As expected and by referring to Figure 15, those facilities that have more high speed exits (exits with lower angles and higher radiuses of arcs), tend to show higher values of exiting speeds. This fact can reflect that when pilots have to take runway exits which have long path lengths, since they know that there will be enough pavement along their evacuation way, they take those exits at the PC point with higher speeds. Therefore, not only they can reduce their runway occupancy times, but also they will continue on reducing their speed along the path of the runway exit until they either reach a desirable taxing speed or stop at the exit hold-bar. According to the information which is presented in Figure 27, BWI had the lowest average exiting speed with just a value of 19 Knots, while the highest average was for DEN airport with a value of 51 knots. Both values are logical since BWI doesn't have plenty of high speeds and most of its runway exits

are either right angle or non-standard with short path lengths and for the case of DEN because of higher elevation airplanes fly faster and the airport is equipped with plenty of high speed exits which helps the pilots to take the PC points at higher speeds. SLC had the highest standard deviation of exiting speeds which might be because of its obvious bi-modal behavior of exiting speeds according to Figure 27. Another interesting fact about the shown distribution of exiting speeds, is the number of facilities which show obvious bi-modal behavior in terms of exiting speeds. This can be due to considerable share of operations which take low-speed and high-speed exits on the runways at those airports. Considering the fact that in Figure 23, we didn't observe bi-modality in ROT behavior, this primary comparison of the distribution of exiting speeds and the distribution of runway occupancy times, tells us about the complex relations between the landing parameters and the overall ROT. Therefore, not all the times having high speed exits would result in lower values of ROT and depending on the location of the runway exits, we might observe high variations in ROT values.

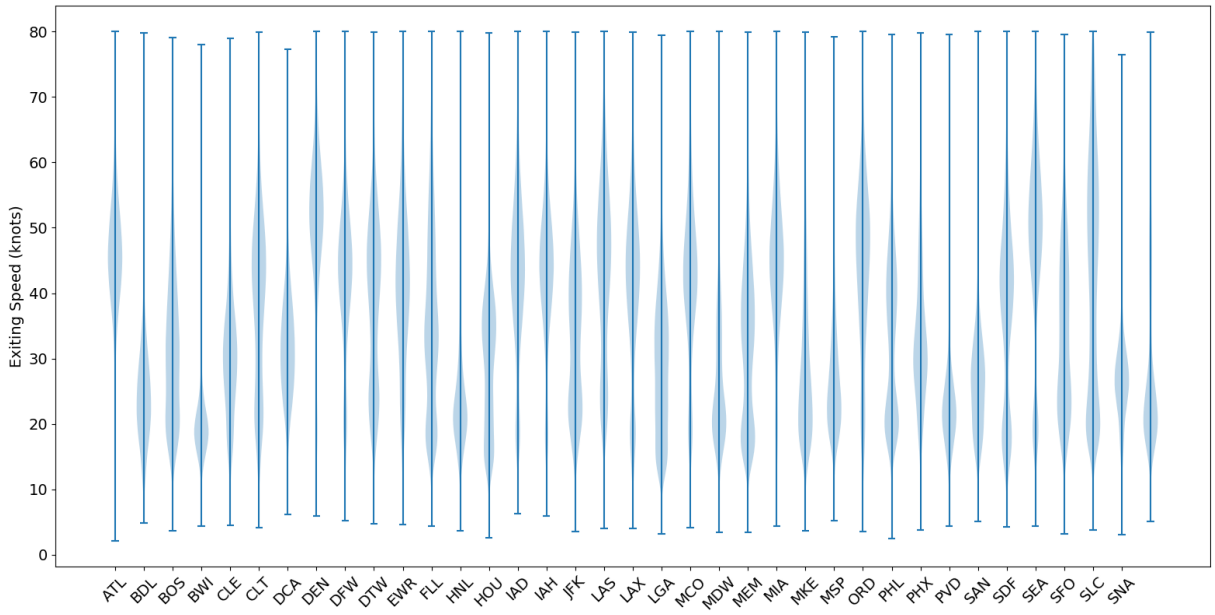

Figure 27. Variability of Exiting Speeds at Different Airports.

2.7 Conclusion

Airport Surface Detection Equipment Model- X (ASDE-X) surveillance system has been in use at 37 airports around the United States to avoid potential runway and taxiway incursions and provide better vision for air traffic controllers to navigate flights. For the first time in this study, we parsed and analyzed two years of ASDE-X data to extract critical landing parameters for more than 12 million arrival flights. The outcome of the explained procedures in this chapter was a computer application called Landing Database, which provides many useful visualizations and insights about the landing parameters for 274 distinct aircraft types from 37 airports. Users can study the distribution of approach speeds, touchdown speeds, exiting speeds, touchdown locations, nominal deceleration rates, runway occupancy times, and exiting distances for various aircraft types. The outputs of this database can help evaluate runway exits at busy US airports in terms of their runway occupancy times and exit utilizations. This functionality can help many airports to understand the importance of each of the operational runways and runway exits better. In case of future constructions or configuration changes in the airport master plan, with the help of the output distributions of this developed database, they can estimate the current and future capacity and the amount of traffic that should be diverted temporarily. Another usage of this database's outputs is in airport simulation models, where users simulate the flight operations from gate to gate. Most of those models like SIMMOD do not use accurate distributions for runway occupancy times and users usually end up entering general normal distributions for every class of aircraft. Since the purpose of running those simulation models is to find the potential delay of certain flight schedules, it is essential to have accurate distributions of runway occupancy times for every unique aircraft type. With the help of the developed landing database researchers, analysts, and airport planners can export valid distributions of runway occupancy times for each aircraft type and use them as

input parameters for a bigger airport to airport simulation scenarios. This way not only the models will have more realistic assumptions based on the real-world operations, but also many sensitivity analyses can be running to understand how vital runway occupancy times can be in estimating total delays at airports.

Finally, due to the recent improvements in aircraft separation systems at airports and the fact that FAA is moving to newer separation systems which will reduce the in-trail separation between arrival pairs, many times the runway occupancy times of the leader planes will become the critical minimum separation between arrival flights. Therefore, having a clear understanding of valid distributions of runway occupancy times of certain runways with certain runway exit configurations is essential for air traffic controllers in order to help them separating the arrival traffic both safely and efficiently. Moreover, by understanding the accurate distribution of runway occupancy times, controllers can avoid more go-arounds which is a very important aspect in improving the traffic flow at airports and all of those required input information can be obtained from the outputs of this chapter.

Chapter 3. Runway Exit Design Model Version 3

3.1 Introduction

Reductions in in-trail wake vortex separations in the future will make runway occupancy time an essential parameter in assessing runway capacity. The Federal Aviation Administration (FAA) proposes using a minimum of 2 nautical miles of in-trail separation under the newly developed Re-Categorization separation rules (RECAT Phase 2) for narrow-body aircraft operations. With such small wake separation, runway occupancy time could become a limiting factor in runway operations.

This study focuses on arrival operations at airports. Runway Occupancy Time (ROT) is the time that an airplane spends on an active runway. In the past two decades, several techniques have been used to estimate runway occupancy time and estimate optimum runway exit locations. The Virginia Tech Air Transportation Systems Laboratory developed a Monte Carlo simulation model to estimate aircraft landing roll profiles for various aircraft with the final goal to predict ROT times [25]. A dynamic programming approach was used to find the optimum location of runway exits based on simulated landing roll profiles [13][14][15]. More recent studies further demonstrated the importance of runway occupancy time in airport capacity and mixed runway operations through simulation [7][16][18][19][20]. In another study, the impact of various ROT distributions on runway arrival throughput was studied [21]. There have been studies to determine the influence of runway occupancy time on the airport throughput [20]. Other studies compared the arrival capacity of airports considering the minimum separation between arrival pairs based on their wake vortex categorization. The airport capacity with minimum separation between arrival pairs was based on the runway occupancy time of the lead aircraft [21]. In a very similar approach various

percentiles of ROT were tested to find the impact on airports arrival throughput when the minimum separation can be the ROT of the lead aircraft [5]. In another study, runway landing occupancy times for airplanes of different wake categories are used to model the capacity of closely-spaced parallel runways [22]. In another study the arrival ROT was calculated as part of the taxing phase for arrival flights [23]. Most fast time simulations like SIMMOD Pro, TAAM, and AirTOp require user-defined (or default) runway occupancy times to simulate aircraft arrival operations [24]. Simulation model users are required to either collect runway occupancy time statistics in the field or employ dedicated runway occupancy time simulation models developed two decades ago [7]. Another study used runway occupancy times for departure and arrival flights to solve the problem of aircraft-sequencing at airports by using genetic algorithms [26]. The dispersion of runway occupancy times for arrivals at an airport, could create significant losses in airport capacity, create delays in handling airport operations, and cause reductions in precise trajectory adherence [27]. In another study the runway occupancy times and arrival separation times of arrival operations at LaGuardia airport during July 1984 were analyzed [28]. Since runway occupancy times are very essential for the traffic flow at airports, NASA developed a dynamic runway occupancy time measurement system which was used in an analyses aimed at improving the efficiency and safety of surface operations [29]. The impact of reduced inter-arrival separations and runway occupancy times were analyzed in another study [30]. Specifically, for high speed exits, the optimal suggested locations of runway exits were identified with a dynamic programming optimization [15]. Detailed performance of airplanes taking high speed exits were simulated by using Monte Carlo approaches [14]. Trani used distributions of runway occupancy times for developing a simulation approach to estimate the airport runway capacity [39]. The impact of gate locations on aircraft exit utilization behaviors was modelled by defining horizontal distances from the runway threshold [31]. After

analyzing two years of ASDE-X data, we noticed that an advanced data-driven approach is required for modeling aircraft landing behavior and estimating runway occupancy times. The other attempts for estimating runway occupancy times were not sophisticated enough to replicate the individual aircraft behavior for the current 274 unique aircraft types in the national airspace system [30].

Runway occupancy time is a stochastic parameter dependent on many factors including runway length, exit locations, gate locations, pilot motivation, and aircraft type. Since many airport simulation studies require ROT data at either individual or group levels, it is essential to have an accurate model to predict runway occupancy times under various operational conditions. Runway occupancy times can vary from airport to airport for many of the reasons stated. Analysis of Airport Surface Detection Equipment Model-X (ASDE-X) data illustrates the point (see Figure 28). Figure 28 shows the variability of runway occupancy times at Atlanta Hartsfield-Jackson International Airport (ATL). Runway length, aircraft fleet mix and runway exit differences yield large differences in the medians of ROT according to the Figure 28. Runway 08L (a primary landing runway) has two well-located, high-speed runways exits resulting in median ROT values close to 40 seconds (to aircraft nose reaching the runway imaginary plane). Runway 26L is primarily used for departures and has two high-speed exits located far downrange into the runway. The median ROT time for this runway is 15 seconds higher than runway 08L. This implies that for similar aircraft fleet mix, a set of poorly located runway exits may increase the runway occupancy time substantially.

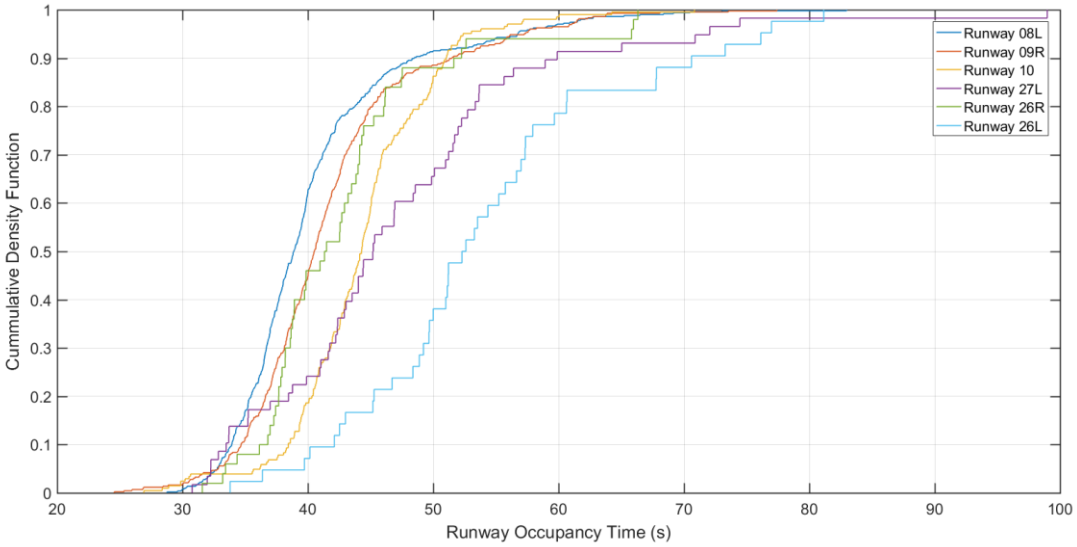

Figure. 28 Atlanta Hartsfield-Jackson International Airport Cumulative ROT Distribution Plot.

Some factors affecting runway occupancy time are more difficult to quantify. For example, gate location and pilot motivation can play a significant role in runway occupancy times. Consider the case of San Diego International Airport (SAN). Analysis of ASDE-X data indicates that Southwest Airlines flights landing at the airport vacate the runway earlier due to the location of the Southwest Airline terminals (see Figure 29). Figure 29 presents the distribution of runway occupancy times for narrow-body aircraft operated by three airlines at SAN landing on runway 27. Figure 29 shows Southwest Airlines flights in blue, United Airlines in orange and American Airlines in yellow. Southwest Airlines pilots are clearly motivated to use earlier runway exits to reduce taxiing times to the gates assigned to the airline. Figure 29 shows that for the same aircraft class, airline pilots will extend or shorten their landing roll to match suitable runway exits closest to their assigned gates. Delaying the exit location further downrange, can have a substantial effect on runway occupancy times as shown in Figure 29.

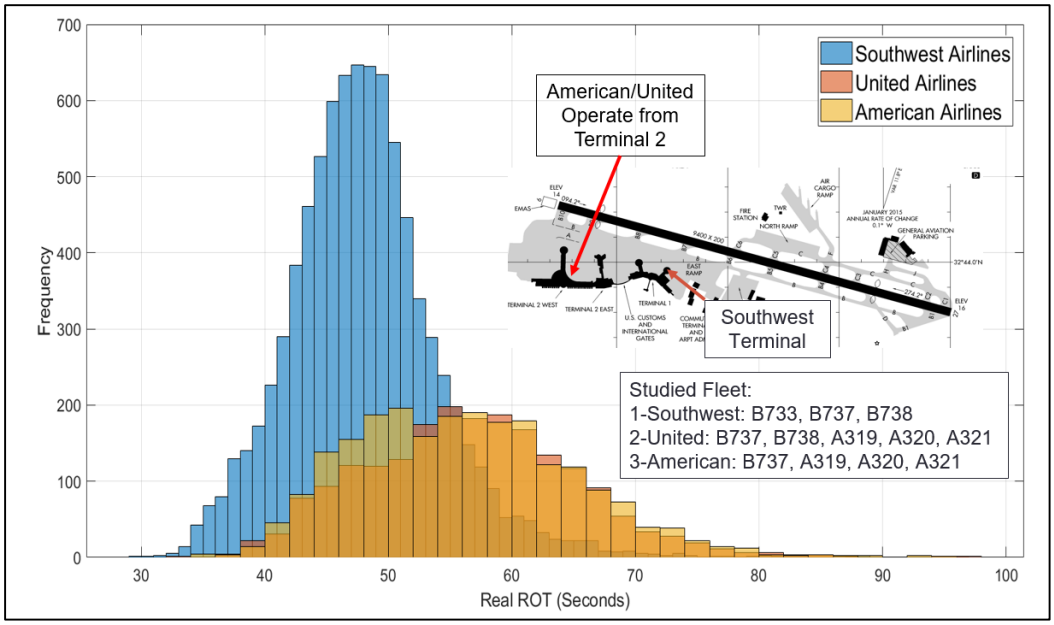

Figure. 29 Variability of Runway Occupancy Times for Similar Aircraft Types Operating at Different Gate Locations.

3.2 REDIM Model Version 2

Runway Exit Design Interactive Model (REDIM) was initially developed in 1990 for NASA [17][25]. The model was built to assess the runway occupancy times on runways and find the optimal location of runway exits and geometries to minimize the weighted average runway occupancy times. The input data for the earlier versions of that model were derived from collected video data. After converting the recorded landing videos to numerical data, many relations were extracted to find the projected behavior of pilots on runways while crossing the runway threshold, touching down, braking on the runway and eventually taking a runway exit to evacuate the runway. The original version of the model had an evaluation module that would run various iterations with a Monte Carlo simulation approach to simulate landings on existing runways with known environmental conditions such as runway length, runway width, percentage of wet and dry, and runway elevation. The output of evaluation module was a weighted average runway occupancy time, and an exit utilization table which showed the user how many times each of the entered

aircraft in the fleet mix share used a specific runway exit. The other critical feature of the model was its optimization module which used dynamic programming to let the users know about the optimal location of runway exits on an empty runway [39][45][46[47]. The optimization module was very essential in designing brand new runways around the world, as analysts used REDIM to design optimum locations for the runway exits on various runways [25]. REDIM model was used for designing the location and geometries of runway exits on new runways at many facilities including:

1- John F. Kennedy International Airport (JFK)
2- Seattle Tacoma International Airport (SEA)
3- Los Angeles International Airport (LAX)

The model has also been in use for producing cumulative density functions of runway occupancy times to be used in airport delay estimation via advanced node-link structured simulation applications such as SIMMOD.

Although the earlier versions of REDIM model were essentially important in analyzing the runway occupancy times and optimal exit locations, there are many inefficiencies in the assumptions and input data for the early versions of REDIM model which makes it not as useful as it used to be for analyzing more recent operations at big airports.

The following bullet points represent some of the shortages of the earlier versions of REDIM model which makes it less efficient in designing new runway exits based on recent operations at airports:

1- The collected video data which resulted in numerical equations for REDIM2 includes only five distinct aircraft types with their performance charts updated at or prior to 1990. Today

based on the developed landing database, we know that there are 274 unique aircraft types which every single of them show particular sort of behaviors on runways which should be modeled accordingly.

2- REDIM2 assumes a linear correlation between touchdown location, touchdown distance, and nominal deceleration with the runway lengths. Therefore, for various aircraft types, for each specific runway length, there will be a single value assigned to the critical landing parameters. Today we know that there can be a correlation with the centrality of each of those distributions with runway lengths, however many different combinations are observed that yield a more complicated situation compare to a single output of some linear functions. For each of the mentioned parameters, we observed large distributions of data with specific behavior on each runway. Therefore, for each aircraft type, there's a need to upgrade the algorithms for generating critical landing parameters.

3- In REDIM2, the exiting speed should be entered by the user, therefore there is a single value associated with the exiting moment whenever a simulated arrival flight wants to evacuate the runway. If the user chose the default value for exiting speed, for very limited number of runway exits, the average observed value from the video data would be selected for each exit type. Today, based on the observations from the landing database, we know that there is much variety in runway exit geometries than the typical acute-angle, right angle, and back-turn exits used for categorizing runway exits. Moreover, we have more variety in the geometry features. Still, we have also seen distributions of speeds at the PC point for various types of runway exits for multiple types of aircraft. Therefore, there is a need for improving the functionality of the runway exit design model for generating more realistic exiting speed values for different aircraft types.

4- Finally, REDIM2 was trying to model and simulate the nominal behavior for arrival flights. Based on our observations, we noticed that some carriers based on their preferred taxiways or terminal location show some motivational factors while evacuating runways. This kind of behaviors cannot be considered as nominal. There are some extreme cases when pilots either pass by the runway exits which they could easily take in order to take further runway exits and save taxi times, or they brake harder than their nominal performance to optimize the ROT and shorten their taxing distance towards the allocated terminal for their airline. We will discuss the proposed methods in the new version of the REDIM model in chapter 5 in more details.

3.3 Methodology

3.3.1 Runway Exit Clusters and Exiting Speeds Distributions

As we mentioned earlier in this chapter, one of the inefficiencies of the earlier versions of the REDIM model was that the exiting speed at the PC point was defined by users and it was a single value for limited number of exit types. After reviewing the final distributions extracted from the landing database, we noticed that each aircraft type has various values of exiting speeds at the PC points, which the overall range of those numbers might vary due to differences in runway exits geometry features. For example, in Figure 30 we represent the CDF plots for the exiting speed distributions of Airbus A319 at three traditionally classified runway exits as high speed exit, right angle exit, and back-turn exit. As shown in Figure 30, the values of speed from the represented distributions are clearly separated from each other. Here by high speed exit we mean an exit angle of 30 degree and a radius of 1800 (ft.) and for right angle exit we mean an exit angle of 90 degree with a radius of 200 (ft.) and for back-turn exits we mean an exit angle of more than 105 degrees with a radius of 161 (ft.). While the average exiting speed at high speed exits for A319 was around

51 knots, that aircraft took right angle exits with an average of 20 knots and the lowest average exiting speed was for back-turn exits with 17 knots. Obviously, the runway exit geometry has impact on the values in the exiting speed distribution. For estimating the proper values of exiting speeds at PC points, first we have to understand the number of true categories for runway exits that we collected in our database. In chapter 2 we mentioned that we collected the geometry information for 3'385 runway exits from all the 37 ASDE-X supported facilities in the country. For each of those exits we collected three parameters: exit angle, radius of the arc, and the path length from the point of curvature to the exit hold-bar. Previously, FAA used to classify runway exits based on their angles [26]. There were some thresholds for the exit angles that would identify the type of an exit. However, we noticed that in many facilities while the exit angles might match the defined ranges for specific exit categories, there are significant differences among the radiuses of the arcs and the exit path lengths. One approach is to call all of those exits as non-standard, however when we monitored all the parameters extracted for the runway exits, we noticed that there are multiple categories and we need to cluster our non-labeled data to find out the true categories for the runway exits.

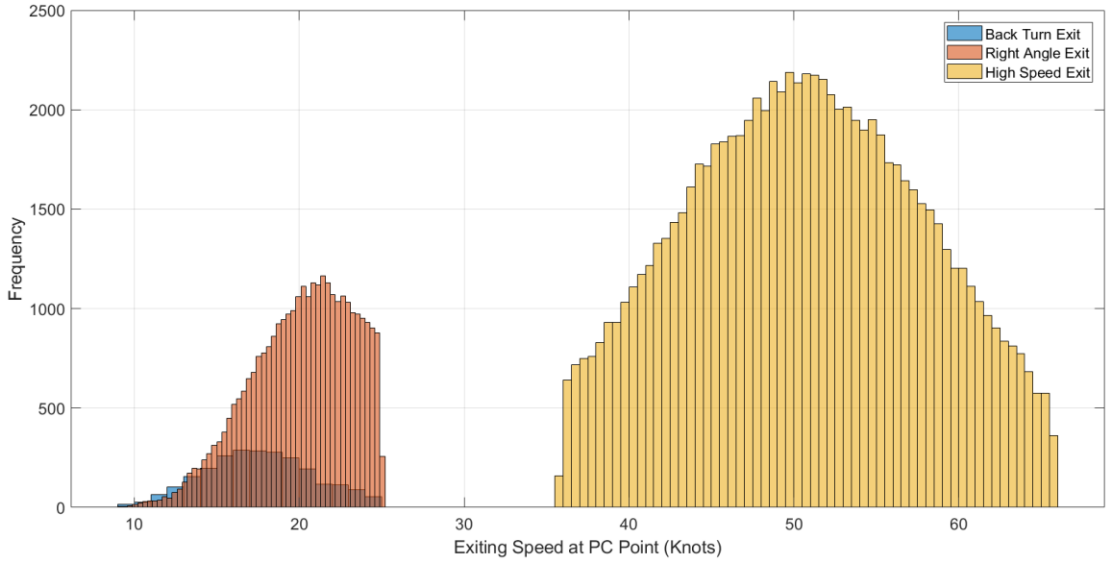

Figure 30. Distribution of Exiting Speeds of Airbus A319 at Traditionally Classified Runway Exits.

The best way to understand the information for runway exits is to visualize the three available features that we have. In chapter two in Figure 13 we saw the histograms for each of the parameters and noticed that the majority of the runway exits in the country are right angle exits. Here we

demonstrate a 3 dimensional visualization by using all the features together to see whether we can extract meaningful patterns among our runway exits or not.

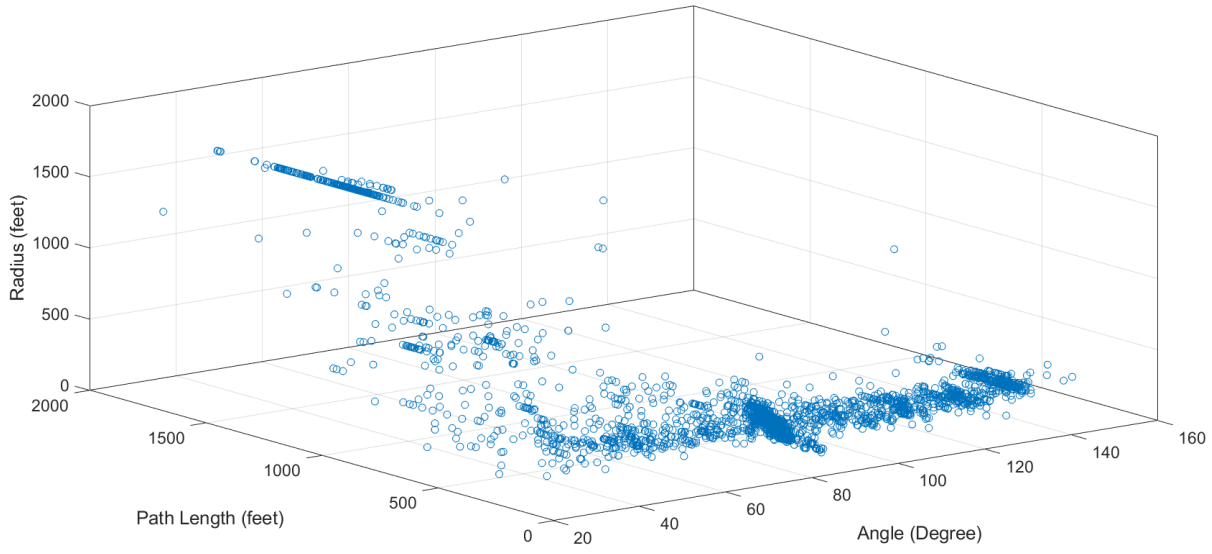

Figure 31. 3 Dimensional Plot for all the Collected Runway Exits Geometry Parameters.

As we can see in Figure 31, just based on the values shown on the x-axis which are the exit angles, we cannot cluster our runway exits efficiently. The 3 dimensional graph clearly tells us that the categories of the runway exits can be identified by analyzing all the three features together. Therefore, a k-means clustering algorithm was used to identify the label of the runway exits. K-means clustering is a popular methodology for identifying potential groups among unlabeled data [32]. Since, at the beginning of the analysis we are not sure that how many exit clusters can represent all of our 3'385 runway exits, we ran our clustering algorithm from 1 to 50 clusters and check the elbow-plot of our clustering steps and find the optimum number of clusters that yields the minimum sum of distances from cluster centroids. Moreover, since the range of values among the three features of the data are significantly different, we standardized all the features before running the clustering analysis by using the z-score method. Even though we selected k-means algorithm for clustering our runway exits, it is always better to evaluate the distances of the input

data in the space from each other by analyzing the dendrogram of the input data after calculating the linkages. Dendrograms are useful for visualizing the clustering groups of hierarchical clustering results [33]. For this purpose, we calculated the average distance between every pairs of data points in the space and created the following dendrogram.

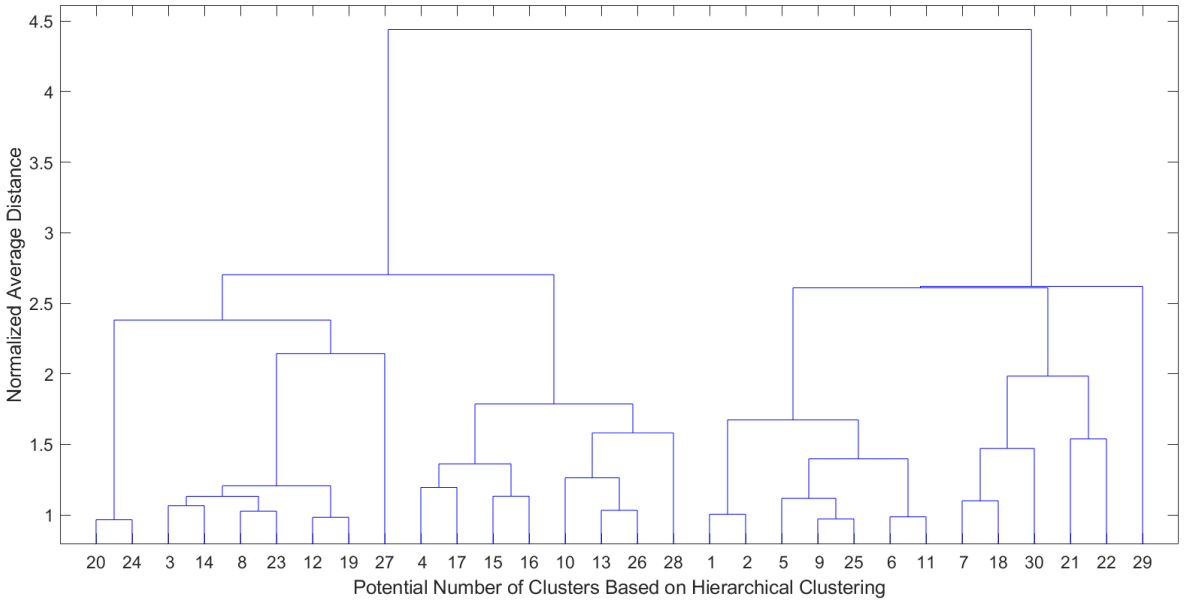

Figure 32. Dendrogram of Runway Exits Average Distances Based on their Geometry Features.

As Figure 32 suggests, based on the hierarchical clustering algorithm fed by average distances between every pairs of data points, there are potentially 30 exit clusters that can represent all of our runway exits. Therefore, we can reduce the maximum number of clusters that we wanted to check from 50 to 30 and run the k-means algorithm from 1 cluster to 30 clusters and identify the optimum point. When we face an unsupervised learning problem similar to what we have here, there are usually no absolute correct answer for the number of clusters. Depending on the research purposes or different aspects of data people can select their own desired number of clusters. However, here we try to choose the optimum representative number of clusters as technically proven as possible [34]. As shown in Figure 33 which depicts the sum of distances from clusters'

centroids for various numbers of clusters, after 20 clusters the graph doesn't show considerable difference, therefore we can select any number equal or above 20. For keeping our problem and data analysis as simple as possible, we chose 20 clusters to categorize each of our runway exits within each of those cluster families.

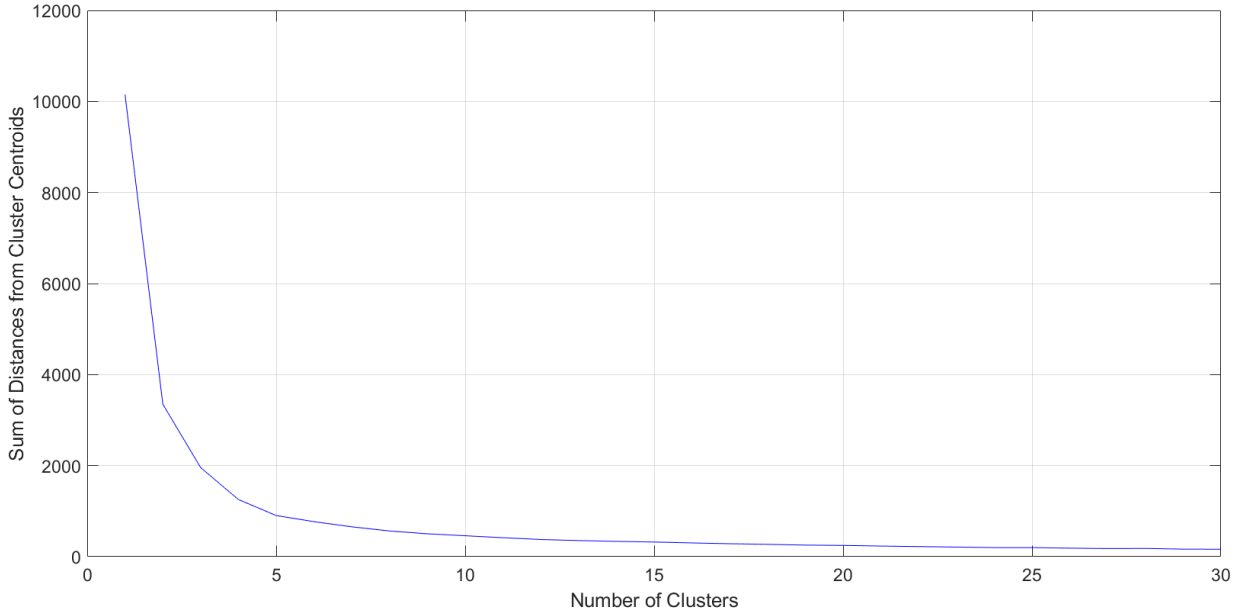

Figure 33. Knee Plot for Runway Exits Identification of Optimum Cluster Number.

Before moving on and predicting the exit speed for each aircraft at the PC point based on our recent clustering algorithm, we take a closer look at our data again but this time we label each data point in the runway exit database with their associated cluster label. Remember that we have 20 clusters now, so we represent all of our exits within the cluster family that they had the minimum distance from the generated centroid of that family. Figure 34 represents the distribution of runway exits among each cluster family. As it is shown in Figure 34 and we talked about it earlier right angle exits and generally non-standard exits are amongst the most popular ones in the runway exit database. Lots of those exits were clustered in groups 1,7,8, and 19.

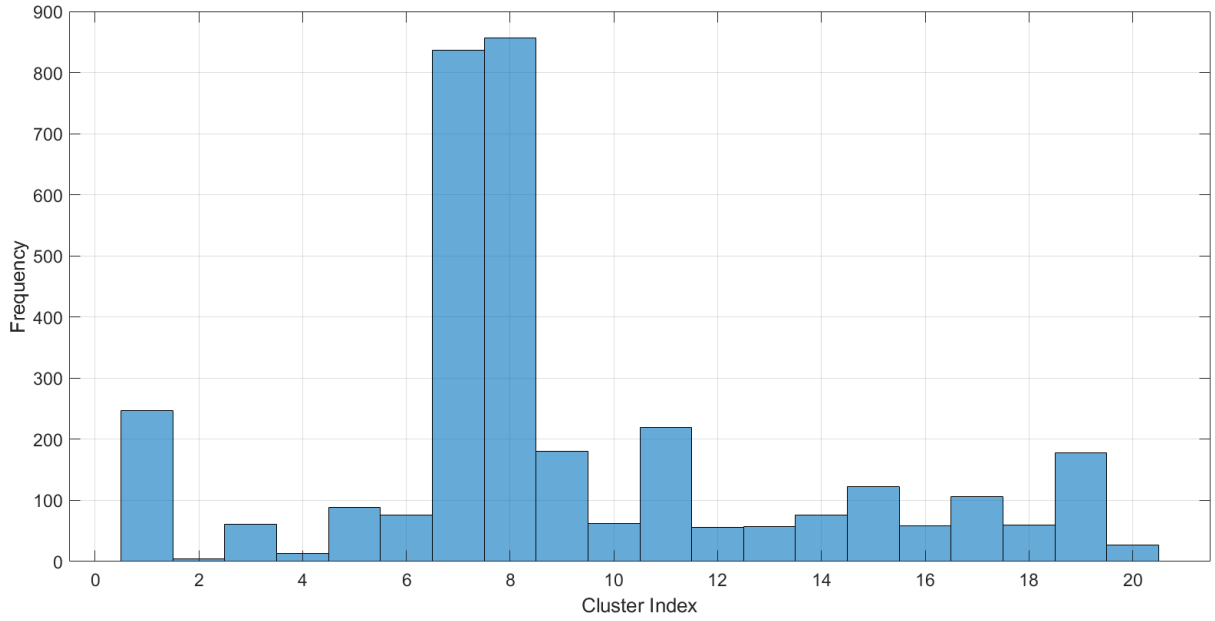

Figure 34. Number of Members in Each Exit Cluster.

Since we had the 3 dimensional visualization of our exits, we can now re-draw them in the 3D space and evaluate how they're grouped together into different clusters. Figure 35 represents the 3D graph of runway exit geometry parameters and their assigned clusters. To avoiding confusion, we represented the parameters for runway exits belonging to 10 clusters out of 20. It is obvious from Figure 35 that different ranges of values of radius, path length, and exit angle help in differentiating runway exits from each other and can validate our clustering approach. Moreover, with the help of clustering algorithms, we can identify outliers and bad data points which could have collected incorrectly at the time of measurements.

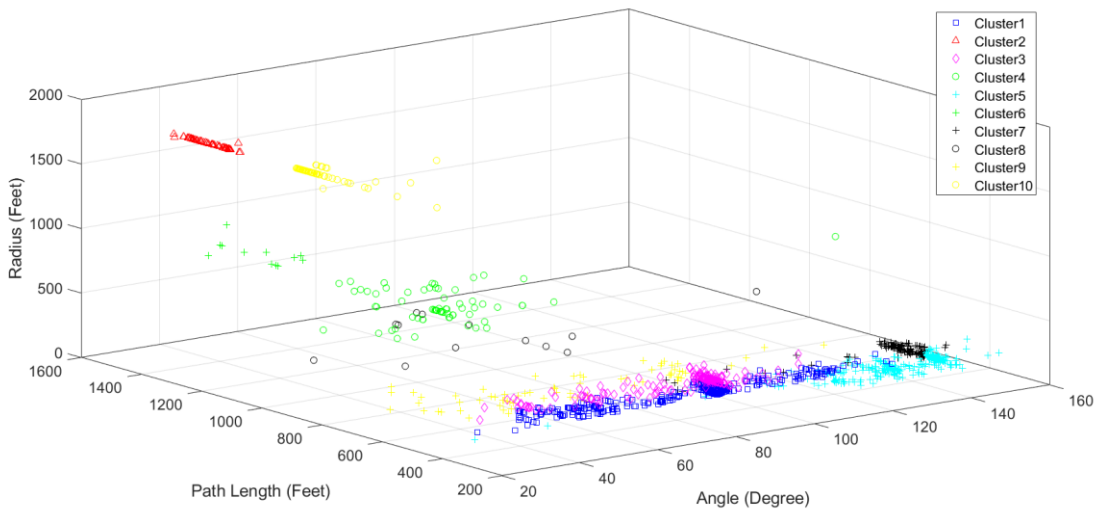

Figure 35. 3 Dimensional Graph of Runway Exits with Their Assigned Cluster Groups for 10 Clusters out of 20 Total Groups.

Now that we clustered the runway exits based on their geometry features, we need a procedure to retrieve proper exit speeds for individual aircraft types. We know that the geometry of the exits has an impact on the range of exiting speed values, but coming up with a general linear formulation doesn't sound reasonable since each of the unique aircraft types in the database has shown various speed ranges at different runway exits. Many factors such as the time of the operation, the demand for landing, the commands from the ATC tower, and pilot preferences based on either the carrier guidelines or self-experiences play role in the aircraft speed at the PC point. Therefore, we should either break the problem into many sub-problems and ask the user to enter enormous amount of input information such as the time of the operation, the carrier type, etc. or we can come up with an acceptable approach in deriving suitable values from the data. For this study we chose a data-driven approach. Therefore, for every cluster that we formed we collect all the incidents from the ASDE-X data that individual aircraft types used each of the exit clusters, then we assign non-parametric Kernel distributions to all the collected values within each cluster for every individual aircraft type. This way we make sure that not only all of our exiting speeds are coming directly

from the data, but also the assigned Kernel distributions will be unique for each aircraft type in each cluster. We truncated the distributions between their 10^{th} and 90^{th} percentile values to avoid having extreme numbers in our data. For each group a non-parametric Kernel distribution was assigned to the runway exit speeds at the point of curvature of the exits. Figure 36 represents the histograms for the exiting speeds of a popular commercial airplane Airbus A319 for all the 20 runway clusters. The ranges of the distributions shown in Figure 36 clearly represent the unique behavior of each runway exit cluster in terms of the exit speed values. For example, runway exit clusters 3 and 20 represent high-speed runway exits with low exit angle and high equivalent radius and path lengths. As it is shown in Figure 36 for the mentioned exit groups the distributions show higher exit values compared to the rest of the exit clusters which is rational.

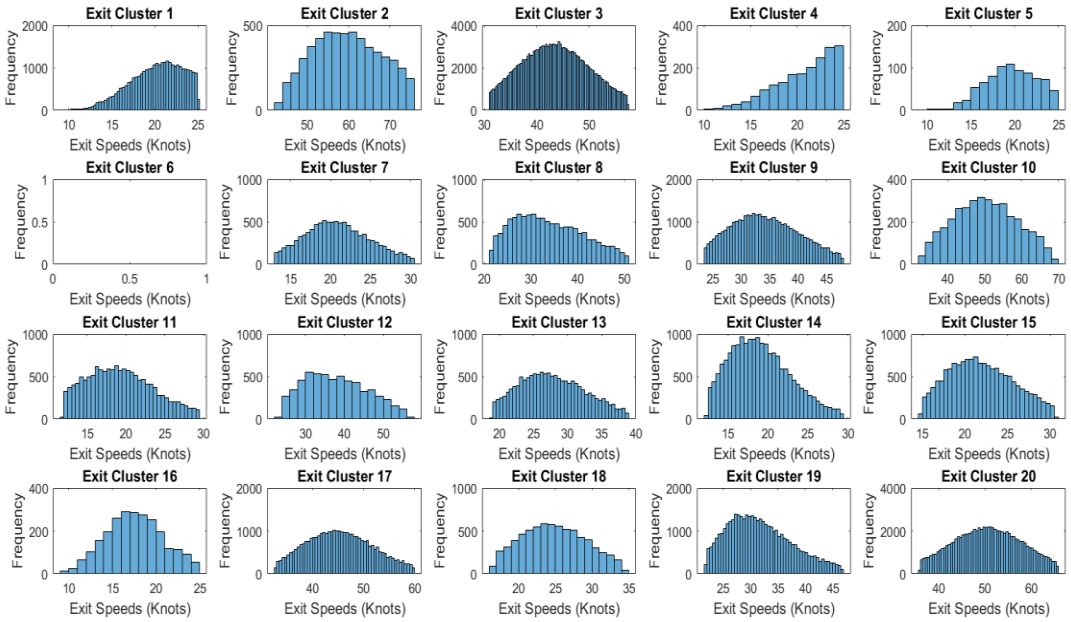

Figure 36. Airbus A319 Distributions of Exiting Speeds for Each Runway Exit Cluster.

Figure 36 clearly shows different ranges of exiting speeds for each runway exit cluster that we can retrieve proper values with the help of Kernel distributions. The differences in the distribution

values are very obvious among multiple exit clusters. Airplanes take high speed exits with higher speeds as expected. There might be some observed low speeds, but the centrality of data for high speed exit clusters is towards higher values. With this approach by re-sampling enough number of iterations for each exit type in our simulation scenarios we can make sure that a valid range of exit speeds will be used during each run of the model. The other benefit of this approach is that not only the exit speeds are cluster based, but also they're aircraft based as well. Different airplanes might take the same PC point of the same runway exit at different speeds due to their dimensions. The following figure for example represents this obvious difference among 6 distinct aircraft types from different dimensional categories. Later in this chapter we will explain the replacement of individual aircraft types to higher level grouped surrogates in cases that we didn't observe sufficient number of incidents within each cluster. The minimum number of observations for each individual aircraft type within each cluster for assigning a Kernel distribution is 30. In the Figure 37 we represent the cumulative density function for 6 distinct aircraft types from 6 different Aircraft Design Groups (ADG). Later in this chapter we explain more aircraft general groupings. The figure transfers many interesting findings about the exiting speeds. These speeds belong to the similar runway exit cluster index 20 which has runway exits with an average angle of 30 degree, and an average radius of arc of 1784 (ft.), in addition to an average path length of 1322 (ft.). This cluster can be considered as one of the high speed runway exit clusters. Based on the chart we can see the monotonic pattern up to MD11, where the average exiting speed increases by increasing the dimensionality of the aircraft, however we can observe that for ADG-5 and ADG-6 representatives which are B789 and A388, we have lower captured exiting speeds. That's because when the airplanes pass a certain size threshold, the pilots should care more and they cannot travel

too fast while taking a runway exit. As a summary for the figure here we present the median exiting speed for each of the shown airplanes in the figure:

1- Cessna C172: 39.8 Knots
2- Cessna C56X: 43.1 Knots
3- Embraer E190: 46.7 Knots
4- McDonnell Douglas MD11: 43.8 Knots
5- Boeing B789: 39.8 Knots
6- Airbus A388: 41.1 Knots

It is true that by considering the entire distribution for each of the mentioned airplanes, we can run a hypothesis test and actually test which aircraft had higher values in overall, however a simple comparison of the medians can tell us about the centrality of the captured values for each of the mentioned aircraft types. With the help of non-parametric Kernel distribution through our clusters we can make sure that the resampled exit speeds in each iteration of our simulation represent the behavior of each individual aircraft at the PC point of runway exits in the real world.

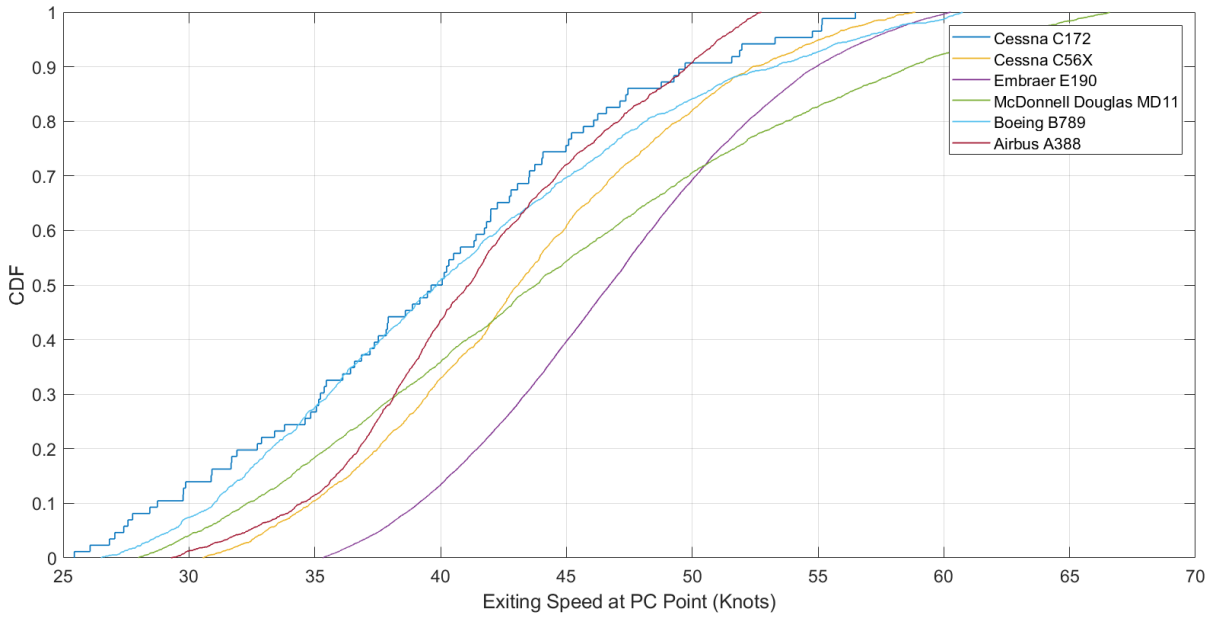

Figure 37. CDF Plot for 6 Distinct Airplanes from 6 Distinct ADG Groupings.

Every time we label a set of data points through an unsupervised learning, we need to train classifiers in case someone wants to enter their desired input parameters for the initial input data. Here we initially clustered our runway exits based on the 3'385 data points that we collected from all the 37 ASDE-X supported airports in the United States, however if in future a user would desire to enter their own customized parameters for each runway exit, we need to let them do that. For that purpose, a classification model trained on the current labeled data is required to classify a new customized runway exit based on the user input information.

For the classifier, we used the bagging method for decision trees. Decision trees are simple and popular classifiers that try to derive rules from the train data to classify their labels based on those rules. Even though it is very easy to train a decision tree classifier, since they can easily over-fit on the train data, it is recommended to use ensemble methods to avoid overfitting and improving the classification accuracy. One well known ensemble method is bootstrap aggregating or bagging method. In this method several random decision trees combine with each other and form the final

classifier to find the labels of the input data [35][36]. This way we train multiple decision trees randomly, and at the end we take the average of all the classifiers for our final model for continuous predictions and we take the most common vote for categorical predictions. Using the average of multiple random decision trees will reduce the variance in output results and as mentioned before helps with the overfitting problem. We selected 50 random decision trees to form our final classifier on customized runway exits. Since the data points were few, we selected 80% of the runway exits as train points and the remaining 20% as test points to evaluate the performance of our classifier. The trained TreeBagger gained an accuracy of 97.5% on the test set. Figure 38 represents the tree style set of rules that the final trained classifier utilizes for labeling the data.

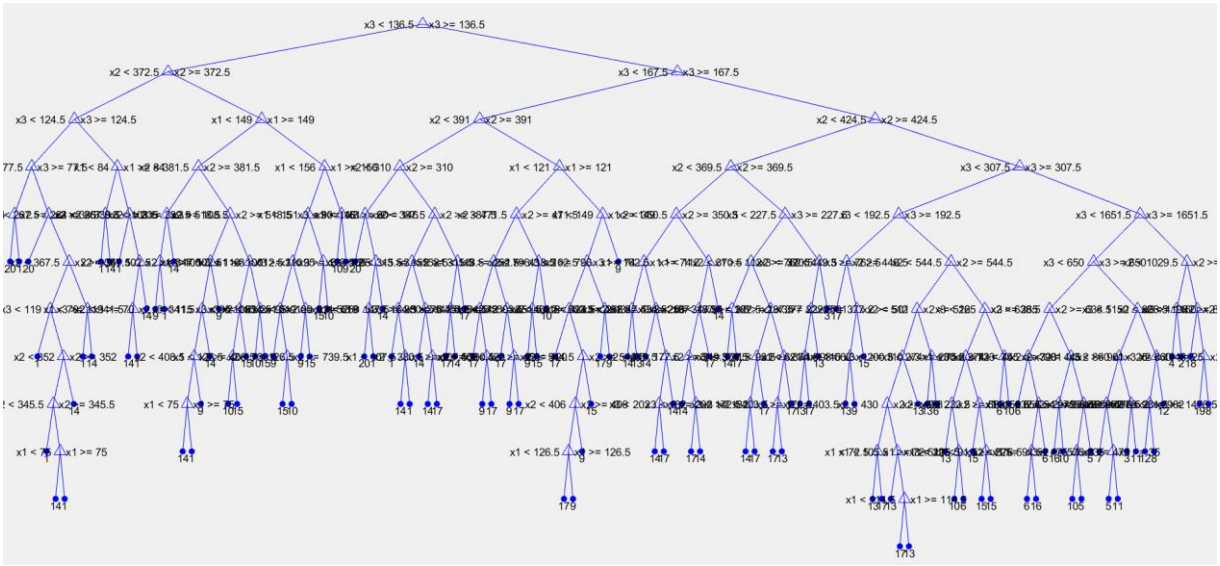

Figure 38. Final Set of Rules for the Trained Classifier Which Labels Customized Runway Exits.

In the final interface for the model application, the users will have the option of selecting from the provided 20 exit clusters. The users will also have the option of entering their own measured parameters for their desired runway exits and the trained classifier will identify the runway exit cluster label and will retrieve the proper exiting speeds based on the selected fleet mix. In the

Appendix A the runway exit clusters are attached to the initial estimated geometry features for each runway exit.

3.3.2 Runway Clusters and Landing Parameters Distributions

For simulating the arrival flights on the runway, we need to have a deep understanding of the critical particles of a successful landing profile from the runway threshold to the runway exit hold-bar. The most significant variables for each arrival flight while landing on the runway are threshold crossing speed, landing speed, landing distance, nominal deceleration rate, nominal speed, and exiting speed. We analyzed the exiting speeds in the previous section and could derive the proper distributions for exiting speeds for each individual aircraft type. Therefore, we will discuss the essential speed and deceleration values prior to the runway exit. Very similar to the way that we extracted the exiting speeds based on the geometry of runway exits, we will try to derive the proper speeds and deceleration rates based on the geometry of the landing runway for each distinct aircraft type. We know that there is some relation between the landing parameters and the runway geometry features such as elevation, and length. However, after analyzing millions of landing profiles we figured that the correlation between runway geometry features and landing critical parameters is way more complicated than the earlier assumptions made in earlier versions of the REDIM model. The following matrix scatter plot shows an example of such complexity for CLT airport. As we can observe in the plot, the relation between each pair of parameters is not clearly linear and heavily correlated. This means that for example if previously there were assumptions that every time a flight land on a short runway, they would have a short touchdown distance, and harsh nominal deceleration rates, we cannot assume the same way anymore. Similarly, assuming longer touchdown distances and shallower braking rates for long runways are not the case anymore. There are definitely some logical relations between the centrality of distributions and the

geometry conditions, however as we observed the same behavior for runway exiting speeds, here again we need to retrieve the entire associated distributions for each individual aircraft for specific runway geometry parameters.

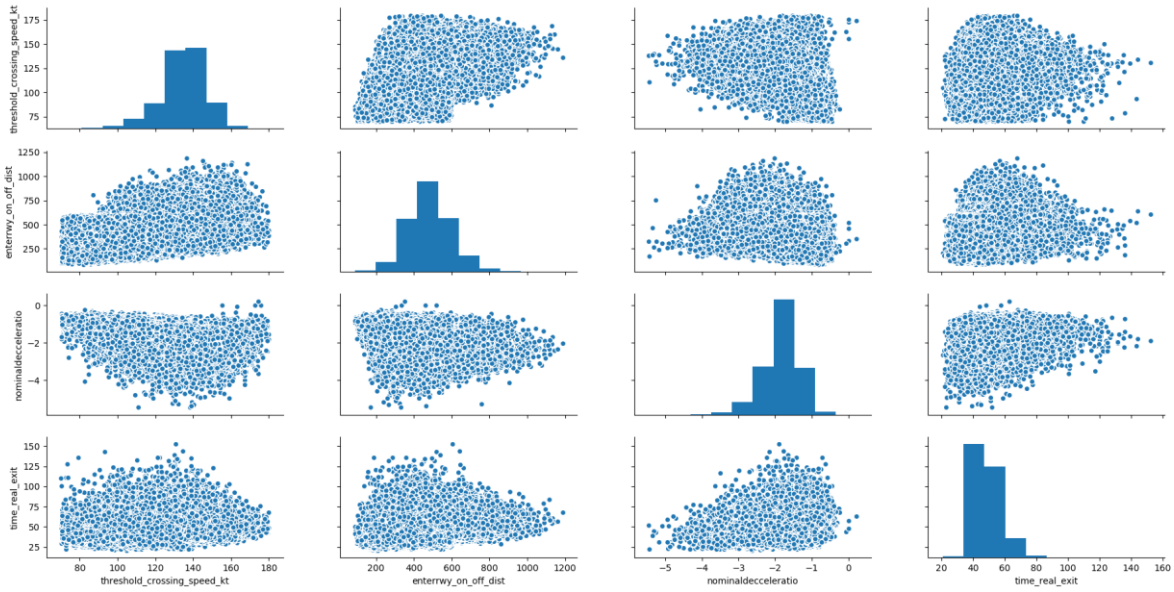

Figure 39. Matrix Scatter Plot of Threshold Crossing Speed, Touchdown Distance, Nominal Deceleration, and ROT Fuselage of all the Operations at CLT.

Since we observed the variability in each parameter and we are still aware of the potential relation between critical landing parameters and the landing runway geometry features, we repeat the same approach that we took on runway exits, but this time by using the collected geometry parameters for the runways. We clustered 290 distinct runway ends that we have in the database based on their length, number of runway exits beyond 2000 (ft.), distribution of runway exits along the runway length (ratio of PC distances over runway length), and the average distance of runway exits from the threshold. All of those features were selected as they have impact on the runway exit selection for each landing flight. Similar to the way that we selected the potential number of clusters for runway exits, we repeated the hierarchical clustering method to examine our 290 runway ends and

see how many cluster groups can potentially represent them with respect to the selected features. Similar to our runway exit clustering, we have a first guess that we can start with 30 clusters at maximum. Therefore, we form our elbow plot again with a variable number of clusters from 1 to 30 and see when we can find a proper index where the sum of distances from centroids is not changing anymore.

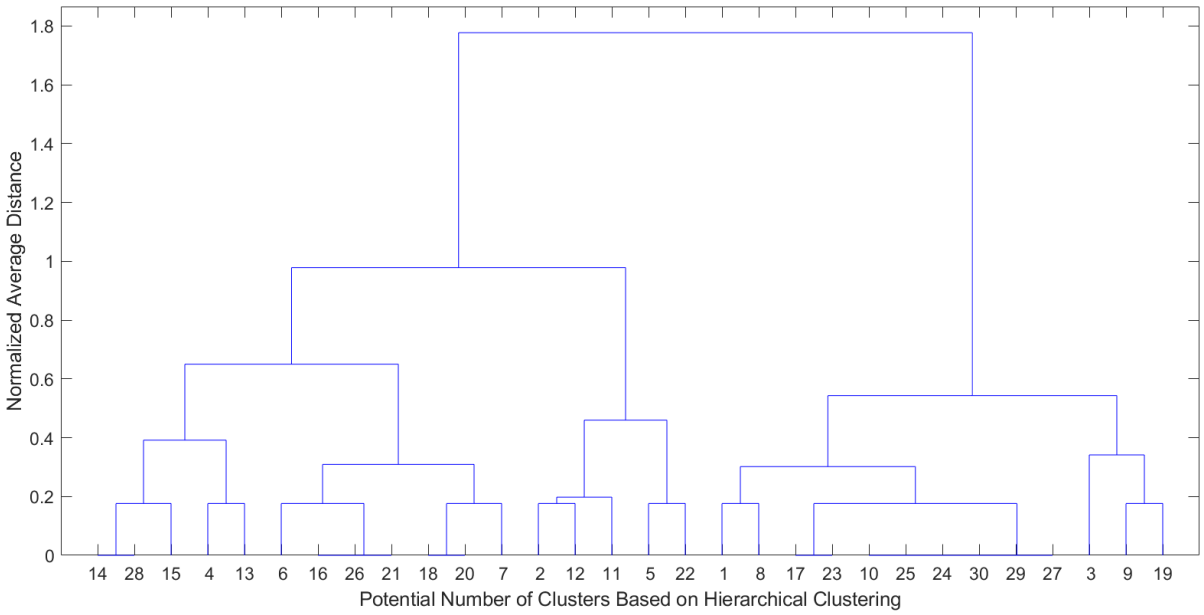

Figure 40. Dendrogram of Runways Average Distances Based on their Geometry Features.

Based on the observations from the knee plot for runway clusters, we selected 20 clusters as the sum of distances from the centroids did not show considerable changes beyond that index. After having our runways clustered, it is beneficial to take a look at the cluster distributions and see how many members are in each cluster family. Figure 41 represents the runway lengths and the number of runway exits on those runways in addition to the allocated cluster for each group. The importance of the runway length in defining the runway clusters is obvious from the plot. There is

also a weak correlation between the runway length and the number of runway exits on those runways, as we can see a weak linear relation between the values shown.

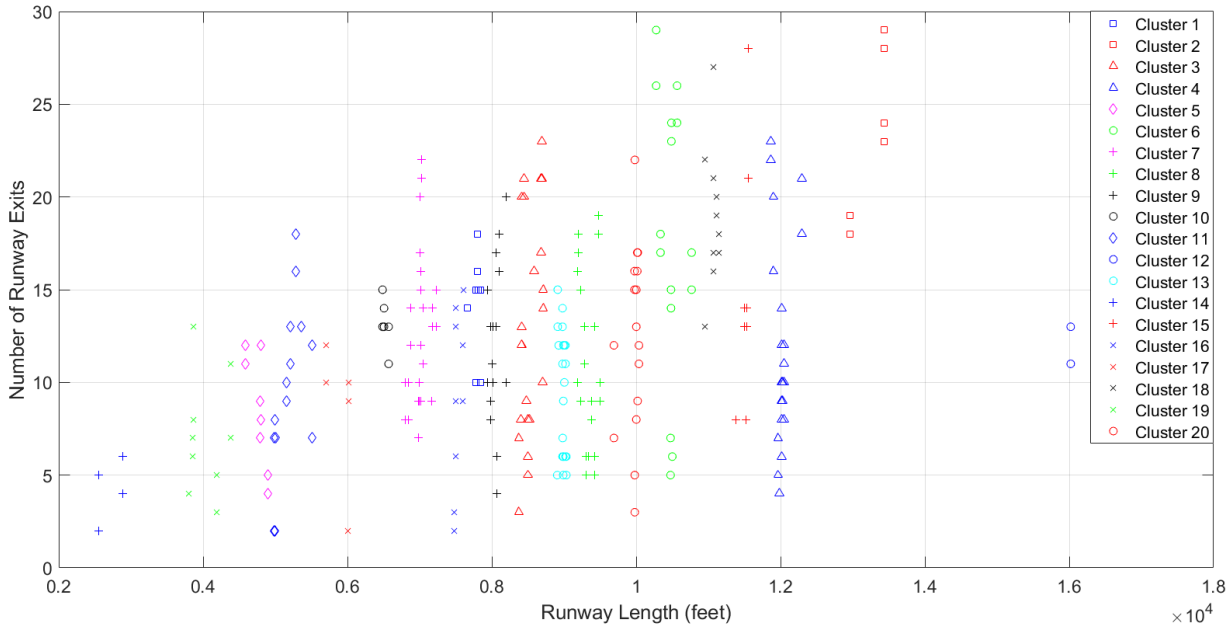

Figure 41. Number of Runway Exits vs. Runway Lengths Among Different Runway Clusters.

Now that we identified the runway clusters among all the 290 distinct runway ends that we have, we should collect the distributions for critical landing parameters for each individual aircraft type within each runway cluster. The runway clusters will play significant role in selecting the appropriate Kernel distributions for threshold crossing speeds, touchdown distances, and nominal decelerations. Therefore, every time a user enters a specific runway geometry, after finding the correct runway cluster label for the entered runway, Kernel distributions for the landing parameters are retrieved for each of the selected aircraft types in the fleet mix table. With sufficient number of iterations that we will explain later in this chapter, we can make sure the algorithm will retrieve enough data points to reflect the nominal behavior of each individual aircraft type on that specific runway. Figure 42 shows an example of touchdown distributions for Boeing B737-800 among all

the runway clusters which this aircraft operated in the landing database. For each of the assigned Kernel distributions, after removing outliers we truncated the values between the 10th percentile and the 90th percentile of the distribution values in order to remove the extreme low and high observed values from the database. In the figure the two parallel vertical red lines represent the 10th and 90th percentile of each distribution accordingly.

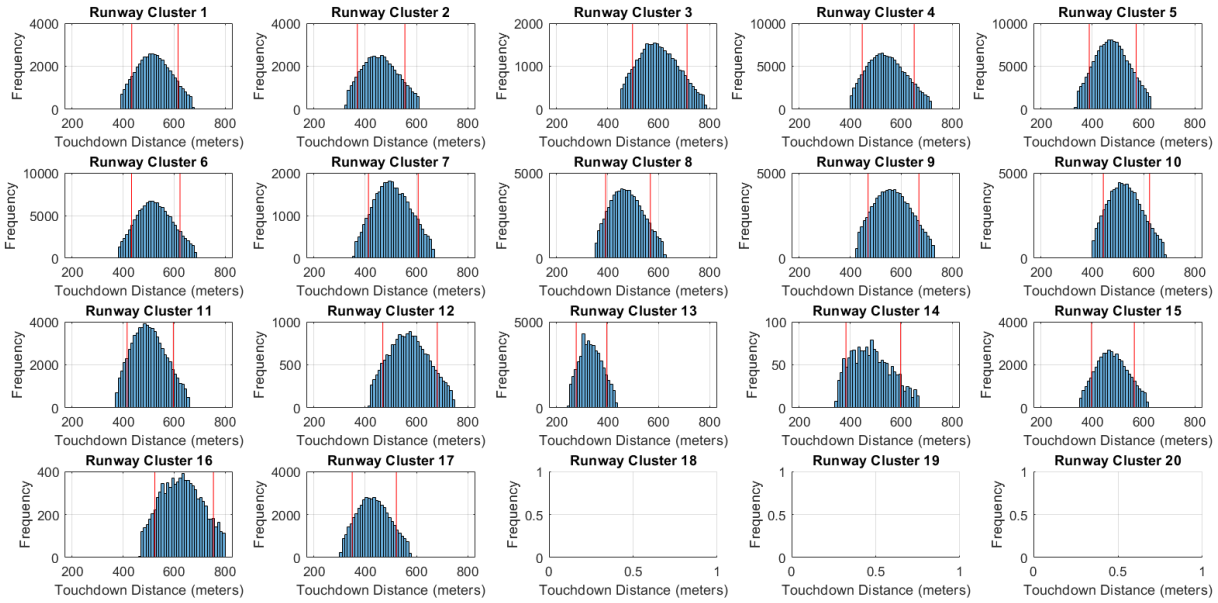

Figure 42. Distribution of Touchdown Locations for B738 on Various Runway Clusters.

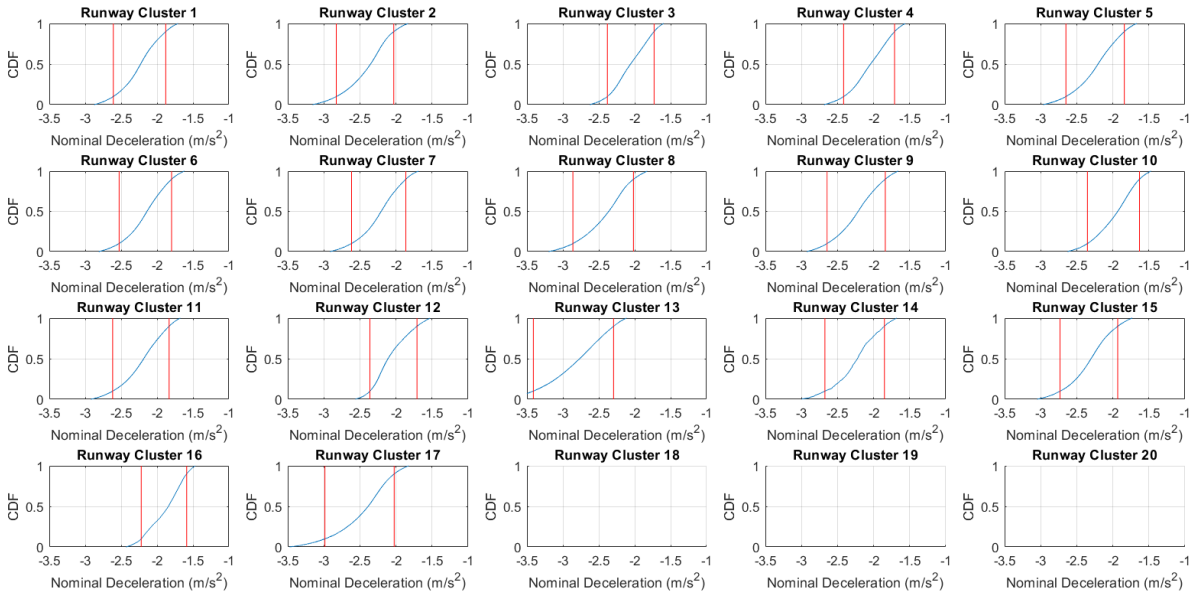

Figure 43. CDF Plots for B738 Nominal Deceleration on Different Runway Clusters.

Figure 42 and Figure 43 clearly represent different behaviors on different runway clusters. For example, if we take a look at the values in both plots for runway cluster 13, we can see that not only the touchdown locations are shorter compare to many other runway clusters, but also the values for nominal decelerations are on the higher side. The average runway length in cluster 13 is 6’673 (ft.) which is relatively short and basically pilots who land on those runways don’t have long available landing distances, therefore they have to land short and brake hard in order to make to the runway exits successfully. Moreover, the average PC location of the runway exits located on the runways in cluster 13 family is 3’811 (ft.) which tells us again that it makes sense to observe a pattern in flights behavior similar to what we see in Figures 42 and 43.

Similar to runway exits that we trained a classifier after labeling our non-labeled runway exit database, we trained 50 random decision trees and bagged them to come up with a final classifier for runways in case a user wants to enter their own desired parameters for the simulation runway.

Therefore, whenever a user enters his or her own parameters for the runway, the trained classifier identifies the label for the brand new runway and then based on the entered fleet mix proper runway distributions will be picked and we randomly generate critical parameters for each iteration of our simulation model. Later in this chapter we represent a simple example of an evaluation case and we will explain about the generated critical landing parameters.

3.3.3 Speed Corrections for Altitude

The elevation of the runway end has an impact on aircraft approach speed. The higher the elevation, the faster the aircraft approach speed will be since by increasing the elevation we will have less density and that causes speed gain. Therefore, one of the critical environmental parameters for the simulation of landing flights is runway elevation. We need that input from the user to correct the approach speeds from the sea level. The following equation is what we use to correct the approach speed at a different altitude. Equation 1 shows the correction formula for editing approach speed at a certain altitude in regards of its sea level approach speed. In this equation V_2 is the speed at the desired altitude, V_1 is the speed at sea level, ρ_1 is the density ratio of the air at sea level and ρ_2 is the density ratio of the air at the desired altitude. Density ratios can be interpolated based on the standard ISA conditions which define the air density ratio as a function of the temperature and altitude.

$$V_2 = V_1\sqrt{\frac{\rho_1}{\rho_2}}$$ Equation 1. Approach Speed Correction Formula.

3.3.4 Algorithms for Aircraft Runway Evacuation

We talked about the critical landing parameters. We also talked about the procedure for randomly generating stochastic values for exiting speeds. However, after reaching to the PC point of the

runway exit, the aircraft still has to traverse the remaining distance from the PC point all the way to the runway exit hold-bar. This part will take another few seconds on the runway and depending on the aircraft exiting speed, deceleration rate along the path length of the exit, and the distance to the hold-bar it can take a range of values to evacuate the runway entirely. For defining the time and distance that it requires the aircraft to evacuate the runway entirely, we integrate the location of the aircraft numerically with steps of 0.1 seconds and appropriate deceleration rate, until the entire fuselage is recognized to be fully out of the runway. In chapter 2 we talked about the aircraft dimension database, therefore we know what is tail span and wing span for each of the vehicles in our model. We just need to identify a procedure to calculate the deceleration rate along the path length of the runway exit and use it in our numerical integration method.

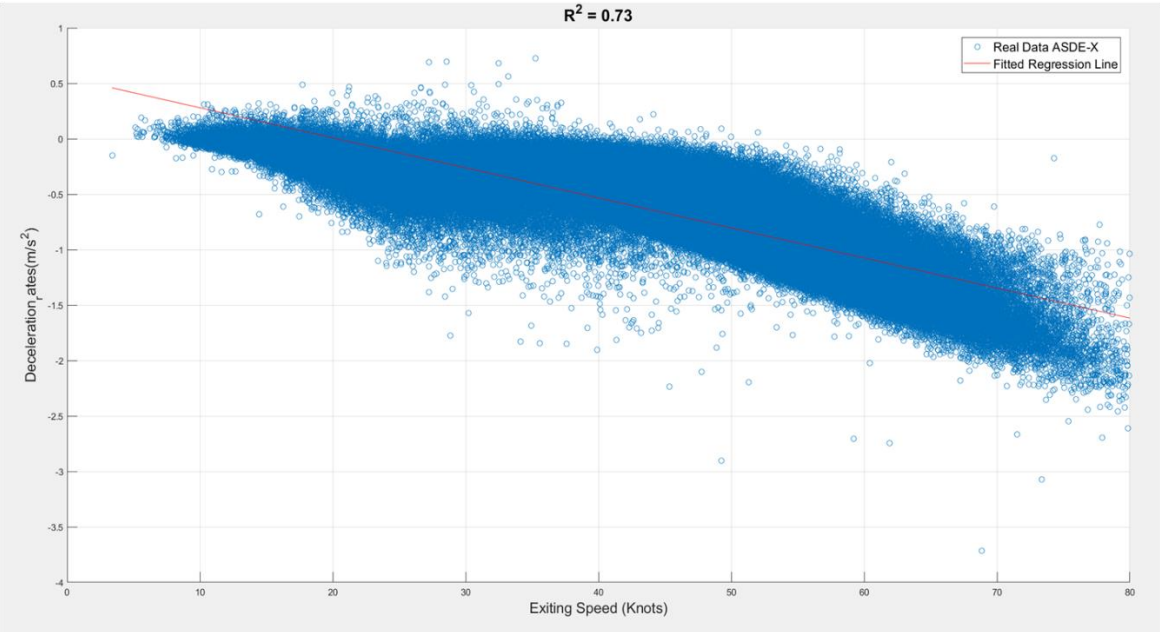

Figure 44. Exiting Speeds for Various Flights from ASDE-X Data at the PC Points vs. Average Deceleration Rates Along the Exit Path.

Figure 44 shows a strong linear correlation between the speed at the PC point of runway exits and the average deceleration rates along the runway exit path. For predicting new values, we fitted a linear regression model to the speed values in knots to predict the deceleration values in meter per

squared seconds. The following equation represents the relation between exiting speeds in knots and the deceleration rate along the exit path from the PC point to the hold-bar of the runway exit in meter per squared seconds. The R-squared value for this fitted equation is 0.73.

$$Deceleration\ Rate = -0.0270993813190620*(Exiting\ Speed\ Knots) + 0.550469480264916$$

Equation 2. Linear Equation for Finding the Deceleration Rate Along the Exit Path Based on the Exiting Speed.

For examining our fitted equation, we tested the numerical integration algorithm for 3'000 randomly generated Airbus A319 airplanes. The deceleration rate along the exit path is derived from Equation 2. Figure 45 represents in the 3D plot for the simulated test flights. As we can see in the plot, there's a logical correlation between seconds required for vacating the runway, the selected deceleration rate, and the speed at the PC point. Basically, the faster airplanes would be at the PC point, the sooner they can vacate the runway, but they have to brake harder to reduce more speed before getting to the exit hold-bar.

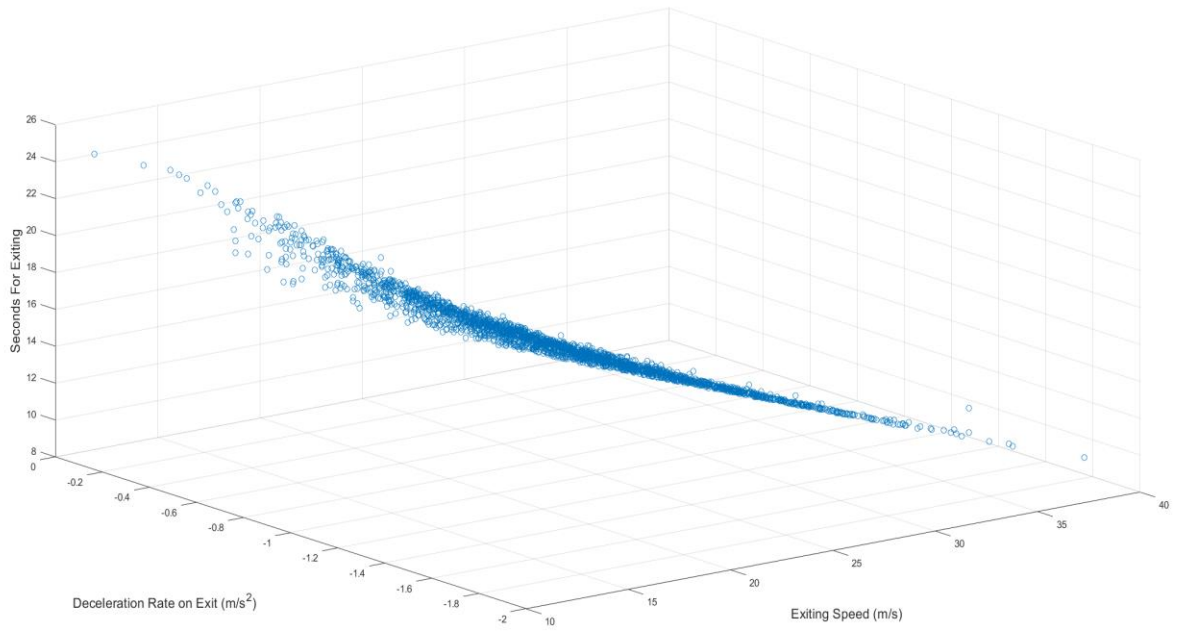

Figure 45. 3 Dimensional Plot for Average Deceleration Along Exit Path, Exiting Speed, and Evacuation Time Required for Exiting Runway.

3.3.5 Wet and Dry Conditions

Another important environmental parameter which has impact on the intensity of the friction between the runway pavement and the aircraft landing gear and nose gear, is the percentage of wet and dry pavements. This input parameter should be entered as two separate percentages which sums up to 100 percent. Basically each of the entered percentages define the amount of time the pavement is wet or dry. This parameter can be estimated by designers while they're analyzing their preferred facility based on the historical weather data. In the simulation model we consider a 15% loss in nominal deceleration rate and deceleration rate along the runway exit path. Therefore, whenever a sample from the percentage of the wet pavement is sampled, the stochastic value for its randomly generated nominal deceleration will be reduced by 15% of its value. Moreover, after the simulation logic chooses a feasible runway exit for evacuating the runway, the value of the deceleration rate after the exit PC point will be reduced by 15%.

3.4 All Parts Combined Together – A Simple Example

In this section, we discuss the hybrid method to simulate individual aircraft landing roll profiles to estimate Runway Occupancy Time (ROT) and exit distance location. We use a Monte Carlo simulation approach for simulating critical events of each aircraft landing and then connect those events using simple kinematic rules. In order to generate stochastic landing parameters for each landing profile, we use parameter distributions extracted from ASDE-X data. Figure 46 shows the critical landing roll events selected for the simulation model. In the simulation, each landing instance begins with a randomly generated threshold crossing speed based on the Kernel distributions associated with the generated aircraft type on the defined runway cluster. Like all other landing parameters, the landing speed is obtained from distributions based on the ASDE-X

data. A nominal deceleration rate is generated from ASDE-X data for individual aircraft types from the proper distribution retrieved for the simulation runway cluster. In the model, we define the concept of nominal speed as the speed and time event where a pilot starts evaluating the current aircraft position and runway exits located further downstream. The nominal speed is normally associated with the search for suitable runway exits. After analyzing of hundreds of ASDE-X speed profiles, we found that the nominal speed for most of the commercial aircraft ranges from 85 to 70 knots. Small General Aviation aircraft are observed to have significantly lower nominal speeds (40-55 knots). Since there is a wide variety of velocity profile behaviors for different classes of aircraft, we define the nominal speed based on the approach speed of every aircraft in the simulation. For the landing roll, simulation is based on the Aircraft Approach Category (AAC) groups. In the modeling paradigm adopted, a pilot will continuously assess the speed of their aircraft and runway exits located downstream that may be suitable to exit the runway. In general, pilots have a priori information about runway exits before landing. Such information is contained in airport diagrams available in either printed or electronic form (i.e., electronic flight bag). For each landing iteration, we generate random exiting speeds for each unique runway exit type on the runway. The stochastic generated speeds are based on the Kernel distribution of the associated aircraft type and runway exit cluster. The generated speed works as a control parameter to limit the highest value of runway nominal speed obtained in the Monte Carlo simulation. Before finalizing the exit utilization in each iteration we check if the deceleration rate from the nominal speed decision point to the point of curvature exceeds a maximum deceleration threshold. If the ratio of the mentioned deceleration rate over the previously generated nominal deceleration is below 120%, we allow that exit assignment and we continue on estimating time parameters, otherwise we don't finalize the exit assignment and we keep checking the remaining runway exits

until we pass all the mandatory conditions. The ratio that we picked for this control loop is 1.2 and that means that we let the flights to even brake 20% higher than the first phase if they can make it to the closer runway exit. While the average ratio from the ASDE-X data is around 95%, we have observed many regional jets using an extra braking power to evacuate the runway earlier. For avoiding runway overruns and making our simulation scenarios more realistic, in every simulation case we place a right angle exit at the end of the runway. Those right angle exits might be taken in situations that generated random events would belong to the tail of the distributions.

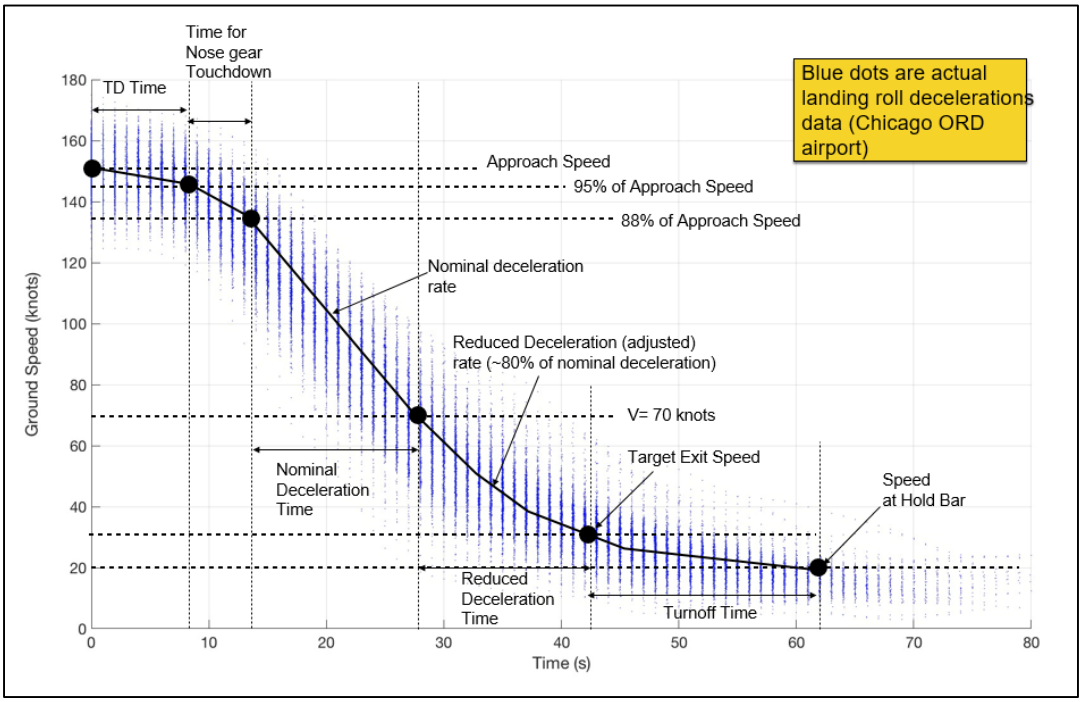

Figure 46. Velocity Profile Phases Modeled in the Monte Carlo Simulation Model.

In each simulated landing iteration, once a flight is assigned to an exit, we estimate the ROT time. ROT time is the summation of the individual times for key parameters defining the generated landing profile. The landing roll profile includes: a) air time from threshold crossing point until touchdown moment, b) free roll time from main gear touchdown until braking, c) activating brakes time until reaching the nominal speed, d) nominal speed until the runway exit point of curvature

location is reached, and e) runway exit point of curvature speed until the aircraft vacates the runway.

To estimate the landing roll turning time, we use a numerical integration algorithm (depending upon aircraft) that integrates the instantaneous position of the aircraft with small time steps into the future. For generating meaningful stochastic values for every shown phase in Figure 46, we construct useful distributions of airplanes behaviors from ASDE-X data. We parsed, analyzed, cleaned, and mined around 12 million arrival flights from 37 ASDE-X airports in the United States. An important difference between the algorithm described in this paper and old algorithms such as those contained in REDIM 2 is that the new algorithm has the capability of modeling individual aircraft behaviors. Having 37 ASDE-X data sets helped us gathering information for 274 unique aircraft.

In this section we represent preliminary results using the newly developed simulation algorithm. The results which we represent in this section are related to runways evaluation cases where users can run the simulation model with the fleet mix of their choice, and their preferred runway exit types and locations on the runways to estimate the weighted average runway occupancy time. We chose runway 10C from Chicago O'Hare Airport for our case study. Table 4 represents the selected fleet mix for the case study that we ran our simulation for.

Table 4. Fleet Mix for the Simulation Case Study.

Aircraft Type	Fleet Mix
Airbus A319	20%
Airbus A320	20%
Boing B738	20%
Boing B772	20%
Embraer E190	20%

Figure 47 shows runway 10C at Chicago O'Hare International airport with the runway exits on the runway. For the simulation tool we designed an interactive map system that users can select their favorite airport and runway and then from a list of existing runway exits, they can select the ones that they prefer to keep open during the simulation scenario or they prefer to close and not letting any airplanes using them. This functionality is extremely helpful for the occasions where airports have undergoing construction projects and they have to close some runway exits. In Figure 47 we represent the open exits with green and the closed exits with red. The imaginary exit arc from the point of curvature all the way to the exit hold-bar is drawn as well. For making our test case more realistic, we closed the right-turn exits and turn-back exits on the runway, therefore all the open exits will lead to the main terminal areas of the airport and provide enough space for airplanes to have higher exit speeds at the point of curvature.

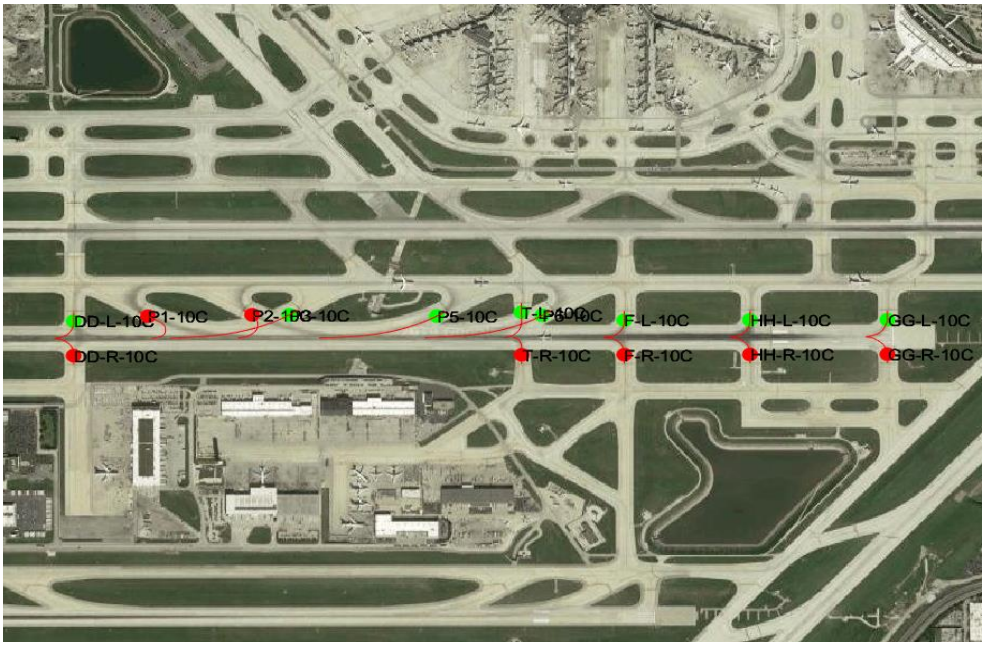

Figure. 47 Runway 10C at Chicago O'Hare International Airport with the Open and Close Exits for the Simulations Scenario.

We ran 10,000 landing aircraft iterations for the test case with the given fleet mix and exit condition. The weighted average ROT for the given condition was 58.9 seconds. Figure 48 shows

the cumulative density function graph for exit utilization in the tested scenario. We can see in Figure 48 that runway exit P6 attracts close to 40% of the entire fleet mix. This high-speed exit is located 6,300 (ft) from the runway threshold point. Around 90% of our simulated flights leave the runway by using available exits prior to 9,000 (ft) from the runway threshold.

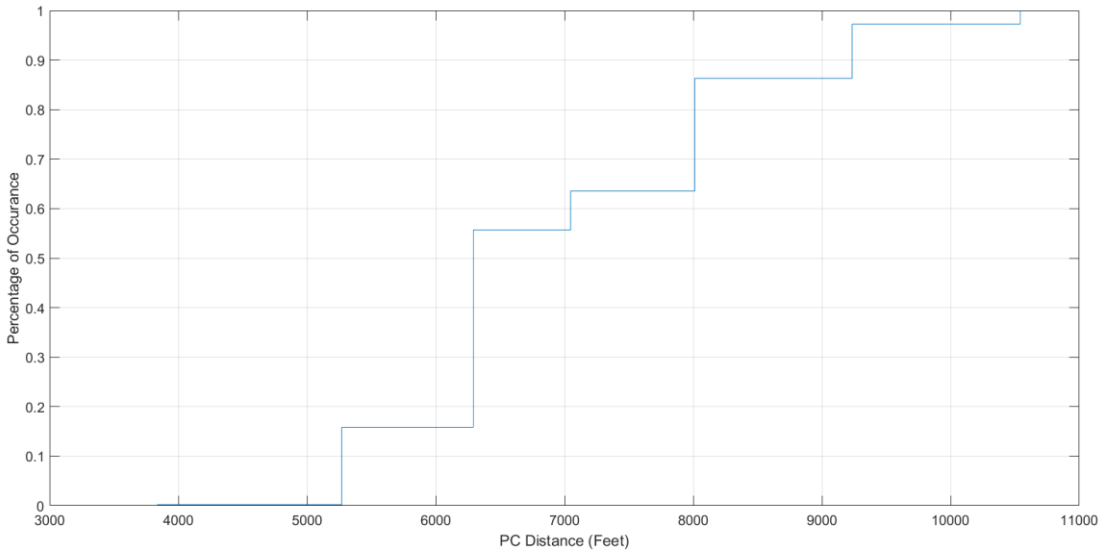

Figure. 48 Exit Utilization Cumulative Density Function Plot.

Figure 49 shows the speed-distance profiles for simulated flights in the model test case. The figure shows that aircraft approach speeds are limited to narrow ranges due to aerodynamic laws driving the process. The general trend of reductions of speed and slowing down on the runway is shown in Figure 49. An important aspect of the new algorithms presented, is the ability to produce stochastic speed values up to the exit speed point. The character of continuous distributions is clearly shown in Figure 49 where every speed profile ends at the point of runway exit curvature.

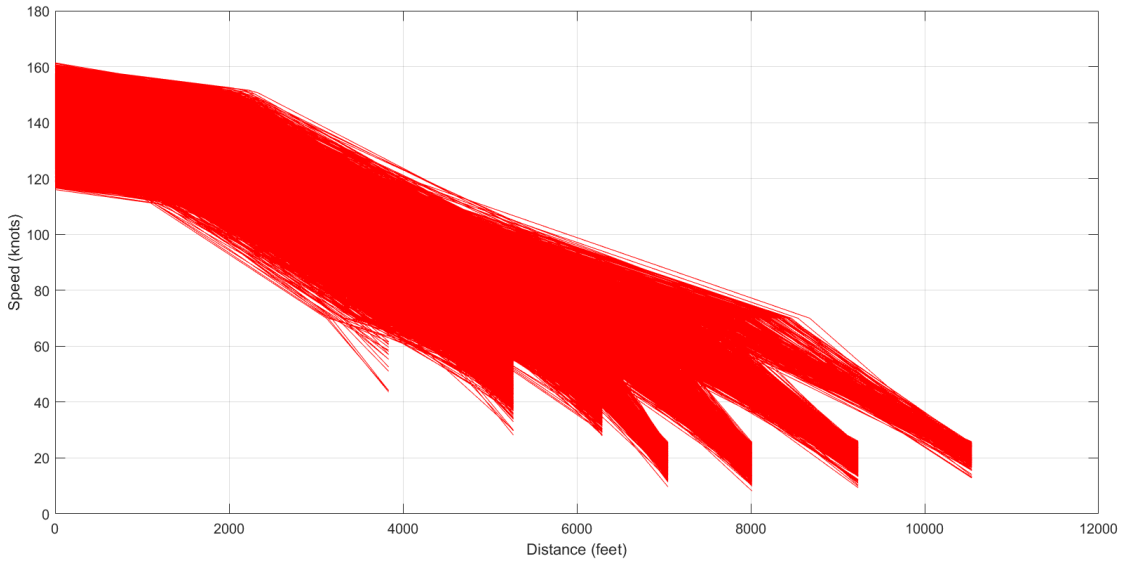

Figure. 49 Speed- Distance Profiles for the Simulated Flights.

Figure 50 shows a summary of every landing event generated for simulated flights in a stacked bar format showing individual components. The red dots in Figure 50 represent taken runway exits and other colors in the stacked bars show different generated random events that construct a complete simulated landing profile for each flight.

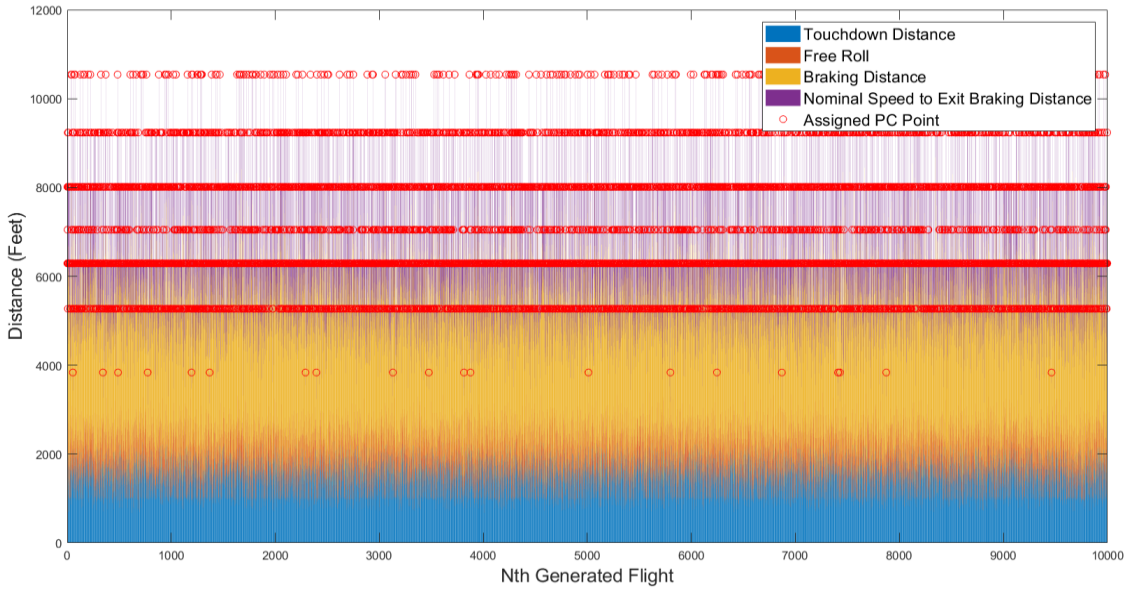

Figure. 50 Generated Random Events for Each Simulated Flights.

3.5 Aircraft Groupings as Surrogates

As mentioned earlier in this chapter, the developed hybrid Monte Carlo approach for estimating the runway occupancy times and exit utilizations is entirely data-driven. Therefore, for each selected aircraft in the fleet mix for every simulation scenario we need sufficient data points within each runway and runway exit cluster to be able to retrieve random numbers from the assigned Kernel distributions. The minimum threshold for the number of operations within each cluster is 30. There are plenty of aircraft types which had either fewer operations than 30 operations during years 2015 and 2016 in ASDE-X or they didn't even have any operations on some specific runway clusters. This can be because of the limitations of specific airports in accepting specific aircraft types. For example, there are only two facilities in the US which have considerable number of operations from Airbus A388 and they are LAX and JFK. Many airports in the database do not have the capability of hosting this type of aircraft due to short runway lengths. On the other hand, most of the facilities that we have surveillance data for, do not host small prop aircraft types and would cause lack of data for forming Kernel distributions for many small airplanes on long runways. For addressing this issue, whenever we have lack of data and the original aircraft type lacks sufficient data points on specific runways or runway exits, we move to a higher level and use the distributions assigned to larger groupings of airplanes. For this purpose, we use two traditional accepted grouping methods of aircraft types by FAA named as AAC (Airplane Approach Category), and ADG (Airplane Design Category). The following two tables define the criteria for each of the mentioned grouping methods for different aircraft types.

Table 5. AAC Grouping Criteria Based on Approach Speeds.

AAC Grouping	Approach Speed (Knots) at Maximum Landing Mass
A	< 91
B	91-120
C	121-140
D	141-165
E	> 166

Based on the criteria in Table 5, we labeled all the 274 aircraft types in the database with their appropriate AAC group. Therefore, when we need a distribution for any of the stochastic parameters of the simulation model, if the user wants to use AAC grouping as the surrogate for airplanes with no data on the simulated cluster, we retrieve the landing parameters from the Kernel distributions created for the AAC groups. The Kernel distributions for both landing parameters and the exiting speeds were created for AAC groups in a similar manner that we did it for individual aircraft types.

ADG grouping has its own criteria based on the tail height and wingspan. The Table 6 represents the criteria for ADG grouping.

Table 6. ADG Grouping Criteria Based on Aircraft Dimensions.

ADG Grouping	Tail Height (feet)	Wingspan (feet)
I	<20	<49

II	20-30	49-79
III	30-45	79-118
IV	45-60	118-171
V	60-66	171-214
VI	66-80	214-262

In the final version of the model, we gave the user the option of choosing either AAC or ADG groupings as the surrogate for those aircraft types that don't have sufficient data points for having an assigned Kernel distribution. The following figure shows the nominal deceleration distributions on each of the runway cluster families for ADG group I. The values shown in figure 51 are for nominal deceleration rates for all the aircraft types which are grouped in ADG I. The usage of surrogate is beneficial to simulate the landing behavior of any non-popular aircraft in the ASDE-X data, based on the similar vehicles to them.

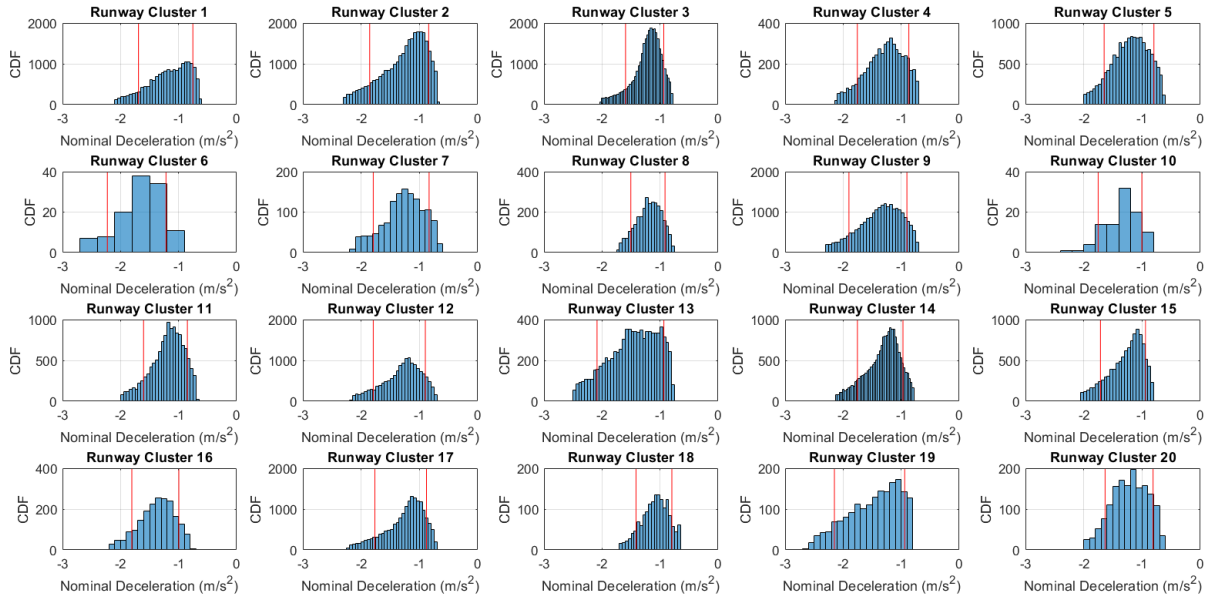

Figure 51. Nominal Deceleration Distributions for ADG I. These Values will be Used at Surrogates for Aircraft Types that Don't Have Sufficient Data.

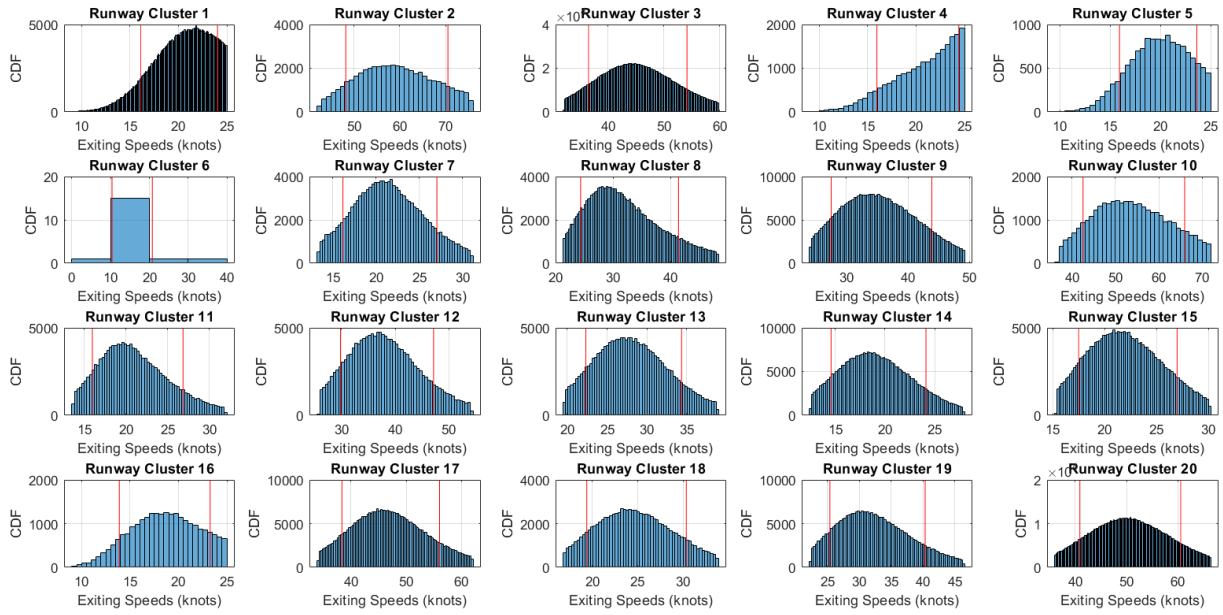

Figure 52. Exiting Speeds for ADG III aircraft Group and the 10th and 90th Percentiles of the Values.

Figure 52 represents the exiting speeds for various ADG groups and the 10th and 90th percentiles of the data points within each cluster.

3.6 Different Modes of the Model

The new version of the hybrid simulation model is capable of running in different modes and giving users useful outputs with various functionalities. There are 3 major types of analysis that the new developed simulation model is capable of doing:

1- Evaluate an existing runway: in this mode, the user knows the fleet mix of usage at the modeling facility, the environmental conditions, runway geometry, and also exit configuration and geometry. The existing runway mode or the evaluation mode is for situations where people are mostly focused on evaluating the performance of ROT and exit utilizations at their desired current facilities. For the new version of the simulation model, users can either pick any of the 37 ASDE-X supported airports and select their desired runway, or they can draw a new existing runway from scratch and enter the information for each runway exit manually. The benefit of having the ASDE-X supported airports in the evaluation mode, is that users don't have to enter the runway exits for those facilities anymore since the data is driven from the runway exit database automatically after choosing the airport. Moreover, there's a new implemented visualization system that shows the live Google Earth layout of the airport and users can evaluate their simulation facility more accurately. More details of the new features of the user interface will be explained later in this chapter.

2- Improve an existing runway: in this mode the user knows the runway geometry information, aircraft fleet mix, and the runway exit configuration. However, they want to utilize an existing gap between two or more runway exits to construct a new exit and improve the runway occupancy times. A dynamic programming approach is used to

optimize runway occupancy time and select the best location for a new runway exit if the minimum separation between current exits and the new one will be met.

3- Design a new runway: in this mode the user just knows the runway geometry information, and aircraft fleet mix. This mode is good for constructing brand new runway and locating the optimum runway exits along the runway length to optimize the runway occupancy times. Again we use a dynamic programming approach to find the best locations for the new runway exits. The user has to enter the desired number of exits and based on that constraint and the minimum separation between runway exits the model identifies optimum locations for runway exits.

In the following section, we will give one simple example for each mode and explain the functionality of the model within each mode.

3.6.1 Evaluate an Existing Runway

As we mentioned earlier, in this mode the user has information about runway exit configurations. Therefore, we just run multiple iterations of the simulation model (based on the entered iteration number) to randomly generate arrival flights for each of the entered aircraft in the fleet mix. For each generated random flight the correct Kernel distribution assigned to the runway cluster and runway exit cluster will be chosen. We demonstrate an example with a sample fleet mix of aircraft for CLT runway 36L. Notice that in this mode we enable the user to either enter the runway configuration itself or chooses one of the 290 existing runway ends from the landing database. Table 7 shows the aircraft fleet mix selected for this evaluation run on CLT runway 36L. The fleet mix shown in the table is based on the real fleet mix on runway 36L of CLT airport during years 2015 and 2016 from ASDE-X data.

Table 7. CLT Runway 36L Fleet Mix for Evaluation Case.

Aircraft Type	Fleet Share (%)
A319	16
A320	6
A321	17
B712	1
B737	1
B738	2
B752	1
CRJ2	19
CRJ7	7
CRJ9	18
DH8A	1
DH8C	3
E120	1
E145	1
E170	5
MD88	1
Total	100

The following exit configuration was used to run this evaluation case. For being more realistic the first two back-turn runway exits were selected to be close since they are very close to the runway threshold and most probably commercial aircraft types can’t make it to the first two exits.

Figure 53. Selected Runway Exit Configuration for the Evaluation Case.

We ran 50,000 iterations for this simulation run. The model has multiple outputs listed as following:

1- An exit utilization table showing the percentage of the time each individual simulated aircraft type used any of the open runway exits.
2- Weighted average runway occupancy time (ROT) for all the simulated flights.
3- A graph showing all the simulated critical parameters in terms of the distances from the runway threshold stacked on top of each other.
4- A graph representing the speed-time profile for all the simulated flights.
5- An output table for each of the simulated flights and the parameters that successfully led the simulated aircraft to evacuate the runway. This file has the aircraft name, the approach speed, touchdown speed, touchdown time and distance, nominal deceleration rate,

deceleration rate from nominal speed all the way to the PC point of exit, runway exiting speed at the PC point, deceleration rate along the exit path length, and the total runway occupancy time.

One of the most important output results of the simulation model is the cumulative density plot for the exit utilization. This output can help the user to identify the essential runway exits at the facility and it can be helpful in evaluating the efficiency of runway exit types and distances from the threshold. Figure 54 represents the CDF plot for exit utilizations for all the simulated flights in the evaluation case. As we can see in the figure 84% of the simulated flights used the first high speed exit on the runway to evacuate. Almost 15% used the second high-speed exit and around just 1% of the remaining flights used the next right angle exit. These utilizations resulted in a weighted average runway occupancy time of 52 seconds overall among all the simulated flights. The logic in the model is in a way that if any sets of randomly generated numbers wouldn't be able to vacate the aircraft within the provided runway exits on the runway, we re-sample a new set of stochastic values for each of the critical landing parameters until the flight would be able to evacuate the runway. Note that we don't resample the earlier generated runway exit speeds and we just resample critical landing parameters on the runway.

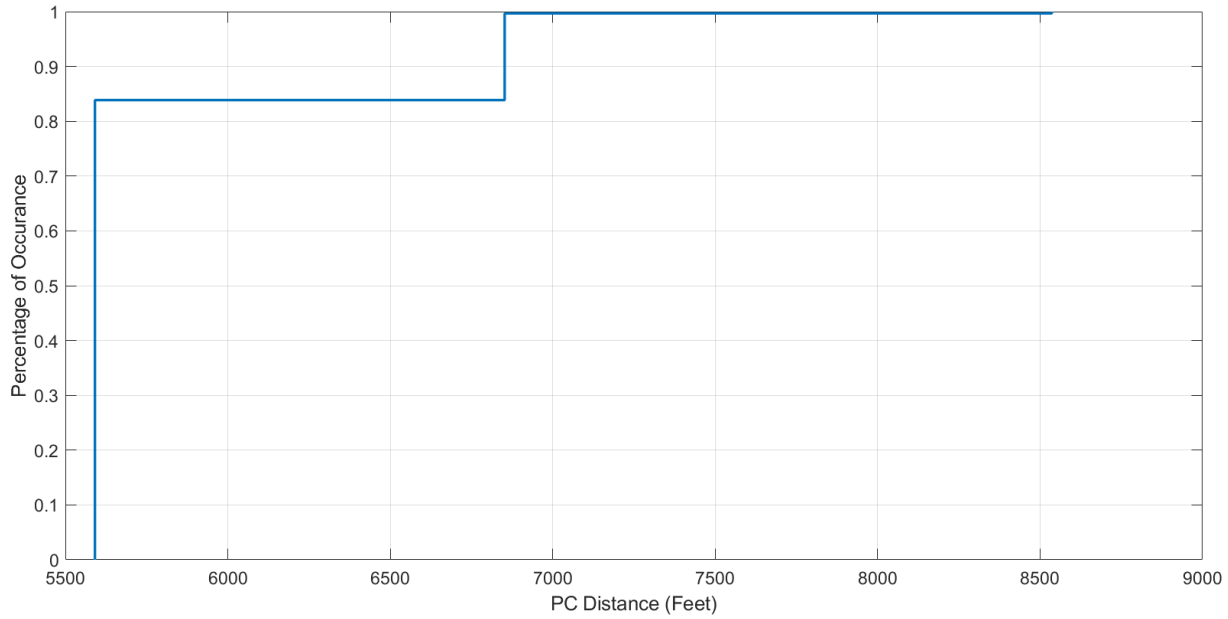

Figure 54. CDF Plot for the Exit Utilization of All Simulated Flights.

Here we show the speed-distance profile for all the simulated flights in the test evaluation mode. The profiles in the Figure 55, clearly represent the runway exits which were used for our evaluation case. The stochastic behavior of approach speeds, touchdown speeds, and exiting speeds are visible in the graph. Moreover, with the help of such plots we can identify the exit types based on the speed distributions that airplanes had at the PC points. For example, the first two high speed exits W7 and W8 located at 5,591 and 6,852 feet from the threshold absorbed many flights with high speed values, while the remaining flights took the right angle exit W9 at lower speed values.

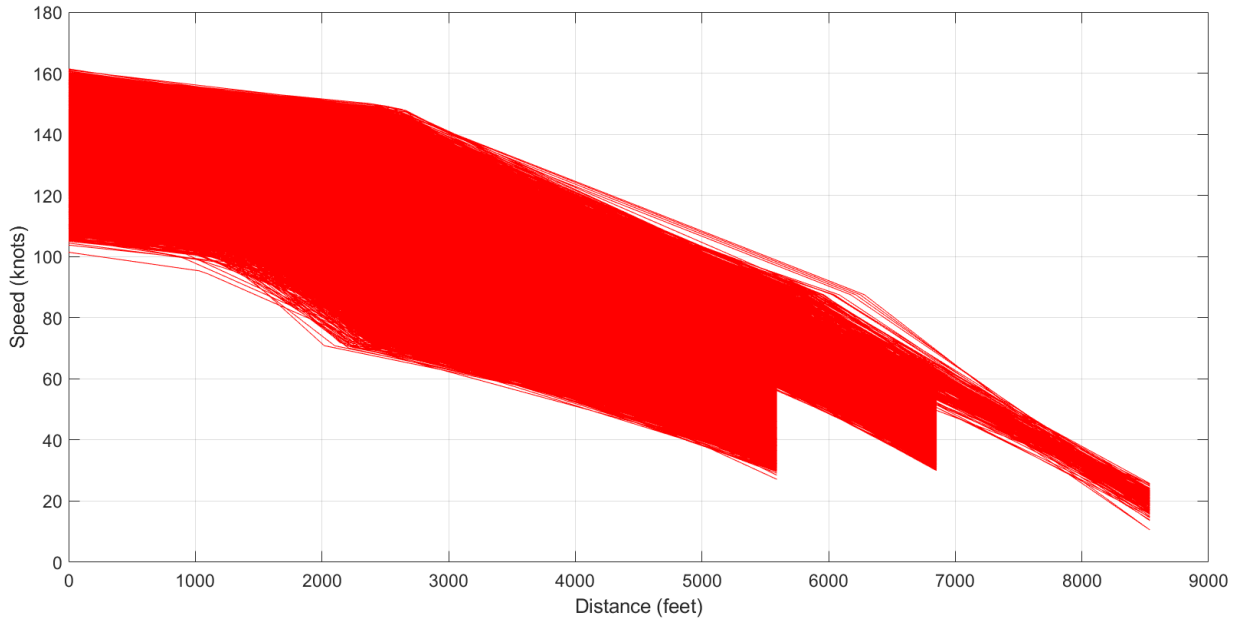

Figure 55. Simulated Flights Speed-Distance Profile.

Figure 56 represents the critical simulated landing parameters for all the landings in the evaluation case. This is an important chart to validate the goodness of simulated events for each phase. We sacked each event in terms of their distances from the runway threshold to make sure that runway exit assignments are logical and valid. The intensity of the red dots at the location of the two high speed exits tell us that those exits were taken by most of the planes. We can validate the distribution of touchdown locations, and as it is obvious from the graph, those flights who didn't meet the 1.2 ratio of deceleration from the nominal speed to PC point over nominal deceleration, had to pass the first upcoming exit and take the next available one which meets the deceleration ratio criteria.

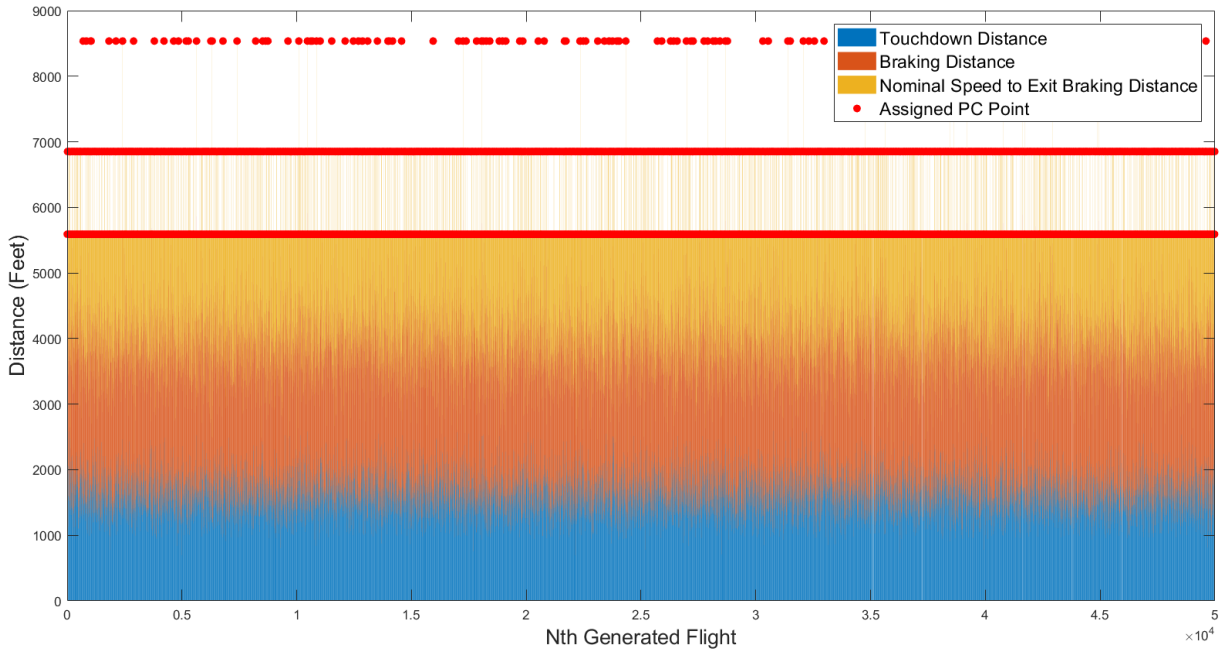

Figure 56. Critical Landing Moments for all the Simulated Flights in the Evaluation Case.

Table 8 shows the exit utilizations for each individual aircraft type for each runway exit and the average runway occupancy time for each runway exit. As expected the closer a runway exit to the runway threshold, the lower the runway occupancy time would be. Those runway exits which were selected to remain closed for the simulation didn't have any assigned flights and ROT values. It is interesting that E120 which is a small aircraft had relatively lower utilization rate at the first high speed exit compare to bigger airplanes. This is because the ASDE-X data does not represent the behavior of single engine planes very accurately as the pilots of those planes don't have a lot of pressure to vacate early on long runways. We addressed that issue in creating design charts by selecting specific percentiles of nominal deceleration for those airplanes to reflect their performance more realistically.

Table 8. Exit Utilization Table for all the Simulated Aircraft in the Evaluation Mode.

ExitDist	A319	A320	A321	B712	B737	B738	B752	CRJ2	CRJ7	CRJ9	DH8D	E120	E145	E170	MD88	Average_ROT
1401	0	0	0	0	0	0	0	0	0	0	0	0	0	0	0	
2720	0	0	0	0	0	0	0	0	0	0	0	0	0	0	0	
5591	95	87	67	87	99	86	90	85	88	81	99	73	95	94	68	51.99677274
6852	5	13	32	13	1	14	10	15	12	19	1	24	5	6	30	58.07153745
8536	0	0	1	0	0	0	0	0	0	0	0	3	0	0	1	69.5072818
8798	0	0	0	0	0	0	0	0	0	0	0	0	0	0	0	

3.6.2 Design a New Runway

Designing a new runway requires the user to have knowledge about only the aircraft fleet mix, runway geometry information such as length, elevation, wet/dry percentage, and the number of desired runway exits. The Original REDIM2 manual [25] defines the dynamic programming (DP) algorithm very clearly. The difference in the new version of the simulation model is that for generating exit candidates we run the hybrid data-driven approach which we explained earlier in this chapter. Each flight will have all the phases of its landing simulated except the exiting part on runway. Therefore, we generate samples all the way to the required distance for reaching to an exit speed which is generated from its associated runway exit cluster for each individual aircraft type. There are two types of exit candidates which are being fed into the dynamic programming approach: primary and secondary candidates. Primary candidates are identified after running the landing role simulator similar to an evaluation case with a difference that airplanes decelerate directly all the way from touchdown point to an imaginary location which they meet a randomly generated exit speed based on the user defined exit type. Secondary candidates are defined based on the minimum separation criteria between every two runway exits. Currently FAA mandates a minimum separation of 750 (ft.) between the point of curvature of two consecutive runway exits to avoid any pavement overlaps. This parameter is another input value that users can define based on their own desire for the minimum separation between runway exits. If we collect all the exit

candidates and we consider the number of exit candidates to be K, we can index each of the candidates as k where k ranges from 1 to K.

Imagine that we have M aircraft for our simulation runs. We also have two surface conditions wet and dry. If we assume i from 1 to M, and j for surface conditions from 1 to 2, and p_j representing the probability for wet and dry surface conditions entered by the user, we can formulate our optimization problem mathematically.

If the number of exits that the user wants to build is N, the following binary decision will be checked for all the generated candidates.

$$X_k = \begin{cases} 1, if\ candidate\ k\ is\ selected \\ 0 \end{cases} \text{ for k = 1:K}$$

$$Y_{ijk} = \begin{cases} 1, if\ aircraft\ i\ is\ assignged\ to\ exit\ candidate\ k\ on\ surface\ condition\ j \\ 0 \end{cases} \text{ for i= 1:M,j= 1:2, k} \in A(i, j)$$

Then the objective function for the optimization is to minimize the weighted average ROT for all the generated flights at every feasible exit candidate on each runway surface condition. The following equations represent the objective function and the constraints for this problem.

$$Minimize \sum_{i=1}^{M} \sum_{j=1}^{2} \sum_{k \in A(i,j)} a_i p_j T_{ijk} Y_{ijk} \quad \{3.3\}$$

$$Subject\ to \sum_{k \in A(i,j)} y_{ijk} = 1 \quad \text{for i=1:M, and j=1,2} \quad \{3.4\}$$

$$\sum_{k \in S(k)} x_k \leq 1 \quad \text{for k = 1: K} \quad \{3.5\}$$

$$\sum_{k=1}^{K} x_k \leq N \quad \{3.6\}$$

$$y_{ikj} \leq x_k \quad \text{for i = 1:M; j=1,2; k} \in A(i,j) \quad \{3.7\}$$

The equations above represent the formulation for the optimization problem. Equation 3.3 is the objective function for minimization of the weighted average runway occupancy time. Equation 3.4 is about the constraint that every aircraft should get assigned to an exit, while equation 3.5 is to ensure a feasible mix of runway exits. Equation 3.6 ensures that we won't exceed the maximum number of allowable exits, and the last equation is to make sure that only the constructed runway exits will be utilized.

For understanding how the optimization algorithm works, we show a simple example of designing a new runway with three suggested high-speed exits. For this run we chose a runway with 9,000 (ft.) length and the following fleet mix of aircraft. We asked the optimization algorithm to give us three suggested locations for high speed exits and a minimum separation criteria of 750 (ft.).

Table 9. Fleet Mix for Optimization Mode Example.

Aircraft	Fleet Share
A319	10
A320	10
A321	10
B737	10
B752	10
CRJ2	10
DH8D	10
E145	10
E170	10
E190	10
Total	100

For the optimization example we ran 100,000 iterations of the simulation to generate landing roll points initially. After the first set of candidates are generated, we find the minimum landing roll distance for any of the airplanes within the fleet mix table. That point becomes our first candidate and we then create our secondary exit candidates. The secondary exit candidates are built based on the minimum separation criteria between every consecutive runway exits. Therefore, we pre-

allocate a vector from the minimum landing roll distance all the way to the given runway length with steps of 750 (ft.). After running the DP algorithm three runway exits will be selected in a manner which they could minimize the weighted average runway occupancy times. Figure 57 represents the imaginary test runway, the generated landing roll distances all the way to the candidate exit location, and the associated runway occupancy times for each generated profile. 98.5% of the generated flights are assigned to the three given locations. The remaining 1.5% of the random flights will be assigned to pseudo right-angle exit which is automatically built at the end of the runway end for each set of runs.

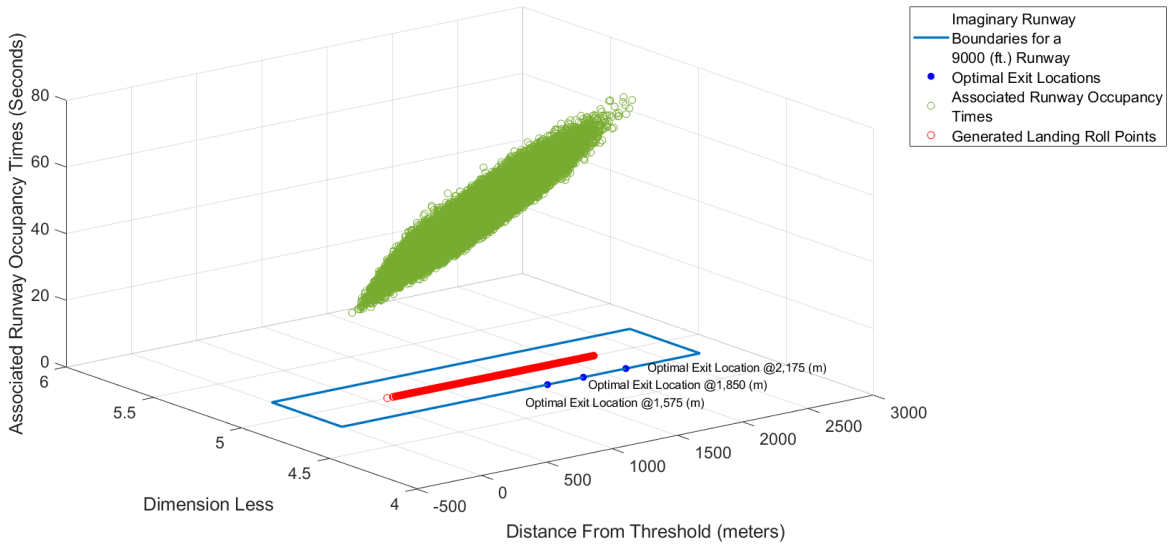

Figure 57. Generated Landing Roll Distances, Associated Runway Occupancy Times, and Suggested Optimal Exit Locations for the Optimization Test Case.

3.6.3 Improve an Existing Runway

In this mode the user wants to improve the ROT by utilizing the existing gap between some runway exits and building a new runway exit. The improve mode in the new version of the model is very similar to designing a brand new runway, with a minor difference. In this mode instead of having

the minimum generated landing distance as the first potential candidate for a new runway exit, we have a given horizontal distance on the runway entered by the user, as the first potential candidate. Similarly, for the last candidate instead of the runway length, we have a second entered horizontal distance on the runway which identifies the final threshold for constructing a new runway exit. Note that it is very important whether each of the entered distances (runway exits) are considered to be open for arrival flights or not. If the user mentions that the beginning and ending of the desired gap are close to flights, we consider the input distances as allowable candidates for new runway exits, otherwise depending on whichever of the input exits to be closed, we consider the first candidate as 750 (ft.) from each of the opened exits.

3.7 Results and Evaluation

In this section, we look at our model's results for all the airports after running the ordinary evaluation model. We compare the ROT values resulting from the simulation model with those observed from the real data. For evaluating the results, we compared the weighted average ROT at each facility for both simulation and real data, and we reported the absolute error and squared root error between the predicted values and real ones. The following table summarizes all the information regarding the validation process by showing the average ROT from simulation, average ROT from data, the absolute error between those values, and the squared root errors. We reported the weighted average errors by considering the number of total operations collected from the ASDE-X data. The values shown in Table 10 are related to the weighted average ROT, but we considered the exit utilization patterns and the cumulative density functions for exiting distances while calibrating the estimator logics. In chapters four and five exit utilization comparison graphics are shown for validating the logic of model not only in estimating correct runway occupancy time, but also the correct exit assignment for each individual aircraft type.

Table 10. Comparison of Real ASDE-X ROT Collected Data and Simulation Results for all the 37 ASDE-X Supported Facilities.

Airport Code	Weighted Average Data ROT (s)	Weighted Average Simulation ROT (s)	Absolute Error (s)	Squared Error
ATL	47.3	48.4	1.1	1.21
BDL	57.7	56.8	0.9	0.81
BOS	49.6	50.3	0.7	0.49
BWI	52.9	51.8	1.1	1.21
CLE	50.9	52.1	1.2	1.44
CLT	48.7	48.5	0.2	0.04
DCA	43.0	41.9	1.1	1.21
DEN	58.1	57	1.1	1.21
DFW	52.1	51.5	0.6	0.36
DTW	51.9	51	0.9	0.81
EWR	44.0	42.8	1.2	1.44
FLL	48.3	46.9	1.4	1.96
HNL	59.7	59.2	0.5	0.25
HOU	47.2	46.9	0.3	0.09
IAD	50.0	50.4	0.4	0.16
IAH	53.5	54.4	0.9	0.81
JFK	52.4	52.9	0.5	0.25
LAS	49.9	48.7	1.2	1.44
LAX	51.4	51.6	0.2	0.04
LGA	42.6	43.2	0.6	0.36
MCO	55.9	54.6	1.3	1.69
MDW	42.6	43.9	1.3	1.69
MEM	59.6	59.2	0.4	0.16
MIA	53.4	52.9	0.5	0.25
MKE	51.8	50.6	1.2	1.44
MSP	50.3	50.8	0.5	0.25
ORD	48.2	48.7	0.5	0.25
PHL	50.1	51	0.9	0.81
PHX	49.6	48.3	1.3	1.69
PVD	52.9	51.7	1.2	1.44
SAN	49.9	50.7	0.8	0.64
SDF	55.2	54	1.2	1.44
SEA	49.6	48.4	1.2	1.44
SFO	58.9	60	1.1	1.21
SLC	52.0	52.8	0.8	0.64
SNA	47.2	46.8	0.4	0.16
STL	55.4	54	1.4	1.96
Weighted Average ROTs	50.7	51.3	-	-
Mean Absolute Error (MAE)	0.82			
Root Mean Squared Errors (RMSE)	0.89			

As shown in Table 10, the real ROT values observed at the airports are pretty close to the estimated values from the data-driven simulation approach. For generating the numbers in Table 10, the real fleet mix of each facility on each runway was utilized. We ran the simulation model on each runway with the associated unique fleet mix for that runway, and we collected the weighted average ROT from each runway at each facility. Then we calculated the weighted average ROT based on the number of operations on each runway for each facility. Those results are shown in the third column of Table 10. The associated ROT values from the ASDE-X data were calculated in the same way from the real data and they are shown in the second column of the table. As you can see the overall weighted average mean absolute error of ROT values between the real data and simulation model for all the operations at all the 37 supported airports is 0.82 seconds. The root weighted mean squared error for ROT values were 0.89 seconds. In 59% of the studied cases the simulation model predicted lower weighted average ROTs compared to the real data. This happens for potentially non-efficient exiting behavior at those facilities in the real world operations. In the remaining 41% of the cases the estimated values were higher than the real weighted average ROT times with a maximum difference of 1.1 seconds and a minimum difference of 0.2 seconds. After evaluating the error between observed and estimated ROT times, we ran a regression analysis between those set of values. The ordinary R-squared of regression between real ROTs and estimated ones was 95.8% and the adjusted R-squared was 95.6% which are promising results and shows the goodness of our data-driven approach in estimating ROT values. A more detailed visualization of the regression study can be found in Figure 58 where each data point represents the observed and estimated values for weighted average ROT at each facility. As we can see all the data points are within acceptable margins from the fitted line and estimated values are very close to the observed ones.

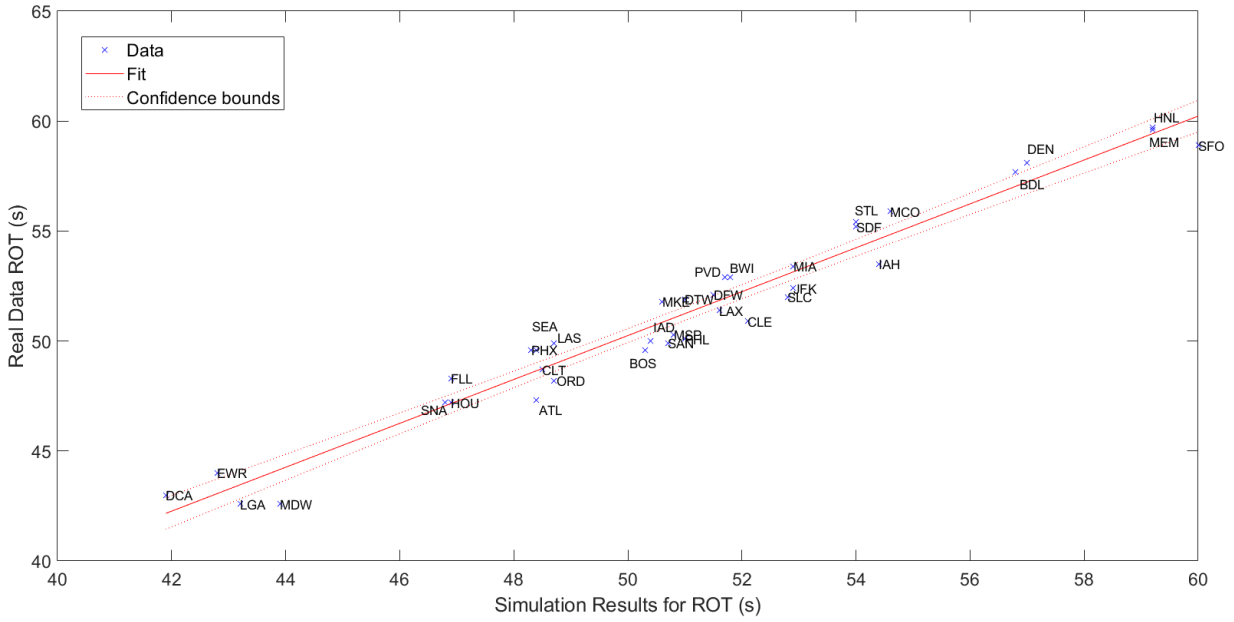

Figure 58. Linear Correlation Between Real ROT Values and Estimated Ones from the Simulation Model at the Airport Level.

3.8 Graphical User Interface (GUI)

A user interface was developed to implement the hybrid application for many tasks. There are currently three separate functionalities that the computer program can handle:

1- Evaluating an existing runway with its current runway exits and geometry in terms of exit utilizations and runway occupancy times prediction with user defined fleet mix.

2- Evaluating a new runway with user defined runway exit types and geometries in terms of exit utilizations and runway occupancy times predictions with user defined fleet mix.

3- Locating optimum exit types on a new runway without any knowledge of exit location and geometry (dynamic programming approach).

All the mentioned tasks can be done by the developed computer application with many interactive features provided for the users to evaluate various runway conditions.

The interactive computer application was developed originally in MATLAB, but a compiled executable format is available now. One of the most helpful features of the new designed program is its capability of showing the real airport layout of any of the 37 ASDE-X supported facilities around the US. Not only a user can look at the facility and its runway exit information, but also they can have a list of runway exits and the associated geometry information like the arc from the point of curvature to the exit hold-bar. The list of runway exits is sorted based on their distance from the runway threshold and an option is provided for the user to open or close whatever exit for their simulation scenarios. The visualization on the map can help the user to understand the impact of opening or closing specific runway exits which can be extremely helpful for planning purposes. Figure 59 shows the first screen of the computer application with all the provided features for different simulation scenarios. As you can see in the figure, there is a map axis provided for real runway simulations or user-defined runways. There are pull-down menus for airports in the database and their associated runway exits. There is a menu for 274 individual aircraft types that can be selected by the user with their desired percentages. The number of generated flights for each scenario can be defined by the user and also there's an option for running on dry or wet surfaces.

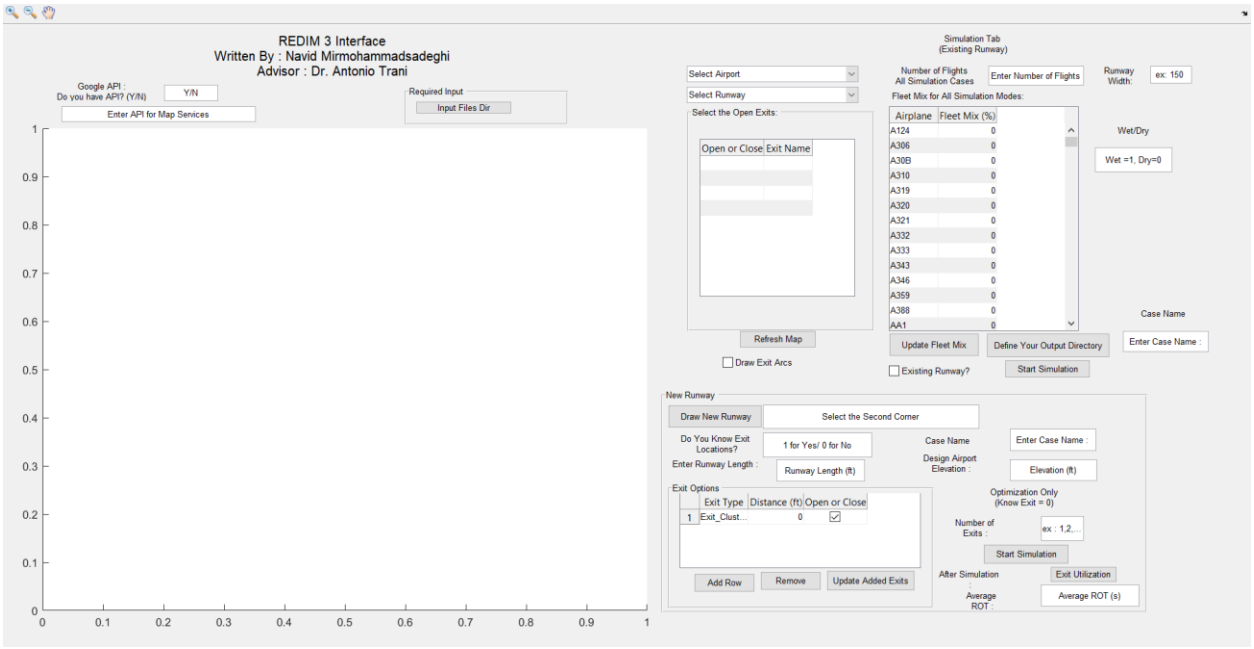

Figure 59. First Screen of the Developed New Interactive REDIM Application.

The user can select any of the 37 airports which have ASDE-X technology and evaluate the exit geometries and runways at those facilities by reviewing their real time Google map layouts. Moreover, by selecting the desired runway at the selected airport, the user will see a list of available runway exits based on the exit database that we have access to. The default for all the exits at all the locations is to keep them open for any simulation scenario, however based on operational constraints or user preferences the user can close whatever exit on the runway. Therefore, for that scenario the model won't assign any operations to any of the closed runway exits. Figure 60 shows the Charlotte International Airport (CLT) and runway 18L selected by the user.

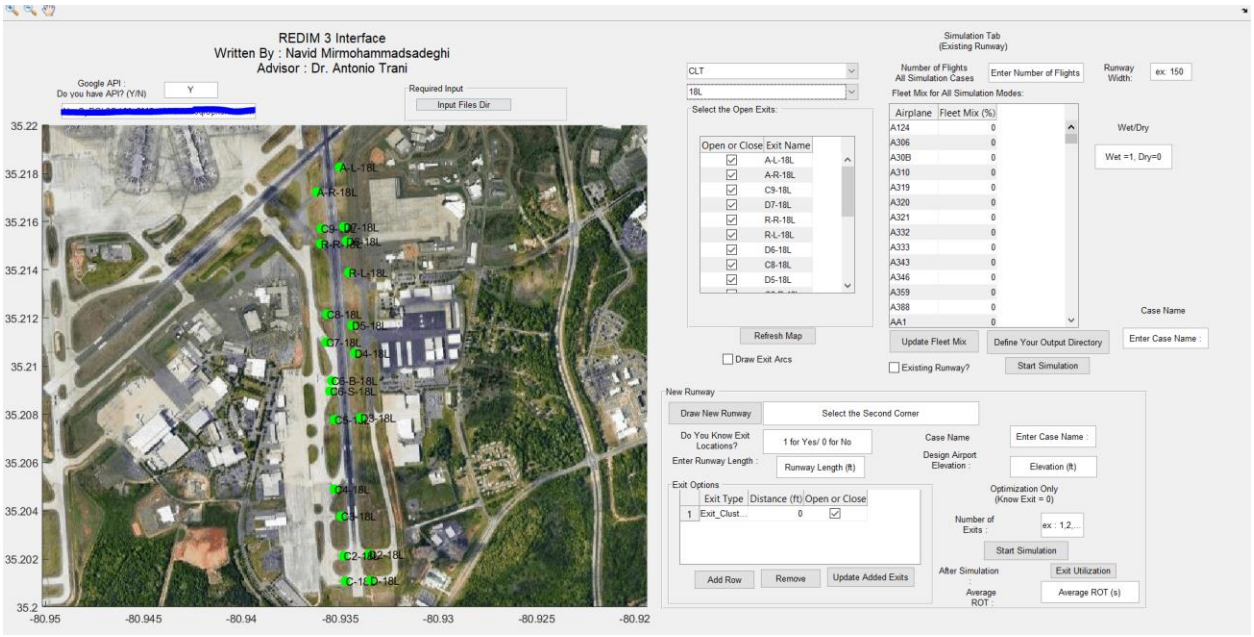

Figure 60. CLT Airport and Runway 18L Selected by the User for Analyzing ROT.

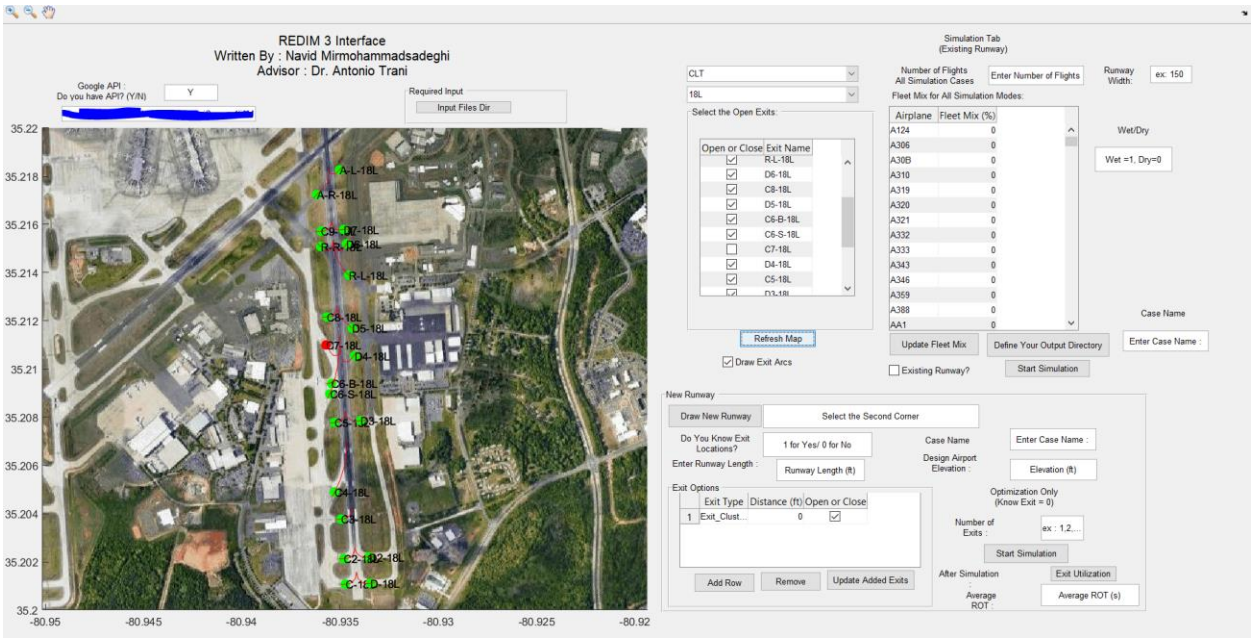

Figure 61. User Closed a Back-Turn Exit and you Can See the Exit Color Became Red.

Not only users can select any of the 37 airports from the database, but also they can run their own desired runway scenarios by drawing a rectangle in an AutoCAD-like environment, and then either

adding their preferred exit types and locations or asking the model to give them the optimum locations of exits.

Figure 62 shows a new runway that the user drew and they put three exits of their preferred types at three locations on the runway.

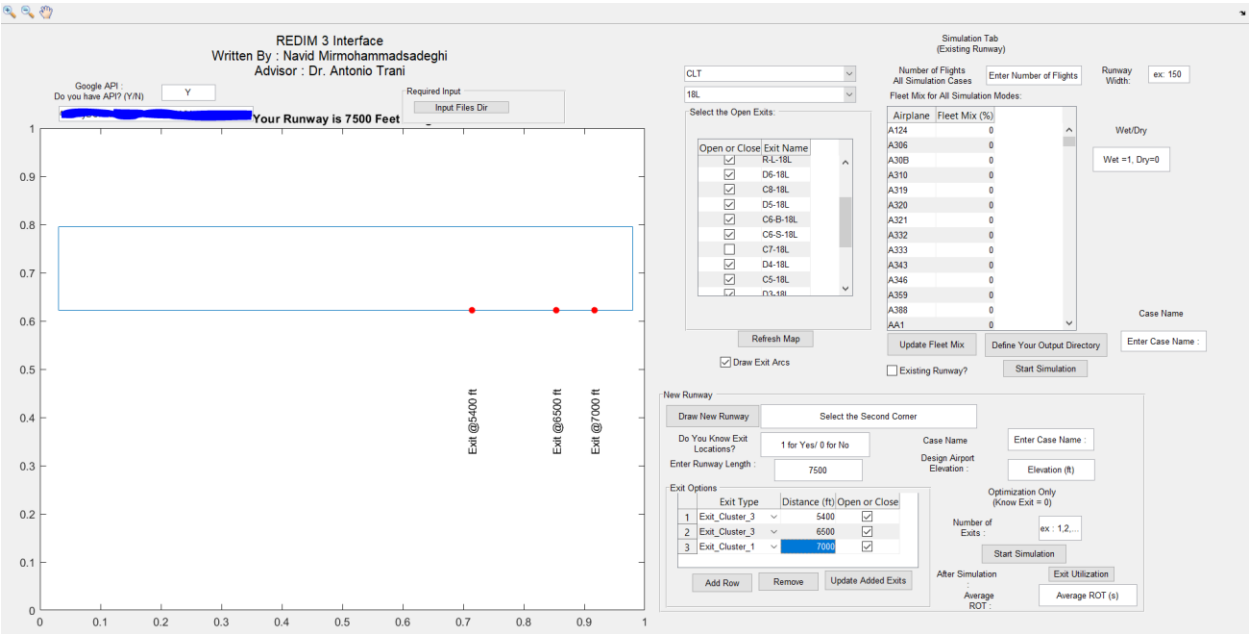

Figure 62.User Defined Runway with Known Exit Locations and Geometry.

The last analysis mode available to the users from the user interface is the optimization mode or new runway design. Here as we mentioned before the user should just draw a new runway in the provided section on the left hand-side, enter the aircraft fleet mix, enter the runway width and elevation, define the percentage of wet/dry, give the simulation case a given name and choose an output directory for the final output files to get saved there, and finally selecting the number of desired runway exits that he/she wants to construct on the new runway. The model runs the dynamic programming algorithm to find the optimum locations, draw the final found locations

over the runway (in addition to their distance from the threshold), and after that it runs an evaluation case with the new set of runway exits to calculate a weighted average runway occupancy time and to create the exit utilization table. Figure 63 shows a test runway drawn by the user and the length was selected to be 9,000 (ft.). After running the optimization algorithm, as you can see in the plot three optimal locations are shown with blue dots and their correspondent distances from the threshold considering a scale based on the drawn rectangle side length and the given input length for the simulation runway length. Not only for each run a comma separated value (.csv) file will be saved in the defined output directory which includes the generated random numbers for each simulated flight, but also users can click on the exit utilization tab in front of "After Simulation" panel and they can see the exit utilization for each individual aircraft type at each of the runway exits. Clicking on that option not only opens up a new window in the application environment, but also it saves an excel file in the output directory in case the user wants to do some statistical analysis on the output data.

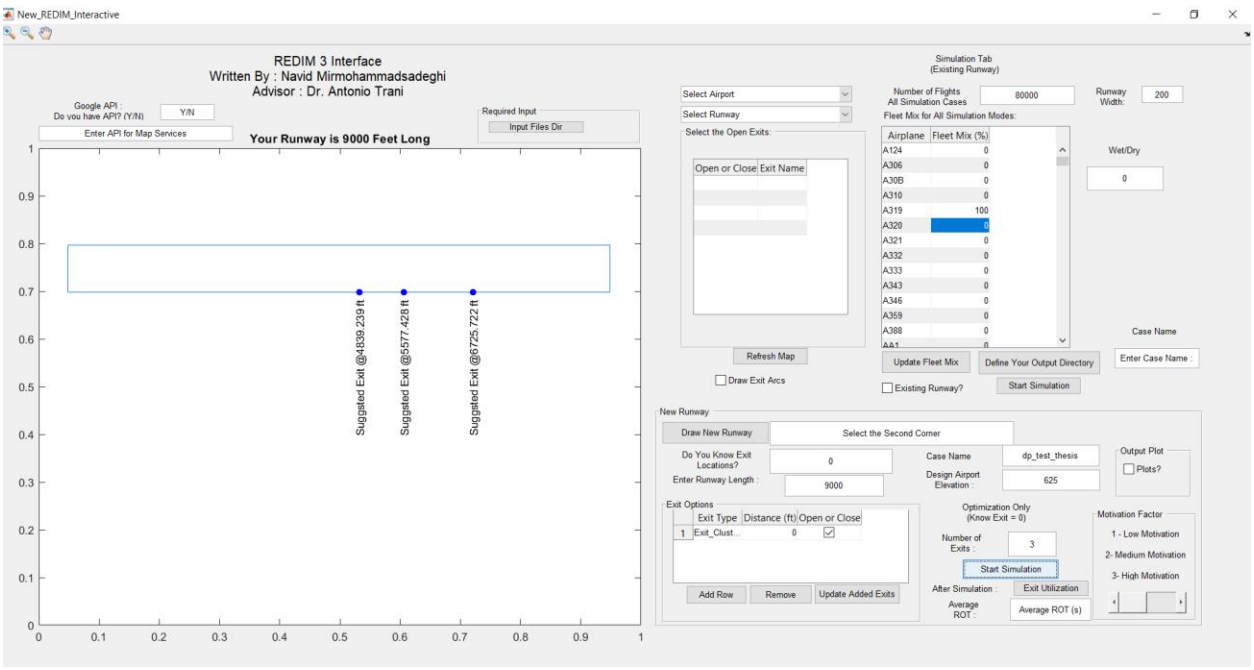

Figure 63. Results of the DP Algorithm Are Shown on the Imaginary Drawn Runway with Their Associated Distances from the Threshold.

3.9 Conclusion

In this chapter, we covered the material for the new simulation model that can simulate arrival flights and calculate runway occupancy times. Since the air traffic control regulations had significant improvements recently, the pair-wise separation between arrival flights has reduced considerably. Therefore, for many aircraft pairs, the minimum separation is the runway occupancy time of the leader plane. This means that for having safe and smooth operations at airports and to avoid many go-arounds which cause extra fuel burn, money loss for carriers, and extra travel time for passengers we have to have an accurate knowledge about the distribution of runway occupancy times for each class of aircraft on each specific runway with various runway exit configurations. Understanding the landing behavior of various aircraft types can also help the ground movement at airports to be smoother and more efficient. Since there are not many practical attempts for

predicting runway occupancy times under various circumstances, we developed and upgraded an older version of the Runway Exit Design Interactive Model (REDIM) to help the airport planners and authorities modeling their facilities in a very realistic way to predict the distributions of the runway occupancy times and runway exiting distances for their fleet mix. The new version of the model implements a data-driven approach to model the landing profile of airplanes for the first time. Previous attempts for predicting runway occupancy times were based on naïve video data or manually collected data. The data used for this study comes from Airport Surface Detection Equipment Model-X (ASDE-X) which is a surveillance system installed at 37 US airports. Two years of data was analyzed and engineered to form the required distributions for the simulation model. One important aspect of this novel simulation approach is that it is aircraft-based. Meaning that users can model single individual aircraft types while they're certain that data behind each aircraft type is unique and belongs only to that aircraft type. Another new aspect of this model is the capability of modeling exiting speeds stochastically. Previous version of the model was programmed based on single data entry for limited runway exit types, while the new version covers a big variety of runway exits and group them based on their geometry features and then within each iteration of the simulation it randomly generates appropriate exiting speeds which makes the modeling of aircraft behavior more realistic. This is the first time that such application is developed based on the recent collected airport surface data, which can reflect the performance of the new generation of commercial aircraft types better than older versions of the runway exit model which was calibrated based on limited video data for few aircraft types. Moreover, for the first time, this model provides deep insights about the weighted average runway occupancy times and exit utilizations, but it also saves useful output files for the users and gives them detailed information for each simulated flight and the generated random events. This way users can analyze the results

even further and get deeper understanding about their simulation scenarios. The novel methodology represented in this chapter is the first of its kind which combines machine learning and Monte Carlo simulation techniques. For the first time, clustering algorithms were used to categorize runway exits and runways based on their geometry features. Then, non-parametric Kernel distributions were formed for critical landing moments. Monte Carlo simulation was used to replicate landing profiles from the appropriate distributions selected from clustering algorithms. This is the first time that big data was handled by using a combination of machine learning and Monte Carlo simulation to predict runway occupancy times and exit utilizations. The output of this model can be used in airport master plans for future improvements or constructions. Since the results are proved to be accurate mathematically, this model can help many consulting firms and airport authorities to include the results in their project proposals or airport master plans.

Chapter 4. Real World Case Studies of Four Airports Using New Version of REDIM Model

After calibrating the simulation model and evaluating it on various runways and at various airports, upon request of FAA, we tested the new developed simulation model on some real-world test cases to provide deeper insights into some facilities' performance in terms of the runway occupancy times. Air traffic controllers, airlines, and airport authorities constantly monitor the airports' operations to find bottlenecks and improve traffic flow and ground movement efficiency at airports [40]. Obviously, one of the major areas of operations at airports are runways and arrival flights have important role on the overall traffic flow at airports. Since many airports in the United States were built many years ago and the demand and number of operations have changed significantly through years, many of those airports don't have the efficient infrastructure to handle the operations more optimally. One of the bottlenecks on the runways is runway exit configuration. Depending on the runway exit type and distance from the threshold and the type of aircraft that uses the facility, we might see various behavior while landing and vacating the runways. Therefore, many times due to non-standard runway exit construction or non-optimally located runway exits or non-adoptive exit configuration based on new aircraft fleet mix, we can see inefficiencies in runway evacuation phase. In such situations many airplanes have to stay on the runway for extra non-necessary time and would reduce the arrival capacity under new separation systems. Moreover, by having non-efficient taxiway designs, the overall taxi time for airplanes increases, which is not desirable for passengers or operators. Since runways are considered as entrance gates for arrival flights to the airports, improving the traffic flow on runways has considerable impact on the overall ground movement of arrival flights at each airport.

Each studied scenario is a current ongoing project at both the FAA and the airports of the study. Each case has unique characteristics and the requested items for each study might vary. For example, at some facilities there is a task for finding the optimum location for new high-speed exits. While at some facilities the importance of specific runway exits is asked and the question is that if due to construction projects one or few runway exits will be closed, what will be the impact on the ROT values. This chapter will look at the case studies at each airport and provide practical answers to the challenges at each facility. The results and findings were presented to both FAA and each of the studied airports' administrations. The findings for each case study can help decision making for future construction projects and perform the cost-benefit analysis for each facility.

4.1 Boston Logan International Airport (BOS)

Boston Logan International Airport (BOS) is the first case study that we analyzed after calibrating the new version of the runway exit simulation model. Upon request of FAA, we had to analyze a couple of scenarios at this facility and look for improvement options for two runways to improve ROT's performance on those runways. BOS had 368,074 validated arrival operations in the landing database. This airport has 6 runways and hence 12 runway ends which based on the data retrieved from the landing database we could find operations on 11 runway ends captured by the ASDE-X system. Figure 64 represents the layout map for BOS airport including all of its runways and terminal areas [37][38].

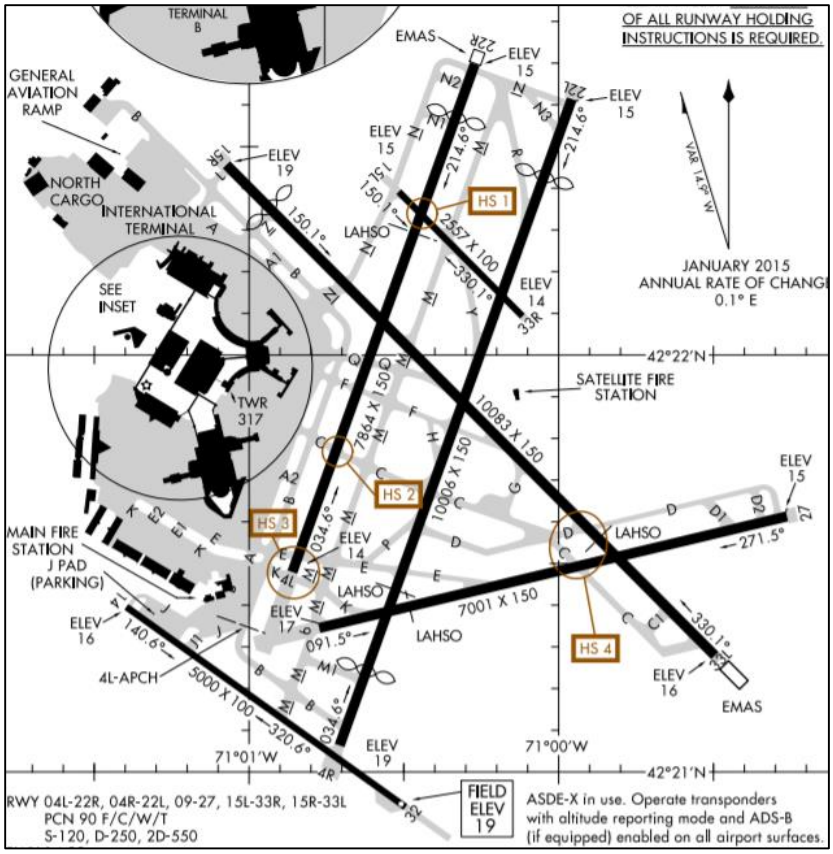

Figure 64. BOS Airport Layout for Runways and Terminals. [Source: FAA]

Before reviewing the problem statement for this facility, we took a look at the statistics of the operations at BOS. Figure 65 for example, depicts the share of operation counts on each runway end during years 2015 and 2016. Based on the data shown in the plot, 27.4% of the arrival flights at BOS land on runway 04R. After that runway we have the following runway ends which account for 61.2% of the entire operations together: 22L, 27, and 33L. Since the area of study for each of those runways is the runway occupancy time, we have to study the airport fleet mix and runway occupancy times distributions.

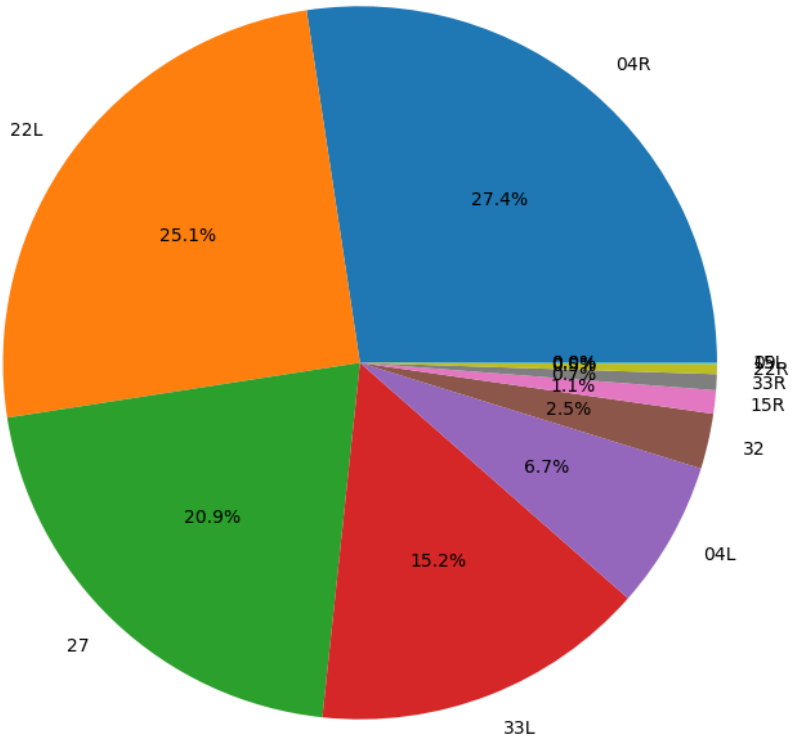

Figure 65. Share of Operations Counts on Different Runway Ends at BOS Airport.

Figure 66 shows the cumulative density function for the runway occupancy times on different runway ends at BOS airport. This plot has some interesting patterns about the ROT data. The very left CDF line represents the values for runway 15L which is just 2,557 (ft.) long and it has the lowest average ROT with a value of 32.9 seconds. The main arrival runway at this facility is runway 04R and its average ROT is 45.8 seconds with a standard deviation of 10.5 seconds. This value is very similar to the parallel runway which is runway 04L and its average ROT is 46.5 seconds.

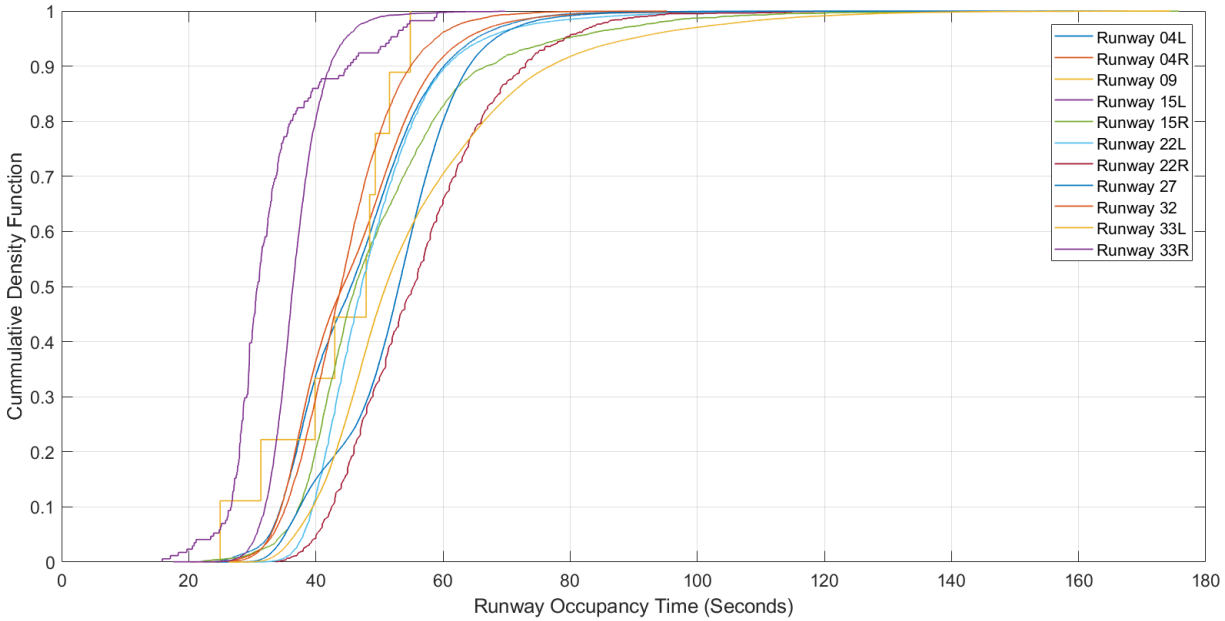

Figure 66. CDF Plots of Runway Occupancy Times on Different Runway Ends at BOS Airport.

Figure 67 represents the fleet mix of aircraft types at BOS for all the planes which showed up in ASDE-X data from 2015 to 2016 more than 500 times at this airport. The top two popular aircraft types at BOS were Embraer E190 and Airbus A320. This facility doesn't have many big airplanes of class heavy and there are small percentages of Boeing B747-400s, Boeing B767-300s, and Boeing B767-300s.

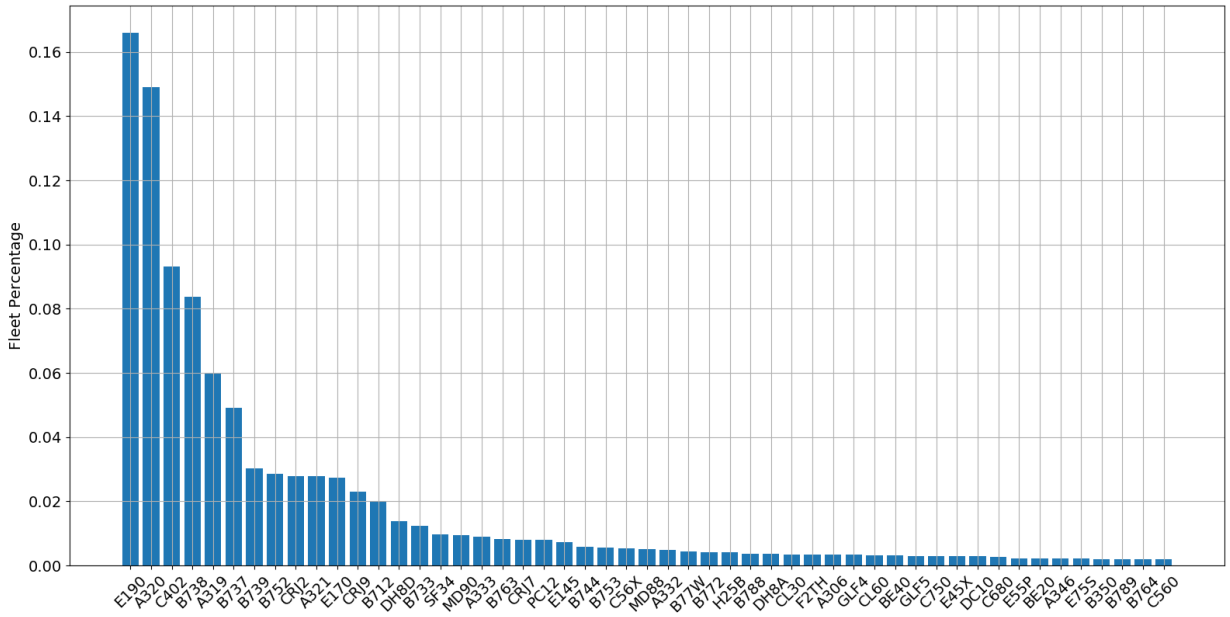

Figure 67. BOS Airport Fleet Mix Share for Each Aircraft type.

4.1.1 Runway 04R

One of the runways that the study focuses on is runway 04R. This runway is the primary arrival runway at BOS airport and it needs further research on landing behavior and ROT performance. Table 11 represents the exit utilization and average ROT for each runway exit utilized on this runway. As we can see 25% of flights on this runway take runway 33R-15L for evacuating the runway. This is not a standard runway exit and pilots take the intersecting runway as an option for vacating the runway. Since the average exiting speed for this intersecting runway is just 19 knots, airplanes had to slow down and stayed on the runway for longer time, therefore the runway occupancy time increases due to non-standard geometry of this exit. The airport authorities are interested to see how they can improve the ROT behavior on the runway by eliminating runway 33R and replacing that with high-speed exit in the open area between runway exits Y and R.

Table 11. BOS Runway 04R Exit Utilization and Average ROT.

Exit Name	PC Distance (feet)	Exit Utilization (%)	Average Runway Occupancy Time (s)
D	2052	0	30
P	2098	0	36.5
C-L	2590	3	33.7
H	3005	3.5	33.6
F-L	3502	2	38.6
15R	4038	4	44.1
Y	4457	45	39.4
15L	5731	25	52.7
R	6524	17.5	56.7
N	8592	0	117.5

Since the intersecting runway 33L-15R is absorbing 25% of the flights on this runway and it is located between two high-speed exits, it is worth it to take a look at the exiting speed distributions for each of those exits and see whether it makes sense to demolish the existing short runway and replace it with a high-speed exit which provides better geometry features or not. Figure 68 plot represents the current exiting speeds at each of the utilized runway exits on runway 04R.

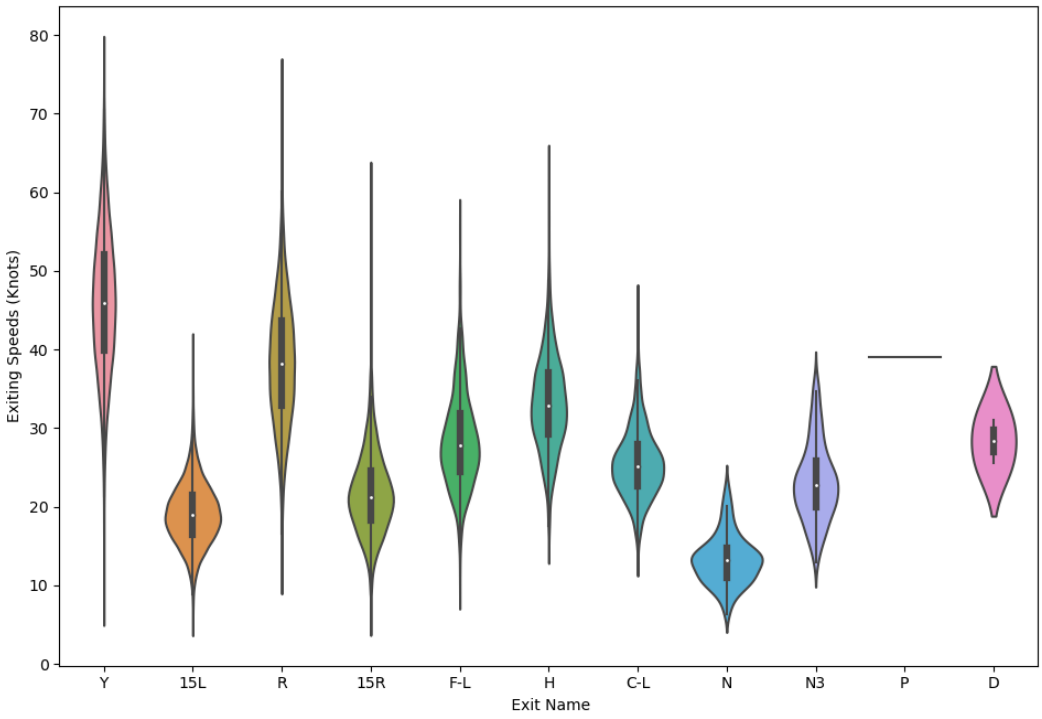

Figure 68. Violin Plot for Exiting Speeds at the PC Point for Each Exit on Runway 04R at BOS.

As we can see in Figure 68, intersecting runways 15L and 15R had very low exiting speeds due to their restricted geometry, while the two high-speed exits on the runway which are Y and R had higher exiting speeds and therefore they could help reducing the ROT time. This analysis proves to us that it makes sense to demolish the intersecting runway 33R-15L and construct a new high speed exit in the opening gap. This problem is a typical improvement case where we already have a runway and bunch of runway exits, but we explore our options for constructing new exits to optimize the runway occupancy time. By using the fleet mix for this runway and the exact runway exit configurations, we ran the improvement algorithm which is a dynamic programming model trying to find the optimal location of the new high-speed exit. Since the airport authorities want to not only close runway exit 15L, but also to improve the location of the current two high speed exits on the runway, the potential gap will be between runway exit 15R at 4,038 feet and high-

speed exit R at 6,524 feet. We ran multiple scenarios and compared the ROT among all of them. Table 12 represents the scenarios that we ran for this specific runway.

Table 12. Simulation Scenarios for Runway 04R at BOS.

Scenario	Location of New High-Speed Exit (ft)	Remarks
Baseline	Not applicable	All exits open
Scenario 1	Not applicable	Do not allow use of Runway 15L/33R as a runway exit
Scenario 2	5,000	Replace Yankee with a new high-speed exit
Scenario 3	5,100	Replace Yankee with a new high-speed exit
Scenario 4	5,500	Replace Yankee with a new high-speed exit
Scenario 5	HS1 = 5,000 HS2 = 6,000	Replace Yankee with a new high-speed exit Replace Romeo with new high-speed exit
Scenario 6	HS1 = 5,000 HS2 =5,750	Replace Yankee with a new high-speed exit Replace Romeo with new high-speed exit

There are two important parameters which we are looking for:

1- The reduction in the weighted average runway occupancy time for improved scenarios

2- The reduction in the standard deviation of runway occupancy times after improving the configuration. This parameter is important since it can be a good reference for controllers and they would know that the new configuration will restrict the variability of behaviors on the runway and in future their confidence for applying separations will be higher as airplanes have better predictable ranges of ROT.

The following bar chart reflects the simulation results for each scenario. Based on the DP algorithm the optimal location of a new high speed exit, will be at 5,000 feet and by eliminating current exits Y and 15L, the WROT will be reduced by 2 seconds while the standard deviation will be reduced

by 3.2 seconds which is a significant change. The other scenario which yielded the same gain was scenario 6, however the ROT gain by moving current taxiway Romeo was not very significant.

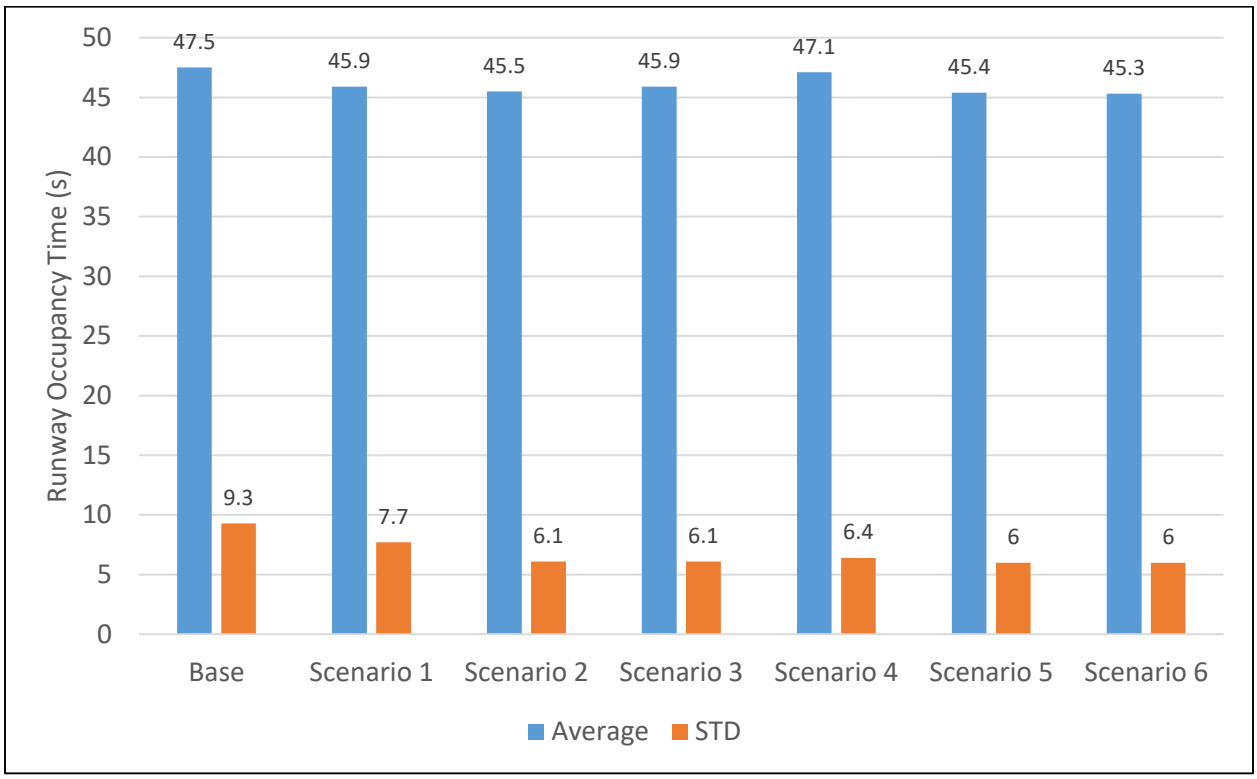

Figure 69. Different Scenarios on BOS Runway 04R, Average and Standard Deviation ROTs.

Therefore, our recommendation after this study for this runway is to demolish the current intersecting runway and replace the exit Y location from 4,457 feet to 5,000 feet and that will save 2 seconds of WROT and 3.2 seconds in ROT standard deviation. Currently taxiway Romeo absorbs around 17% of the operations and our study shows that it is not recommended to replace its location and it would be better to keep that runway exit at its current location.

4.1.2 Runway 33L

Runway 33L accounts for 15.2% of the operations at BOS airport. Not all the times airport controllers are interested in just reducing the ROT times. Sometimes due to many dependencies on intersecting runways they might be interested to evaluate the impact of re-configurations of

runway exits to see whether it's worth it to help the arrival flow by changing ROT or not. This is the case for this runway. The airport authorities wanted to see what would be the impact on the ROT values by closing a high-speed exit and moving it further down on the runway, or closing the current and new proposed high-speed exits and construct a right-angle exit further down the runway. Figure 70 shows runway 33L at BOS and all of its current runway exits. We can see in the plot that high-speed exit Q is colored as red which means that we don't want to assign any flights to that. The main operational reason is that flights who take this taxiway will have to continue taxing on another active runway and that causes many dependencies with the intersecting runway.

Figure 70. BOS Runway 33L Exit Configuration with Taxiway Q Shown as Closed.

Table 13. BOS Runway 33L Exit Utilization and Average ROT.

Exit Name	PC Distance (feet)	Exit Utilization (%)	Average Runway Occupancy Time (s)
D-L	2500	0.04	33.9
G	3763	0.01	48.5
F	4035	16.6	40.5
04R	5072	0.06	58.6
Q	5188	53.8	47.6
M-L	6117	0.6	57.2
M-R	6206	0.1	69.3
04L	6715	5.5	62.1
N-LS	7426	0.03	78.3
N-LB	7492	19	73
N-R	7539	0.08	82.4
Z	8946	1.5	93.5
L	9860	2.5	110

As we can see in Table 13, runway exit Q is an essential exit for runway 33L. This runway exit absorbs around 54% of the operations on this runway and provides a very reasonable ROT performance with an average of 47.6 seconds. This means that if arrivals on this runway won't be able to take this exit, they're going to have higher values of ROT. The following violin plot represents the exiting speeds at PC points on this runway and clearly tells us the reason behind acceptable ROT performance for high-speed exit Q. As figure 71 represents, the three high speed

exits on this runway were taken at higher speeds at their PC points, therefore they could help reducing the WROT on the runway. High-speed exit Q has two taxi-way branches leading to two different hold-bars, however the path length and radius all the way to the branching point is the same. That is the reason that two high-speed exits are related to Q (Q1 and Q2). As you can see branching didn't have that much impact on the exiting speed at the PC point. All in all, from the exit utilization and ROT study in this analysis, we noticed that exit Q is very essential and the potential proposal for replacing with a further high-speed exit or right-angle exit would probably increase the weighted average runway occupancy time.

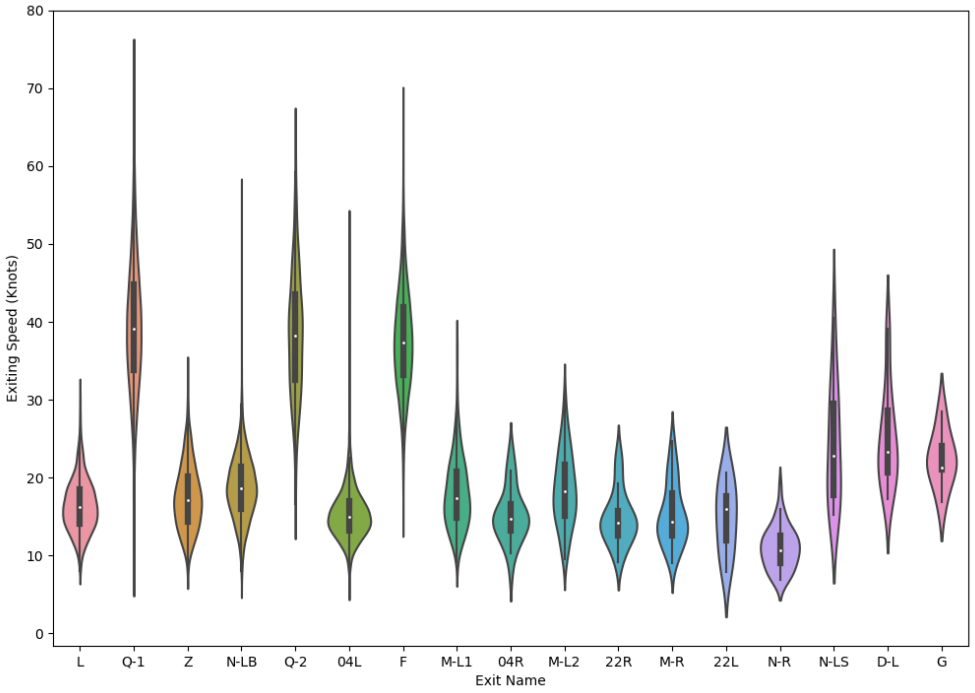

Figure 71. Violin Plot for Exiting Speeds at the PC Point for Each Exit on Runway 33L at BOS.

Similar to runway 04R, we ran multiple scenarios on the runway to evaluate the airport authorities' proposal for re-configuring the runway exits. Table 14 summarizes the scenarios that we ran for runway 33L.

Table 14. Simulation Scenarios for Runway 33L at BOS.

Scenario	Location of New High-Speed Exit (ft)	Remarks
Baseline	Not applicable	All exits open
Scenario 1	Not applicable	Close Quebec (Q)
Scenario 2	5,350	Replace Quebec with a new high-speed exit at 5,350 feet. New HS exit has a 37 degree angle, 1500 ft radius and 700 feet distance to hold bar. Runway exit Mike (M) is still usable.
Scenario 3	7,010	Close Quebec (Q) and proposed Uniform (U) exits Add a new runway exit with radius 200 feet (path length 400 feet) and 115 degree angle.

The problem on runway 33L at BOS is interesting since airport controllers are curious to evaluate a situation where they will avoid taxing on another active runway after evacuating runway 33L, while they're not sure about the additional runway occupancy time as the consequence of changing the runway exit configuration. This is a classic example where a reliable simulation model can be used to help decision making. This point is critical as we know many runways all around the world might have non-efficient runway exit configuration or have taxing restrictions. Without using a simulation model it is hard to judge what would happen if significant changes were applied to the runway exit configuration. Therefore, designers and planners can use the new version of the hybrid simulation model to evaluate any changes on the runway before making non-optimum decisions.

The following bar graph summarizes the results for all the four scenarios that we ran for BOS runway 33L. As we predicted demolishing taxiway Q and replacing that with any high-speed exit or right-angle exit further down range of the runway will have a negative impact on the runway occupancy time.

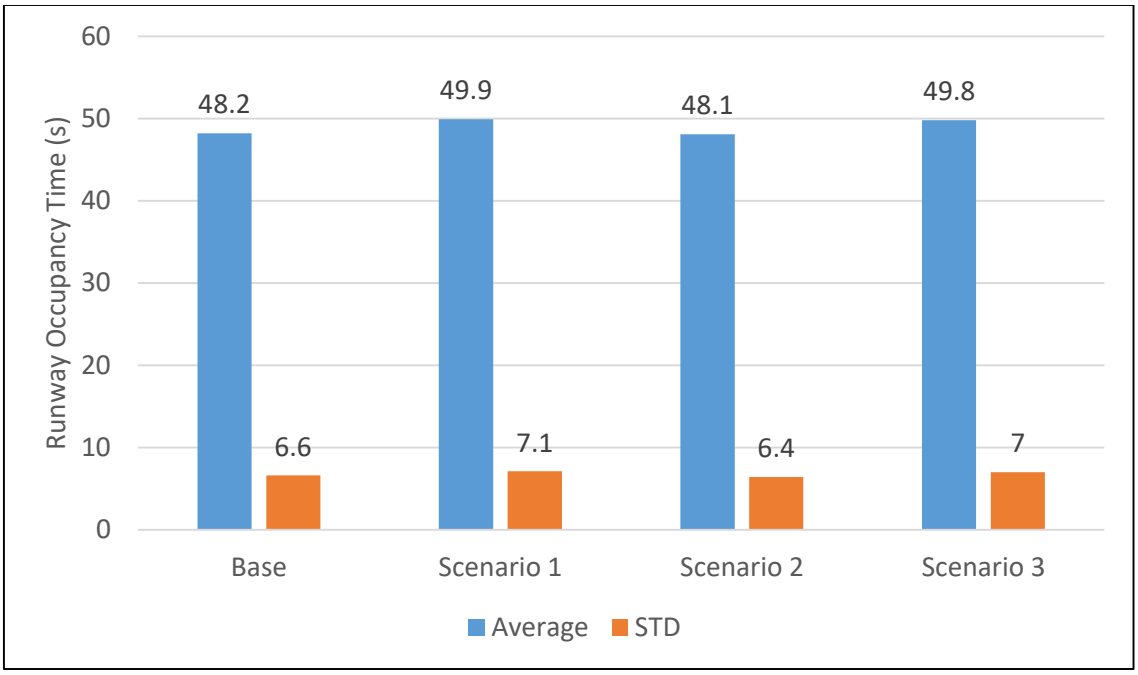

Figure 72. Different Scenarios on BOS Runway 33L, Average and Standard Deviation ROTs.

Our conclusion on this study is that by replacing high-speed Q from 5,188 feet to 5,350 feet, we won't have much difference in both weighted average and standard deviation of runway occupancy times and there's going to be a difference of 0.1 seconds. However, the runway will potentially have an increased weighted average runway occupancy time for 1.6 extra seconds in weighted average and 0.4 seconds in standard deviation if we close high-speed exit Q and build a new right angle exit at 7,010 feet from the threshold. Both of the case studies were presented to FAA sponsors and BOS airport authorities and relevant consulting firms which were trying to do the same analysis.

4.2 Philadelphia International Airport (PHL)

Philadelphia International Airport (PHL) was the second real world case study that upon request of FAA, we were tasked to utilize the new version of the simulation model and study the ROT performance at this facility. This airport accounts for 376,822 arrival flights in the landing database. The airport layout of PHL is shown in the following figure.

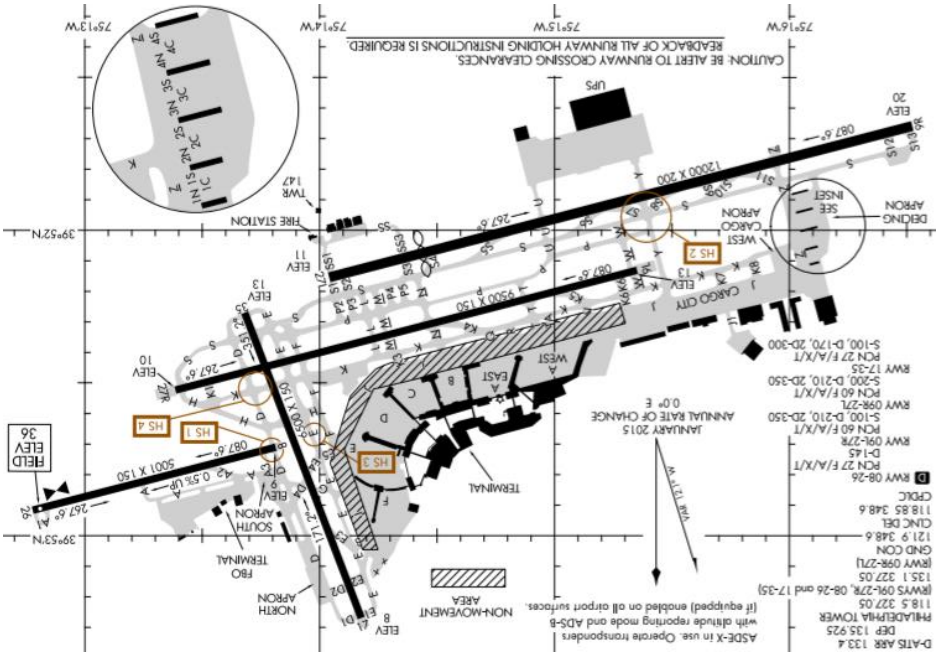

Figure 73. PHL Airport Layout. [Source: FAA]

The runway for this study is 27R which is actually the primary arrival runway at PHL. According to the following pie chart this runway accounts for 48.6% of the entire arrivals at this airport which is a significant share. The fact that this runway is responsible for almost half of the arrival operations, rings the bell that in terms of capacity and traffic flow this is an essential part of the entire airport. Both FAA and the airport authorities are seeking ways to improve the arrival operations ROT performance on this runway, therefore we review a few more statistics about the operations on this runway and then analyze the problem in more detail.

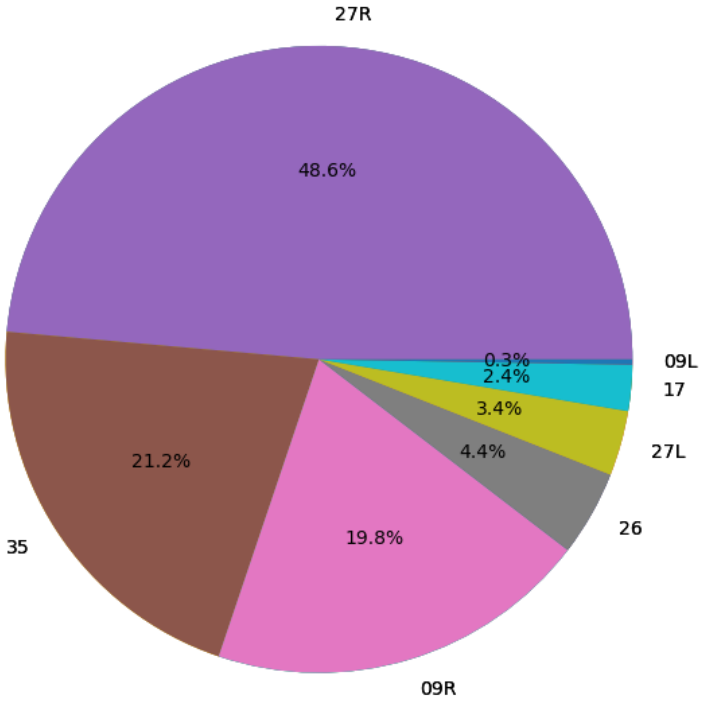

Figure 74. PHL Share of Arrival Operations on Each Runway End According to the Landing Database.

As usual we need to know the operational fleet mix of airplanes for each of our case studies. The following bar chart represents the fleet mix percentage for every aircraft that showed up in the database for more than 100 times during years 2015 and 2016. Based on this chart CRJ-200 with a fleet percentage of 22% was the dominant aircraft in the fleet mix. After that, we have Embraer E170 and De Havilland DH8A with 11%, and Airbus A321 with around 9% of all the operations. We model all the aircraft types from the fleet mix for all of our simulation scenarios and we choose a high number of iterations for each run of the model, in order to make sure that the behavior is steady for every entered aircraft from the fleet mix.

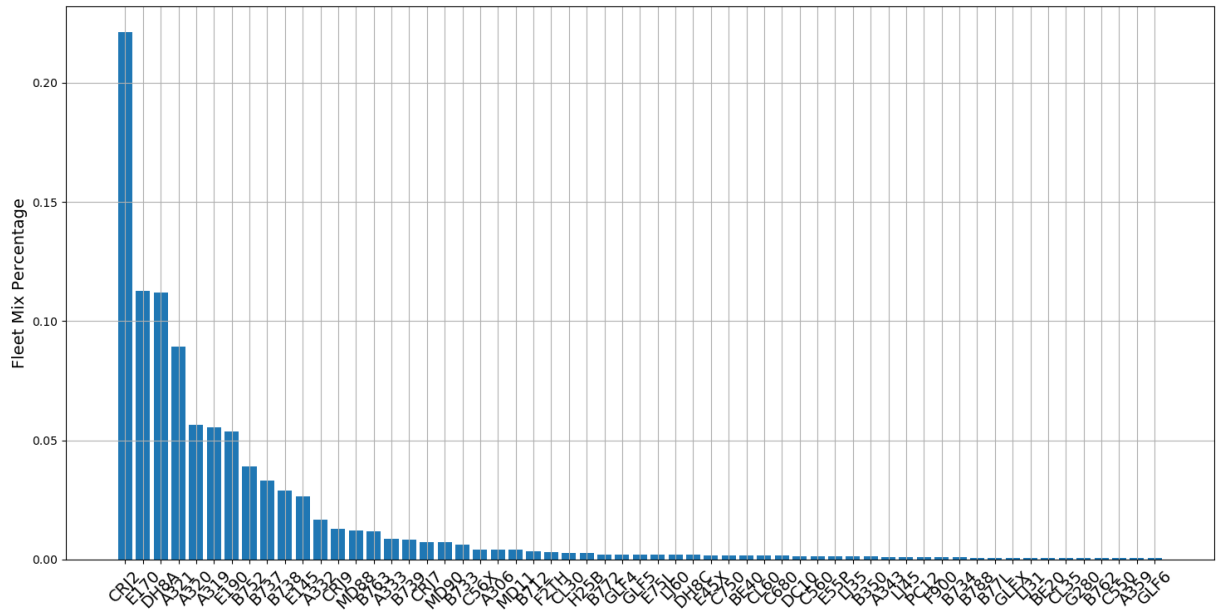

Figure 75. PHL Fleet Mix of Different Aircraft Types Based on Landing Database.

Since we are studying the ROT behavior of the runway ends at PHL, it is valuable to take a look at the cumulative density plots for ROT on every runway end. The following figure represents the CDF plots for ROTs on each runway end at PHL.

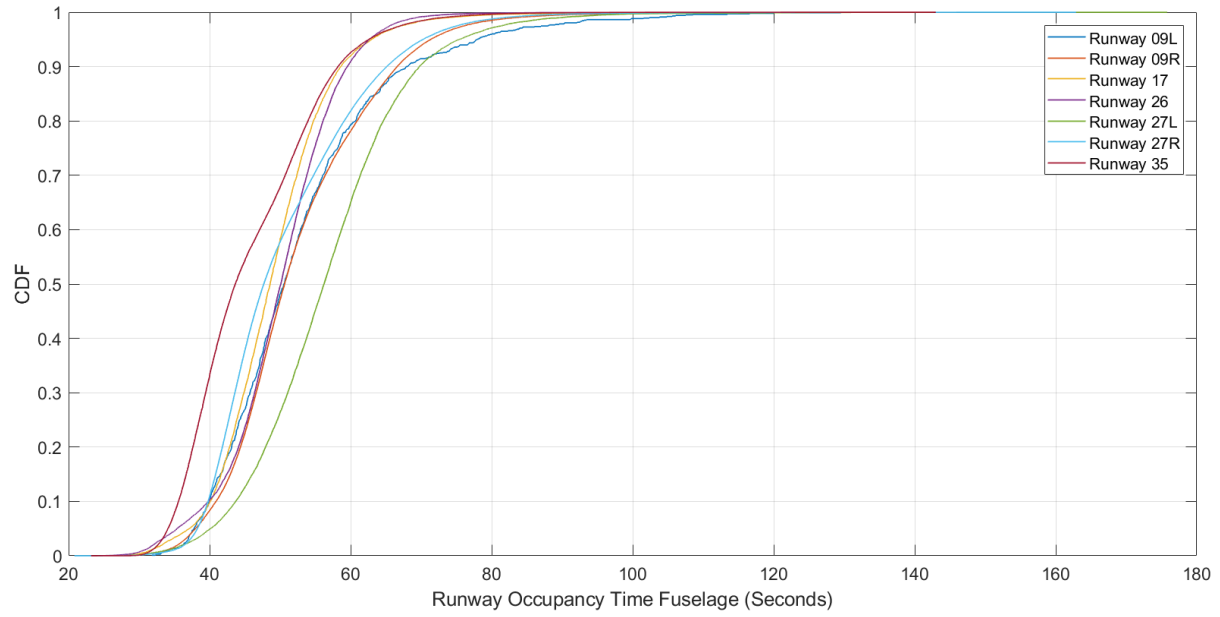

Figure 76. CDF Plots for ROT Values on Different Runway Ends at PHL.

Based on the CDF plots shown in Figure 76, the average ROT on runway 27L is 56.8 seconds and its standard deviation is 11.1 seconds. The lowest average ROT at this facility is for runway 35 with a value of 45.9 seconds. Runway 27L has an available landing distance of 9,912 feet which means that this runway is relatively long and also it has many runway exits which causes the standard deviation of the ROT values to be high. This primary analysis shows us that we can look for a more optimum runway exit configuration that will reduce the weighted average ROT and decreases the standard deviation as well.

4.2.1 Runway 27L

The problem that we are trying to solve on this runway, is to find the optimal location of a high-speed exit between current taxiways S5 at 3,719 feet from the runway threshold and S9 at 6,443 feet from the runway threshold. Right now all the available exits in this gap are either right-angle exit or back-turn which are not suitable for vacating the runway as quickly as possible. The airport authorities feel that by constructing a new high-speed exit and replacing that with the current low-speed exits in that range, they can reduce the ROT time on the runway. Similar to other case studies, first we review the exit utilization and average ROT for all the runway exits. Table 15 summarizes that information.

Table 15. PHL Runway 27L Exit Configuration and Utilization.

Exit Name	PC Distance (feet)	Exit Utilization (%)	Average Runway Occupancy Time (s)
U-R	2721	0.2	38
S5	3719	5.9	40.1
S4	3781	0.05	45.6

Y-R	4817	3.8	45
Y-L	4840	18.6	49.8
S6	5194	0.3	52.4
S7	6151	10.5	54.7
S9	6443	57.5	61.2
S8	6555	0.05	59.2
Z	7567	1.7	63.8
S10	9802	1.3	83
S	10297	0.06	95

As we can see in Table 15, high speed exit S9 is the most popular exit on this runway. There's an earlier high speed exit on this runway which is S5, but the reason behind its low exit utilization is that this exit was constructed very close to the runway threshold, therefore many narrow body airplanes can't utilize this runway exit while landing on runway 27L. As usual for proving our case about higher exit utilizations for high speed exits, we can take a look at the violin plot for exiting speed distributions on this runway. Figure 77 represents the exiting distributions for each runway exit. As we can see in the figure two high speed exits S9 and S5 had relatively higher exiting speeds as expected. The only difference that we noticed after comparing the same violin plots generated in earlier cases, is that the distribution of exiting speeds at S5 is clearly having a higher central point. The reason is that not only this exit is a high speed exit, but also it is located very close to the runway threshold. Therefore, successful evacuation via that runway exit required airplanes to maintain higher exiting speeds.

After reviewing the data shown in Figure 77 and Table 15, we also noticed that between the current two high speed exits we have a gap of 2,724 feet which is filled with right angle or turn-back exits. This causes a higher value for weighted average ROT, therefore it makes sense to replace all of those exits with a new high speed exit and improve the performance.

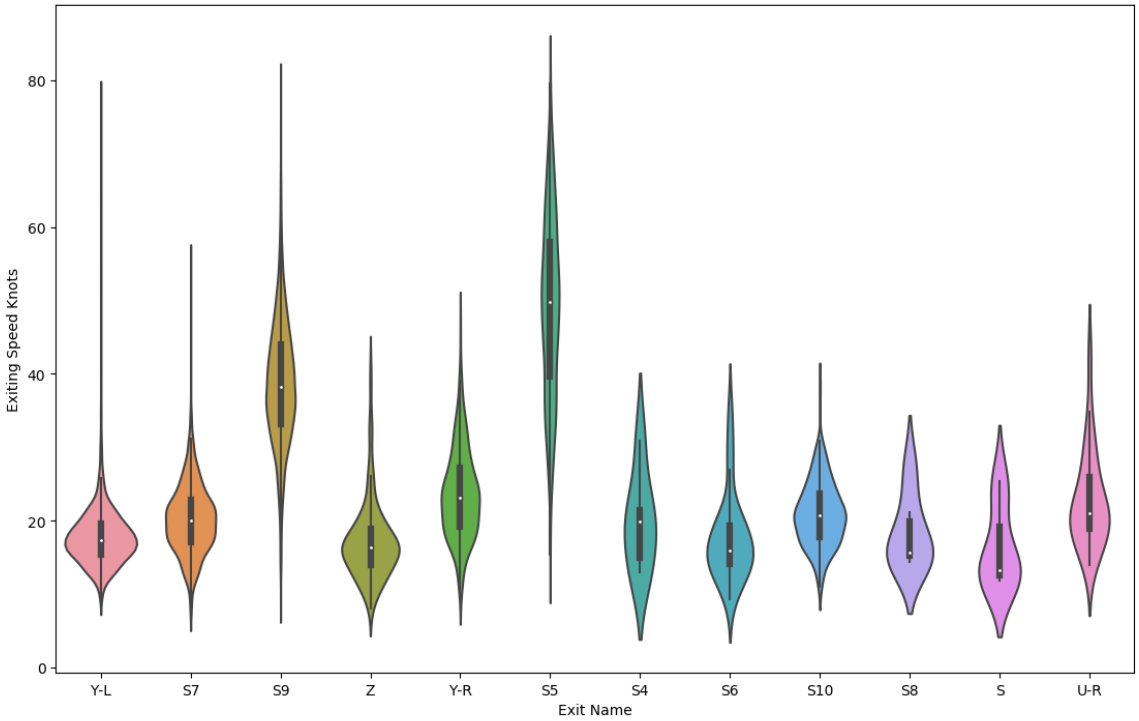

Figure 77. Violin Plot for Exiting Speeds on Runway 27L at PHL.

We ran three different scenarios for this runway. Upon request of the airport authorities we ran an extra scenario with a different share of wet/dry condition than our usual mix of 90%/10%. For running the second scenario we ran the improve case with the simulation model, and the dynamic programming algorithm gave us the location of the new high speed exit at 5,190 feet for 90/10 wet/dry scenario and 5,280 feet for 80/20 wet/dry scenario.

Table 16. Simulation Scenarios for Runway 27L at PHL.

Scenario	Location of New Optimal High-Speed Exit (ft)	Wet/Dry Mix (%/%)	Remarks
Baseline	Not applicable	10/90	Open exits: U, S7, Y, S9, S11, S12 and S13
One High-Speed Runway Exit, 10/90	5,190	10/90	Open exits: U, S7, Y, NewHS1, S11, S12 and S13
One High-Speed Runway Exit, 20/80	5,280	20/80	Open exits: U, S7, Y, NewHS1, S11, S12 and S13

Figure 78 represents the results for the three scenarios that we ran for runway 27L at PHL. As we can see by considering a wet/dry condition of 90/10, the weighted average ROT can be reduced for 4.4 seconds after constructing a new high speed exit at 5,190 feet from the runway threshold and replacing it with all the non-high speed exits in the available gap. This new configuration can also reduce the standard deviation of ROTs for 1.4 seconds. By changing the wet/dry percentages, the suggested optimal location for the new high speed exit moves further down on the runway and we see that the difference for WROT becomes 4.2 seconds and the standard deviation difference becomes 1.5 seconds which are both significant changes for this runway. We have to keep in mind that for all of the case studies that we present here, the final weighted average runway occupancy time is by considering the overall impact on the entire fleet mix, however by looking at detailed changes for each individual aircraft type, we see even higher difference rates compare to the average differences. For this reason, in Figures 79 and 80 we represented the ROT times to the new proposed high speed exit under both pavement conditions and compared them with the ROT

times to the second current existing high speed exit on this runway. By looking at the plots we see that based on individual aircraft types there will be ROT gains of 4.4 seconds to 5.8 seconds.

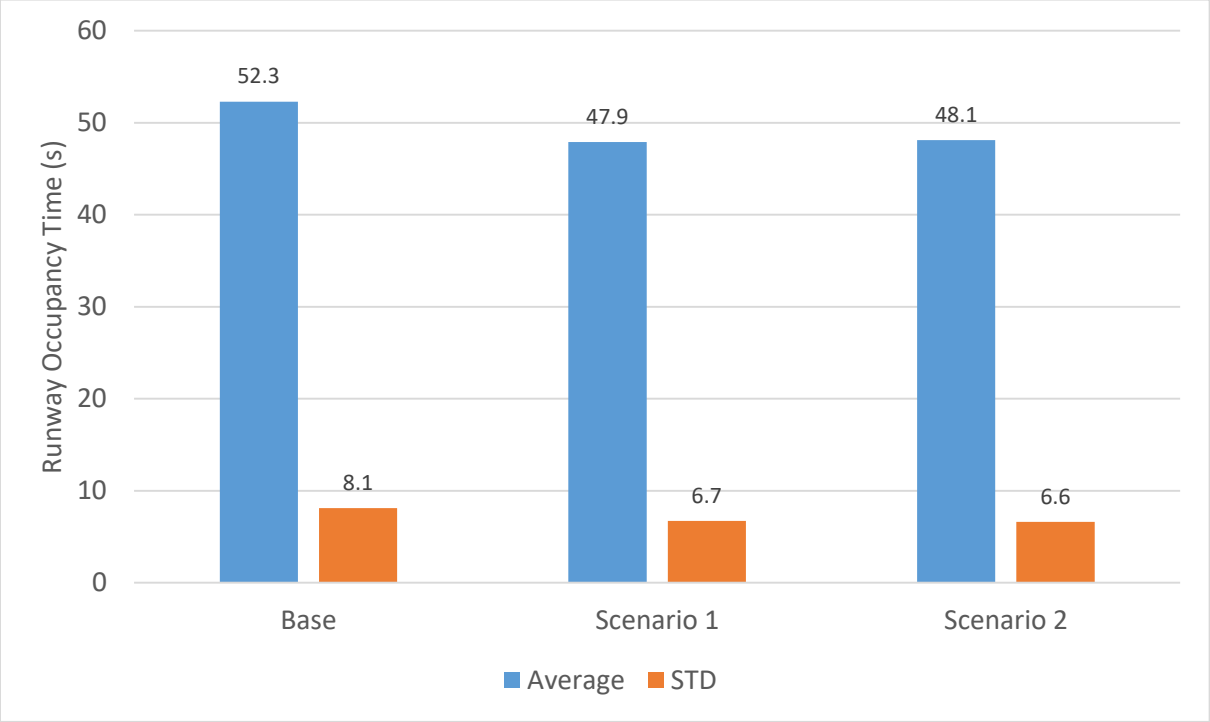

Figure 78. Different Scenarios on PHL Runway 27L, Average and Standard Deviation ROTs.

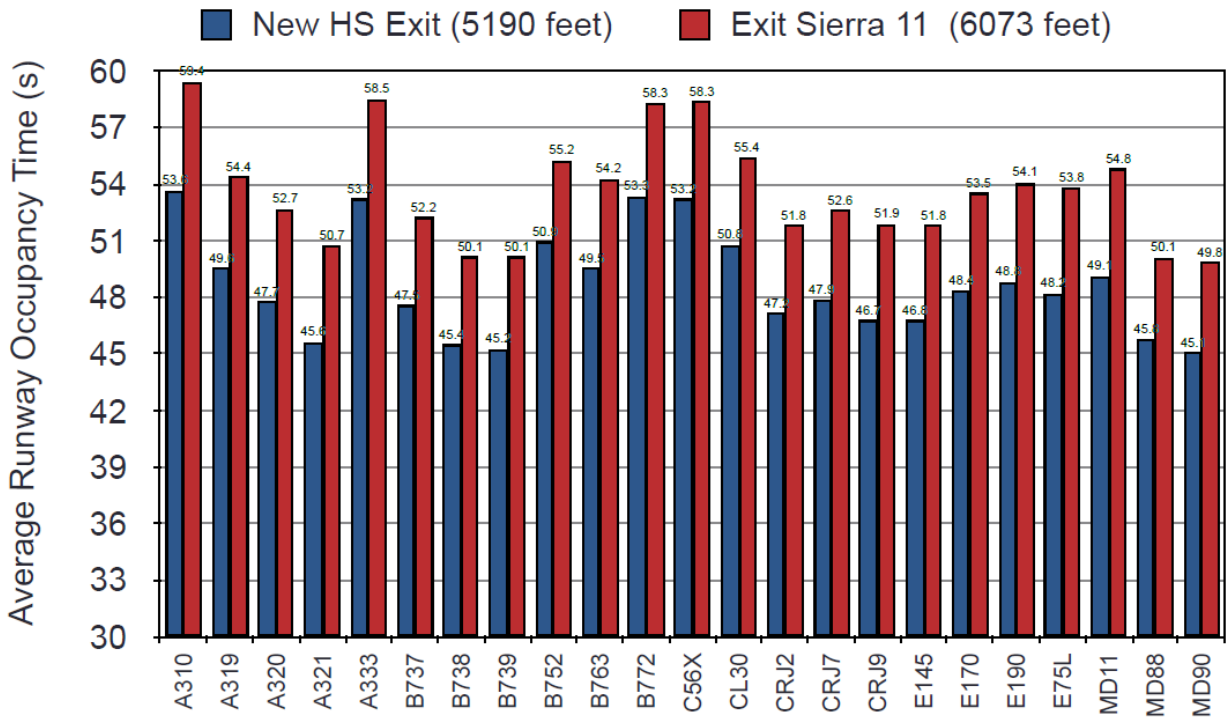

Figure 79. Individual ROT Differences for Airplanes Taking New High Speed Exit and the Second Existing Current High Speed Exit, Wet/Dry 90/10.

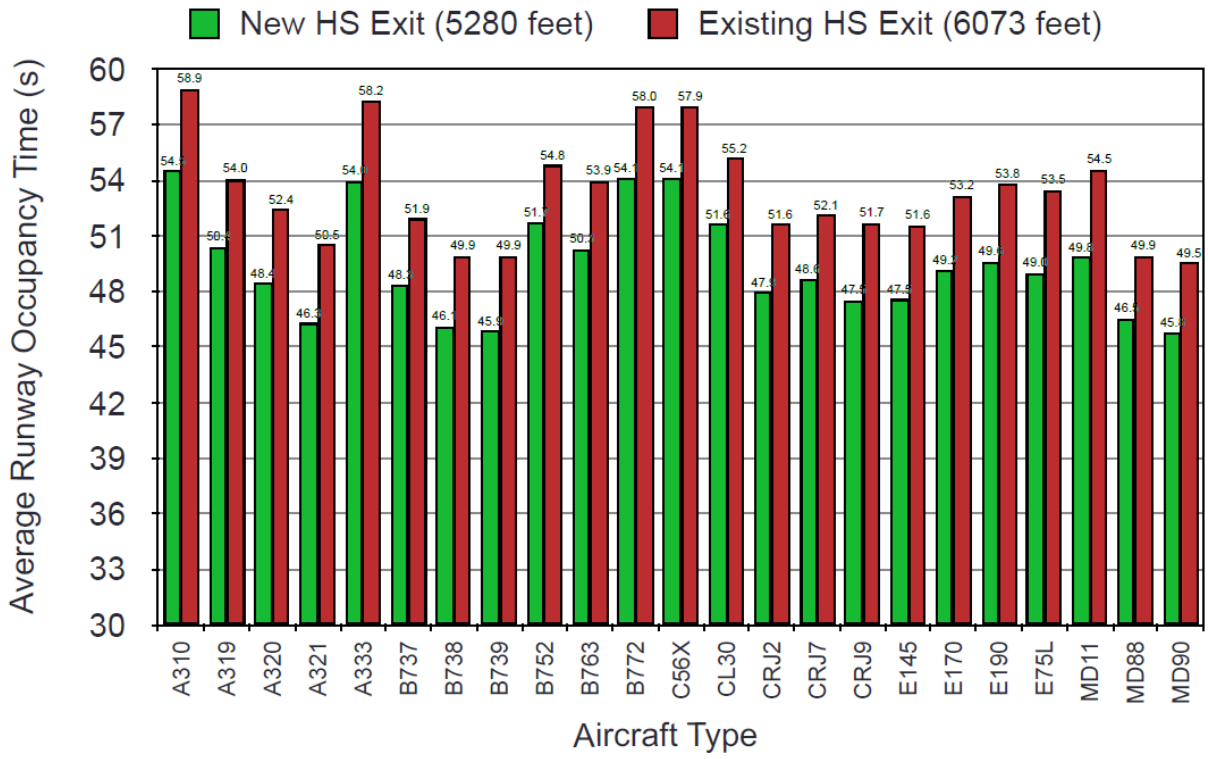

Figure 80.Individual ROT Differences for Airplanes Taking New High Speed Exit and the Second Existing Current High Speed Exit, Wet/Dry 80/20.

Therefore, our conclusion for this runway is that since there's a significant gain in weighted average runway occupancy time after constructing a new high speed exit at 5,190 feet from the runway threshold, it is beneficial for the airport traffic flow and arrival capacity on runway 27L to demolish the exits between S5 and S9 and construct a new high speed exit.

4.3 Denver International Airport (DEN)

Denver International Airport (DEN) is the next candidate that we were asked to evaluate for potential improvements in runway exit configuration. This airport accounts for 539,212 arrival operations in the landing database. Upon request of FAA, we evaluated the ROT performance of runway 16R at DEN airport and explored any optimum strategies for improving the ROT performance on this runway. Runway 16R is the longest runway available in our database with a length of 16,000 feet. Also, DEN airport is a unique facility as it is built 5,430 feet from the sea level. Such high elevation increases the approach speeds for planes and represent very unique behavior compare to the rest of the airports in the database. Figure 81 depicts the layout of runway 16R at DEN airport.

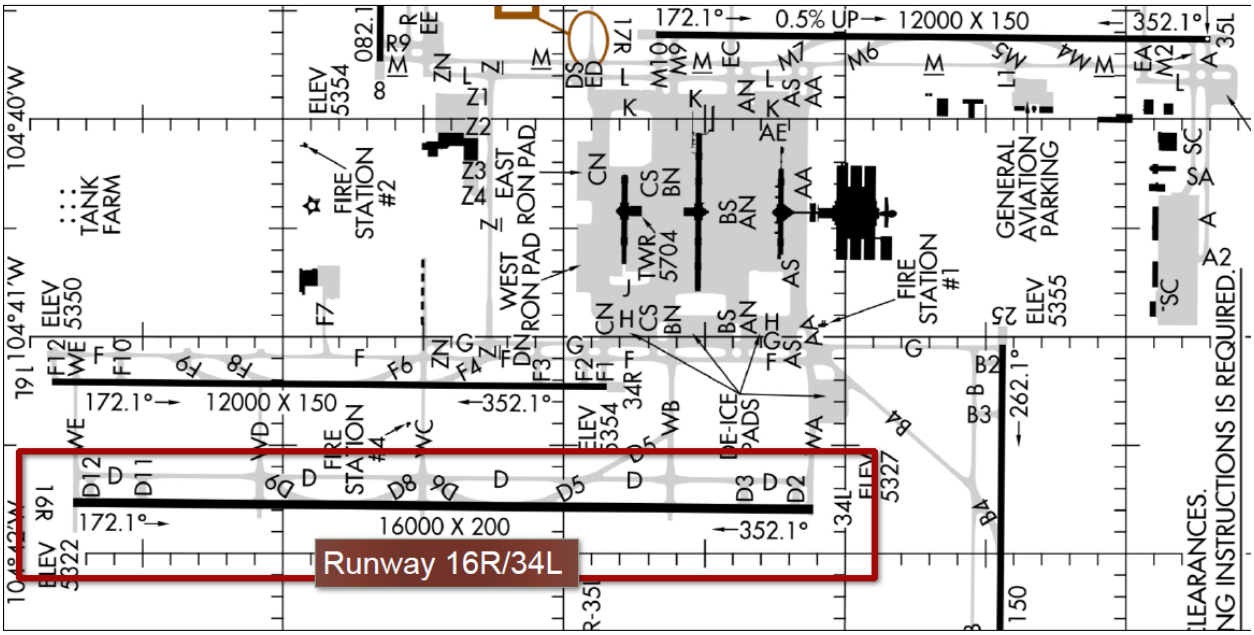

Figure 81. DEN Runway 16R Layout. [Source: FAA]

Runway 16R is the third popular arrival runway end at DEN airport. This runway stands after 35L and 16L in terms of number of recorded landings from the landing database.

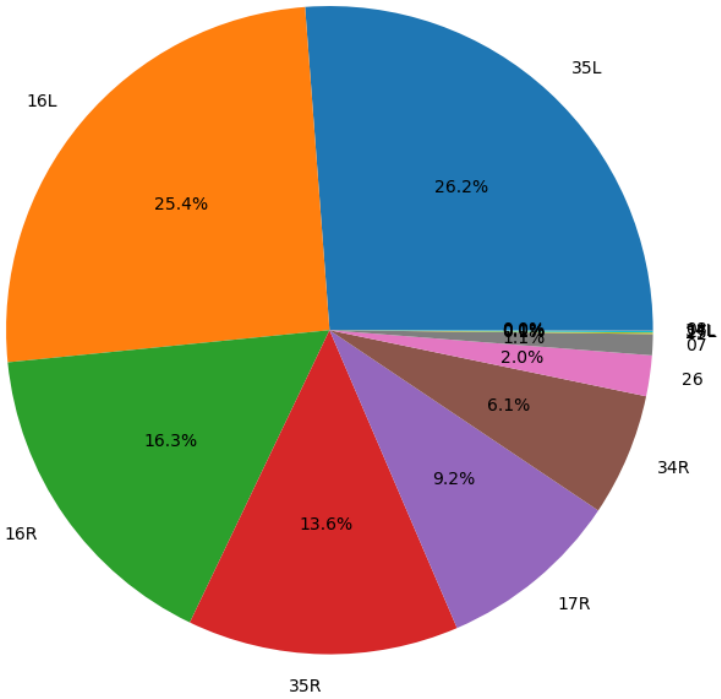

Figure 82. Percentage of Operations for Each Runway End at DEN Airport According to Landing Database.

Now that we know the number of operations at DEN and the ranking of each runway end in terms of number of operations, similar to other case studies we take a look at the airport fleet mix because it is a critical input data for our simulation model. As we can see in Figure 83, the most dominant aircraft type at DEN during years 2015 and 2016 was Boeing B737-700 with approximately 15% share of the entire operations. After B737, CRJ-200, Airbus A320, and Boeing B737-800 had highest number of showings at the airport.

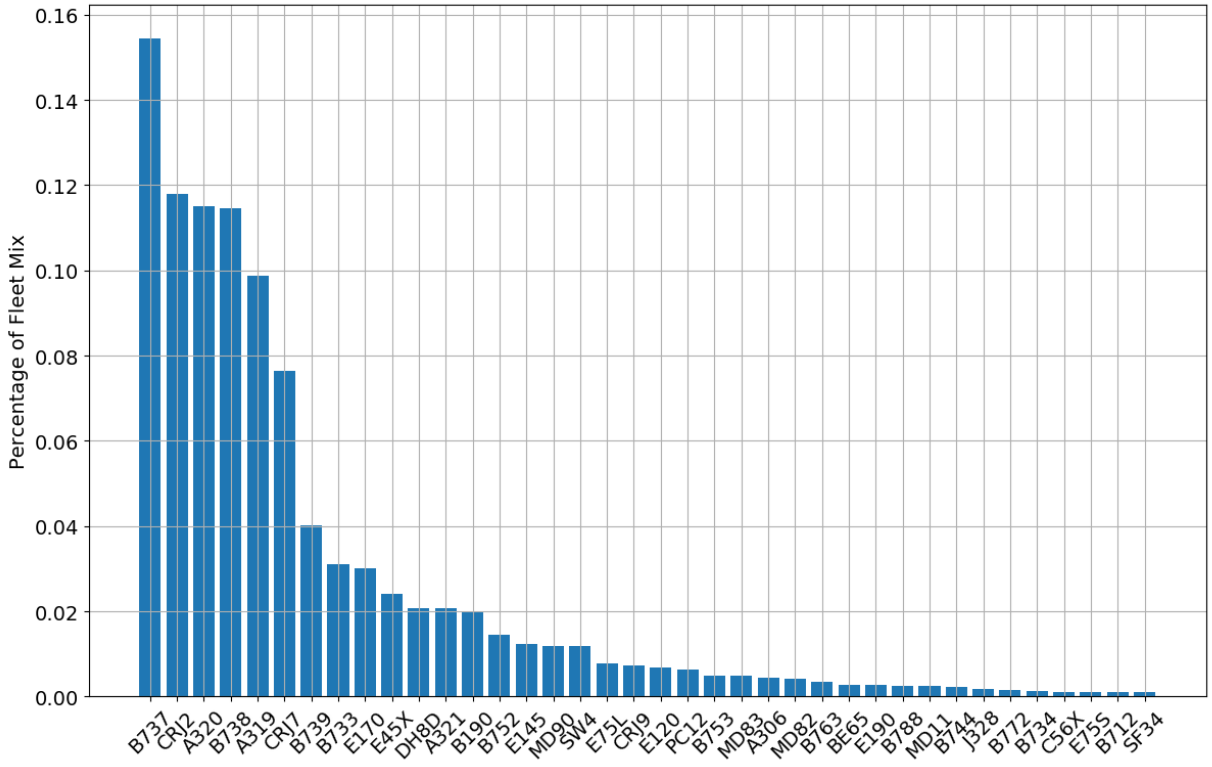

Figure 83. DEN Fleet Mix Based on Landing Database.

We have analyzed the airport layout, the number of operations on each runway end, and the overall aircraft fleet mix at DEN. Now it is time to take a look at cumulative density functions of the ROT values at DEN for each runway end. The runway that we are studying in this case is runway 16R which is the longest runway at this facility. Figure 84 represents the distribution of ROT values for each runway end at DEN. Based on the information shown in Figure 84, runway 16R had an average ROT value of 67.7 seconds which is relatively a high number. It is true that this runway is very long, however with appropriate runway exit configuration and location we can expect to reduce the runway occupancy time on this runway. The lowest average ROT for this airport belongs to runway end 34R with an average ROT of 50.7 seconds which is 17 seconds lower than our case study runway. One very interesting point is that even though this runway was designed symmetrically in terms of runway exit configurations from both ends (16R and 34L), the average

runway occupancy time on 34L is 56.9 seconds, which is approximately 10.7 seconds lower than the other runway end. The number of recorded arrival flights on 34L was very few –just 191 in two years- however, the main reason behind the low ROT values for that runway end is that flights took high speed exit D6 which is closer to the runway threshold. We will explain the exit utilization on runway 16R in the next section with more details.

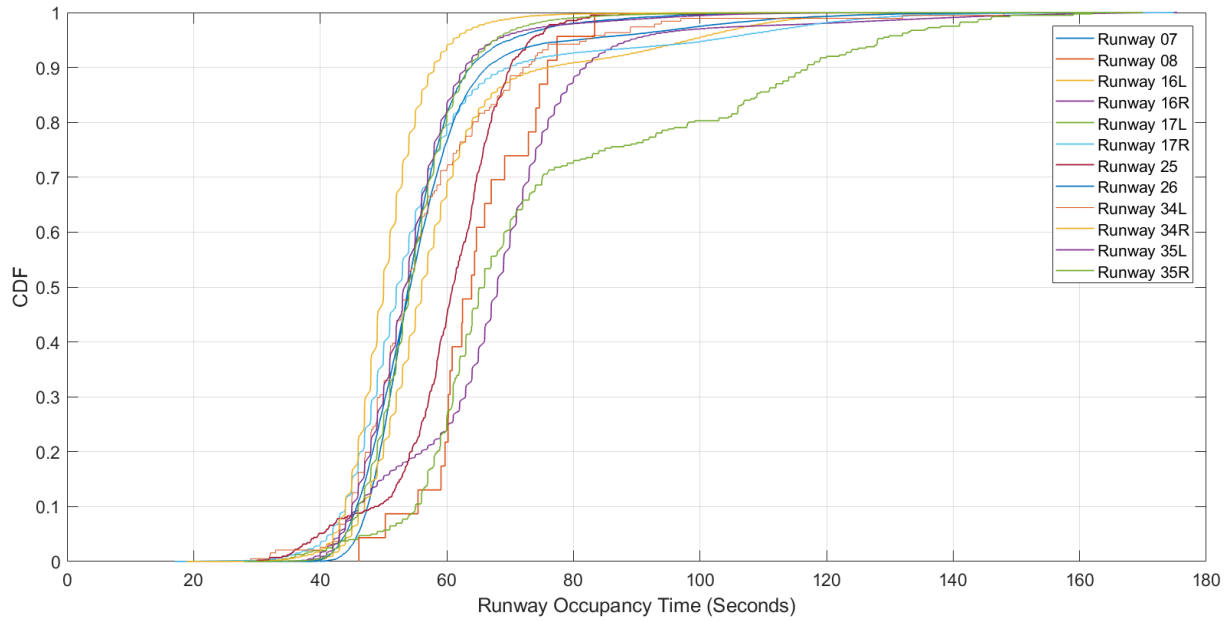

Figure 84. CDF Plots for ROT Values on Each Runway End at DEN Airport.

4.3.1 Runway 16R

The problem that we are trying to solve for runway 16R at DEN is to find potential solutions that will reduce the runway occupancy times on this runway. So far we noticed that the average ROT on this runway is very high and more importantly we noticed that the standard deviation for ROT values are 16.5 seconds on this runway. These values are very big and will cause too much uncertainty for the controllers when the new wake separations will be applied at this airport. For understanding our options in improving the ROT behavior, we first take a look at the runway exit utilization and average ROT on this runway. Table 17 represents the runway exits on runway 16R

and their exit utilizations. The interesting operational information about the runway exit configuration on this runway is that the third available exit on the runway is a high speed exit labeled as “D8”. This exit is located at 5,775 feet from the runway threshold that is relatively a short distance for DEN elevation. That’s why only 19% of the flights could make it successfully to that exit. As expected the remaining right angle and back-turn exits didn’t absorb too many flights, but the second high-speed exit on the runway absorbed the majority of the arrival flights. High speed exit D5 which is located at 9,341 feet from the threshold could absorb 75.2% of the flights with an average ROT of 71.4 seconds. The gap between the two existing high speed exits is 3,566 feet which is an adequate spacing for constructing at least a new high speed exit. This proposal sounds logical as the average ROT on the runway is shifted to the right because of the location of the most popular runway exit on the runway.

Table 17. Runway Exit Utilization and Average ROT for Exits on Runway 16R at DEN.

Exit Name	PC Distance (feet)	Exit Utilization (%)	Average Runway Occupancy Time (s)
WD	3871	0.07	38.2
D8	5775	19	46.5
WC	7383	3.16	57.1
D6(1)	8208	0	58
D6(2)	8208	0.04	64.3
D5	9341	75.2	71.4
WB	12734	0.17	99.2
D3	14334	0.03	118.3
D2	15453	0.02	136.6

WA	15750	2.3	135

Similar to other case studies that we represented earlier, we review the exiting speed distributions for each runway exit to have better understanding on flights' behavior on the runway. The following graph depicts the violin plots for each runway exit on runway 16R and the airplanes' distribution of exiting speeds. Similar to many other cases that we showed earlier in this chapter, the difference between speed values at the PC point for high-speed exits and right-angle exits is obvious. Again we see that the speed distribution for the earlier high speed exit is slightly higher than the values for the second high-speed exit. The fact that we don't have any high speed exits between D8 and D5, and that all the exits between those two push the pilots to slow down a lot, tells us that we need to construct at least one high speed exit in this available gap. Therefore, we run the improve case on DEN and ask the DP algorithm to give us the optimum location for a new high-speed exit between 5,775 feet and 9,341 feet.

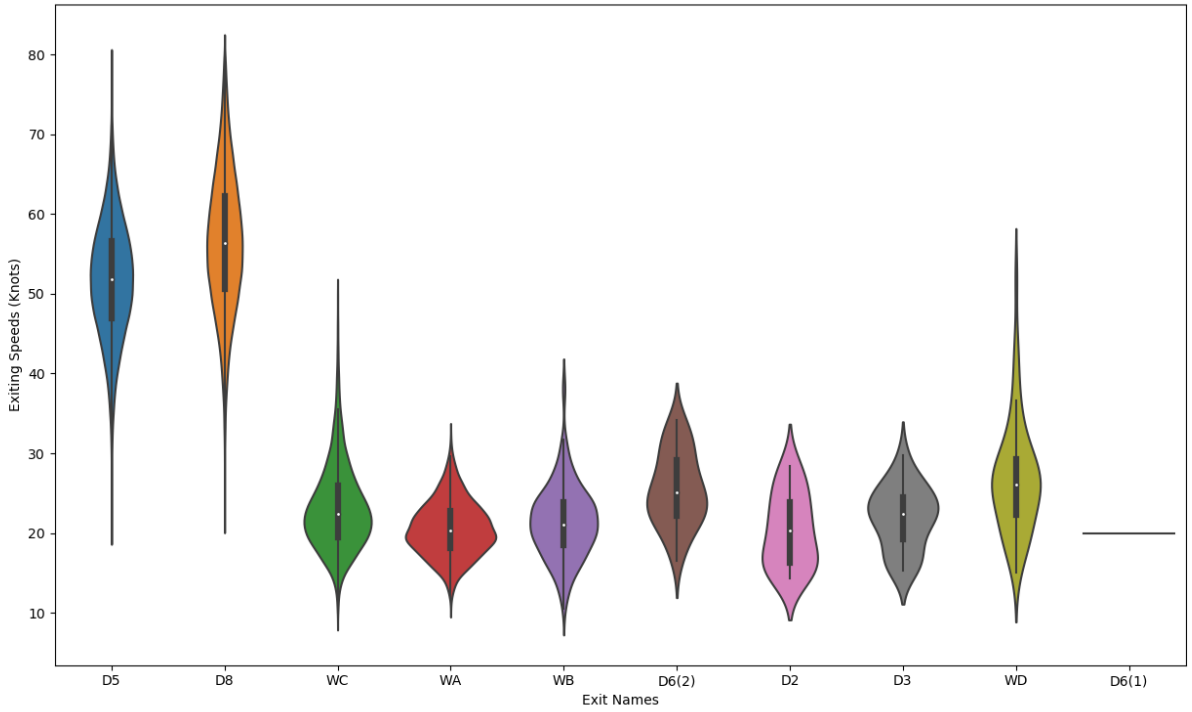

Figure 85. Violin Plot for Exiting Speeds on Runway 16R at DEN.

We ran 5 different scenarios for runway 16R after finding the initial optimal candidate for constructing a new high-speed exit. After running the improve case with the extracted fleet mix for this runway from landing database, the algorithm found the optimum location as 7,800 feet for a pavement condition of (90%, 10%) for wet/dry. The suggested location sounds reasonable based on the entered range, however there can be a little bit of pavement overlap between the new proposed high-speed exit and exit D6(1). Therefore, in our evaluation scenarios we moved the proposed exit with steps of 100 and 200 feet to see how much ROT will change. The following table represents the simulation scenarios we ran for this runway.

Table 18. Simulation Scenarios for Runway 16R at DEN.

Scenario	Location of New High-Speed Exit (ft)	Remarks
Baseline	Not applicable	Current configuration
Scenario 1	Optimal at 7800 feet	Optimal location
Scenario 2	New HS exit at 8000 feet	200 feet downrange from optimal location
Scenario 3	New HS exit at 8,200 feet	400 feet downrange from optimal location
Scenario 4	New HS exit at 8,300 feet	500 feet downrange from optimal location Avoids overlapping pavement interaction
Scenario 5	New HS exit at 8,400 feet	600 feet downrange from optimal location Avoids overlapping pavement interaction

Before analyzing the results for all the scenarios, we evaluated the potential exit utilization on this runway after constructing a new high-speed exit at 7,800 feet from the threshold. The following plot shows the CDF of exit utilizations if we construct a new high speed exit between the current existing ones.

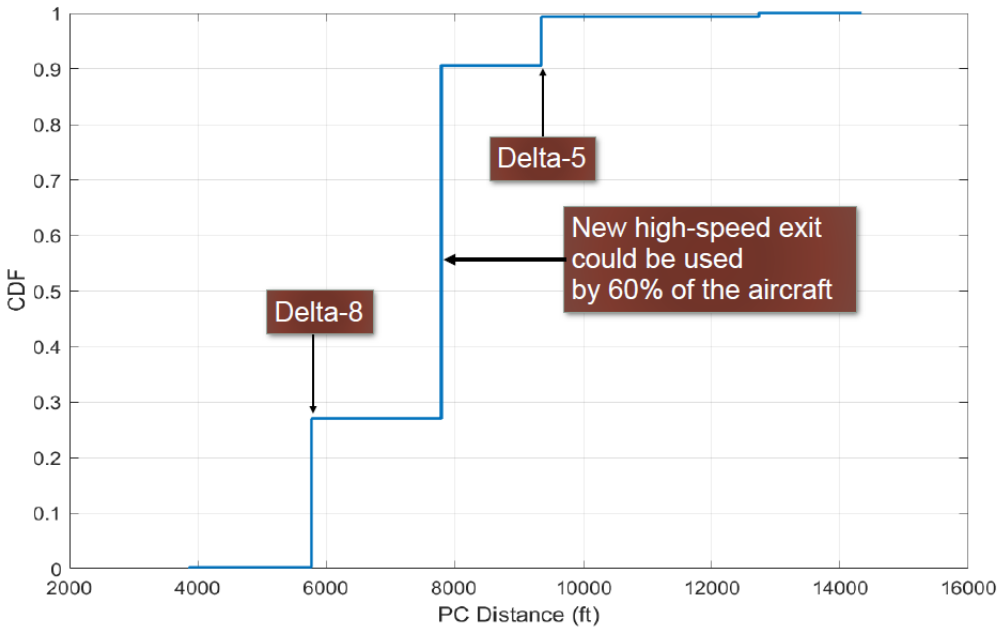

Figure 86. Exit Utilizations on Runway 16R After Building a New High Speed Exit at 7,800 Feet.

Base on Figure 86, a new high speed exit can potentially absorb 60% of the arrival flights and will reduce the weighted average ROT for 9.7 seconds. This new exit can also reduce the standard deviation of ROTs for 7.9 seconds which is a very significant number. Now that we are certain about the benefits of constructing a new high speed exit we ran a sensitivity analysis by moving the new high speed exit to reduce the amount of pavement overlap.

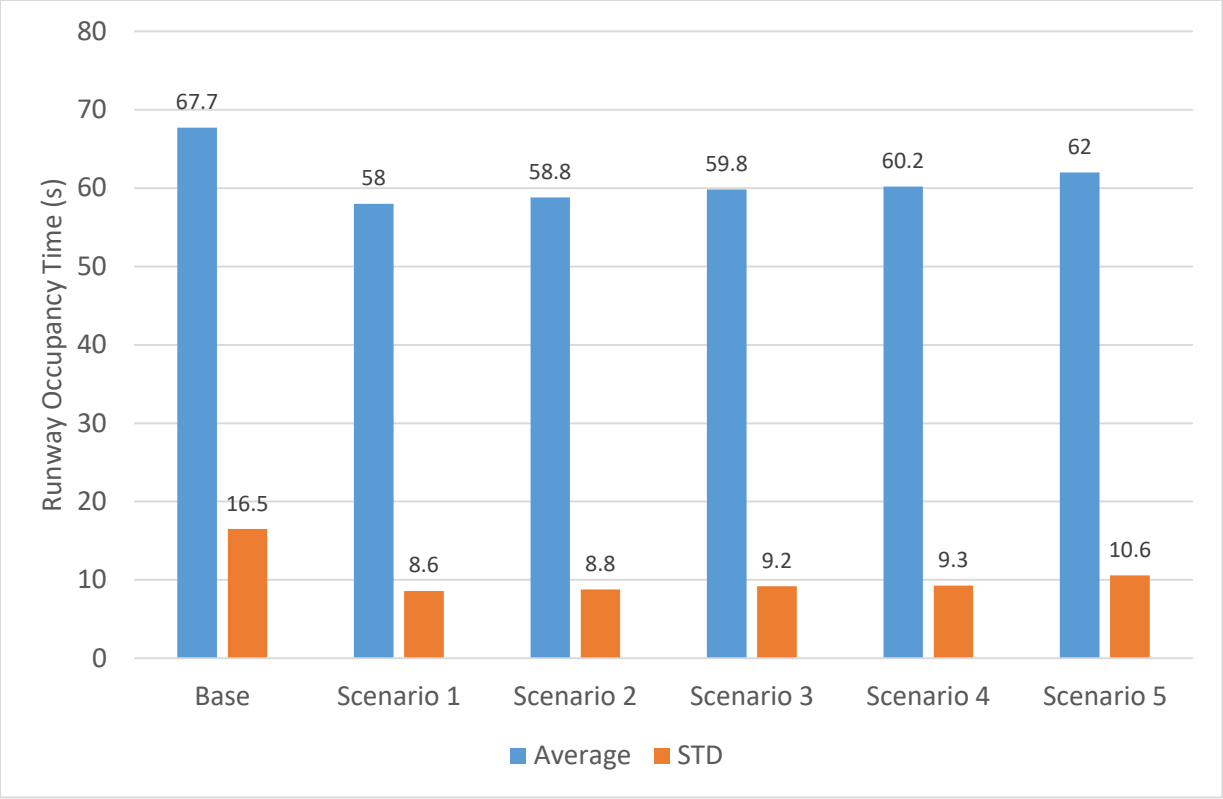

Figure 87. Different Scenarios on DEN Runway 16R, Average and Standard Deviation ROTs.

Figure 87 shows us that even by constructing the new high speed exit at 8,300 feet from the threshold which is 500 feet further than the optimum location we can save 7.5 seconds in average ROT and 7.2 seconds in ROT standard deviation. Therefore, our conclusion for this runway is that by constructing a new high speed exit in the range between 7,800 feet to 8,400 feet from the threshold, based on current fleet mix at the airport, this runway can see ROT gains between 7.5 to 9.7 seconds which is a significant change in ROT values.

4.4 Charles B. Wheeler Downtown Airport (MKC)

Charles B. Wheeler Downtown Airport (MKC) was the last airport that we studied its ROT performance upon request of FAA for analyzing a general aviation facility. One difference between MKC and the other studied airports is that MKC is not an ASDE-X supported facility, therefore we didn't have any landing data for this facility except some fleet mix information which FAA provided for us. Modelling general aviation operations based on the ASDE-X data is very challenging as we don't have many GA flights at commercial facilities. Also, even if piston airplanes show up at bigger airports, due to long runways available for their pilots, they don't perform similar to the times they land on short runways at GA facilities. For all the reasons mentioned, we had some difficulty reflecting the real behavior for this class of aircraft.

Figure 88 shows the MKC layout. For this case study we focused on runway 01-19. The fleet mix data was provided by FAA as we didn't have access to any surveillance data similar to ASDE-X.

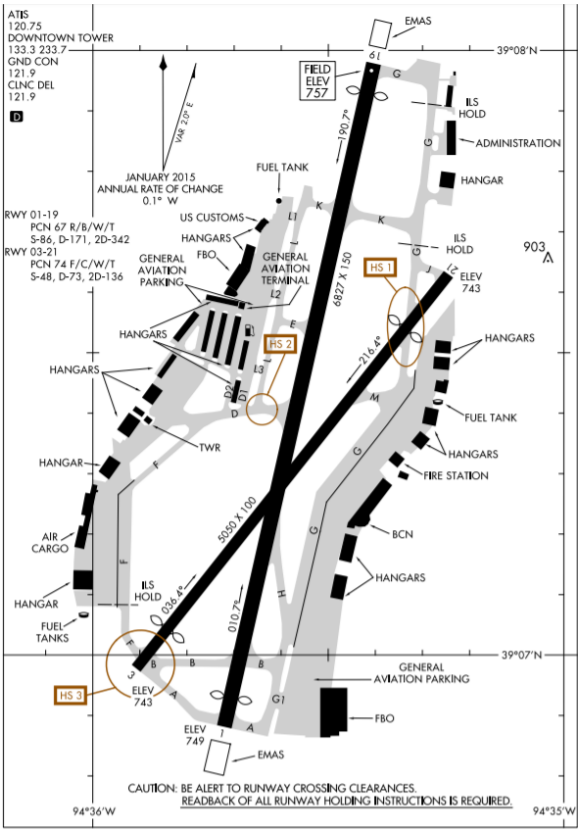

Figure 88. MKC Airport Layout Map. [Source: FAA]

Figure 89 represents the fleet mix of MKC based on extracted data from flightaware.com for month October 2019. In this plot fleet percentages more than 1% are shown. This airport has around 77% piston aircraft, 68% jet aircraft, 21% multiengine, and 6% helicopters in its fleet mix.

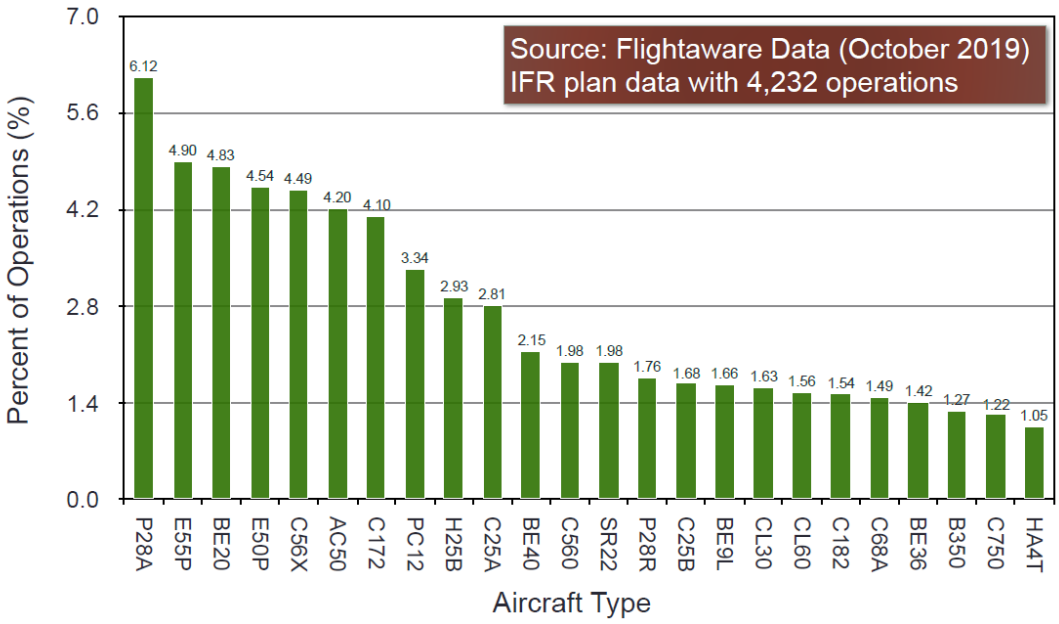

Figure 89. MKC Fleet Mix for Aircraft Types More Than 1% of the Operations.

This study focuses on runway 01-19 at MKC and explains the solution for improving the ROT performance. This runway is relatively a short runway and it is just 6,827 feet. Except the intersecting runway 03-21 which can be used as a pseudo high-speed exit, the rest of the runway exits are right-angle or back-turn. The main reason behind such exit configuration is that FAA mandates facilities to have at least 30 arrival flights per hour in order to construct high-speed exits. Table 19 shows the geometry and information for each available runway exit on runway 01 at MKC. Figure 90, shows the histogram of number of operations during different hours of the day at MKC considering the arrival flights on both runways. As we can see based on the available data during peak hours, this facility has at most 20 operations, therefore we can't consider constructing any high-speed exits for our proposal.

Table 19. MKC Runway 1 Exit Configuration and Geometry Information.

Exit Name	Point of Curvature from Runway Threshold (ft)	Angle (deg)	Equivalent Radius (ft)	Path Length to Hold Bar (ft)	Location (meters)
H-right	1,480	150	75	620	451
Runway 3-21	2,061	30	1300	1200	628
D	2,850	110	170	374	869
E	3,790	90	170	374	1,155
K	5,076	90	170	374	1,548
G-right	6,632	90	170	374	2,022

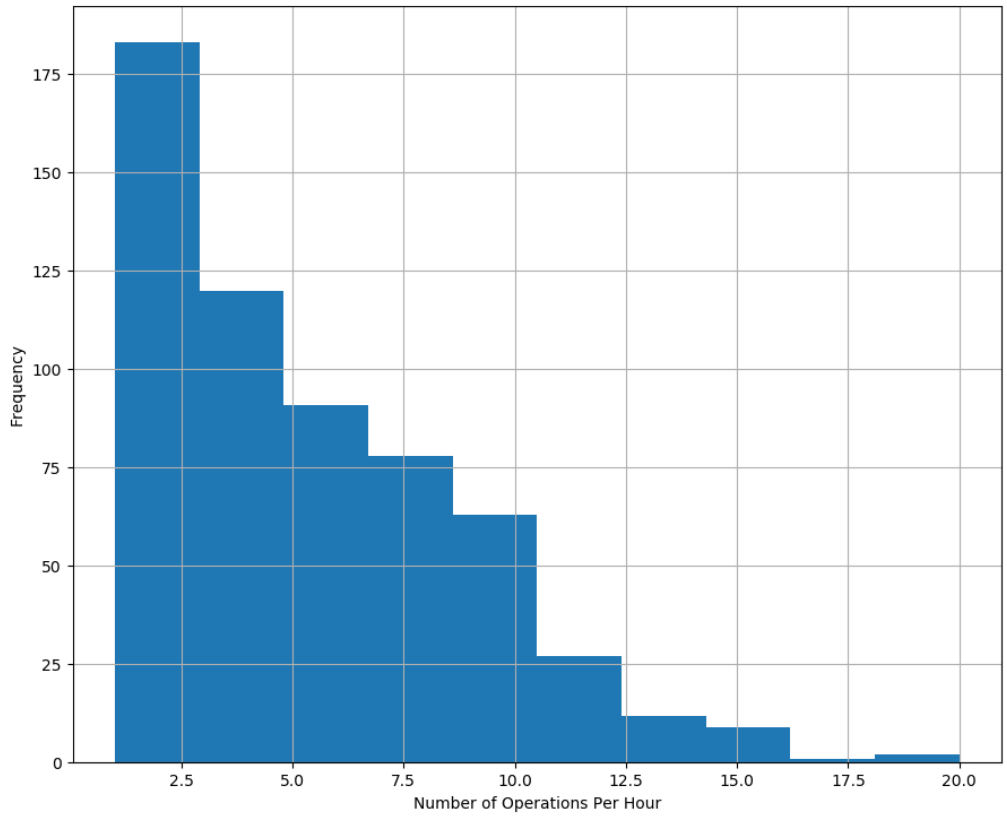

Figure 90. Number of Operations Histogram for MKC, Based on Hourly Number of Operations. [Source: FAA Data for July 2019]

Based on the airport layout we can clearly identify the potential gap for constructing a new right-angle exit to help airplanes vacate the runway faster. The best location for constructing the new right-angle exit is between current exits “E” and “K”. Prior to exit “E” we have the intersecting runway and there’s limited spacing for constructing a new exit. After exit “K” we don’t have direct access to the terminal area, therefore airplanes should go to the end of runway, take taxiway “G”, taxi back, take taxiway “K” and pass the active arrival runway, and finally taxi towards the gate locations. Hence, our best option for the improvement case is to ask the DP algorithm to give us the optimum location of a new right angle exit between exits “E” and “K”. We did so and the suggested new location for a right angle exit was 4,285 feet from runway threshold. Since we don’t have access to any radar data from this facility, we need to run the base case as simulation as well

and then compare it with the optimal case. Figure 91, depicts the exit utilization percentage for 250,000 simulated flights on runway 01 at MKC. The weighted average runway occupancy time for the base case scenario is 45 seconds. As you can see in the plot around 11% of the flights could make it to the first exit which is a pseudo high-speed exit, but the majority of flights used exits "D" and "E". Figure 90, represents the stacked random events on top of each other for showing the exit utilization and generated random events. This plot helps us to validate the exit assignments and to see what was the range of generated random events for each simulated incident.

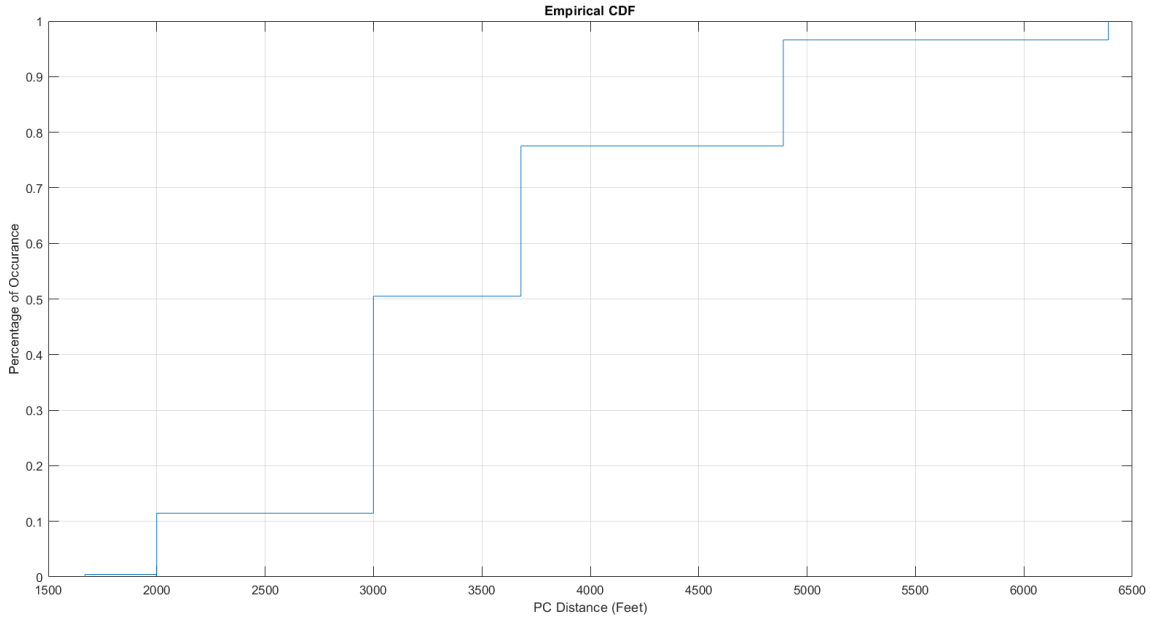

Figure 91. Exit Utilization for Base Case Simulation on Runway 01 at MKC.

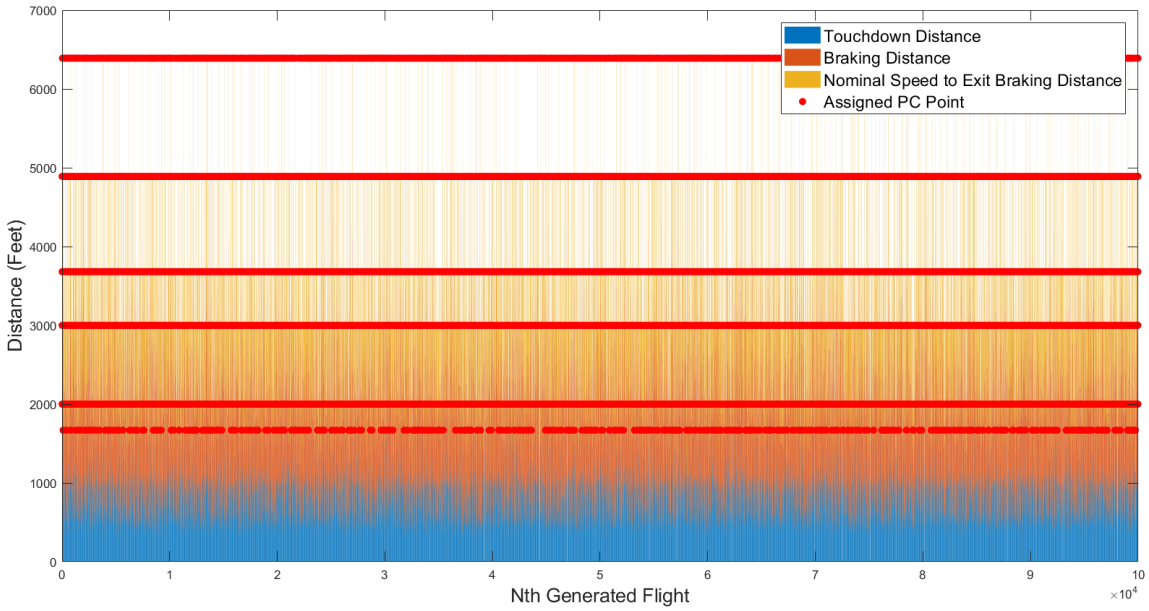

Figure 92. Generated Random Events for Base Case Simulation.

Now that we have the base case scenario, we can run the second scenario where we added the new right angle exit at 4,285 feet. Figure 93, represents the exit utilization CDF plot for 250,000 simulated flights on an improved version of runway 01. As you can see by adding the new right angle exit around 18% of the flights who were assigned to exit "K" are now assigned to the new right-angle exit and that caused saving 2.1 seconds in weighted average ROT. This result tells us that we picked the correct location for construing a new right-angle exit and we could save a considerable amount of time by avoiding assignments to the last two right angle exits. The new ROT with the new right-angle exit will be 42.9 seconds.

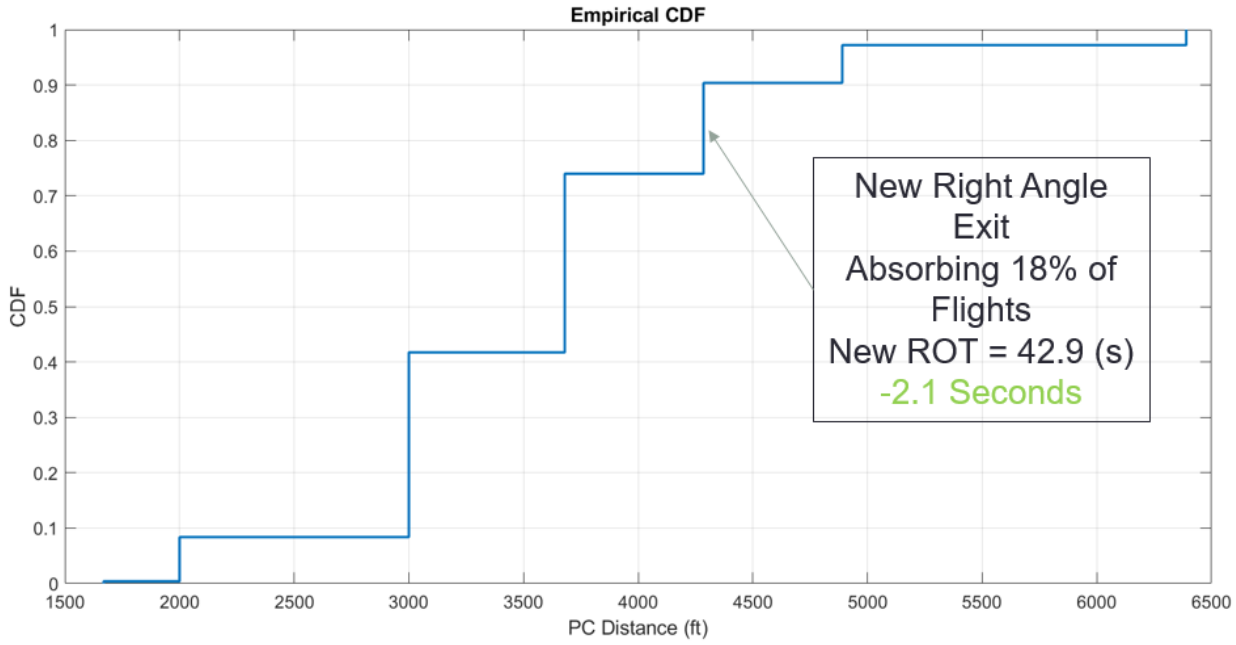

Figure 93. Exit Utilization for Scenario with the New Right Angle Exit.

As we mentioned earlier, modeling general aviation behavior based on ASDE-X data is challenging as pilots are not pushed to perform at their limits on longer runways. Since we classify every new runway to the nearest geometry information that we collected from ASDE-X data, there's always the chance for small airplanes to have lower values of nominal deceleration compare to their typical braking rates on short GA runways. For this purpose, we shifted the distribution of nominal decelerations and picked the 30th and the 20th percentiles of nominal deceleration to see the impact on exit utilizations. We expect to see a shift towards left in exit assignment tables and observe more flights getting assigned to earlier exits as we are pushing the planes to brake harder. Figure 94, represents the exit assignment CDF for 250,000 simulated flights on modified runway 01 at MKC by using 30th percentile of nominal deceleration for airplanes. As you can see the assignments are shifted to the left and more than 84% of the flights are already evacuated by 4,285 feet. This change reduced the assignment to the new proposed right-angle exit from 18% to 14% and reduced the runway occupancy time for 4 seconds compare to the base scenario. Figure 95, represents a similar graph but this time for 20th percentile of nominal deceleration. As we expected

the assignment to the new right-angle exit will be reduced to 9% and the weighted average ROT will become 40 seconds which is 5 seconds less than the base case scenario.

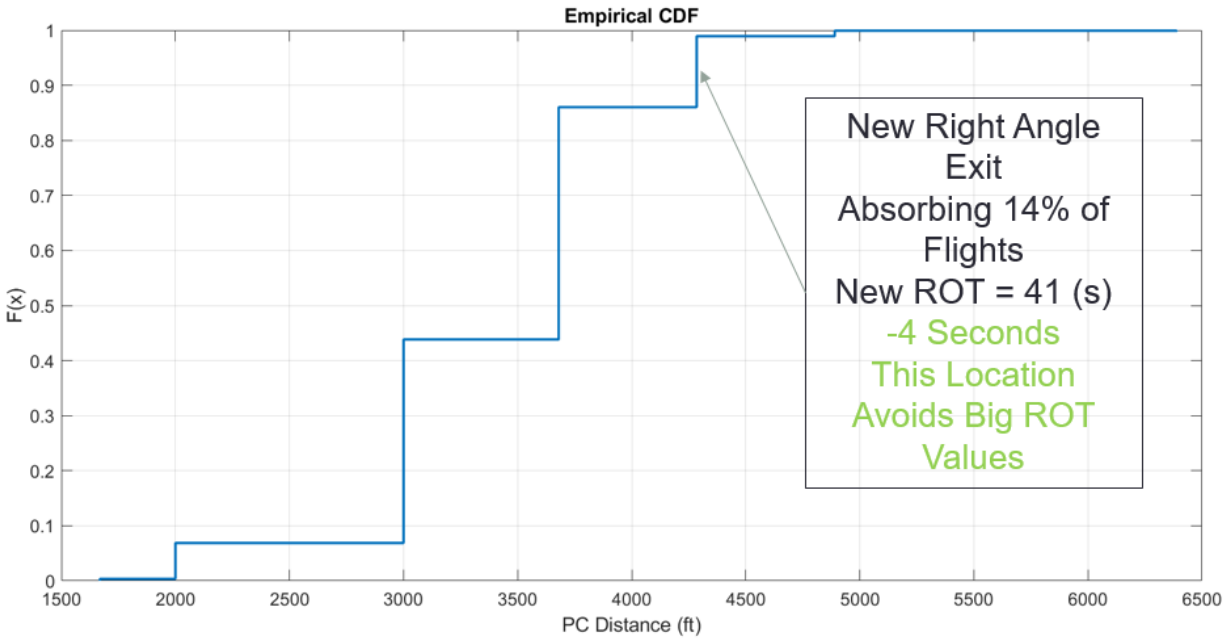

Figure 94. Exit Utilization for Scenario with the New Right Angle Exit, 30th Percentile of Nominal Deceleration.

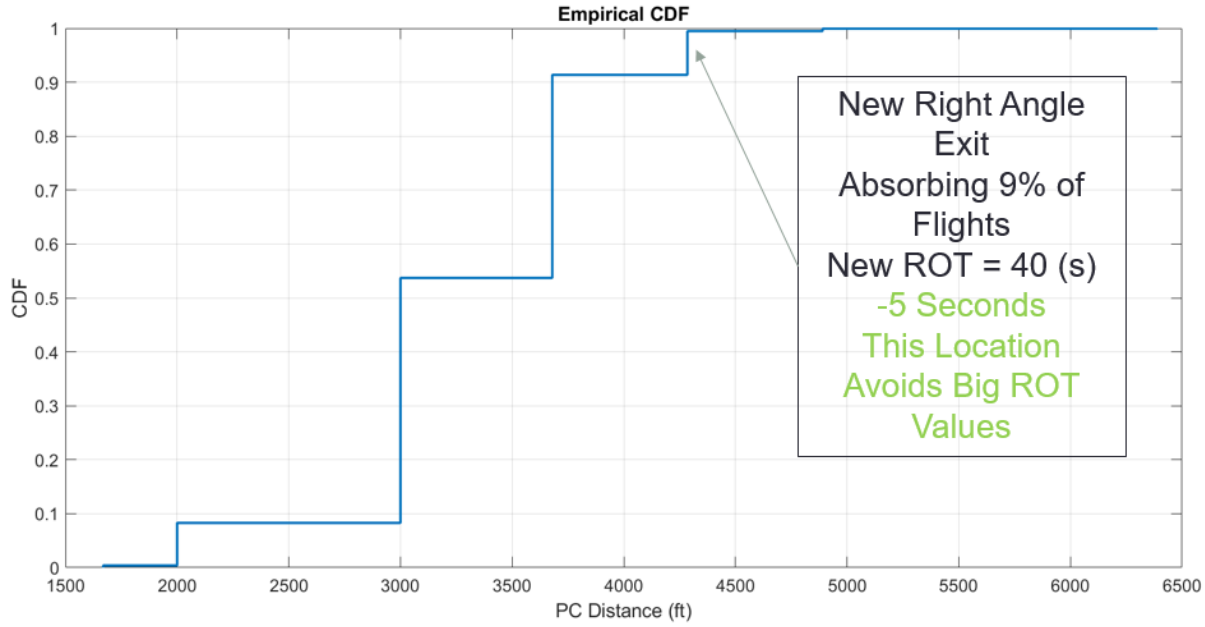

Figure 95. Exit Utilization for Scenario with the New Right Angle Exit, 20th Percentile of Nominal Deceleration.

4.5 Conclusion

In this chapter, the results of the simulation model were presented for four airports. The test cases we reviewed in this chapter were real-world scenarios identified by airport authorities and the Federal Aviation Administration (FAA). This was a great exercise to tune and evaluate the simulation model on real-world scenarios and improve the efficiency and arrival capacity. The four analyzed airports were as following: Boston Logan Airport, Philadelphia Airport, Denver International Airport, and Charles B. Wheeler Downtown Airport. The first three airports are equipped with ASDE-X system, however the last facility is not an equipped ASDE-X airport and we had to ask the authorities to provide us with some operational data. For each case, initially we ran the model on the base runway exit layout by allowing the model to assign aircraft to every possible runway exit in the field. Then we tried various cases for each facility based on potential improvements or proposed solutions by the air traffic controllers for each airport. This exercise clearly showed the power of such a simulation model in analyzing the runway occupancy times at various airfields with different characteristics such as elevation, number of available exits, runway length, and exit configurations. The final results shown in each section of this chapter were presented to FAA and airport authorities of each facility and we provided valuable consulting points to help managers decide based on scientific experiments. The author of this document ran all the test case scenarios and model runs and he provided some suggestions in addition to the proposed solutions from the airport authorities. One of the most important lessons learned from this phase of the analysis is the capability of developing a practical simulation model which can be used not only by US airport planners, but also by any airport consultant anywhere around the world for analyzing the ROT behavior of their facilities. In all cases, we showed the room for

improvements in ROT times by constructing new runway exits or avoiding the usage of low-speed exits at those facilities.

Chapter 5. Pilot Motivational Factors

We talked about the landing parameters and behavior for airplanes that we extracted from the ASDE-X data. Based on the analyzed data, we formed the distributions. By combining machine learning approaches with Monte Carlo simulation, we built our hybrid model, which can estimate the runway occupancy times and exiting distances for various aircraft types under different environmental conditions. Our attempts for modeling the landing profiles all the way to exit evacuations are based on nominal behaviors that we extracted from the data. For this situation, we assume that a pilot is trying to perform nominally at each critical point on the runway, but meanwhile, we try to optimize the runway occupancy time. However, after analyzing data at some facilities for some specific aircraft types and carriers, we noticed that sometimes pilots are motivated based on multiple reasons to stay on the runway for a shorter or even longer amount of time compared to a nominal stay. Various reasons might motivate a group of pilots or certain airlines to change the nominal landing behavior on the runway. We could identify the following potential reasons for motivated pilots:

1- Terminal and gate locations sometimes play a role in a pilot's decision to choose a specific runway exit on the runway [31]. This decision results from pilots' experience from previous taxing phases at the same airports [49]. They know that by choosing a specific runway exit, they can get to their gates faster, therefore they want to either brake harder and take early exits or brake shallower and coast on the runway. We will demonstrate some examples for both conditions later in this chapter.

2- On rare cases, the air traffic controllers advise the pilots to take specific runway exits due to heavy arrival traffic or to avoid crossing other active runways after evacuating the arrival runway.

Due to limitations in exit geometry or runway length, pilots have to focus on evacuating the runway at a safe exiting speed after a successful touchdown and braking. Some carriers also provide specific regulations for their pilots and prohibit them from taking exits at very high speeds due to maintenance costs. However, a few times, pilots of specific carriers took earlier exits based on the observed data, which they had to brake harder than usual for making to those exits. Since we had to model the nominal behavior without pushing the vehicles beyond their mechanical capacity, we relied on normal landing profiles on runways. It is nice to have an add-on feature in the model to enable users to check the feasibility of taking specific runway exits within rational ranges of collected distributions. This extra feature can help designers evaluate the percentage of particular flights that could evacuate particular runway exits closer to their assigned gate area. We review some observations of pilot motivations from the ASDE-X data and then present three methods to model motivational factors while simulating a landing profile.

5.1 Real Observed Motivational Behavior from ASDE-X Data

5.1.1 San Diego Airport (SAN)

SAN airport is an exciting facility as it has just one runway. Analyzing landing behavior on this runway is less challenging than the remaining 36 airports because it has a simpler layout for runway and terminal area. We observed the first signs of a motivational factor at this facility. Figure 96 represents an interesting behavior related to Southwest Airlines flights on runway 27 at SAN. As shown in the figure, due to the Southwest terminal location, most of its airplanes take an earlier exit to reduce their taxi time until they arrive at their associated gates. The histograms shown in this graph represent lower ROT values for similar aircraft types belong to Southwest airlines compare to the ones that belong to American and United Airlines. While Boeing B737-700s of Southwest brake a little harder on the runway to take an early right-angle exit with higher

exiting speeds, United and American flights coast on the runway and stay on it for a longer time because their gate areas are closer to the runway end.

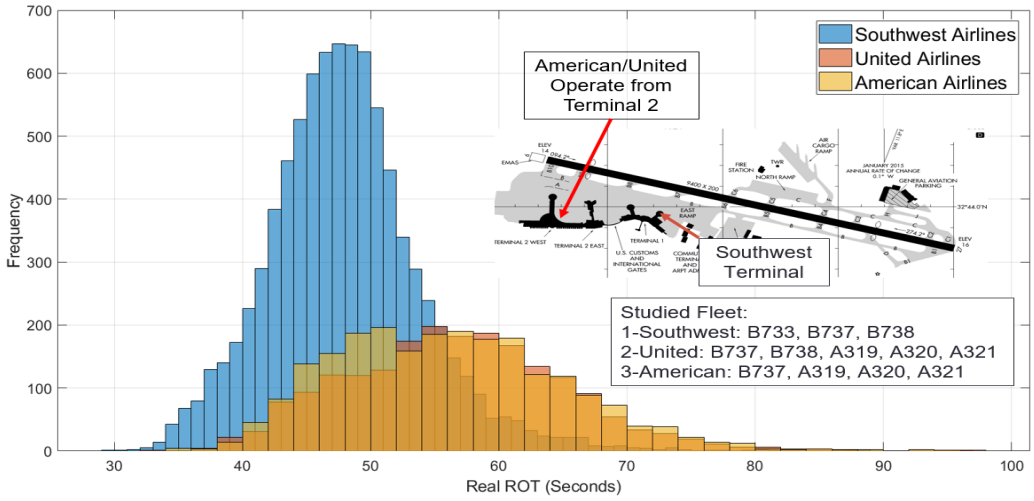

Figure 96. Variability of Runway Occupancy Times for Similar Aircraft Types Operating at Different Gate Locations.

Southwest airlines is the major carrier at SAN airport. This airline accounts for 35% of the total operations at this airport. The following pie chart represents the percentage of occurrence by airlines at SAN based on the ASDE-X data for years 2015 and 2016. In the chart we can see that American airlines and United stand on the next ranks with around 9% of operations each. Southwest airlines (SWA) uses different versions of Boeing B737 – B733, B735, B737, B738, B739- so for analyzing the ROT behavior of similar aircraft types with different associated carriers, we filtered the data from SAN for all the operations of B737 family for all the airlines. Figure 98 shows the distribution of Runway occupancy times and exiting speeds for the studied group of airplanes for the 6 major carriers at SAN.

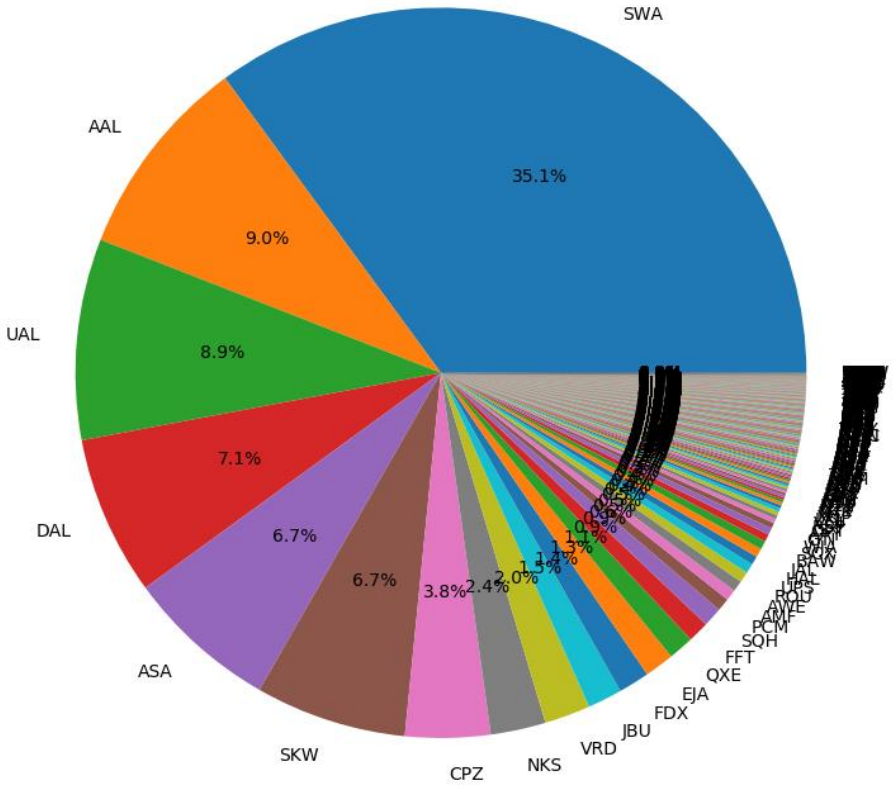

Figure 97. Percentage of Occurrence Based on Airlines at SAN.

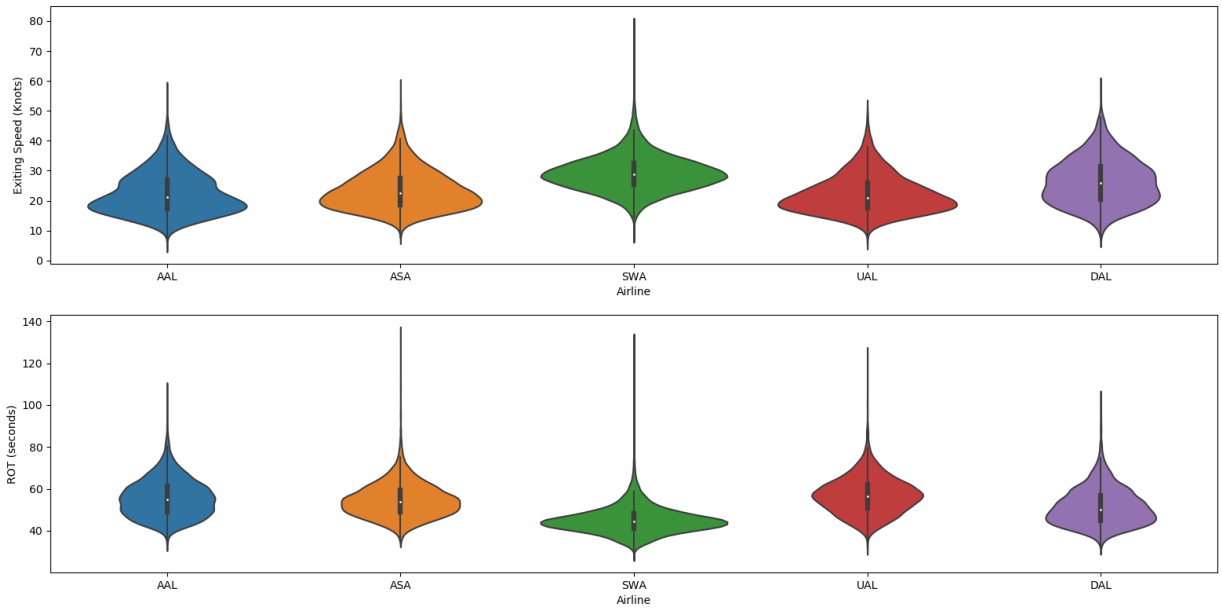

Figure 98. Top 6 Major Airlines' Distributions of ROT and Exiting Speeds.

SWA average runway occupancy time is 45 seconds, whereas the same values for American airlines flights with similar aircraft type is 56 seconds and for United it is 57 seconds. Therefore, SWA pilots not only save time for travelling to their gate area, but also they save 12 seconds of ROT in average compare to the other major carriers. This is interesting that when we take a look at average exiting speeds based on airlines, we notice that SWA stands at top with 29 knots while American and United flights took the right angle exits with 22 knots on average.

5.1.2 Los Angeles International Airport (LAX)

We observed motivational factors in pilot behaviors in LAX data as well. Similar to SAN airport, the motivated carrier at LAX airport is Southwest airlines. The runway that we analyzed for motivational factors is runway 24R which is located at the far north of the airport. This runway absorbs 39% of the entire arrival operations at LAX. The runway length is 8,926 feet and it has operations of Airbus A380-800 which is the largest commercial aircraft besides Antonov A225. The average ROT on this runway is 51 seconds. American airlines is the dominant carrier in LAX with 13.2% of the operations, while SWA stands on the second rank with 12.5% of the flights. Figure 99, shows the distribution of ROT times on runway 24R for the top 6 major airlines which operate at LAX. We can clearly see that SWA flights had an overall lower ROT values on this runway, therefore we were curious to see whether there are any motivational factors playing role on this runway or not. For this purpose, it is always valuable to analyze the nominal deceleration or speed parameters on the runway, in addition to exiting distances. Before reviewing the critical landing parameters, we take a look at the runway layout and its exit configuration to see whether there were any popular runway exits on this runway or not. Figure 100, shows the exit configuration on runway 24R at LAX airport. This runway has only 5 exits, which the most popular

one is taxiway “AA” which is a high speed exit, however there’s another high speed exit called as “Z” which is closer to the threshold and some flights use that as well. The reason behind the bi-modality of ROT behavior for many carriers according to Figure 99, is the existence of two high speed exits on this runway. We noticed that around 72% of SWA flights behaved in an extremely unnominal way and broke extremely hard to make it to the first turn-back exit called as taxiway “Y”. Table 20 represents a complete data analysis on exit utilizations and ROT statistics for the top major carriers which had operations on runway 24R in the landing database. The values in table clearly tell us that SWA flights utilized taxiway “Y” 72% of the times as they could save taxing times towards their gate locations as the consequence for their exit selection.

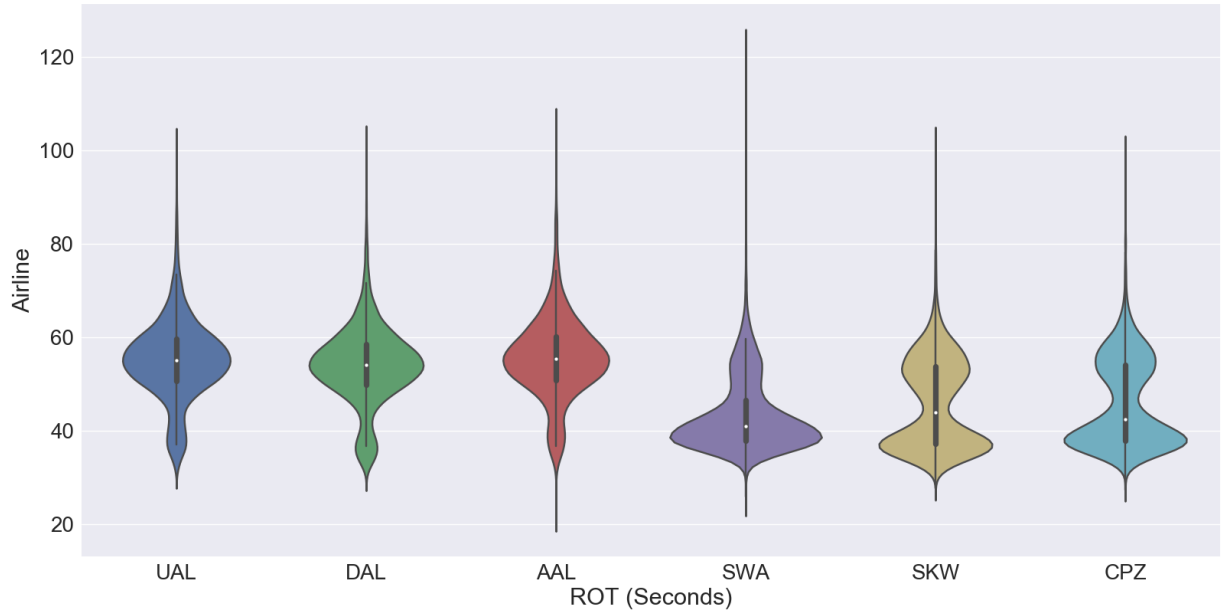

Figure 99. Distribution of ROTs for Top Major Airlines at LAX on Runway 24R.

Figure 100. Runway 24R at LAX Exit Configuration.

Table 20. Exit Configuration, Flight Utilization, and ROT Stats on Runway 24R at LAX for Major Airlines.

Exit Name	PC Distance (feet)	Airline	Average ROT (s)	Average Exiting Speed (Knots)	Count of Flights
W	2640	SKW	27.7	21.8	1
		SWA	27.3	23.7	8
Z	4275	AAL	39.9	48.5	1843
		CPZ	38.9	46.2	13605
		DAL	37.6	51.8	2237
		SKW	37.6	50.6	12979
		SWA	39.2	53.1	3566
		UAL	39.3	50.2	1683
Y	4680	AAL	40.4	19.9	16
		CPZ	40.7	20.5	52
		DAL	39.7	22.5	6
		SKW	38.2	22.9	44
		SWA	40.2	21.2	36688
		UAL	41.4	20.1	15
AA	6541	AAL	56.8	41.2	16015
		CPZ	55.6	42.4	9419

		DAL	55.4	44.4	18615
		SKW	54.2	45.6	12014
		SWA	55.1	43.8	10397
		UAL	56.4	42.4	13845
BB	8733	AAL	76.1	17.5	443
		CPZ	75.9	20.2	143
		DAL	75.2	19.9	445
		SKW	75.4	20.6	202
		SWA	77.1	20.1	257
		UAL	76.6	18.1	374

Clearly the majority of SWA flights take an early turn-back exit on runway 24R which help them reducing their ROT values considerably. However, we have to understand that the average exiting speed at the PC point for a runway exit like taxiway “Y” on runway 24R is just around 21 knots even for SWA flights. Therefore, for successfully evacuating the runway via this specific taxiway, pilots should brake harder than their nominal behavior on such a long runway. We validated our assumption for the impact of hard braking by looking at the distributions of nominal deceleration rate for SWA and non-SWA flights. Figure 101, shows the histogram of nominal deceleration rates and the fitted normal distributions for SWA and non-SWA flights.

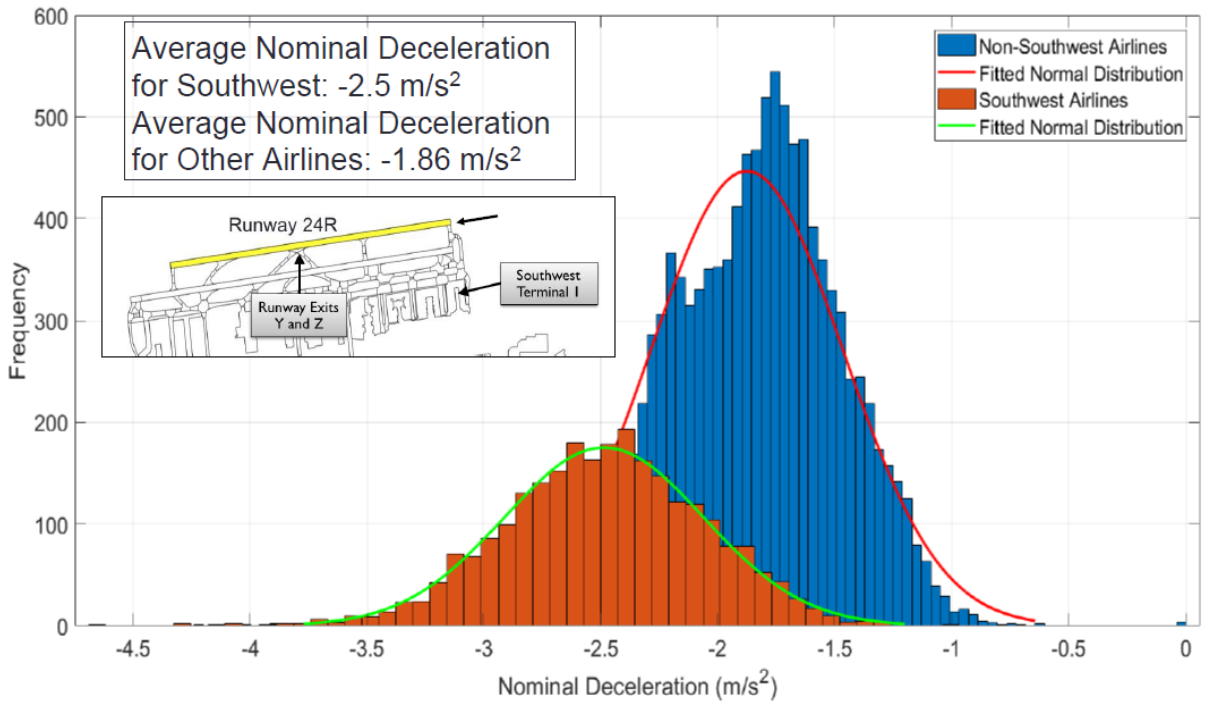

Figure 101. Distribution of Nominal Decelerations for Southwest and Non-Southwest Flights on Runway 24R and the Fitted Normal Distributions to Each.

The most popular runway exit on this runway is taxiway "AA" which is considered as a high speed exit with an angle of 30 degrees, a radius of 1,800 feet, and a path length of 1,000 feet from its PC point all the way to the exit hold-bar. This exit absorbs 58% of all the arrival flights on this runway. Taxiway "Z" and taxiway "Y" stand on the following ranks with utilization percentages of 21% and 19% in order. Taxiway "Y" geometry restricts the airplanes' exiting speed at the PC point as it has an angle of 135 degrees, a radius of 125 feet, and a path length of 377 feet from PC to hold-bar. For understanding the impact of braking rate on taking different exits, we compared the nominal decelerations for the top carriers on runway 24R which used high speed exit "AA" for evacuating the runway, with the nominal deceleration values for SWA flights which took the early turn-back exit. Figure 102, clearly represents higher braking rates for SWA flights when they took taxiway "Y" compare to the rest of the airlines when they took taxiway "AA". Similar to other parameters, most of the carriers had very similar behavior while using the same runway exit

according to the graph. Table 21 represents more detailed information about the nominal deceleration rates for different airlines on runway 24R at LAX. As we can see, SWA pilots had to brake harder than other pilots in case they wanted to vacate the runway by using taxiway “Y”. The average nominal deceleration for SWA flights who evacuated using exit “Y” was -2.73 m/s^2 which is even lower than 15th percentile of nominal decelerations for all B738s who landed on that runway. This tells us that for having an algorithm which replicates the motivated behavior for pilots, we have to modify the deceleration rate. Later in this chapter under section “Modifying the Braking Rate on the Runway”, we will explain a proposed method which deals with adjusted braking rates.

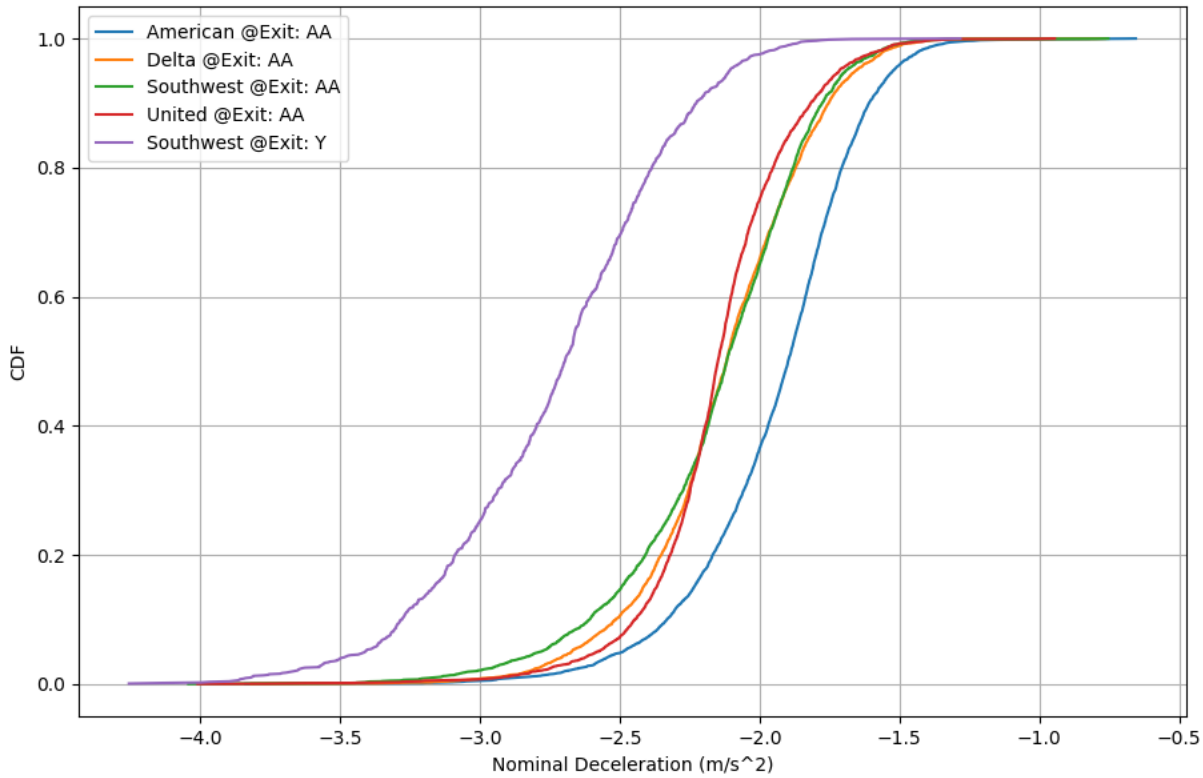

Figure 102. CDF Plots for Nominal Deceleration Values for American, Delta, United and Southwest Airlines Flights Which Took Exit "AA" and Southwest Flights Which Took Exit "Y".

Table 21. Major Airlines' Nominal Deceleration Rates for Taking Different Exits on Runway 24R at LAX.

Airline	Exit Name	Mean Nominal Deceleration (m/s^2)	Standard Deviation	15th Percentile (m/s^2)	20th Percentile (m/s^2)
American	AA	-1.94	0.3	-2.23	-2.17
Delta	AA	-2.13	0.31	-2.42	-2.35
United	AA	-2.15	0.27	-2.37	-2.32
Southwest	AA	-2.15	0.34	-2.49	-2.41
Southwest	Y	-2.73	0.41	-3.16	-3.1
All B738s On LAX 24R	All Exits	-2.14	0.4	-2.52	-2.42

5.1.3 Denver International Airport (DEN)

So far we talked about some observed motivational behaviors at SAN and LAX airports. At LAX we learnt that SWA flights brake harder to take an early turn-back exit which would help them saving more time on taxing towards their gate location. We observed the same behavior again for SWA flights at SAN, while for American and United flights we saw that pilots stay on the runway, as their associated terminal areas are closer to the end of runway. Generally, a motivational factor behavior is to save more time beyond the exit hold-bar and that's why pilots focus on taking specific runway exits at some facilities. Our take on this challenging problem is to analyze the feasibility of reducing ROT times as much as possible since the simulation model's major task is to minimize ROT. However, we can practice some approaches to model a behavior when the ROT will not be optimum, but the utilized runway exit is the desired one for the pilot. Our observation at DEN airport falls into this category. As we mentioned earlier, by running multiple improvement scenarios we proved that by constructing a new high speed exit on runway 16R, we could reduce

ROT by 8 seconds in average. This tells us that maybe high utilization of the second existing high speed exit on runway 16R, is because the location of current exits is not optimum. However, we saw that the assignment to the first high speed exit was almost 25% of the assignment to the second high speed exit. After analyzing the airport layout, we figure out that a specific design of a certain taxiway – D5- helps the flights to easily diverge to the parallel taxiway to the runway, and this maneuver decreases extra turning moves. The following figure represents the taxing path for flights which take high speed D5 on runway 16R. Figure 103, represents the layout of runway exits on runway 16R at DEN airport with taxiway D5 highlighted. This picture clearly shows how well-connected this taxiway is to the major path towards the terminal area, and airplanes would have to have the least number of maneuvering turns to taxi to the gates. As we mentioned before around 75% of arrival flights utilize this high speed exit, which is mostly due to the appropriate location of this runway exit. In contrast with those cases of motivational factors that pilots were seeking ways to evacuate the runways faster, here they have to coast for a longer time until they reach their desirable taxiway. This behavior is not basically a goal in our modeling because we don't want to increase ROT, however among the proposed methods we addressed some ways to report percentage of feasibility for utilizing each runway exit. This way a planner can evaluate the number of flights which can take a desirable runway exit no matter how it would impact the ROT.

Figure 103. Taxiway D5 on Runway 16R at DEN, Which Leads Airplanes Easily Towards the Terminal Area.

5.2 Defining Desired Horizontal Distance on the Runway

Now that we showed multiple examples of motivational factors on various runways, it is time to evaluate a few proposed methods for modeling that sort of behavior. The first method that we present here is named the horizontal distance. Each motivated pilot focuses on a limited number of runway exits, among those they can take to evacuate the runway successfully. The location of those exits while running an evaluation mode can be identified by the horizontal distance from the runway threshold. Therefore, a user who knows where the allocated terminal area would be for a

set of airplanes belonging to a specific airline will identify the percentage of flights that should be preferably assigned to particular exits determined by their horizontal distance from the arrival threshold. In this method we consider the absolute difference of aircraft exiting distance and desired horizontal distance to be less than or equal to 100 feet. Hence, when we run our evaluation scenario with motivational factor options, the model tries to repeat each iteration of motivated flights until it can get assigned to the preferable runway exits by checking the absolute difference criteria in distances. Here we present an example from SAN airport where we simulated 100,000 Airbus A319 flights and compared the exit utilizations with the ones at SAN on runway 27. We present three different scenarios:

1- Simulating without motivational factors
2- Simulating with one desired horizontal distance for all the samples of a specific aircraft type
3- Simulating with multiple desired horizontal distances with assigned weights to each of them

Before reviewing the simulation results, it is valuable to take a look at SAN runway 27 runway exit configuration and types. When landing on runway 27 around 49% of the flights take runway exit “B8” which located 5,226 (feet) from the threshold. Runway exit “B9” is the second popular exit which absorbs around 33% of the entire arrivals. You can see the location of popular exits and their labels in the following figure.

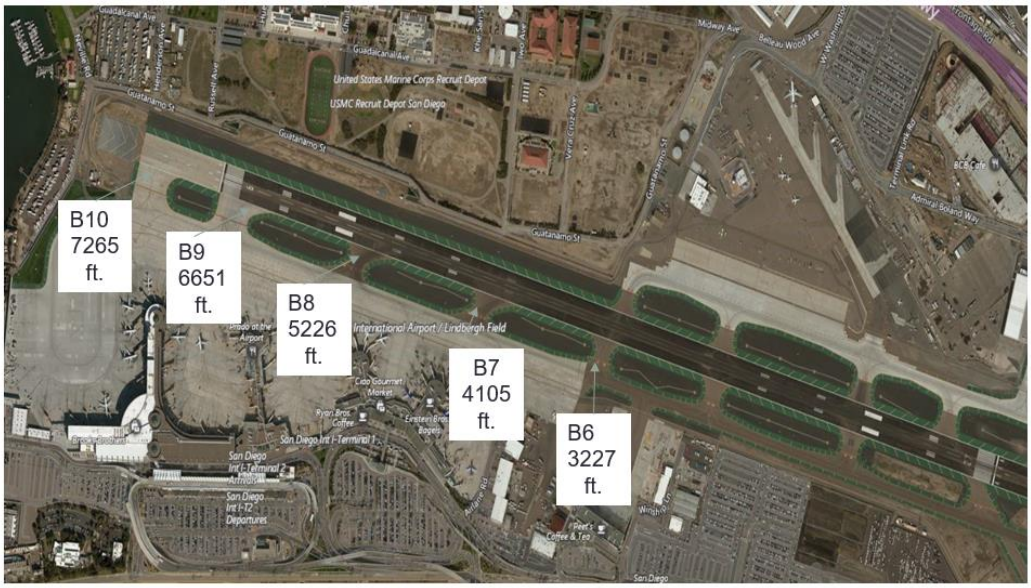

Figure 104. SAN Runway 27 Runway Exit Configuration and PC Distances of Popular Exits.

We have data for 180,997 arrival flights at SAN from years 2015 and 2016. Among those arrivals 6,636 flights were operated by Airbus A319 which 1,980 of them were for Spirit Airlines, 1,393 belonged to United Airlines, and 1,200 belonged to Frontier Airlines. 51% of A319s vacated the runway by using exit "B8", 42% used runway exit "B9", and the remaining 7% used the rest of the exits. Therefore, there's a tendency among A319 flights to take "B9" as it is located closer to the desired terminal areas, however "B8" would provide lower ROT values as it is closer to the threshold. Hence, in such situation we have a motivational factor which is not following our simulation strategy that is to optimize ROT. For addressing this challenge, we compared a simulation scenario without motivational parameters and the exit utilization of A319s on this runway. The following figure shows the CDF plot for 100,000 simulated A319s on runway 27 and their real exit utilization from ASDE-X data. As shown in Figure 105, the simulation logic is to vacate airplanes based on their nominal behavior as soon as possible, however for this specific case this doesn't match the observed behavior at SAN due to preferred taxiway leading to the terminal area at the end of the runway. From the exit utilization CDFs, we can interpret that there

are two desired locations for this aircraft type on this runway: one at 5,226 (feet) and another one at 6,651 (feet).

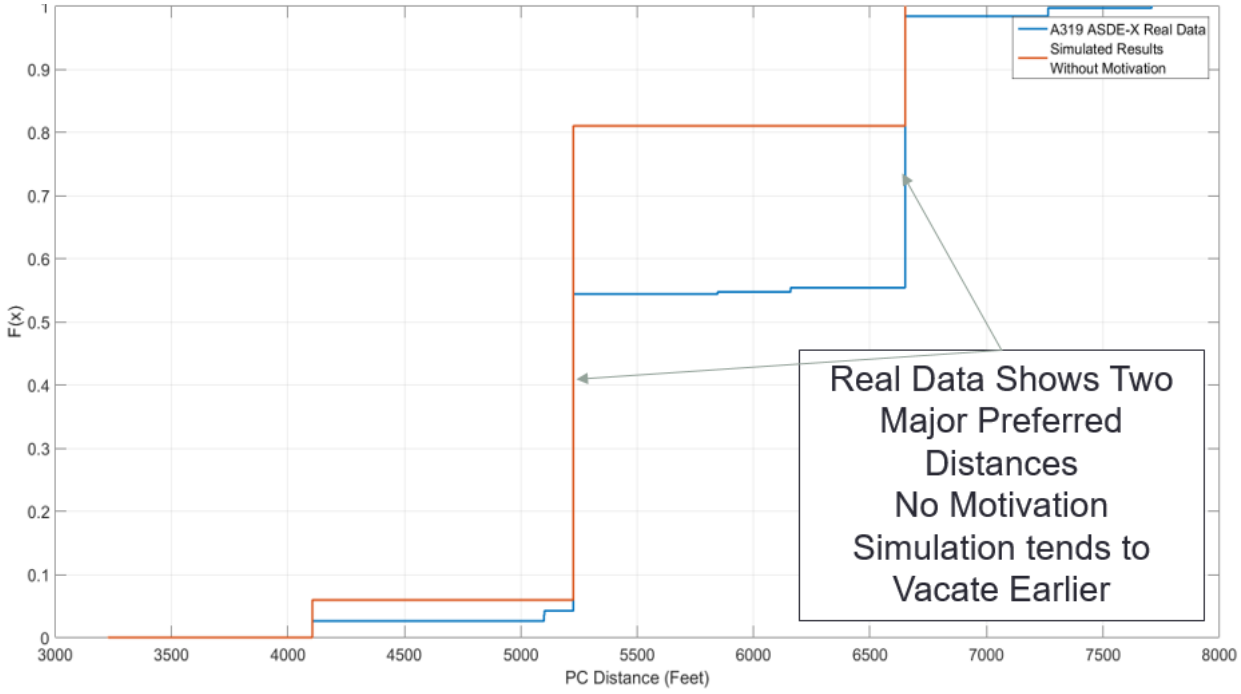

Figure 105. Exit Utilization for Nominal Simulation Scenario and ASDE-X Data for A319 Flights on Runway 27 at SAN.

As shown in Figure 105, the simulation strategy is towards saving ROT times when we don't include any motivational parameters. Keep in mind that average ROT to "B8" is 48 seconds, while average ROT to "B9" is 59.4 seconds, therefore based on our model logic it doesn't make sense for flights to skip using runway exit "B8" unless their generated random parameters wouldn't pass the criteria for taking this exit successfully. That's why around 81% of the simulated flights are already vacated the runway by the position of taxiway "B8" and just 19% are assigned to "B9". As we mentioned earlier the first proposed method to reflect the motivational behavior is to ask the user to enter a desired horizontal distance and the algorithm in evaluation case repeats the same steps until it get to exit assignment procedure. If the next feasible exit would be within 100 (feet) from the desired entered horizontal distance, the set of generated random events will be saved and

we check that instance as a successful candidate. If the mentioned criteria won't be met, we resample all the landing parameters until we get a set of them which can evacuate the airplane successfully from the preferred exit location. Of course this option is tricky for naïve users who are not familiar with individual aircraft type characteristics and they might enter unreasonable desired locations. In that case the model might never converge to a feasible solution within multiple iterations, therefore we put a threshold for number of total attempts in generating landing profiles. If the total number of failed attempts would be 2.5 times the number of required landings for each aircraft in the fleet share, we stop the simulation and tell the user that the entered desired distance is not appropriate for that aircraft on that runway cluster with the provided runway exits. If we think about the recent process, there might be some cases that would be lucky to pass the threshold cap with tiny margins. For addressing that issue, we report the success rate among all the attempts for the specific entered horizontal distance. That way users can understand how likely is for their entered fleet mix to successfully evacuate runway at the preferred location. Now let's continue on our A319 case on runway 27 at SAN airport and try to test the proposed algorithm with 100% of the A319s to be preferably assigned to "B8". The following graph shows the CDF plot for exit utilizations of 100,000 simulated A319s and real ASDE-X data. as we can see the model assigned 100% of the simulated flights to "B8" with a success rate of 97%. This means that our algorithm works well and the majority of the generated instances could make it to "B8", however the model had to resample more instances to compensate for that 3% which couldn't evacuate by taxiway "B8" location. Now we know that we can restrict the flights to a certain exit location and the model tells us a success rate for that. Let's try repeating this analysis for 100% motivational factor for exit "B9" by entering the desired horizontal distance as 6,651 (feet).

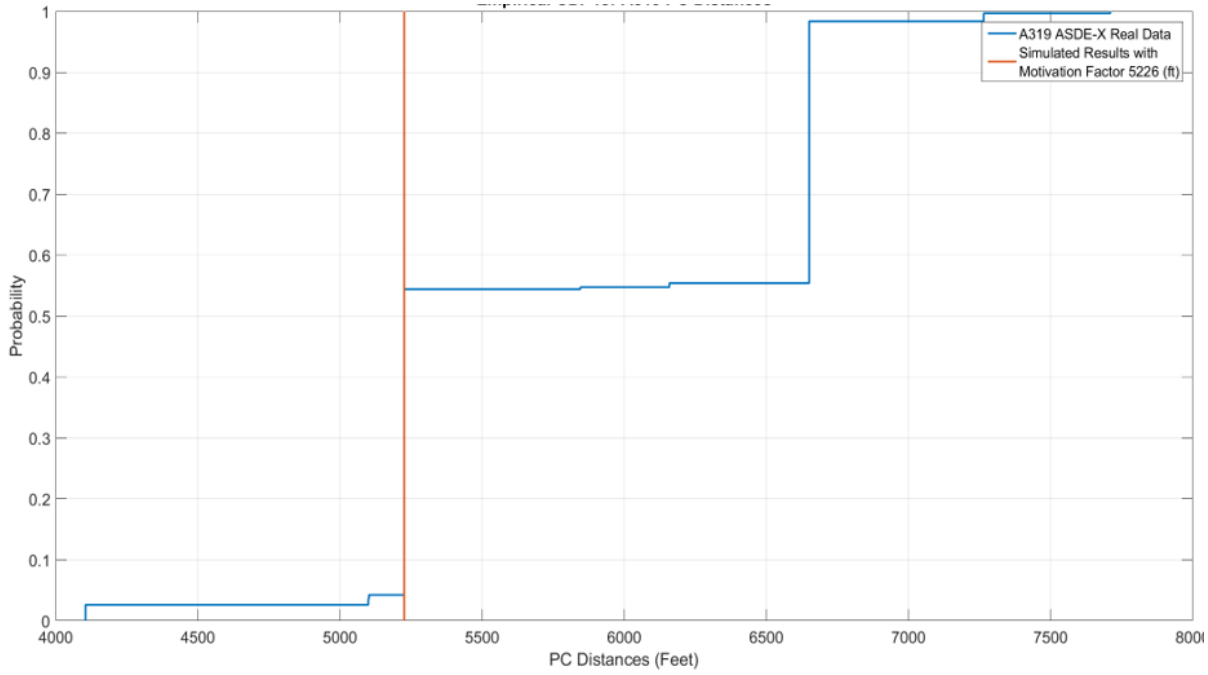

Figure 106. Exit Utilization for Motivated Simulation Scenario with Desired Exit Distance as 5,226 (ft.) and ASDE-X Data for A319 Flights on Runway 27 at SAN.

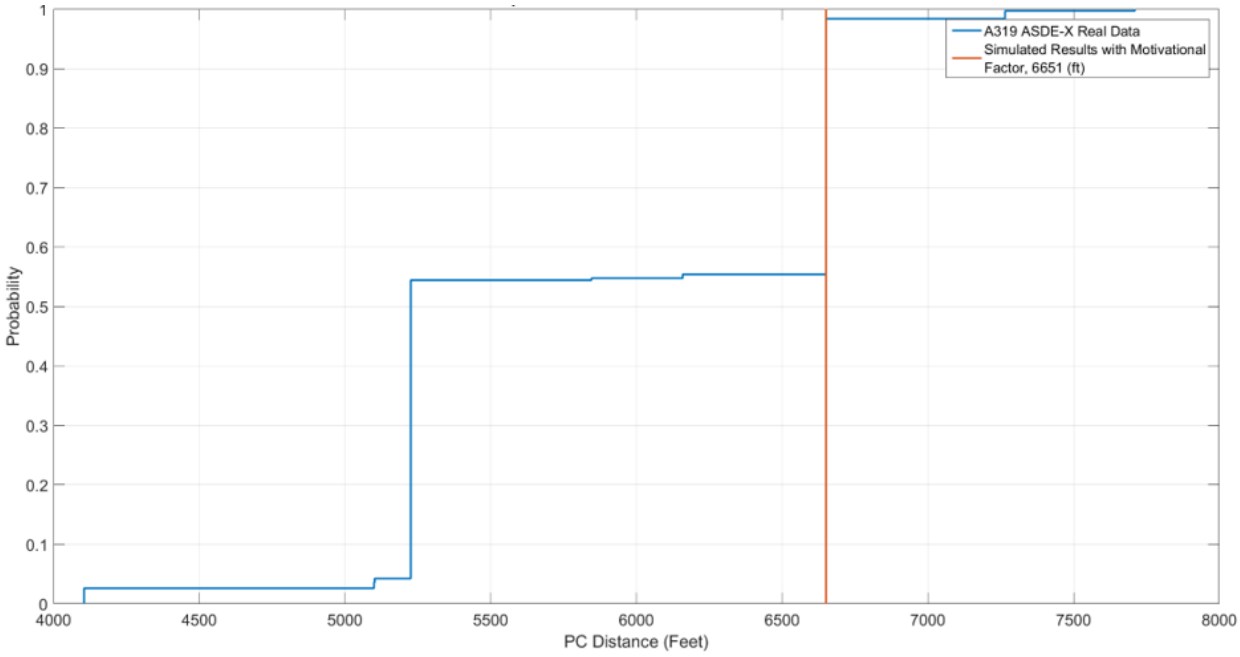

Figure 107. Exit Utilization for Motivated Simulation Scenario with Desired Exit Distance as 6,651 (ft.) and ASDE-X Data for A319 Flights on Runway 27 at SAN.

Figure 107, represents the second motivated scenario where we entered the preferred horizontal distance at the location of exit "B9". As we can see in the graph the motivated simulation algorithm

assigned 100% of the simulated flights to exit “B9” with a success rate of 100%. This makes sense since this exit is located almost at the end of the runway and many generated instances of a narrow body airplane like A319 can easily use that exit to vacate the runway. Now that we learnt the patterns and validated the results of the algorithm, we can run the case which is very close to the real exit utilization for A319s at SAN on runway 27. As we mentioned around 51% of A319 flights utilized exit “B8” and 42% utilized exit “B9”. Since the remaining exits are either very close to the threshold or very far, we round the utilizations to 50% for each of the preferred runway exits. This is a solid assumption as we know flights in the real world which used exits prior to “B8” or after “B9” had extreme values in any of their landing parameters. So by entering equal weights of 50% to two desired horizontal distances one at 5,226 (feet) and another at 6,651 (feet) we ran the third motivated scenario. The following figure represents the exit utilization for 100,000 simulated A319s versus the real ASDE-X data for this aircraft type. As we can observe in Figure 108, the algorithm successfully assigned half of the flights to the first desired location which was exit “B8” and the remaining half to the second desired location which is where exit “B9” is located. As expected the success rate for this scenario is 100%. This brings us to the conclusion for this proposed method that overall the algorithm does an acceptable job in assigning defined percentages of specific airplanes to defined preferred locations, however the issue is that we repeat exactly the same sample generation as we do for a nominal evaluation case. The only difference is that we resample until we assign to the desired exit location and we repeat this process until we meet the number of required iterations entered by the user. We can definitely improve this process by generating candidates more intelligently and not relying on pure random procedure. We explain a new proposed method in the next section which tries to model the motivational factor more

intelligently and also it is well-aligned with our primary goal in reducing ROT. Therefore, next section attempts to see whether we could push the airplanes to vacate the runway sooner.

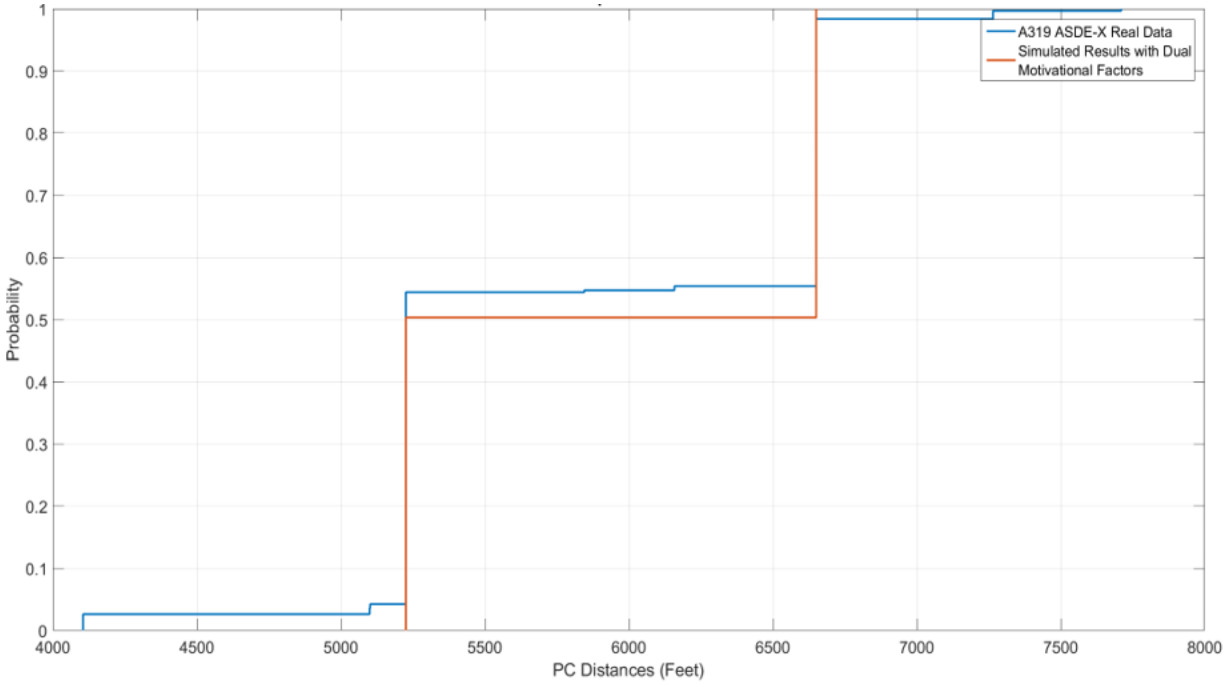

Figure 108. Exit Utilization for Motivated Simulation Scenario with Equally Weighted Desired Exit Distances as 5,226(ft.) and 6,651 (ft.) and ASDE-X Data for A319 Flights on Runway 27 at SAN.

5.3 Modifying the Braking Rate on the Runway

The second method that we propose for modeling motivational factors is about adjusting the required acceleration for making to certain runway exits. In the previous method, we saw that the model was trying to resample as many instances until the required number of iterations of arrival flights successfully vacated the runway by a certain distance. This method is suitable for those cases when the nominal performance of the selected aircraft types generally matches the set of required parameters for desired exit locations. For example, in the case study at SAN airport, we saw that with high success rate A319s could utilize the right angle exit at the end of the runway as it is not a hard runway exit to be taken for narrow-body airplanes. However, in cases like LAX runway 24R, where we saw very aggressive behavior by SWA flights, we might meet the threshold

cap for failed scenarios and would never converge to a feasible solution. For those cases, we can't rely on random events anymore, as most of the times pilots don't show such high motivation and we don't have enough occurrences in any of the distributions related to landing parameters. There have been some studies about adjusting braking rates for airplanes while landing and automating the selection of runway exits even before the landing. The most famous system in the world which is using such adjustments is called Brake to Vacate (BTV), which is an extra software designed by Airbus to reduce the chances of runway overruns [42][43]. The BTV system also enables the pilots to select their desired runway exit before the landing. By back-engineering the required braking rate it checks the feasibility of taking the selected runway exit and notifies the pilot. This system was initially designed for Airbus A380-800 which is a giant aircraft and there's always a risk for overrunning runways specifically on wet pavement, but thanks to BTV the avionics on board help the pilot to vacate the runway safely. After huge success in A380 airplanes, Airbus started to implement this system on massive scales on A320 aircraft family and A350 series. This system constantly evaluates the speed and deceleration of the airplane and sends the flight crew feedback about the required next steps. For example, it tells the pilot based on its calculated deceleration rate for making to the PC point of a specific runway exit, what level of braking and which combination of braking and thrust reversers should be implemented in order to have the airplane in a proper speed at the PC point of selected runway exit. This system also evaluates the feasibility of making to a defined exit based on the pavement condition and if the runway would be too short, it gives the pilot an alert via audio and visual signals. The idea of BTV was developed by a PhD student named Fabrice Villaumé back in 1998, and after testing the process on an Airbus A340, in March 2005 the first landing test was accomplished. BTV system was initially tested with an A380 flight in May 2008 [42].

After familiarizing with the BTV process, we thought that we could implement a similar procedure for modeling motivational factors on runways. What happens with BTV is that the avionics on the board calculate the required deceleration rate for a given exit based on predicted speeds on the runway for the aircraft. When we simulate a landing profile nominally, we generate a threshold crossing speeds based on the runway cluster, we generate a touchdown location based on runway cluster, and then we generate a nominal deceleration again based on the runway cluster. Now if the deceleration from nominal speed to the PC point which its speed is generated based on exit clusters, would be less than or equal to 1.2 times the nominal deceleration, we accept those set of random numbers and assign the flight to the successful exit candidate. The issue here is that we might've generated a low nominal deceleration rate and our aircraft might not be able to vacate early due to its shallow generated braking rate. Therefore, the solution can be inspired by the BTV procedure. If we let the algorithm generating random values for threshold crossing speed, and touchdown location, but instead of generating a nominal deceleration from the distribution we back-engineer the required deceleration rate for making to the exiting speed for each upcoming runway exit, we can make sure that we are not blindly selecting a random deceleration rate which might not be feasible for early exits. Having all the required deceleration rates for every upcoming exit on the runway beyond the nominal speed point is helpful, however meanwhile we don't want to out-perform the aircraft and push it beyond its capabilities. The reasonable way for checking the feasibility of braking for that specific aircraft type with the new calculated deceleration is to see where in the distribution of nominal decelerations collected for that aircraft in the runway cluster, the new deceleration rate stands. We defined certain percentiles to give users a better statistical feeling about the amount of pressure they're implementing over the braking values. Basically, for each upcoming exits on the runway the algorithm checks whether the required

deceleration will be in a certain range of nominal distribution of the aircraft or not. So for running the evaluation mode with motivational factor option we follow these steps:

1- The algorithm generates a random threshold crossing speed based on the runway cluster and aircraft type.
2- The algorithm picks a touchdown location based on the aircraft type and runway cluster.
3- Then it assigns random exiting speeds to all the open exits on the runway based on their cluster groups and aircraft type.
4- Now that we know the beginning and ending speeds, we can calculate the required deceleration from the touchdown point all the wat to the PC point by the following constant speed formula:

$$a = \frac{V^2_{Exiting\ Speed\ at\ PC} - V^2_{Touchdown\ Speed}}{2 * \Delta(Distance\ Between\ Touchdown\ Location\ and\ Exit\ PC\ Point)}$$

5- The required deceleration calculated in step 4 then will be compared to a certain percentile of the Kernel distribution of nominal decelerations for the same aircraft type on the specific runway cluster. Three modes were defined to let the user know about the amount of braking in terms of percentiles of the data. Those modes are:
    a- If the user selects the “low” motivational factor mode, the required deceleration from touchdown point to the PC point should be greater or equal than 20^{th} percentile of the nominal deceleration distribution for that aircraft on that runway cluster to assign the flight to the nearest exit which satisfies this criterion.
    b- If the user selects the “medium” motivational factor mode, the required deceleration from touchdown point to the PC point should be greater or equal than 15^{th} percentile

of the nominal deceleration distribution for that aircraft on that runway cluster to assign the flight to the nearest exit which satisfies this criterion.

c- If the user selects the “high” motivational factor mode, the required deceleration from touchdown point to the PC point should be greater or equal than 5^{th} percentile of the nominal deceleration distribution for that aircraft on that runway cluster to assign the flight to the nearest exit which satisfies this criterion.

Notifying the user about the selected percentile can give him/her a better understanding of the situation and we help them to judge it themselves if they want to push their chosen fleet mix to brake that hard or not. We will review some examples and explain the procedure on real-world scenarios to see how well the new proposed algorithm works. Previously we mentioned an example of observed motivated behavior by SWA flights on runway 24R at LAX. Here we try to see how different percentiles of nominal deceleration will change the exit utilization. As you can see in the following plot, for each motivational level, we cover a certain part of the entire nominal deceleration distribution for B738 on the cluster family of runways, including 24R at LAX. The values shown in the figure for each of the motivated scenarios are heavily dependent on the location of each available exit for the simulation agent. After calculating the required braking rate from touchdown point to the PC point of every upcoming exit, we check whether the required deceleration passes the criteria of maximum available deceleration or not.

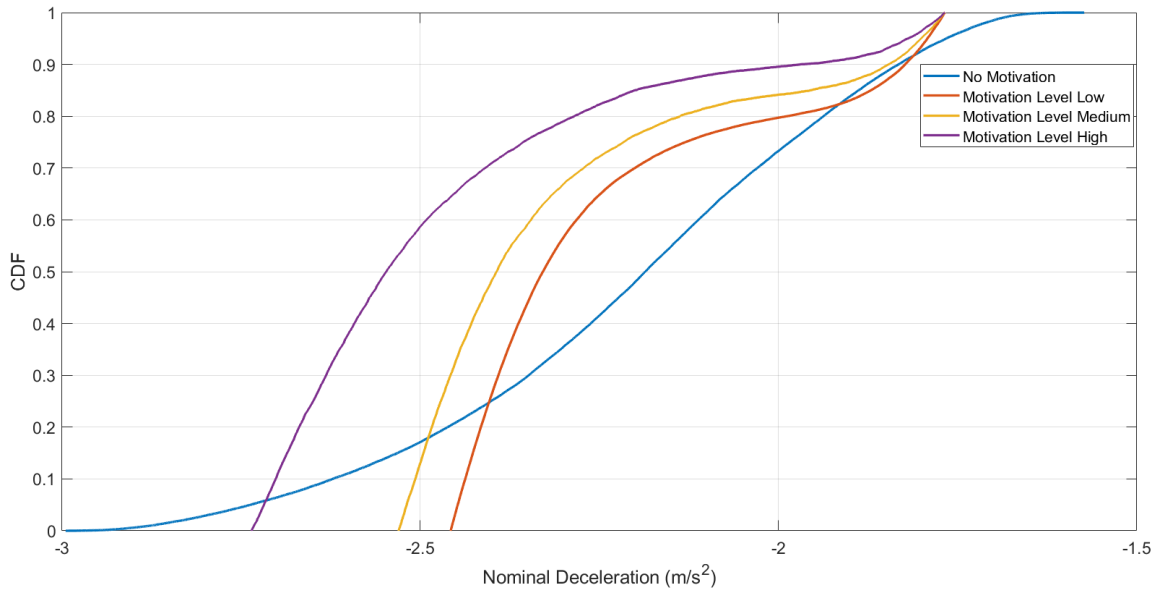

Figure 109. Deceleration Values for 4 Different Simulation Scenarios of B738 on Runway 24R at LAX.

Now we take a look at the exit utilization for each of those scenarios to see the impact of shifting the braking rate to the required deceleration from the touchdown location all the way to the PC point. As we can see there's a drastic change in exit utilization by using the new proposed motivational algorithm. For this specific case we can see that from approximately 16% of utilization for the first high speed exit, by forcing the algorithm to accept deceleration rates as big as 20th percentile of nominal decelerations on this runway cluster, 48% of B738s could take the first high speed exit and around 80% were already vacated the runway by taxiway "Y". If you remember we mentioned earlier that 72% of SWA flights utilize taxiway "Y", which means that they had to brake very hard and that was the inspirational for our new proposed motivational algorithm.

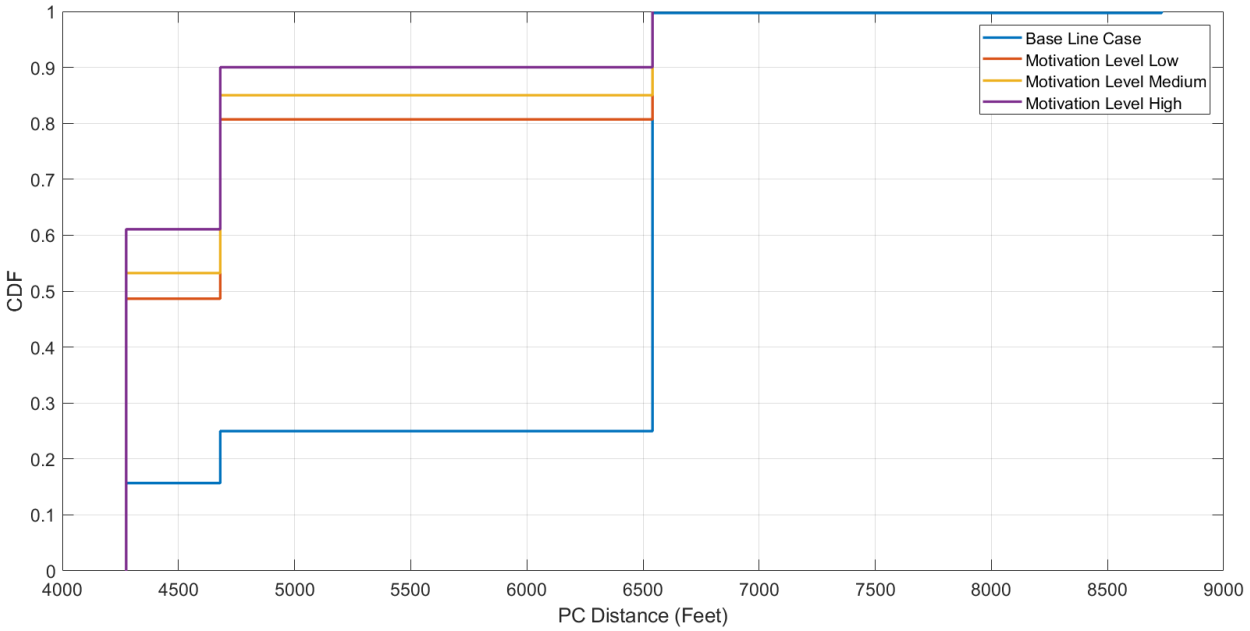

Figure 110. Exit Utilization for Different Motivated and Non-Motivated Simulation Scenarios for B738 on Runway 24R at LAX.

Calculating the required deceleration and having a percentile threshold for vacating the runway earlier seems to be working well. However, this option will allow the user to assign flights to runway exits, which requires pilots to brake really hard for utilizing them. As the result, the designers will construct high-speed exits at short distances from the runway threshold and they might not be very comfortable for every pilot. Even though we can reduce ROT times drastically by shifting the deceleration values to smaller percentages, it might not be safe for most operations that behave nominally. Therefore, it is recommended that in addition to selecting harsher braking rates, we notify the user about the success rate of each scenario. In that case, users of the model can assess whether it makes sense to push more pressure on the pilots for braking harder based on the reported success rates or not. In the next section, we review a similar approach with the difference that this time we notify the user about the number of total attempts for the convergence of simulation results if they choose different levels of motivation.

5.4 Modifying the Braking Rate and Desired Horizontal Distance

In this chapter, we reviewed some real examples of motivated behavior at ASDE-X supported airports. Then we proposed two methods to replicate that behavior in our simulation model. First, we offered a way that users would enter a preferred distance and the algorithm keeps resampling until it converges to the defined number of required flights. Second, we offered an algorithm which was inspired by the BTV system, which calculates the required constant deceleration from the moment of touchdown to every upcoming runway exit and if that deceleration would be within certain range of nominal deceleration distribution on that runway cluster, we assign that flight to the runway exit which passed the criteria. In either of those approaches, we had one degree of freedom. In the first approach, our degree of freedom is the entered distance by the user, and in the second approach, it is the deceleration rate required to vacate the runway within a certain allowable range. Each of those methods yielded good results as we represented the drastic change in exit utilizations, however there are some shortages in each approach that might not be as practical as possible. In the first approach, the algorithm still generates random events on a nominal behavior from the collected distributions and it continues to resample until it converges. Even though we allowed the simulation loop to repeat itself for certain amount of iterations, there can be some cases that wouldn't end up with many successful candidates. Hence, the algorithm will tell the users that their desired distance is not feasible. In the second approach, we solved that challenge by choosing the deceleration rate more wisely. When we calculate the required constant deceleration to every upcoming exit and check whether they're within a certain range of nominal decelerations, we increase our chance for evacuating at certain exits rather than relying on pure random numbers. However, in the second approach, we tend to assign the aircraft to the nearest feasible exit which is ideal for reducing ROT, but we observed some behaviors that users might

be interested in saving taxi times by exiting at further locations which are closer to the terminal areas. Moreover, even with a threshold for the number of total attempts, the user is still blind about the process's success rate. Therefore, we thought that the most sophisticated way is to combine both of the mentioned approaches and deliver better outputs to the user. In the new proposed approach, we consider two degrees of freedom. First will be the desired distance that the user wants certain airplanes to vacate the runway, and second the desired motivational level that the user wants to test. As a result, we check that motivated planes will be vacated at a particular location, but we also adjust their braking rates. This time, we also report each scenario's success rate for the user and assess whether that's a reasonable location for their desired runway exit. Here we present a few examples and explain the new approach with more details.

Imagine that we have a 16,000 (ft.) runway and we want to evaluate the utilization percentages for each of them at certain distances from the runway threshold. Let’s choose B738 as our test flight on this runway. This is a narrow-body aircraft which has the flexibility of braking hard and landing early on such a long runway, however we should keep in mind that for such a long runway at sea level the touchdown locations will be shifted further down range on the runway. For our first case study we imagine that the user has two desired locations for constructing high speed exits. One at 6,500 (ft.) and another at 9,000 (ft.) as based on our observations these locations are good candidates for absorbing most of the traffic for such a runway length that we have here. We ran the analysis with a base case scenario where we applied our nominal simulation methodology and the success rate is simply the exit utilization percent without any motivational factors. Then we repeated the simulation by considering motivational factors regarding the desired entered distance and desired deceleration percentile. For both of our case studies we stuck with our previous definitions for motivation levels:

1- Motivation level low: 20th percentile of nominal deceleration

2- Motivation level medium: 15th percentile of nominal deceleration

3- Motivation level high: 5th percentile of nominal deceleration

Similar to the base case for each scenario, we reported the success rate in addition to the average runway occupancy time of all simulated flights for each case. Note that we ran 100,000 iterations in each scenario for the selected fleet mix which is Boeing B738 in this case. The following table summarizes the results for all the scenarios. As shown in Table 22, by changing from nominal behavior to motivated ones, we see a significant change in success rates specially for the runway exit which is closer to the threshold. This example clearly tells the user that what is the success rate and average ROT for each scenario to each of the desired exit locations. This approach is better than only entering desired distances as we could modify the braking rates. Also, it is also better than only modifying the braking rates since we know what is the success rate for each motivational level. With this new algorithm every user can evaluate various desired locations for various aircraft types and assess the situation with higher confidence. As we enabled the users to create output files after each simulation scenario and review the generated values for each critical landing event, users can analyze the range of deceleration rates which was used for each of the motivated scenarios and evaluate their initial decisions on their preferred exit locations.

Table 22. Exit Utilizations and Average ROT for B738 on an Imaginary Runway, for Motivated and non-motivated Scenarios.

Exit Location (feet)	Zero Motivation/ ROT	Motivation Low/ROT	Motivation Medium/ROT	Motivation High/ROT
6,500	43%/53 s	49%/52.5 s	65%/52 s	75%/51.8 s

9,000	99%/73 s	100%/66.7 s	100%/66.6 s	100%/66.6 s

Now let's try another example on a long runway where we can evaluate the location of many hypothetical runway exits. This time we test our proposed algorithm on a 10,500 (ft.) runway at 650 (ft.) from the sea level. This geometry information is very similar a popular runway at ORD which is runway 10C. For this test we pick another narrow-body aircraft which is flexible enough to perform braking at various levels. Our selected plane for this case study is Airbus A319. Note that we focused on narrow-body planes for our motivational studies as we just observed such behavior among different carriers who dominantly use narrow-body planes. Definitely harsh ranges of braking rates are not feasible for heavy or super-heavy aircraft and small planes can easily utilize early exits. Therefore, the challenge is for narrow-body planes where they can cover a wide range of exit distances. For running our sensitivity analysis on hypothetical desired exit locations, we located high speed exits at 4,000 (ft.), 5,000 (ft.), 6,000 (ft.), 7,000 (ft.), and 8,000 (ft.) from the runway threshold.

Table 23. Exit Utilizations and Average ROT for A319 on an Imaginary Runway, for Motivated and non-motivated Scenarios.

Exit Location (feet)	Zero Motivation/ ROT	Motivation Low/ROT	Motivation Medium/ROT	Motivation High/ROT
4,000	10%/43 s	13%/42 s	15%/42 s	18%/42 s
5,000	69%/49 s	74%/49 s	84%/48 s	95%/48 s
6,000	98%/55 s	99%/55 s	100%/55 s	100%/55 s

7,000	100%/64 s	100%/63 s	100%/63 s	100%/63 s
8,000	100%/73 s	100%/73 s	100%/73 s	100%/73 s

As shown in Table 23, by pushing the simulation agent in terms of braking rates, the utilization for earlier runway exits increases as expected. This example is a nice representation for the potential of narrow-body airplanes in utilizing early runway exits by adjusting the nominal deceleration factor. The benefit of this method is that not only the user will have an understanding of the success rate for each desired location of runway exits, but also it can evaluate the impact of the percentile of deceleration used in each of the scenarios. Therefore, whenever an airport planner wants to evaluate the probability of taking specific runway exits at certain locations on the runway, they can adjust the motivation level in terms of braking pressure and select the scenario which yields the best ROT with a reasonable percentile of nominal deceleration. Another great aspect of this functionality, is that we don't apply the required deceleration without checking the historical performance of each vehicle, and this would assure the user that the resulted success rate at each preferred location is within the braking capabilities of each aircraft based on their collected historical data.

We here conclude this chapter by reviewing the material presented in it. First, we showed some real examples of observed motivated behavior at three airports in US from the ASDE-X data. We showed that in some situations, some carriers behaved with motivations for either vacating the runway earlier or later than their typical exiting distance. The main reason behind motivated behavior is to save some taxi time after evacuation of the runway, therefore pilots sometimes choose runway exits that can take them to their final terminal destination faster. After analyzing the observed behavior from real data, we proposed three methods to replicate the motivational

behavior in our simulation model. Our first proposed approach was to ask the user to enter a number of preferred locations for those airplanes that it wants to vacate at those locations. We explained that we model with a new distance criterion in a way that every successful candidate should vacate the runway within a small range from entered preferred locations. We resample until the number of required flights are met. If the failed cases pass a certain number compare to the total required flights, we notify the user that those locations are not feasible for the selected fleet mix. In the second proposed approach, we adjust the braking rate based on the location of every upcoming exit. This method is specifically useful for reducing ROT by allowing the airplanes to brake harder. We explained that we calculate the required constant deceleration from the touchdown point to every upcoming runway exit, and if that value would be equal or less than the maximum allowable deceleration rate, we consider that instance as a success. The same threshold for failed cases that we used with our first proposed approach was used in this method as well. Finally, we combined the first two methods and added an extra feature to them and we presented the third method. In this method the user is provide with two flexibilities in choosing input parameters. They can not only select a set of preferred locations for specific airplanes, but also they can choose what level of braking is allowed for airplanes on the runway. With this method we report the success rate for each of desired locations that the user fed into the model. This way planners will have a better understanding for the possibility of reducing ROTs with two degrees of freedom which are desired distances, and braking rates.

5.5 Conclusion

In this chapter, we talked about motivational factors while evacuating the runway. The idea for dedicating a chapter related to this subject was formed when the author of this document observed some fascinating behavior at San Diego airport for Southwest Airlines flights. They showed

extremely motivated patterns of braking for reducing runway occupancy times and evacuating the runway at specific runway exits. Three distinct methods for modeling motivational factors were presented in this chapter that can be reviewed by airport planners or airline analysts to analyze airplanes' behavior from the beginning of the braking phase to the full fuselage out moment of the aircraft. The proposed methods are based on either certain exiting distance or certain braking threshold or both of those factors combined. The chapter begins with various observed examples from the ASDE-X data and then we examined each of the proposed methods with real observed behaviors. All methods are valuable as add-on features to the simulation model. Users can use this new functionality to examine the possibility of reducing ROT times by assigning preferred exit locations or braking rates for their arrival fleet. All three methods were successfully tested against the real data and could replicate a motivated behavior for simulated planes. The difference of proposed methods is either in choosing a factor between desired exit location or desired braking rate, in addition to the amount of information which they provide for the users. In the third proposed method, which is the most sophisticated one, users can see the percentage of successful runway evacuations for every desired distance and braking rate scenario for every individual aircraft within their selected fleet. This functionality can provide in-depth information for users who are not familiar with each aircraft's technical performance. They are also curious about potential changes in exiting patterns that could save ROT or taxi time. The proposed motivational factors in this study are not delivered as part of the new REDIM model to the sponsor of this research study, however they're supposed to be added to the simulation model as add-on features in future phases of the study. The motivational factors implemented in the beta version of this model were programmed in a binary manner, where users can either use them or dismiss using them and run the model in the nominal version.

Chapter 6. Machine Learning Models for Predicting Runway Occupancy Times (Feedforward Neural Networks)

Runway occupancy time is an essential parameter to estimate the performance of airport operations. With improvements in airport surface radar surveillance technology, estimating runway occupancy time and aircraft exit distance on runways is possible. Past studies have predicted runway occupancy times using traditional simulation-based methods aided with airport observations. However, there are not many attempts to use deep learning and more recent data science algorithms to predict runway occupancy times. This paper describes a neural network algorithm for predicting runway occupancy times for arrival flights at airports. The algorithms used to predict runway occupancy time are data-driven. The data employed in this study is extracted from two years of the Airport Surface Detection Equipment Model-X deployed at 37 airports in the United States. The algorithm's input layer is defined using estimated speed and acceleration parameters for individual aircraft operating at different airports. We studied the performance of our model for fourteen distinct aircraft types at eight different airports and the weighted average R-squared values of the regression analysis between observed and estimated values for our predicted runway occupancy time model was 0.9. The R-squared value for predicted exiting distances was 0.94.

6.1 Introduction

Flight operations at large airports continue to increase as the demand for air transportation grows Worldwide. Runway capacity is an essential factor in assessing the practical capacity of an airport. With reduced aircraft in-trail wake vortex separations, runway capacity will be a necessary part at

improving the operational efficiency of the airport. By increasing the number of arrival and departure flights on runways, airports can handle more flights per hour and address the growing demand for air transportation services.

6.2 Input Data for Neural Network

6.2.1 ASDE-X Data

Airport Surface Detection Equipment Mode-X (ASDE-X) is a surveillance system using radar, multilateration and satellite technology that allows air traffic controllers to track the movement of aircraft and vehicles on active runways and taxiways [7]. There are 37 airports in the United States with ASDE-X equipment installed. The combination of radars and multilateration technology can detect airplanes up to 60 nautical miles from the airport. The ASDE-X data employed in this study includes landing operations at 37 airports for years 2015 and 2016. The ASDE-X data was used to create an interactive landing events database for the FAA. The two-year raw ASDE-X data is equivalent to 37 TeraBytes. ASDE-X data contains the geographically-referenced aircraft position (latitude/longitude) with high precision (i.e., millisecond level). Moreover, each ASDE-X record has information about the aircraft type, flight ID, and aircraft altitude.

Using the instantaneous position of each flight in ASDE-X data, we estimate the aircraft speed and acceleration every second. Similar to other radar surveillance data, ASDE-X data has “noise” in the reported positions and times. Smoothed speed profiles are generated in order to obtain reasonable values. Figure 111 represents the calculated and smoothed speed profiles for one aircraft event. We used the moving average technique to smooth aircraft speed data.

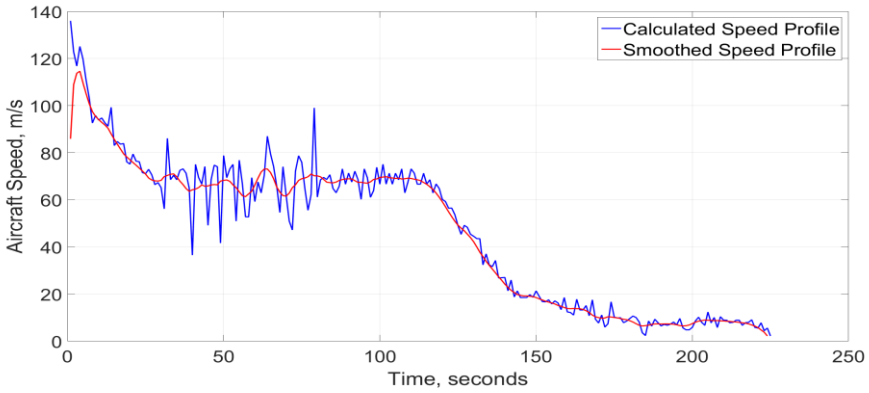

Figure 111. Calculated and Smoothed Speed Profiles for a Single Landing Event.

The primary focus in analyzing ASDE-X data is to predict the landing aircraft behavior on the runway. The aircraft landing profile starts at the point where the aircraft crosses the runway threshold and ends at the exiting point where the aircraft physically vacates the runway (i.e., leaves the imaginary plane of the runway).

6.2.2 Runway Database

To study the runway performance, we created a database of 145 runways at 37 US airports. Each runway is represented by a polygon used to estimate runway occupancy times. The latitude and longitude of each runway end center point were collected from the FAA airport geometry database [11]. The same source includes information on displaced thresholds for each runway if applicable. Figure 112 presents an example of runway polygons created for Chicago O'Hare International Airport.

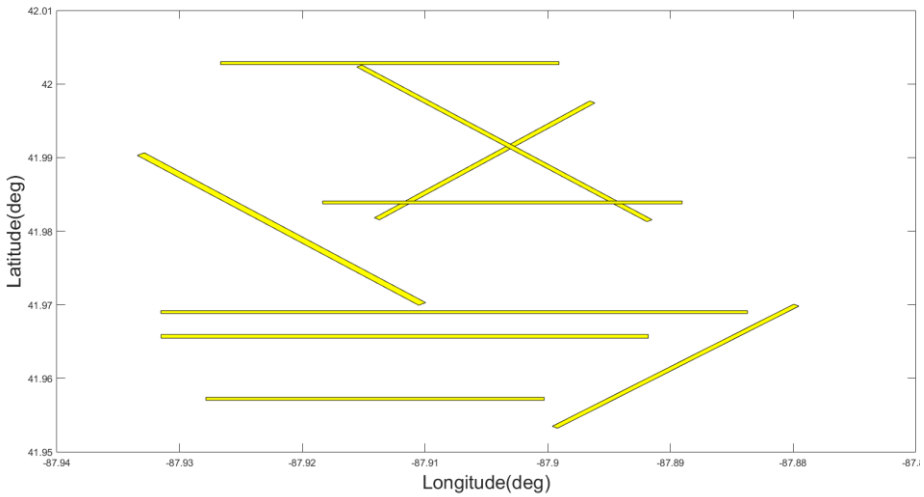

Figure 112. Chicago O'Hare International Airport (ORD) Runway Layout.

6.2.3 Runway Exit Geometry and Information

The runway exit geometry of each runway is a factor in the estimation of runway occupancy time. For this project, we created a database with runway exit geometry information for 3,385 runway exits. The runway exit database includes: exit angle, exit radius, the arc length from the point of curvature to the runway exit hold bar, and the distance from the runway threshold to the point of curvature of each exit. We used Google Earth Pro for creating the runway exit database. Figure 113 presents a sample arc for a high-speed exit at Chicago O'Hare International Airport represented in Google Earth Pro.

Figure 113. Sample Runway Exit Arcs and Other Information for Identifying Runway Exits.

6.3 Methodology

The methodology for estimating ROT and exiting distances utilized in this chapter is completely different than the approaches used in earlier chapters. In chapter 3 we introduced a novel hybrid approach, which used machine learning techniques for creating meaningful distributions for a Monte Carlo simulation, however in this chapter we use machine learning models for estimating ROT and exiting distances. The model that we use in this chapter is a multi-layer perceptron regressor which is also known as artificial feedforward neural network.

We used two, two-layer feedforward neural network models to estimate runway occupancy time and aircraft exit distance, separately. A model to estimate the runway occupancy time can be used in fast-time runway simulations or even in real-time air traffic control decision support models. The first artificial neural network receives an input vector of size six. The following six parameters are the required input format for each operation:

1. Runway Threshold Crossing Speed (knots)
2. Touchdown Speed (knots)
3. Time Difference Between Threshold Crossing and Touchdown (seconds)
4. Touchdown Distance from Runway Threshold (feet)
5. Average Deceleration on Runway (m/s^2)
6. Speed at Runway Exit Point of Curvature (knots)

The target for prediction is the runway occupancy time in seconds (i.e., the point where the aircraft is completely outside of the runway polygon). The artificial neural network includes: sigmoid transfer function in the hidden layer and a linear transfer function in the output layer. We ran all of our experiments with 20 hidden neurons. We programmed all the data processing and neural

network procedures in the MATLAB programming language [44][48]. Figure 114 shows the structure of the two-layer feedforward neural network with 20 hidden neurons.

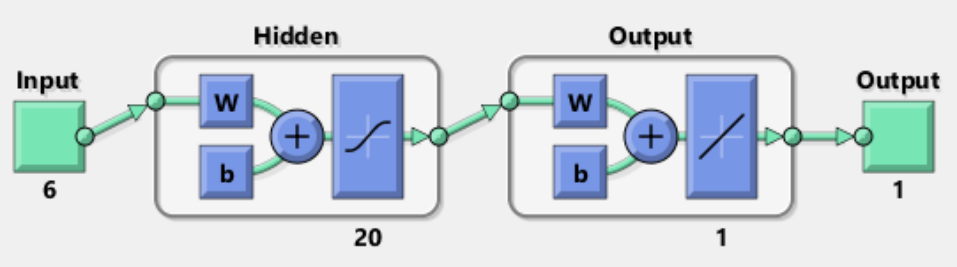

Figure 114. Schema of the Trained Neural Network with 2-Layers.

For training process, we divided the data randomly into three different sets. 70% in the train set, 15% in the test set, and 15% in the validation set. The validation data helps to improve the accuracy of training the model. Test data is selected at random and never used during the training process. The mean squared error is the metric used for improving the performance of the fitted neural network during each epoch.

6.4 Results

In this study, we analyzed three months of ASDE-X data at eight airports. The airports studied are ORD, DEN, DCA, CLT, ATL, SAN, LAX, and JFK. We studied the performance of the prediction models for 14 distinct aircraft types with various wake categorization and runway occupancy time behavior.

The procedure described above, was applied to study runway occupancy time and the exit distance of airplanes. The process is very similar to curve fitting procedure in data analytics. For validating the predicted results, we compared the test sets for each aircraft using the same neural network but at different airports. Error distributions for each aircraft type were helpful to understand the

performance of the model better. However, we used a regression analysis to estimate the goodness of our trained model in predicting ROT and exit distance. We chose the R-squared parameter to evaluate the regression analysis between observed and predicted values from the neural network. Figure 115 shows an example of data for an Airbus A319 at CLT airport with the regression analysis between the observed and predicted ROT values. Figure 115 shows, the neural network did an acceptable job, and overfitting did not happen since the reported performance measures are very similar among all the divided groups of data.

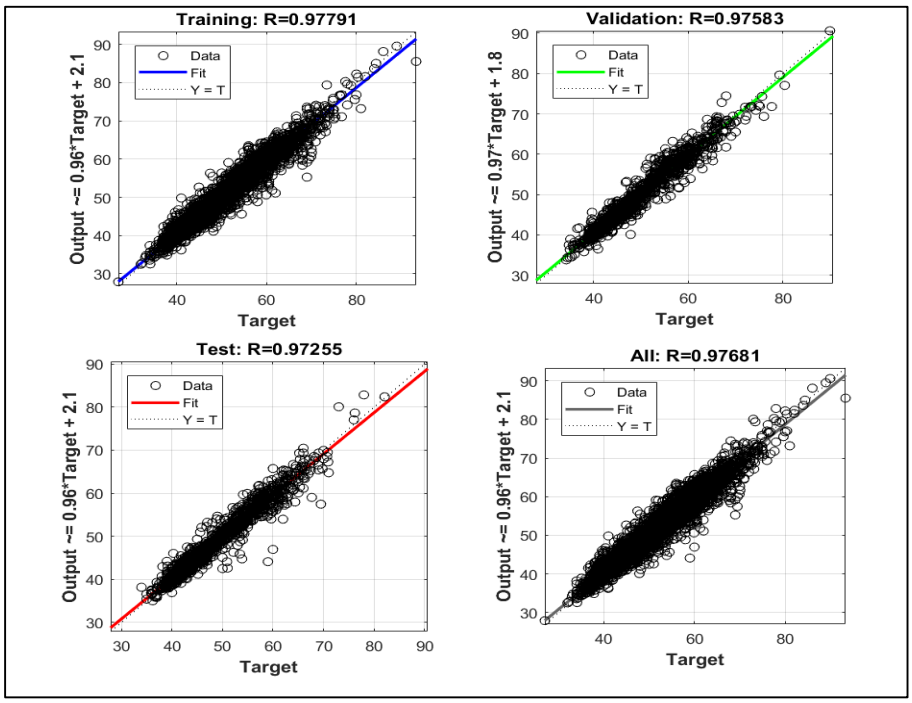

Figure 115. Regression Plots of Different Divided Groups of A319 Data at CLT for Observed and Predicted ROTs.

Figure 116 shows an error histogram illustrating the differences between observed and predicted ROT values for the same aircraft at CLT. As expected, the errors follow a normal distribution with a mean at zero for acceptable model performance. The vast majority of the non-zero errors are within 5 seconds which seems an acceptable error scale for measuring ROT.

We tested our model on 339,142 operations representing 14 distinct aircraft types at eight airports. Table 24 shows the counts of each aircraft type studied.

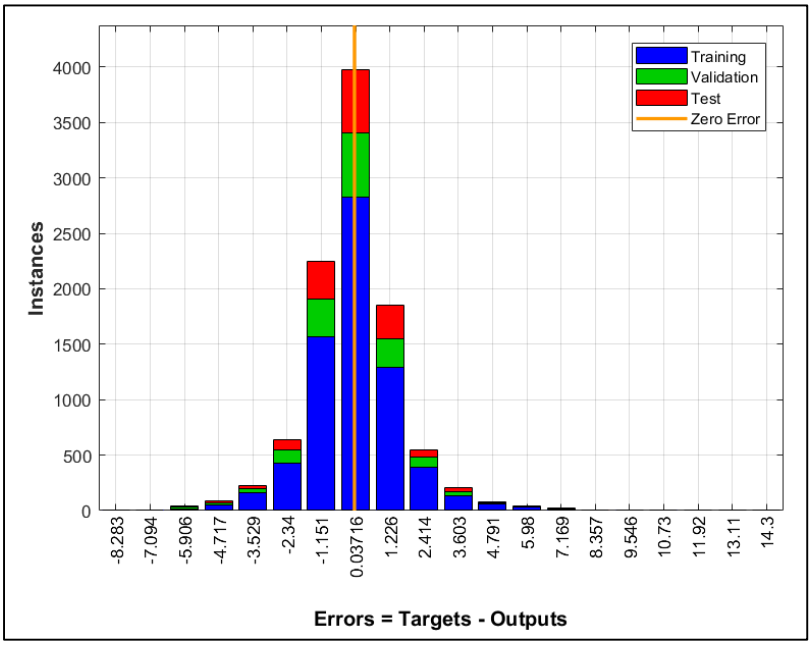

Figure 116. Error Plot for Different Groups of Airbus A319 Aircraft Data at CLT.

Table 24. Count of Aircraft Types Used in the ROT Study.

Aircraft	Landing Operations
A319	36,642
A320	46,761
A321	30,649
A332	3,053
A388	1,548
B738	54,849
B739	22,955
B752	16,450
B744	3,711
B772	4,025
CRJ2	4,083
CRJ7	29,392
CRJ9	26,529
E170	21,495

We do not report the performance metrics for aircraft which have fewer than 150 landing operations. Table 25 represents the calculated R-squared test values from the regression analysis between observed ROT values and predicted ROT.

Table 25. R-Squared Test Values from the Regression Analysis Between Observed True ROTs and Predicted ROTs by Neural Network[1].

	Airport							
Aircraft	ATL	CLT	DCA	DEN	JFK	LAX	ORD	SAN
A319	0.95	0.95	0.58	0.98	0.75	0.96	0.86	0.93
A320	0.95	0.95	0.8	0.99	0.85	0.97	0.90	0.93
A321	0.96	0.94	0.8	0.99	0.88	0.94	0.87	0.90
A332	-	0.91	-	-	0.79	0.93	0.72	0.62
A388	-	-	-	-	0.93	0.91	-	-
B738	0.95	0.95	0.92	0.77	0.88	0.95	0.91	0.79
B739	0.88	0.69	-	0.99	0.54	0.94	0.89	0.91
B752	0.94	0.82	0.79	0.52	0.83	0.95	0.84	0.74
B744	0.90	-	-	0.81	0.83	0.93	0.93	-
B772	0.64	-	-	0.82	0.81	0.91	0.86	-
CRJ2	0.97	0.97	0.82	0.98	0.83	0.66	0.85	0.73
CRJ7	0.93	0.97	0.82	0.99	0.81	0.95	0.87	0.90
CRJ9	0.94	0.97	0.78	0.97	0.78	0.94	0.69	0.85
E170	0.93	0.89	0.79	0.98	0.91	0.96	0.86	0.90

The overall predicted ROT times are presented in Table 25. The values show high accuracy for the model in predicting ROT times for most of the aircraft. 47 percent of the cells in Table 25 exceed an R-squared value of 90%, and 77 percent of the cells in Table 25 exceed an R-squared of 80%. There are still some airplanes at some studied airports which show signs of overfitting. For example, the R-squared values for Boeing 777-200 (B772) at ATL or R-squared values for Airbus A319 (A319) at DCA are good representatives of an overfitting pattern in the neural network because their estimated R-squared on the train sets were high (the train R-squared values were respectively 0.93 and 0.84 for B772 at ATL and A319 at DCA). Repeating the training process with different biases and weights are the best options for improving model performance.

[1] The airplanes with few number of operations during the studied months were eliminated.

However, after trying with a different set of biases and weights, those cells did not change considerably.

For an airplane like the Airbus A380-800 (A388) which belongs to the legacy super heavy wake class (or Group A in re-categorization wake vortex), our model predicted the ROT values with high accuracy. The Airbus A380-800 data was collected at New York Kennedy International Airport (JFK) and Los Angeles International Airport (LAX) airports. This is a positive indication that the model can predict ROT values accurately for aircraft that do not regularly fly at many facilities in the United States.

Another aircraft that showed signs of overfitting at more than one airport was the Bombardier CRJ-200 (CRJ2). The model performance at LAX was not very accurate considering the high reported R-squared values for the associated train data set (0.97), we can interpret that there might be an overfitting pattern happening for CRJ2 planes at LAX. The reason might be related to observed motivational practices at LAX due to gate location. Moreover, the data for CRJ2 aircraft shows large variations in touchdown distance across airports. It would be difficult for a model to avoid overfitting in such cases even with randomly selecting the train and test sets from the data.

Another potential reason behind the weaker numbers in the table is related to the nature of feature extraction from the ASDE-X data. For example, as mentioned earlier, a challenging part of analyzing the landing profile is to identify the touchdown location. Therefore, if there would be non-matching patterns in the input set, we might see some significant errors in predicted ROTs. We could see this pattern in the case of DCA predicted ROTs. The runways at DCA are short, and the touchdown locations are closer to the runway threshold compared to the other airports. However, because of the noise in data, the algorithm might have extracted some touchdown locations which made the ROT values less precise. Another potential reason might be the exit

geometry and properties. At DCA, we have observed some runway exits which cannot be classified with standard exit types. The landing aircraft behavior and pilot motivational practices are very unique at DCA.

Table 26 presents the R-squared values from the regression analysis between observed and predicted exiting distances in feet. Generally, the performance measures for the second model are better than the first model even though both are fed with similar input vectors. A hypothesis behind the better performance for the second model is in the nature of exiting distances. Aircraft exit distance is generally dictated by the exit locations on the runways. Every runway has a limited number of runway exits at defined distances from the runway threshold. Runway exit distances are less stochastic than ROT. This fact increases the performance of the second artificial neural network.

Table 26. R-Squared Test Values from the Regression Analysis Between Observed Exiting Distances and Predicted Exiting Distances by Neural Network[2].

	Airport							
Aircraft	ATL	CLT	DCA	DEN	JFK	LAX	ORD	SAN
A319	0.95	0.96	0.64	0.98	0.91	0.97	0.97	0.85
A320	0.88	0.96	0.94	0.98	0.94	0.99	0.93	0.93
A321	0.94	0.96	0.91	0.96	0.94	0.96	0.95	0.92
A332	-	0.85	-	-	0.64	0.91	0.88	0.88
A388	-	-	-	-	0.89	0.98	-	-
B738	0.94	0.94	0.96	0.95	0.93	0.95	0.96	0.83
B739	0.92	0.88	-	0.98	0.52	0.94	0.94	0.72
B752	0.96	0.88	0.88	0.92	0.91	0.97	0.87	0.90
B744	0.85	-	-	0.80	0.89	0.90	0.93	-
B772	0.64	-	-	0.77	0.76	0.92	0.94	-
CRJ2	0.98	0.97	0.91	0.98	0.93	0.64	0.93	0.88
CRJ7	0.95	0.96	0.87	0.98	0.90	0.97	0.93	0.99
CRJ9	0.93	0.97	0.94	0.96	0.92	0.94	0.90	0.75
E170	0.96	0.96	0.93	0.96	0.58	0.98	0.95	0.99

[2] The airplanes with few number of operations during the studied months were eliminated.

Figure 117 shows the stochastic behavior for exit distances of an Airbus A330-200 operating at CLT airport. As Figure 117 shows, clusters of points which belong to the same runway exit. Exit distances are less stochastic than runway occupancy times.

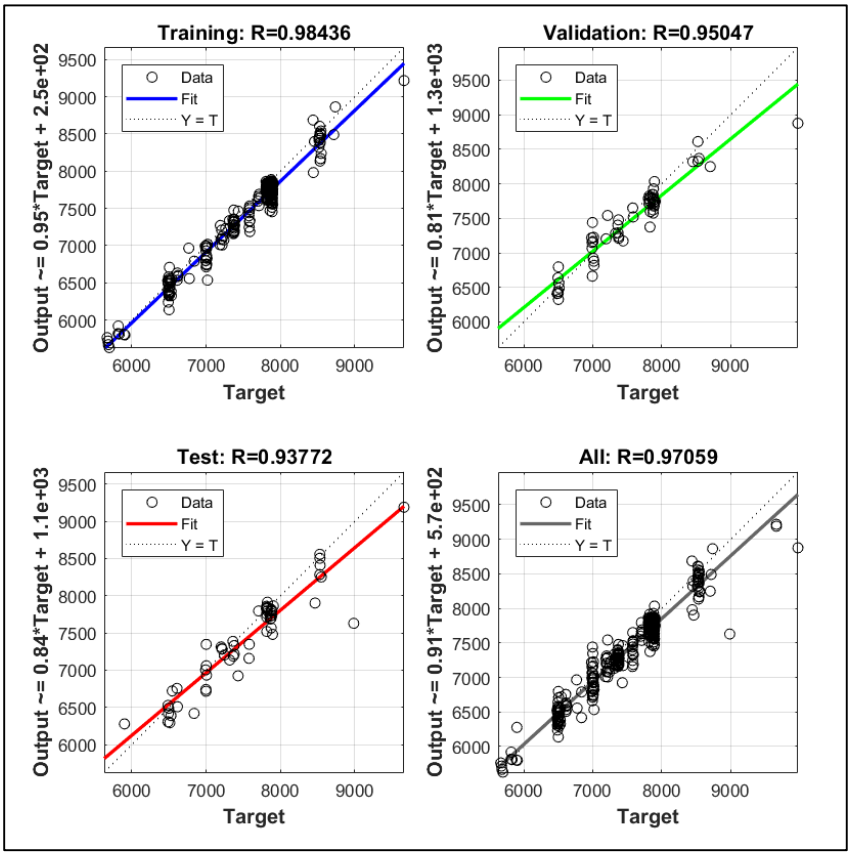

Figure 117. Regression Plots of Different Divided Groups of A332 Data at CLT for Observed and Predicted Exiting Distances.

6.5 Conclusion

Due to the recent reductions in airplane separations for the final landing approach at busy hubs in the United States, which are the results of the advancements in wake vortex in-trail separation systems, runway occupancy times of airplanes are gaining attention. Having capable computer applications and simulation models that would be able to predict runway occupancy times accurately, is valuable for a more efficient and smooth flow of operations at busy airports. The major contribution of this study is not only to provide reliable predictive models for planners to evaluate, analyze, or design new facilities but also to provide deep insights from heavy radar and surface data. The approach used in this chapter for predicting runway occupancy times is different than the proposed approaches in earlier chapters. In this chapter we proposed the usage of artificial neural networks for predicting runway occupancy times and arrival flights' exiting distances. The material provided in this chapter can be useful for those airport designers who seek quick predictive models for estimating runway occupancy times. The structure of the proposed model in this chapter is very simple, however the accuracy of the predictions is promising. This can notify the readers of this document that if they have access to valid input data which is required by the proposed models in this study, they can achieve accurate ROT times. This approach doesn't require entering runway exit configurations, or defining runway geometry features for estimating ROT times. Instead modelers can produce valid distributions of input parameters which are related to critical landing behaviors, and utilize the same recipe for their neural network structure to estimate runway occupancy time and exiting distances for their desired arrival fleet.

Chapter 7. Conclusion

This document is for a Ph.D. dissertation submitted for a degree in transportation systems engineering with a focus on air transportation systems. The author has provided seven chapters to represent his research work and studies during his Ph.D. time. The dissertation begins with an introduction chapter where the motivation for this research study was defined and then the contributions of each chapter were explained to guide the reader.

The second chapter of this dissertation is about parsing, cleaning, storing, analyzing and engineering data called Airport Surface Detection Equipment Model-X or ASDE-X. The author of this document explains the algorithms and methodologies used for architecting a landing database from 37 Terabytes of ASDE-X data. The ASDE-X system is a surveillance technology implemented at 37 airports of the US to avoid taxiway and runway incursions and help air traffic controllers navigate airplanes easier. The focus of this study is on runway occupancy times, therefore most of the features extracted from the raw data are concentrated on defining the landing behavior of airplanes to the moment they were entirely out of the runway. Since the major focus of this research attempt was to design a computer model which predicts airplanes runway occupancy time and distance, the second chapter tries to prepare the user for the material they would see in the following chapters by providing many statistical analyzes of runway occupancy times for various airplanes at various airports. This chapter can be used as a helpful reference for programmers and planners in the aviation industry who work with ASDE-X data for delivering their products. The benefits of this chapter are not restricted to providing technical data engineering details or data massaging of a specific dataset. Beyond helpful guidance for engineering this particular dataset, lots of useful statistical facts about aircraft landing behaviors were revealed. They can all be essential for aircraft manufacturers, airline analysts, airport designers, and air

transportation authorities. In addition to the methodology, a complete list of crucial input files which were developed by the author to analyze ASDE-X dataset are provided in the Appendix section to ease the process of working with this data for readers.

The third chapter of this dissertation explained the author's novel method to model arrival aircraft behavior on the runway. This chapter identifies the methodologies taken for developing the simulation model in detail. The author utilized a data-driven approach as he had access to tons of valuable analyzed data, which he engineered himself. The provided data after procedures defined in chapter two go through the methodologies described in chapter three and the final outputs are predicted runway occupancy times. The author reveals his novel approach to using machine learning models to form the structure of his final predictive outcome. A combination of supervised and unsupervised learning methods was used to categorize each aircraft type's critical distributions. Those distributions were then utilized to form the Monte Carlo simulation model for predicting various parameters related to aircraft landing and runway evacuation behaviors. After defining the methodology, the author represented the model's evaluation results by comparing the predicted results versus the real observed data. The chapter ends with a quick introduction to the graphical user interface, which was programmed entirely by the author. It also helps the reader understand the functionalities of the developed simulation model. The material provided in this chapter is not only great for data science enthusiasts who are interested in learning the usage of machine learning in different fields, but also is a great guidance for aviation data scientists who are specifically interested in using data science for modeling aviation systems. Moreover, this chapter is a thorough review of novel methodologies in predicting runway occupancy times, in addition to a helpful user guide for the final developed application.

In the fourth chapter, the author tested his developed model on four real-world case scenarios, where the problem of runway occupancy time has created some inefficiencies in the airports' capacities. In this attempt, the newly developed algorithms were challenged against potential changes in runway exit configurations, and the final results provided deeper insights for the FAA authorities and airport runners. This chapter represents the necessity of such a model for making better decisions regarding future construction projects at airports. The author kept the format of reporting results similar for all the four facilities. One of the significant contributions of this study can be clearly noted in the fourth chapter, where airport consultants can refer to future case studies for their desired facilities. In this chapter, the author provides the base ROT results, and then he tests various alternatives to improve the ROT performance of the tested airports. The airport authorities suggested some of those alternatives, however the author tested many scenarios based on his experience in studying ROT behaviors and exit utilizations. This chapter can be referred by any documents related to future construction master plans of the mentioned airports or similar facilities. The lesson learned from this chapter was that a developed simulation model for an academic research study could be used for industrial decision making and for guiding managers in making better decisions.

In the fifth chapter, the author represents a new approach for modeling motivated pilots' behavior. This chapter was inspired by observed motivational behaviors at various airports where pilots have desired runway exits and adjust their landing roll behavior to make their desired exits comfortably. After observing some strange performances at a specific airport, the author of this document decided to explore those arrival flights more accurately. He noticed that those motivated pilots pushed the aircraft to brake harder to make it to earlier runway exits. This wasn't the only observed behavior as he observed some flights making it more relaxed in braking to take further runway

exits, which would make their taxi time to their carrier's terminal shorter. Three different approaches were tested in this chapter to represent the pilots' motivational factors for taking pre-determined runway exits. The results were compared to the real observed scenarios to evaluate the goodness of proposed approaches. This chapter can be used by tons of airport planners besides airline analysts to test the potential change in exit utilization patterns of various aircraft types.

In the sixth chapter, a novel approach was proposed to predict runway occupancy times and exiting distances for arrival airplanes. The selected model in this study was a feedforward neural network with a shallow structure. The author attempted on a various number of hidden neurons to improve the performance of the trained model on the test set. This approach is an alternative to the modeling algorithms defined in chapter 3. The author chose to use machine learning to predict ROT times, examine a strong supervised model, and compare the performance with a data-driven hybrid approach. Promising results were achieved on both ROT times and exiting distances. This chapter is a useful guide for those who are interested in exploring the usage of machine learning models in air transportation industry. This chapter also provides useful guidance for airport planners and aviation analysts interested in predicting critical parameters from ASDE-X data and want to use machine learning or deep learning structures rather than simulation models. Finally, the provided recipe can be repeated in any programming language to predict ROT times if the readers would have access to the required input parameters.

In the end, we have to mention that the author of this document dedicated many years to engineering a massive amount of data in aviation to design functional and industrial-level databases and fundamental computer models. The federal aviation administration is currently using models that we represented in this dissertation for future design and improvement purposes. The landing database developed in this study is presently being used by various consulting

companies in the aviation market. Many researchers across the country are using the provided data for analyzing different parts of air travel.

For accomplishing the mentioned achievements in this study, the author exercised fundamental computer programming, data analytics, statistical learning and systems engineering methods to not only deliver decent products to the sponsors of this study, but also to provide decent vision for future research and development in the area of air transportation systems and aviation analytics. This document can be used as a reference for future studies in areas such as air traffic control, airport ground movement, airlines operations, airports capacity analysis, and any studies related to the usage of data science in air transportation.

References

[1]https://www.faa.gov/about/office_org/headquarters_offices/ang/offices/tc/library/storyboard/detailedwebpages/asdex.html

[2] https://en.wikipedia.org/wiki/ASDE-X, online, 2020.

[3] Perl, E. (2006, April). Review of airport surface movement radar technology. In 2006 IEEE Conference on Radar (pp. 4-pp). IEEE.

[4] Spencer, T. L. (2016). Enhanced Air Transportation Modeling Techniques for Capacity Problems (Doctoral dissertation, Virginia Tech).

[5] Hu, J. (2018). Estimation of Runway Throughput with Reduced Wake Vortex Separation, Technical Buffer and Runway Occupancy Time Considerations (Doctoral dissertation, Virginia Tech).

[6] Trani, A. A. (2003). Quick review of airport runway capacity (Doctoral dissertation, Blacksburg: Virginia Polytechnic Institute and State University).

[7] Mirmohammadsadeghi, N. (2017). Improvements to Airport Systems Capacity and Efficiency Using Computer Models and Tools (Doctoral dissertation, Virginia Tech).

[8] Chen, Y. T. (2006). A Modeling Framework to Estimate Airport Runway Capacity in the National Airspace System (Doctoral dissertation, Virginia Tech).

[9] Srivastava, A. (2011, October). Improving departure taxi time predictions using ASDE-X surveillance data. In 2011 IEEE/AIAA 30th Digital Avionics Systems Conference (pp. 2B5-1). IEEE.

[10] Updated Runway Exit Probability Tool to Assist Airports with Optimizing the Location of Exit Taxiways, Air Transportation Systems Laboratory at Virginia Tech, 2020.

[11] FAA. "Airport Data.", Online, 2017.

[12]https://www.faa.gov/regulations_policies/orders_notices/index.cfm/go/document.information/documentID/1029781, 2020.

[13] Sherali, H. D., A. G. Hobeika, A. A. Trani and B. J. Kim. "An integrated simulation and dynamic programming approach for determining optimal runway exit locations." Management science 38(7): 1049-1062, 1992.
[14] Hobeika, A. G., Dona, E. L., & Nam, A. S. (1988). Optimal location of high-speed runway exits using automated landing, rollout, and turnoff. Transportation research record, 1147, 34-39.
[15] Trani, A. A., Cao, J., Kim, B. J., Gu, X., Zhong, C. Y., & Tarrago-Trani, M. T. (1996). Flight simulations of high speed runway exits. Virginia Polytechnic Institute and State University, Department of Civil Engineering, Transportation Systems Laboratory, Blacksburg, VA.
[16] Nam, A. S. (1986). Increasing capacity by the use of optimal runway exits, automated landing, roll out and turnoff in an airport environment (Doctoral dissertation, Virginia Polytechnic Institute and State University).
[17] Kim, B. J., A. A. Trani, X. Gu and C. Zhong. "Computer simulation model for airplane landing-performance prediction." Transportation Research Record 1562(1): 53-62, 1996.
[18] Stamatopoulos, M. A., K. G. Zografos and A. R. Odoni. "A decision support system for airport strategic planning." Transportation Research Part C: Emerging Technologies 12(2): 91-117, 2004.
[19] Mirmohammadsadeghi, N., Hu, J., & Trani, A. (2019). Enhancements to the Runway Capacity Simulation Model Using the ASDE-X Data for Estimating Airports Throughput Under Various Wake Separation Systems. In AIAA Aviation 2019 Forum (p. 3044). doi: 10.2514/6.2019-3044
[20] Kolos-Lakatos, T. “The influence of runway occupancy time and wake vortex separation requirements on runway throughput”, Massachusetts Institute of Technology, 2013.
[21] Hu, J., Mirmohammadsadeghi, N., & Trani, A. (2019). Runway Occupancy Time Constraint and Runway Throughput Estimation under Reduced Arrival Wake Separation Rules. In AIAA Aviation 2019 Forum (p. 3046). doi: 10.2514/6.2019-3046
[22] Janic, M. "Modelling the capacity of closely-spaced parallel runways using innovative approach procedures." Transportation Research Part C: Emerging Technologies 16(6): 704-730, 2008.
[23] Mirmohammadsadeghi, N., Hotle, S., Trani, A., & Gulding, J. (2018). Taxi Event Extraction from ASDE-X Surveillance for Surface Performance Evaluation. In 2018 Aviation Technology, Integration, and Operations Conference (p. 4139). doi: 10.2514/6.2018-4139
[24] ATAC. "Simmod PRO! Reference Manual.", 2001.
[25] Virginia Tech. "REDIM 2.0 User's Manual.", 1992.
[26] Caprì, S. and M. Ignaccolo. "Genetic algorithms for solving the aircraft-sequencing problem: the introduction of departures into the dynamic model." Journal of Air Transport Management 10(5): 345-351, 2004.
[27] Nikoleris, T. and M. Hansen., "Effect of Trajectory Prediction and Stochastic Runway Occupancy Times on Aircraft Delays." Transportation Science 50(1): 110-119, 2015.
[28] Weiss, W. E., & Barrer, J. N. (1984). Analysis of runway occupancy time and separation data collected at la guardia, boston, and newark airports. MITRE CORP MCLEAN VA.
[29] Lee, D. D., Smith, A., Cassell, R., & Abdul-Baki, B. (1999, October). NASA low visibility landing and surface operations (LVLASO) runway occupancy time (ROT) analysis. In Gateway

to the New Millennium. 18th Digital Avionics Systems Conference. Proceedings (Cat. No. 99CH37033) (Vol. 1, pp. 5-D). IEEE.
[30] Koenig, S. E. (1978). Analysis of Runway Occupancy Times at Major Airports (No. MTR-7837). MITRE CORP MCLEAN VA METREK DIV.
[31] Gu, Trani, A. A., & Zhong, C. (1995). Characterization of gate location on aircraft runway landing roll prediction and airport ground networks navigation. Transportation research record, 52-60.
[32] Hartigan, J. A., & Wong, M. A. (1979). Algorithm AS 136: A k-means clustering algorithm. Journal of the royal statistical society. series c (applied statistics), 28(1), 100-108.
[33] Johnson, S. C. (1967). Hierarchical clustering schemes. Psychometrika, 32(3), 241-254.
[34] Bholowalia, P., & Kumar, A. (2014). EBK-means: A clustering technique based on elbow method and k-means in WSN. International Journal of Computer Applications, 105(9).
[35] Breiman, L. (1996). Bagging predictors. Machine learning, 24(2), 123-140.
[36] Friedman, J., Hastie, T., & Tibshirani, R. (2001). The elements of statistical learning (Vol. 1, No. 10). New York: Springer series in statistics.
[37] FAA. "Airport Surface Detection Equipment, Model X (ASDE-X).", 2014.
[38] FAA. "Airport Data.", 2017.
[39] Trani, A. A., A. Hobeika, H. Sherali, B. Kim and C. Sadam (1990)., "Runway Exit Designs for Capacity Improvement Demonstrations", Phase 1: Algorithmic Development, 90-32.
[40]https://www.faa.gov/airports/resources/advisory_circulars/index.cfm/go/document.current/documentNumber/150_5300-13, 2014.
[41] Kumar, V., L. Sherry and R. Kicinger. "Runway occupancy time extraction and analysis using surface track data." George Mason University, 2009.
[42] Villaumé, F., & Jeanneau, M. (2007). Control laws for automatic take-off using robust nonlinear inversion techniques. IFAC Proceedings Volumes, 40(12), 1022-1027.
[43] https://en.wikipedia.org/wiki/Brake_to_Vacate, 2020.
[44] https://www.mathworks.com/help/deeplearning/ref/feedforwardnet.html, online, 2019.
[45] Kim, B. J. (1993). Optimal runway exit design and capacity enhancement (Doctoral dissertation, Virginia Tech).
[46] Kim, B. J. (1990). An integrated approach to the optimal runway exit locations (Doctoral dissertation, Virginia Tech).
[47] Trani, A. A., Hobeika, A. G., Kim, B. J., Nunna, V., & Zhong, C. (1992). Runway exit designs for capacity improvement demonstrations. Phase 2: computer model development.
[48] Haykin, S. (2004). Kalman filtering and neural networks (Vol. 47). John Wiley & Sons.
[49] Hawkins, F. H. (2017). Human factors in flight. Routledge.

Appendix A – Runway Exit Geometry Database and Assigned Exit Clusters

Airport	rw	Exitname	Angle	PathLength	Radius	IndexCluster	PCdist
ORD	04R	Y2	150	539	90	4	1586
ORD	04R	Y3	150	498	60	4	3113
ORD	04R	Y4	30	1030	1500	12	4637
ORD	04R	Y5	40	1129	1000	2	6615
ORD	04R	D	40	653	475	8	7613
ORD	04R	N	100	602	475	19	7613
ORD	22L	Y1	90	523	356	19	7645
ORD	22L	Y2	30	868	1501	12	5910
ORD	22L	Y3	30	898	1503	12	4311
ORD	22L	Y4	150	480	120	4	2365
ORD	09L	M	90	414	200	1	7250
ORD	09L	M1	30	1357	1800	20	5793
ORD	27R	C1	30	1422	1800	20	5636
ORD	27R	Z	90	421	199	1	7240
ORD	10C	GG-L	90	409	200	1	10542
ORD	10C	GG-R	90	408	200	1	10542
ORD	10C	HH-L	90	403	170	1	9235
ORD	10C	HH-R	90	404	170	1	9235
ORD	10C	F-L	90	413	175	1	8013
ORD	10C	F-R	90	413	175	1	8013
ORD	10C	T-L	90	476	175	1	7048
ORD	10C	T-R	90	335	90	14	7143
ORD	10C	P6	30	1270	1800	20	6292
ORD	10C	P5	30	1276	1800	20	5270
ORD	10C	P3	30	1292	1800	20	3836
ORD	10C	P2	150	495	130	4	4491
ORD	10C	P1	150	529	90	4	3655
ORD	10C	DD-L	90	394	175	1	2729
ORD	10C	DD-R	90	393	170	1	2729
ORD	28C	F-L	90	400	190	1	2395
ORD	28C	F-R	90	399	180	1	2395
ORD	28C	T-L	90	362	120	14	3448
ORD	28C	T-R	90	472	175	1	3404
ORD	28C	P6	150	516	90	4	3427
ORD	28C	P5	150	530	90	4	4424
ORD	28C	P3	150	474	130	4	5722
ORD	28C	P2	30	1287	1800	20	5027
ORD	28C	P1	30	1249	1800	20	6062
ORD	28C	DD-L	90	393	173	1	7711
ORD	28C	DD-R	90	392	175	1	7711
ORD	28C	CC-L	90	379	175	1	8960
ORD	28C	CC-R	90	380	175	1	8960
ORD	28C	BB-L	90	386	175	1	9297
ORD	28C	BB-R	90	384	175	1	9297
ORD	28C	AA-L	90	392	210	1	10555
ORD	28C	AA-R	90	390	210	1	10555
ORD	10L	Y-L	90	467	220	1	12659

ORD	10L	Y-R	115	420	128	7	12463
ORD	10L	GG-L	90	371	160	1	10949
ORD	10L	GG-R	95	390	175	1	10931
ORD	10L	EE-L	90	394	175	1	9923
ORD	10L	EE-R	90	400	175	1	9923
ORD	10L	N5	90	828	120	10	9658
ORD	10L	N4	150	469	85	4	8736
ORD	10L	F-R	90	390	160	1	8055
ORD	10L	N3	30	842	1800	3	7115
ORD	10L	T-L	145	511	80	4	6631
ORD	10L	T-R	50	461	158	18	6799
ORD	10L	P4	45	503	160	18	5180
ORD	10L	DD-L	90	388	155	1	2747
ORD	10L	DD-R	90	379	170	1	2747
ORD	10L	N1	130	434	145	11	4930
ORD	28R	EE-L	90	366	165	1	2763
ORD	28R	EE-R	90	372	130	14	2763
ORD	28R	N5	90	345	100	14	3122
ORD	28R	N4	30	787	1800	12	3693
ORD	28R	F-L	90	377	150	1	4633
ORD	28R	N3	150	538	90	4	5324
ORD	28R	T-L	130	429	140	11	5779
ORD	28R	T-R	35	815	1800	12	5779
ORD	28R	P4	135	454	165	11	7318
ORD	28R	DD-L	90	450	190	1	9842
ORD	28R	DD-R	90	474	270	1	9777
ORD	28R	CC-L	90	382	150	1	11169
ORD	28R	CC-R	90	383	155	1	11169
ORD	28R	BB-L	90	375	165	1	11516
ORD	28R	BB-R	90	375	170	1	11516
ORD	28R	AA-L	90	380	190	1	12777
ORD	28R	AA-R	90	380	187	1	12777
ORD	28R	N1	45	468	155	18	7659
ORD	15	T2	45	559	389	8	2745
ORD	15	T3	45	486	286	18	3822
ORD	15	T5	45	547	408	8	4746
ORD	15	T6	45	517	298	18	5790
ORD	15	T7	45	503	320	18	6804
ORD	15	T8	150	478	100	4	7525
ORD	15	K	130	450	170	11	8215
ORD	15	T9-L	90	343	157	14	8297
ORD	15	T10-L	90	424	191	1	8580
ORD	15	N-L	50	515	284	18	9416

ORD	15	N-R	130	421	146	11	9214
ORD	15	L	130	476	170	11	8609
ORD	33	T1	110	377	215	16	9451
ORD	33	T2	135	420	165	11	6364
ORD	33	T3	135	437	160	11	5365
ORD	33	T5	135	414	130	11	4450
ORD	33	T6	135	420	140	11	3428
ORD	33	T7	135	424	110	11	2494
ORD	33	T8	30	740	700	9	1611
ORD	04L	A1	141	439	100	4	2019
ORD	04L	C-L	80	393	190	1	3984
ORD	04L	C-R	100	426	180	1	3899
ORD	04L	M-L	40	614	250	8	5662
ORD	04L	M-R	140	438	55	11	5617
ORD	04L	NN	112	404	155	7	7309
ORD	22R	R2	50	439	80	18	7452
ORD	22R	H1-L	100	342	120	16	7303
ORD	22R	H1-R	80	330	90	14	7363
ORD	22R	H-L	130	409	55	11	6781
ORD	22R	H-R	50	462	150	18	6850
ORD	22R	A2	85	376	185	1	6739
ORD	22R	A1	40	764	1800	12	4875
ORD	22R	C-L	80	411	210	1	3195
ORD	22R	C-R	100	365	110	16	3213
ORD	09R	B	90	436	250	1	7689
ORD	09R	H3	90	475	235	1	7228
ORD	09R	H2	60	450	200	15	6375
ORD	09R	C-L	130	388	100	11	5614
ORD	09R	C-R	50	642	675	9	5515
ORD	09R	M-L	90	333	80	14	4806
ORD	09R	M-R	90	368	150	14	4727
ORD	09R	A1-L	90	321	80	14	2583
ORD	09R	A1-R	90	379	125	1	2510
ORD	27L	C-L	130	373	100	11	1933
ORD	27L	C-R	50	466	200	18	2043
ORD	27L	M-L	90	374	145	1	2931
ORD	27L	M-R	90	351	55	14	2984
ORD	27L	A1-L	30	864	1500	12	4702
ORD	27L	A1-R	90	340	100	14	5207
ORD	27L	H1-L	90	330	100	14	7261
ORD	27L	Runway 4L/22R-L	50	429	225	18	5996

ORD	27L	Runway 4L/22R-R	130	367	80	11	5921
ORD	27L	J-L	90	413	200	1	7696
ORD	10R	W3	30	1232	1800	20	4877
ORD	10R	W4	30	1311	1800	20	5793
ORD	10R	W5	90	368	200	1	7293
ORD	28L	W2	30	1247	1800	20	4854
ORD	28L	W1	30	1204	1800	20	5903
ORD	28L	AA	90	418	190	1	7244
ORD	09R	TT	90	376	150	1	6218
HNL	08L	L	90	361	130	14	4722
HNL	08L	G-R	90	418	250	1	5181
HNL	08L	G-L	90	350	140	14	5286
HNL	08L	N	30	623	315	8	4752
HNL	08L	S-R	104	359	200	16	6764
HNL	08L	S-L	90	464	230	1	6835
HNL	08L	D-R	60	423	250	15	6987
HNL	08L	D-L	120	426	175	7	6803
HNL	08L	Y	30	697	315	8	6743
HNL	08L	H	65	459	300	13	7783
HNL	08L	E-R	54	477	300	13	8549
HNL	08L	E-L	100	376	225	16	8286
HNL	08L	K-R	108	329	80	16	10069
HNL	08L	K-L	82	539	190	19	9975
HNL	08L	C-R	142	433	67	4	11448
HNL	08L	C-L	38	632	350	8	11632
HNL	26R	T-R	45	847	300	8	12292
HNL	26R	T-L	135	416	85	11	12137
HNL	26R	A-R	90	334	100	14	12218
HNL	26R	A-L	90	325	100	14	12218
HNL	26R	RB-R	118	404	190	7	11512
HNL	26R	RB-L	62	353	140	15	11789
HNL	26R	L	90	400	250	1	7222
HNL	26R	G-R	90	389	200	1	6689
HNL	26R	G-L	90	375	200	1	6689
HNL	26R	N	150	442	100	4	7122
HNL	26R	S-R	90	440	185	1	5113
HNL	26R	S-L	75	339	150	15	5216
HNL	26R	D-R	60	438	190	15	5109
HNL	26R	D-L	120	404	165	7	4900
HNL	26R	Y	150	483	115	4	5109
HNL	26R	H	115	336	100	7	4173
HNL	26R	E-R	56	415	180	18	3516

HNL	26R	E-L	127	418	180	11	3234
HNL	26R	K-R	98	445	165	1	1997
HNL	26R	K-L	72	354	139	15	2032
HNL	26R	V	45	532	200	18	11767
HNL	08R	RM	150	621	100	5	3494
HNL	08R	RG	30	1068	1800	3	7699
HNL	08R	RH	90	402	200	1	11331
HNL	08R	RA	90	382	200	1	11769
HNL	26L	RG	150	591	100	5	3527
HNL	26L	RM	30	1059	1800	3	7709
HNL	26L	RC	90	420	200	1	11313
HNL	26L	RB	90	388	200	1	11762
HNL	04L	E-R	90	246	85	6	2977
HNL	04L	E-L	90	346	200	14	2866
HNL	04L	K-R	145	351	61	11	4090
HNL	04L	K-L	45	395	95	18	4206
HNL	04L	C-R	90	309	150	14	6735
HNL	04L	C-L	90	368	150	14	6805
HNL	04L	B	130	325	115	11	2942
HNL	22R	F-R	90	341	185	14	6715
HNL	22R	F-L	90	313	185	14	6715
HNL	22R	D-R	98	325	175	16	5220
HNL	22R	D-L	82	306	130	14	5262
HNL	22R	E-R	90	358	200	1	3708
HNL	22R	E-L	90	256	100	6	3817
HNL	22R	K-R	137	339	65	11	2527
HNL	22R	K-L	35	452	290	18	2549
HNL	22R	B	50	383	200	18	3708
HNL	04R	C-R	90	390	165	1	8726
HNL	04R	F-R	90	378	200	1	1876
HNL	04R	F-L	90	288	85	14	1978
HNL	04R	D-R	98	350	200	16	3303
HNL	04R	D-L	82	307	175	14	3350
HNL	04R	E-R	90	375	200	1	4861
HNL	04R	E-L	90	329	150	14	4899
HNL	04R	P	75	383	200	15	6082
HNL	04R	K	30	945	1800	3	5073
HNL	04R	C-L	90	342	140	14	8744
HNL	22L	F-R	90	353	186	14	6753
HNL	22L	F-L	90	390	200	1	6753
HNL	22L	D-R	98	308	175	16	5319
HNL	22L	D-L	82	398	200	1	5319
HNL	22L	E-R	90	353	200	14	3766

HNL	22L	E-L	90	387	200	1	3766
HNL	22L	P	105	332	100	16	2658
HNL	22L	K	150	418	98	4	3129
HNL	22L	C-L	90	405	175	1	8753
MCO	17L	N3	125	372	150	7	2920
MCO	17L	F	60	819	550	9	5943
MCO	17L	N4	55	821	550	9	6839
MCO	17L	N5	90	354	150	14	8413
MCO	17L	N6	90	345	150	14	8824
MCO	17L	J	120	359	150	7	1754
MCO	35R	N1	90	360	150	14	8809
MCO	35R	N2	90	360	150	14	8399
MCO	35R	N3	55	828	550	9	5236
MCO	35R	F	120	366	150	7	2232
MCO	35R	J	55	825	550	9	6422
MCO	36R	E-L	60	431	200	15	3103
MCO	36R	E-R	120	374	100	7	3043
MCO	36R	B7	120	424	160	7	4210
MCO	36R	Y	90	389	180	1	5357
MCO	36R	B5	123	424	150	7	5819
MCO	36R	J-L	121	412	130	7	8424
MCO	36R	J-R	43	494	200	18	8447
MCO	36R	B2-L	90	371	175	1	11392
MCO	36R	B2-R	90	372	175	1	11392
MCO	36R	B1-L	90	372	175	1	11789
MCO	36R	B1-R	90	375	175	1	11789
MCO	36R	B6	55	1071	600	17	4513
MCO	18L	B10-L	90	401	175	1	11759
MCO	18L	B10-R	90	358	175	14	11806
MCO	18L	B9	90	380	175	1	11255
MCO	18L	E-L	45	494	200	18	8576
MCO	18L	E-R	120	391	115	7	8586
MCO	18L	B7	60	1091	600	17	6700
MCO	18L	B6	90	334	125	14	6330
MCO	18L	Y	90	371	175	1	6271
MCO	18L	B5	57	1101	600	17	5102
MCO	18L	J-L	121	376	105	7	3149
MCO	18L	J-R	59	418	190	15	3242
MCO	17R	H3	130	375	150	11	2316
MCO	17R	H5	130	376	150	11	3906
MCO	17R	E-L	90	357	175	14	4188
MCO	17R	E-R	90	359	175	14	4188
MCO	17R	F-L	90	359	175	14	4487

MCO	17R	F-R	90	355	150	14	4500
MCO	17R	H6	55	1039	550	17	4020
MCO	17R	H7	60	1040	550	17	5393
MCO	17R	H8	50	1050	550	17	6601
MCO	17R	H9	90	340	150	14	9427
MCO	17R	H10	90	357	150	14	9809
MCO	35L	H1	90	347	150	14	9824
MCO	35L	K	90	341	150	14	9824
MCO	35L	H2	90	352	150	14	9416
MCO	35L	H3	50	1075	550	17	6577
MCO	35L	H5	50	1048	550	17	5011
MCO	35L	E-L	90	342	150	14	5515
MCO	35L	E-R	90	344	175	14	5500
MCO	35L	F-L	90	324	150	14	5230
MCO	35L	F-R	90	369	175	1	5174
MCO	35L	H6	130	369	150	11	4913
MCO	35L	H7	121	372	150	7	3536
MCO	35L	H8	130	378	150	11	2312
MCO	36L	E-R	120	418	170	7	3816
MCO	36L	E-L	90	369	180	1	3918
MCO	36L	A2	90	334	100	14	4917
MCO	36L	Y	70	1116	400	10	4549
MCO	36L	J-L	90	385	250	1	7574
MCO	36L	J-R	60	1066	400	17	7003
MCO	36L	B2-L	90	365	175	1	11396
MCO	36L	B2-R	90	367	175	1	11396
MCO	36L	B1-L	90	368	175	1	11782
MCO	36L	B1-R	90	380	175	1	11782
MCO	18R	B10-L	90	395	180	1	11766
MCO	18R	E-R	90	393	250	1	7693
MCO	18R	E-L	60	1074	400	17	7123
MCO	18R	A2	90	332	100	14	6874
MCO	18R	Y	70	1135	400	10	5452
MCO	18R	J-L	120	418	160	7	3940
MCO	18R	J-R	90	376	160	1	4038
MCO	18R	B10-R	90	386	160	1	11788
BOS	14	M	105	338	150	16	2561
BOS	14	22L	105	332	150	16	3533
BOS	32	J	132	322	100	11	4856
BOS	32	J1	106	328	150	16	3761
BOS	32	M	75	335	150	15	2107
BOS	15L	Y	36	576	450	8	1180
BOS	33R	N-R	66	357	150	15	2547

BOS	33R	N-L	109	350	150	16	2403
BOS	33R	M-R	66	356	150	15	1436
BOS	33R	M-L	114	334	150	7	1298
BOS	9	E	159	532	100	4	2126
BOS	9	C-L	122	374	100	7	3676
BOS	9	C-R	58	513	250	13	3782
BOS	9	D1	121	381	125	7	5962
BOS	9	D2	90	376	150	1	6477
BOS	9	D	90	354	150	14	6751
BOS	27	M-R	120	398	200	7	6789
BOS	27	M-L	57	426	190	18	6974
BOS	27	K	50	648	750	9	6057
BOS	27	E	21	892	700	17	4172
BOS	27	C-L	122	359	100	7	2950
BOS	27	C-R	58	372	250	15	3067
BOS	04L	N-R	90	278	100	14	7705
BOS	04L	N-L	90	328	150	14	7619
BOS	04L	N2	90	336	150	14	7360
BOS	04L	N1	90	310	130	14	6830
BOS	04L	Q-L	97	325	150	14	3076
BOS	04L	Q-R	83	308	150	14	3150
BOS	04L	F-L	87	323	150	14	2685
BOS	04L	F-R	93	299	110	14	2726
BOS	22R	Q-L	97	303	100	14	3687
BOS	22R	Q-R	83	329	150	14	3667
BOS	22R	F-L	87	298	100	14	4133
BOS	22R	F-R	93	331	150	14	4062
BOS	22R	C-L	85	317	150	14	5032
BOS	22R	C-R	102	293	120	16	5032
BOS	22R	E-R	82	299	150	14	6680
BOS	22R	E-L	102	337	130	16	6631
BOS	22R	K-R	90	333	150	14	6985
BOS	22R	K-L	90	297	110	14	7022
BOS	04R	P	150	447	175	4	2098
BOS	04R	D	90	364	175	1	2052
BOS	04R	C-L	85	352	175	14	2590
BOS	04R	C-R	90	328	130	14	2639
BOS	04R	H	30	956	350	17	3005
BOS	04R	F-L	90	642	250	19	3502
BOS	04R	F-R	93	289	120	14	3627
BOS	04R	Y	30	1002	1800	3	5495
BOS	04R	R	30	1008	1800	3	6524
BOS	04R	N3	60	610	300	13	8152

BOS	04R	N	90	436	175	1	8592
BOS	22L	B	106	572	150	19	8353
BOS	22L	M1	90	472	150	1	7650
BOS	22L	E-L	102	329	120	16	5985
BOS	22L	E-R	79	378	200	1	7215
BOS	22L	P	30	696	750	9	5076
BOS	22L	D	90	366	175	1	5281
BOS	22L	C-L	90	339	120	14	4786
BOS	22L	C-R	74	461	350	13	4536
BOS	22L	H	150	508	100	4	4164
BOS	22L	F-L	87	279	120	14	3793
BOS	22L	F-R	93	611	250	19	3656
BOS	22L	Y	150	491	85	4	2406
BOS	15R	M-L	115	356	150	7	2667
BOS	15R	M-R	65	513	150	13	2815
BOS	15R	Q	147	642	85	5	3246
BOS	15R	F	157	510	100	4	4538
BOS	15R	G	63	508	400	13	4989
BOS	15R	D-L	60	380	150	15	6516
BOS	15R	D-R	120	381	150	7	6305
BOS	15R	C	120	377	150	7	8658
BOS	33L	L	90	367	175	1	9860
BOS	33L	Z	90	377	200	1	8946
BOS	33L	N-LS	60	463	300	13	7426
BOS	33L	N-LB	90	343	130	14	7492
BOS	33L	N-R	70	334	130	15	7010
BOS	33L	M-L	115	500	130	7	6117
BOS	33L	M-R	65	386	150	15	6206
BOS	33L	Q	33	1155	1800	3	5350
BOS	33L	F	23	833	700	9	4035
BOS	33L	G	117	342	130	7	3763
BOS	33L	D-L	60	414	175	15	2500
BOS	33L	D-R	120	335	85	7	2484
SAN	9	B1	145	376	100	11	8068
SAN	9	B4	90	388	175	1	5102
SAN	9	B5	90	402	185	1	3868
SAN	9	B6	103	327	175	16	2995
SAN	9	B7	145	329	150	11	1897
SAN	9	B8	145	332	150	11	787
SAN	9	C1	142	321	110	11	8179
SAN	9	C2	90	278	110	14	7710
SAN	9	C3	90	407	200	1	5846
SAN	9	C4	90	390	200	1	5100

SAN	9	C5	90	436	220	1	3842
SAN	9	C6	77	376	220	15	3019
SAN	9	D	94	510	160	19	6159
SAN	27	B10	90	349	185	14	7265
SAN	27	B4	90	386	175	1	993
SAN	27	B5	90	387	175	1	2213
SAN	27	B6	77	359	220	15	3227
SAN	27	B7	35	513	450	8	4105
SAN	27	B8	35	503	450	8	5226
SAN	27	B9	90	315	150	14	6651
SAN	27	C3	90	406	175	1	210
SAN	27	C4	90	392	220	1	992
SAN	27	C5	90	437	175	1	2166
SAN	27	C6	103	336	175	16	3168
SLC	17	K1	90	439	250	1	9278
SLC	17	J	90	583	250	19	9278
SLC	17	N	90	370	150	1	7795
SLC	17	P	30	947	1800	3	6116
SLC	17	K4	90	370	150	1	5860
SLC	17	Q	77	440	250	15	4195
SLC	17	K5	53	590	500	13	4168
SLC	17	K6	150	569	85	5	4089
SLC	17	R	150	505	150	4	2173
SLC	17	K7	90	365	150	14	2564
SLC	35	P	150	498	85	4	2465
SLC	35	K4	90	357	150	14	3110
SLC	35	Q	103	414	200	16	4619
SLC	35	K5	127	417	130	11	4619
SLC	35	K6	30	1063	1800	3	4457
SLC	35	R	30	1125	1800	3	6073
SLC	35	K7	90	370	150	1	6405
SLC	35	K8	90	401	200	1	8750
SLC	35	S	100	434	250	1	8900
SLC	35	K9	30	768	450	8	8827
SLC	14	J	61	773	600	9	4881
SLC	14	P-L	57	436	200	18	3279
SLC	14	P-R	123	404	150	7	3550
SLC	14	N	63	537	400	13	3279
SLC	32	P-L	123	375	150	7	991
SLC	32	P-R	57	507	300	13	1129
SLC	32	N	117	397	150	7	1129
SLC	32	Q-L	45	345	150	18	4668
SLC	32	Q-R	104	339	150	16	4500

SLC	34R	H13	90	588	350	19	11687
SLC	34R	H12	90	387	175	1	11433
SLC	34R	H11	90	466	300	1	9608
SLC	34R	H10	90	389	175	1	7986
SLC	34R	S	90	354	150	14	8023
SLC	34R	H9	30	1041	1800	3	6665
SLC	34R	H8	30	954	1800	3	5606
SLC	34R	H7	150	561	120	5	6041
SLC	34R	H6	30	1050	1800	3	3784
SLC	34R	H5	90	415	250	1	4068
SLC	34R	H4	150	481	100	4	3932
SLC	34R	Q	112	410	150	7	3964
SLC	34R	H3	150	536	85	4	2338
SLC	34R	E	70	536	450	13	5990
SLC	16L	H11	90	340	175	14	1947
SLC	16L	H10	90	343	100	14	3741
SLC	16L	S	90	341	100	14	3741
SLC	16L	H9	150	516	85	4	4535
SLC	16L	H8	150	443	130	4	5496
SLC	16L	H7	30	1104	1800	3	5077
SLC	16L	H6	150	478	110	4	7320
SLC	16L	H5	90	426	250	1	7451
SLC	16L	H4	30	1070	1800	3	7160
SLC	16L	Q	68	423	200	15	7701
SLC	16L	H3	34	1051	1800	3	8912
SLC	16L	H2	90	377	175	1	11470
SLC	16L	H1	108	534	250	19	11749
SLC	16L	M	67	552	250	13	11749
SLC	34L	A11	90	412	200	1	11754
SLC	34L	A10	90	423	200	1	11476
SLC	34L	A9	45	1276	800	2	8466
SLC	34L	A8	45	1271	800	2	7273
SLC	34L	A7	45	1292	800	2	6052
SLC	34L	A6	51	1387	800	2	4650
SLC	34L	A5	140	458	150	4	4500
SLC	34L	A4	140	443	150	11	3466
SLC	34L	A3	140	457	150	4	2235
SLC	16R	A9	130	441	150	11	2285
SLC	16R	A8	130	453	150	11	3473
SLC	16R	A7	130	483	150	11	4644
SLC	16R	A6	53	1545	900	2	4681
SLC	16R	A5	40	1392	900	2	6134
SLC	16R	A4	40	1317	900	2	7258

SLC	16R	A3	40	1398	900	2	8378
SLC	16R	A2	90	438	200	1	11456
SLC	16R	A1	90	429	200	1	11732
LAX	07L	T-L	90	361	150	14	1884
LAX	07L	T-R	90	331	150	14	1915
LAX	07L	P-L	90	357	150	14	3015
LAX	07L	P-R	90	357	150	14	3015
LAX	07L	N	90	358	150	14	3441
LAX	07L	M-L	90	362	150	14	4473
LAX	07L	M-R	30	411	150	18	4473
LAX	07L	B6	135	393	85	11	5248
LAX	07L	B5	64	504	450	13	6124
LAX	07L	B4	134	377	135	11	6738
LAX	07L	H2	32	1113	1800	3	6934
LAX	07L	G-L	90	337	150	14	7702
LAX	07L	B3	90	417	175	1	8759
LAX	07L	J-L	90	381	150	1	9372
LAX	07L	J-R	150	373	150	4	9331
LAX	07L	F-L	90	364	175	1	10886
LAX	07L	F-R	90	338	175	14	10914
LAX	07L	B	90	381	175	1	11871
LAX	07L	G-R	90	365	150	14	7656
LAX	25R	U-L	90	334	150	14	10957
LAX	25R	U-R	90	338	150	14	10957
LAX	25R	T-L	90	355	150	14	8943
LAX	25R	T-R	90	431	170	1	8841
LAX	25R	P-L	90	354	150	14	7819
LAX	25R	P-R	90	353	150	14	7819
LAX	25R	N	90	363	150	14	7381
LAX	25R	M-L	149	377	150	4	6291
LAX	25R	M-R	43	720	1000	9	6366
LAX	25R	B6	43	711	1000	9	5320
LAX	25R	B5	40	719	1000	9	4453
LAX	25R	B4	42	727	1000	9	3686
LAX	25R	G-L	83	354	175	14	3167
LAX	25R	B3	90	350	175	14	1986
LAX	25R	G-R	75	339	150	15	3123
LAX	06L	W	90	366	150	14	5975
LAX	06L	Y	45	757	1000	9	3546
LAX	06L	Z	150	418	125	4	3724
LAX	06L	AA	150	415	125	4	1443
LAX	06L	V	90	340	150	14	8754
LAX	24R	BB	90	358	150	14	8733

LAX	24R	W	90	352	150	14	2640
LAX	24R	Y	135	377	125	11	4680
LAX	24R	Z	30	990	1800	3	4275
LAX	24R	AA	30	1000	1800	3	6541
LAX	06R	V-L	90	342	150	14	9339
LAX	06R	V-R	90	366	175	1	9339
LAX	06R	E8	140	383	150	11	9007
LAX	06R	E10	90	334	100	14	7075
LAX	06R	W-L	90	295	120	14	6653
LAX	06R	W-R	90	331	100	14	6653
LAX	06R	Y-L	135	312	120	11	5029
LAX	06R	Y-R	30	966	1800	3	4671
LAX	06R	E13	125	400	85	7	4252
LAX	06R	Z-L	30	645	400	8	3501
LAX	06R	Z-R	150	427	100	4	3221
LAX	06R	AA-L	40	403	200	18	1519
LAX	06R	AA-R	90	370	200	1	1341
LAX	06R	E7	90	328	110	14	9721
LAX	06R	E6	90	334	125	14	10183
LAX	24L	E10	90	330	125	14	2259
LAX	24L	W-L	90	328	120	14	2687
LAX	24L	W-R	90	294	120	14	2687
LAX	24L	Y-L	150	442	100	4	4073
LAX	24L	Y-R	46	406	250	18	4203
LAX	24L	E13	55	750	1000	9	4713
LAX	24L	Z-L	30	800	1000	9	5677
LAX	24L	Z-R	150	380	135	4	5455
LAX	24L	AA-L	58	755	1000	9	7319
LAX	24L	AA-R	140	339	130	11	7669
LAX	24L	BB-L	135	376	100	11	8723
LAX	24L	BB-R	90	308	150	14	8808
LAX	24L	CC	90	362	150	14	9493
LAX	24L	DD	90	351	150	14	9884
LAX	07R	T-L	90	350	150	14	1892
LAX	07R	T-R	90	350	150	14	1892
LAX	07R	H9	147	387	125	4	2434
LAX	07R	N-L	90	358	150	14	3441
LAX	07R	N-R	90	358	150	14	3441
LAX	07R	H8	147	412	100	4	4082
LAX	07R	H6	147	404	125	4	4957
LAX	07R	A7	150	426	110	4	5086
LAX	07R	H4	148	424	150	4	6110
LAX	07R	H3	33	1084	1800	3	5814

LAX	07R	G-L	83	359	150	14	7601
LAX	07R	G-R	98	371	150	16	7560
LAX	07R	H1	30	1103	1800	3	7443
LAX	07R	A4	60	422	250	15	8274
LAX	07R	F-L	90	364	175	1	10882
LAX	07R	F-R	90	371	175	1	10869
LAX	25L	U-L	135	464	175	11	10743
LAX	25L	U-R	90	359	175	14	10885
LAX	25L	T-L	90	357	150	14	8905
LAX	25L	T-R	90	357	150	14	8905
LAX	25L	H9	33	1129	1800	3	7599
LAX	25L	N-L	90	354	150	14	7351
LAX	25L	N-R	78	354	150	14	7351
LAX	25L	H8	33	1112	1800	3	5965
LAX	25L	H6	33	1107	1800	3	5106
LAX	25L	A7	30	1093	1800	3	5028
LAX	25L	H4	30	1124	1800	3	3910
LAX	25L	H3	147	410	120	4	4261
LAX	25L	G-L	82	363	150	14	3225
LAX	25L	G-R	98	363	150	16	3178
LAX	25L	H1	150	385	120	4	2619
LAX	25L	A4	120	381	150	7	2400
PHL	8	A2	150	465	80	4	1200
PHL	8	A	90	361	150	14	2594
PHL	26	A	90	360	150	14	2095
PHL	26	A2	30	717	550	8	3331
PHL	26	A3	85	367	150	14	4607
PHL	26	D-L	95	355	150	14	4796
PHL	26	D-R	85	357	150	14	4831
PHL	17	S-L	84	351	150	14	5886
PHL	17	S-R	90	347	150	14	5886
PHL	17	K-L	84	417	250	1	4723
PHL	17	K-R	95	397	250	1	4664
PHL	17	H-L	90	346	150	14	4038
PHL	17	H-R	90	348	150	14	4038
PHL	17	E4	49	426	200	18	2895
PHL	17	D4	130	371	100	11	2760
PHL	17	G-L	60	412	200	15	2675
PHL	17	G-R	121	343	85	7	2648
PHL	17	E3	150	429	100	4	1642
PHL	17	E-R	100	359	150	16	6306
PHL	17	E-L	90	358	150	14	6306
PHL	35	K-L	84	352	150	14	1427

PHL	35	K-R	96	333	150	14	1427
PHL	35	H-L	90	366	175	1	2149
PHL	35	H-R	90	353	175	14	2149
PHL	35	E4	130	358	85	11	3325
PHL	35	D4	50	431	200	18	3435
PHL	35	G-L	60	382	150	15	3633
PHL	35	G-R	120	350	100	7	3534
PHL	35	E3	30	775	1500	12	4254
PHL	35	E2	128	356	175	11	5680
PHL	35	D2	90	332	100	14	5720
PHL	35	E1	92	365	150	14	6309
PHL	35	D1	90	360	150	14	6309
PHL	09L	K1	90	340	150	14	8703
PHL	09L	D-R	84	338	150	14	7942
PHL	09L	D-L	95	359	175	14	7882
PHL	09L	E-R	84	359	150	14	7100
PHL	09L	E-L	96	381	250	1	6999
PHL	09L	K2	30	945	1800	3	5871
PHL	09L	L-R	45	464	150	18	5789
PHL	09L	L-L	136	398	85	11	5666
PHL	09L	M-R	133	338	110	11	4950
PHL	09L	M-L	47	439	200	18	5136
PHL	09L	K3	90	411	250	1	4793
PHL	09L	N-R	90	392	175	1	4037
PHL	09L	N-L	102	401	250	16	3947
PHL	09L	K4	150	447	90	4	3609
PHL	09L	T-R	90	361	175	14	2114
PHL	09L	T-L	90	405	200	1	1968
PHL	09L	S	101	400	200	16	9176
PHL	09L	H	147	494	150	4	9248
PHL	27R	E-R	96	357	200	1	2100
PHL	27R	E-L	84	345	175	14	2079
PHL	27R	K2	150	441	90	4	2875
PHL	27R	L-R	36	721	1000	9	3278
PHL	27R	L-L	136	388	60	11	3485
PHL	27R	M-R	133	363	90	11	4080
PHL	27R	M-L	48	431	200	18	4226
PHL	27R	K3	90	388	250	1	4245
PHL	27R	N-R	78	392	250	15	5079
PHL	27R	N-L	90	363	150	14	5089
PHL	27R	K4	30	925	1700	3	5154
PHL	27R	T-R	90	402	250	1	7056
PHL	27R	T-L	90	350	150	14	7056

PHL	27R	K5	30	972	1800	3	7391
PHL	27R	K6	90	381	200	1	8940
PHL	27R	W-L	95	346	200	14	9281
PHL	09R	Z	90	345	120	14	2681
PHL	09R	S9	150	437	100	4	3083
PHL	09R	S8	30	946	1800	3	3183
PHL	09R	S7	90	332	120	14	4106
PHL	09R	S6	30	971	1800	3	4522
PHL	09R	Y-L	90	369	120	14	5385
PHL	09R	Y-R	90	356	150	14	5385
PHL	09R	S5	150	457	110	4	5776
PHL	09R	S4	30	944	1800	3	5987
PHL	09R	U-L	90	395	200	1	7401
PHL	09R	U-R	90	348	150	14	7459
PHL	09R	S3	30	949	1800	3	8025
PHL	09R	S2	90	394	200	1	9796
PHL	09R	S1-L	90	383	225	1	10248
PHL	09R	S1-R	90	344	120	14	10329
PHL	27L	S10	90	375	200	1	11163
PHL	27L	Z	100	336	150	16	8928
PHL	27L	S9	30	1088	1800	3	7804
PHL	27L	S8	150	423	90	4	7916
PHL	27L	S7	90	339	150	14	7512
PHL	27L	S6	150	435	90	4	6555
PHL	27L	Y-L	90	353	150	14	6201
PHL	27L	Y-R	90	359	175	14	6178
PHL	27L	S5	30	1086	1800	3	5080
PHL	27L	S4	150	451	90	4	5142
PHL	27L	U-L	90	345	150	14	4115
PHL	27L	U-R	90	366	200	1	4082
PHL	27L	S3	150	446	90	4	3083
PHL	27L	S	105	350	200	16	11658
PHL	27R	W-R	90	356	175	14	9281
DFW	13R	A1	150	607	90	5	2543
DFW	13R	A2	90	369	175	1	3694
DFW	13R	A3	90	384	175	1	5478
DFW	13R	A4	30	1090	1800	3	5991
DFW	13R	A5	90	371	150	1	8849
DFW	13R	A6	90	366	150	14	9111
DFW	31L	A	90	370	175	1	9090
DFW	31L	A1	30	1077	1800	3	6001
DFW	31L	A2	90	394	150	1	5262
DFW	31L	A3	90	369	150	1	3504

DFW	31L	A4	150	594	90	5	2573
DFW	13L	R	90	407	175	1	8766
DFW	13L	R3	90	381	175	1	6996
DFW	13L	R2	150	567	100	5	4228
DFW	31R	R3	90	374	175	1	1700
DFW	31R	R2	30	1109	1800	3	3965
DFW	31R	R1	30	1069	1800	3	6055
DFW	31R	P-L	90	397	175	1	8398
DFW	31R	P-R	90	400	175	1	8398
DFW	31R	N-L	90	405	175	1	8770
DFW	31R	N-R	90	404	175	1	8770
DFW	17L	Q4	150	473	90	4	2258
DFW	17L	Q5	150	488	90	4	3935
DFW	17L	Q6	30	993	1800	3	3831
DFW	17L	Q7	30	1000	1800	3	5831
DFW	17L	Q8	30	995	1800	3	6822
DFW	17L	Q9	90	379	150	1	8038
DFW	17L	Q	90	396	175	1	8295
DFW	17L	EL	90	399	175	1	1439
DFW	35R	Q1	90	389	150	1	8300
DFW	35R	Q2	90	385	150	1	8038
DFW	35R	Q3	30	1020	1800	3	6796
DFW	35R	Q4	30	1011	1800	3	5487
DFW	35R	Q5	30	1001	1800	3	3821
DFW	35R	Q6	150	504	90	4	3918
DFW	35R	Q7	150	506	85	4	1919
DFW	35R	EL	90	417	175	1	6687
DFW	18R	WR-L	90	417	175	1	13168
DFW	18R	WR-R	90	364	150	14	13201
DFW	18R	A-L	75	396	150	15	10880
DFW	18R	A-R	120	449	150	7	10753
DFW	18R	B-L	70	406	150	15	10480
DFW	18R	B-R	127	460	150	11	10301
DFW	18R	E7	30	1018	1800	3	9346
DFW	18R	WM-L	90	382	175	1	9065
DFW	18R	WM-R	90	403	175	1	9046
DFW	18R	E5	150	503	150	4	8422
DFW	18R	E6	30	1088	1800	3	7761
DFW	18R	WL-L	90	422	175	1	7724
DFW	18R	WL-R	90	388	150	1	7774
DFW	18R	E4	30	1036	1800	3	6477
DFW	18R	E3	30	1014	1800	3	5207
DFW	18R	E2	150	468	150	4	5817

DFW	18R	WK-L	90	373	175	1	5176
DFW	18R	WK-R	90	404	175	1	5166
DFW	18R	E1	150	546	90	4	4743
DFW	18R	Z-L	90	371	175	1	2276
DFW	18R	Z-R	90	424	150	1	2292
DFW	18R	Y-L	90	412	200	1	1862
DFW	18R	Y-R	90	456	200	1	1862
DFW	36L	A-L	60	470	150	15	2318
DFW	36L	A-R	106	386	150	16	2194
DFW	36L	B-L	54	466	150	18	2746
DFW	36L	B-R	130	400	150	11	2604
DFW	36L	E7	150	528	90	4	3345
DFW	36L	WM-L	90	396	175	1	3986
DFW	36L	WM-R	90	388	175	1	4011
DFW	36L	E5	30	1113	1800	3	4000
DFW	36L	E6	150	495	150	4	4689
DFW	36L	WL-L	90	386	175	1	5322
DFW	36L	WL-R	90	401	175	1	5294
DFW	36L	E4	150	556	90	5	6189
DFW	36L	E3	150	464	150	4	7284
DFW	36L	E2	30	1057	1800	3	6607
DFW	36L	WK-L	90	416	175	1	7900
DFW	36L	WK-R	90	397	175	1	7900
DFW	36L	E1	30	1019	1800	3	7944
DFW	36L	Z-L	90	432	175	1	10808
DFW	36L	Z-R	90	370	175	1	10794
DFW	36L	Y-L	90	427	175	1	11185
DFW	36L	Y-R	90	373	175	1	11185
DFW	36L	WG	90	376	150	1	12927
DFW	36L	WF-L	90	355	150	14	13220
DFW	36L	WF-R	90	362	150	14	13220
DFW	17R	ER-L	90	370	150	1	13210
DFW	17R	ER-R	90	357	150	14	13210
DFW	17R	EQ-L	90	426	200	1	12864
DFW	17R	EQ-R	90	383	200	1	12901
DFW	17R	EP	90	416	200	1	12602
DFW	17R	A-L	90	376	175	1	11038
DFW	17R	A-R	90	373	175	1	11038
DFW	17R	B-L	90	376	175	1	10663
DFW	17R	B-R	90	371	175	1	10663
DFW	17R	L6	30	1035	1800	3	9404
DFW	17R	EM-L	90	371	175	1	9074
DFW	17R	EM-R	90	372	175	1	9074

DFW	17R	L4	150	539	150	4	8434
DFW	17R	L5	30	1142	1800	3	7759
DFW	17R	EL-L	90	369	175	1	7774
DFW	17R	EL-R	90	370	175	1	7774
DFW	17R	L3	30	1080	1800	3	6471
DFW	17R	K8-L	90	364	190	1	6475
DFW	17R	K8-R	90	366	175	1	6475
DFW	17R	L2	150	595	90	5	5999
DFW	17R	EK-L	90	360	175	14	5180
DFW	17R	EK-R	90	369	175	1	5176
DFW	17R	L1	150	577	90	5	4701
DFW	17R	EJ-L	90	375	175	1	3875
DFW	17R	EJ-R	90	374	175	1	3875
DFW	17R	Z-L	90	379	175	1	2288
DFW	17R	Z-R	90	376	175	1	2288
DFW	17R	Y-L	90	418	200	1	1863
DFW	17R	Y-R	90	413	175	1	1863
DFW	35L	A-L	90	372	175	1	2060
DFW	35L	A-R	90	372	175	1	2060
DFW	35L	B-L	90	371	175	1	2437
DFW	35L	B-R	90	373	175	1	2437
DFW	35L	L6	150	577	95	5	3258
DFW	35L	EM-L	90	371	175	1	4024
DFW	35L	EM-R	90	371	175	1	4024
DFW	35L	L4	30	1135	1800	3	4015
DFW	35L	L5	150	538	150	4	4678
DFW	35L	EL-L	90	372	175	1	5324
DFW	35L	EL-R	90	373	175	1	5324
DFW	35L	L3	150	575	100	5	6147
DFW	35L	K8-L	90	364	175	1	6619
DFW	35L	K8-R	90	363	175	1	6619
DFW	35L	L2	30	1082	1800	3	6625
DFW	35L	EK-L	90	374	175	1	7913
DFW	35L	EK-R	90	360	175	14	7913
DFW	35L	L1	30	1086	1800	3	7923
DFW	35L	EJ-L	90	373	175	1	9224
DFW	35L	EJ-R	90	375	175	1	9224
DFW	35L	Z-L	90	418	200	1	10759
DFW	35L	Z-R	90	386	175	1	10801
DFW	35L	Y-L	90	370	175	1	11187
DFW	35L	Y-R	90	378	175	1	11187
DFW	35L	EH	90	404	175	1	12625
DFW	35L	EG-L	90	382	175	1	12912

DFW	35L	EG-R	90	366	175	1	12925
DFW	35L	EF-L	90	365	175	1	13206
DFW	35L	EF-R	90	345	175	14	13201
DFW	18L	WR-L	90	373	150	1	13211
DFW	18L	WR-R	90	379	175	1	13201
DFW	18L	WQ	90	388	150	1	12931
DFW	18L	WP	90	392	150	1	12656
DFW	18L	A-L	90	373	175	1	11040
DFW	18L	A-R	93	377	175	1	11040
DFW	18L	B-L	90	370	175	1	10664
DFW	18L	B-R	93	380	175	1	10664
DFW	18L	F6	30	1047	1800	3	9391
DFW	18L	WM-L	90	372	175	1	9076
DFW	18L	WM-R	90	382	175	1	9076
DFW	18L	F4	150	541	150	4	8426
DFW	18L	F5	30	1132	1800	3	7771
DFW	18L	WL-L	90	372	175	1	7776
DFW	18L	WL-R	90	377	175	1	7776
DFW	18L	F3	30	1081	1800	3	6469
DFW	18L	G8-L	90	367	175	1	6476
DFW	18L	G8-R	90	367	175	1	6476
DFW	18L	F2	150	571	100	5	5999
DFW	18L	WK-L	90	372	175	1	5176
DFW	18L	WK-R	90	377	175	1	5176
DFW	18L	F1	150	570	100	5	4702
DFW	18L	WJ-L	90	375	175	1	3875
DFW	18L	WJ-R	90	382	175	1	3875
DFW	18L	Z-R	90	382	150	1	2288
DFW	18L	Z-L	90	377	175	1	2288
DFW	18L	Y-R	90	412	175	1	1864
DFW	18L	Y-L	90	411	175	1	1864
DFW	36R	A-L	87	373	175	1	2063
DFW	36R	A-R	90	372	175	1	2063
DFW	36R	B-L	87	377	175	1	2436
DFW	36R	B-R	90	371	175	1	2436
DFW	36R	F6	150	578	100	5	3262
DFW	36R	WM-L	90	378	175	1	4025
DFW	36R	WM-R	90	372	175	1	4025
DFW	36R	F4	30	1085	1800	3	4064
DFW	36R	F5	150	547	150	4	4642
DFW	36R	WL-L	90	379	175	1	5325
DFW	36R	WL-R	90	371	175	1	5325
DFW	36R	F3	150	569	100	5	6148

DFW	36R	G8-L	90	365	175	1	6624
DFW	36R	G8-R	90	366	175	1	6624
DFW	36R	F2	30	1067	1800	3	6632
DFW	36R	WK-L	90	378	175	1	7923
DFW	36R	WK-R	90	373	175	1	7923
DFW	36R	F1	30	1085	1800	3	7912
DFW	36R	WJ-L	90	380	175	1	9225
DFW	36R	WJ-R	90	372	175	1	9225
DFW	36R	Z-R	90	414	175	1	10761
DFW	36R	Z-L	90	379	175	1	10811
DFW	36R	Y-R	90	376	175	1	11188
DFW	36R	Y-L	90	377	175	1	11188
DFW	36R	WH	90	377	150	1	12661
DFW	36R	WG-L	90	374	150	1	12926
DFW	36R	WG-R	90	375	150	1	12926
DFW	36R	WF-L	90	370	150	1	13204
DFW	36R	WF-R	90	369	150	1	13204
DFW	17C	ER-L	90	415	150	1	13201
DFW	17C	ER-R	90	441	175	1	13150
DFW	17C	EQ	90	439	200	1	12871
DFW	17C	A-L	90	411	150	1	11037
DFW	17C	A-R	90	365	150	14	11037
DFW	17C	B-L	90	424	150	1	10662
DFW	17C	B-R	90	375	150	1	10662
DFW	17C	M7	30	1072	1800	3	9363
DFW	17C	M6	30	1116	1800	3	7734
DFW	17C	M5	150	513	150	4	8403
DFW	17C	P2	30	1116	1800	3	8089
DFW	17C	EL-R	90	426	175	1	7737
DFW	17C	EL-L	90	439	175	1	7772
DFW	17C	M4	30	1070	1800	3	6479
DFW	17C	M3	30	1075	1800	3	5145
DFW	17C	M2	150	472	150	4	5829
DFW	17C	EK	90	372	175	1	5163
DFW	17C	EJ-L	90	421	175	1	3833
DFW	17C	EJ-R	90	407	175	1	3833
DFW	17C	Z-L	90	409	175	1	2252
DFW	17C	Z-R	90	408	175	1	2252
DFW	17C	Y-L	90	415	175	1	1862
DFW	17C	Y-R	90	420	175	1	1862
DFW	17C	M1	150	566	90	5	4744
DFW	35C	A-L	90	366	175	1	2058
DFW	35C	A-R	90	411	175	1	2058

DFW	35C	B-L	90	373	175	1	2436
DFW	35C	B-R	90	427	175	1	2436
DFW	35C	M7	150	578	90	5	3287
DFW	35C	M6	150	517	150	4	4659
DFW	35C	M5	30	1053	1800	3	4045
DFW	35C	P2	150	534	110	4	4406
DFW	35C	EL-R	90	432	150	1	5324
DFW	35C	EL-L	90	394	175	1	5324
DFW	35C	M4	150	600	90	5	6190
DFW	35C	M3	150	489	150	4	7242
DFW	35C	M2	30	1089	1800	3	6609
DFW	35C	EK	90	371	175	1	7912
DFW	35C	EJ-L	90	413	175	1	9176
DFW	35C	EJ-R	90	404	175	1	9200
DFW	35C	Z-L	90	420	175	1	10762
DFW	35C	Z-R	90	383	150	1	10812
DFW	35C	Y-L	90	408	175	1	11148
DFW	35C	Y-R	90	405	175	1	11148
DFW	35C	EG	90	361	150	14	12931
DFW	35C	EF	90	366	150	14	13191
DFW	35C	M1	30	1075	1800	3	7906
PHX	07R	G4	90	363	150	14	3062
PHX	07R	H4	90	363	150	14	3062
PHX	07R	G5	43	675	800	9	4479
PHX	07R	H5	42	679	150	8	4479
PHX	07R	G6	45	1026	800	17	5043
PHX	07R	H6	90	894	150	10	5593
PHX	07R	H7	90	372	150	1	6502
PHX	07R	G7	45	1002	800	17	5956
PHX	07R	G8	90	373	150	1	7580
PHX	25L	G1	90	362	150	14	7615
PHX	25L	H1	90	361	150	14	7615
PHX	25L	H2	90	371	150	1	7304
PHX	25L	G2	45	1040	800	17	6365
PHX	25L	G3-S	45	1024	800	17	5266
PHX	25L	H3-S	45	1025	800	17	5266
PHX	25L	G4	90	367	150	14	4432
PHX	25L	H4	90	368	150	14	4432
PHX	25L	G5-S	90	357	150	14	2690
PHX	25L	G5-B	135	398	125	11	2690
PHX	25L	H5-S	90	361	150	14	2690
PHX	25L	H5-B	135	406	125	11	2690
PHX	25L	G6	135	432	100	11	1796

PHX	25L	G3-B	90	384	150	1	6035
PHX	25L	H3-B	90	378	150	1	6035
PHX	07L	E5	90	402	150	1	1974
PHX	07L	E6-B	135	418	125	11	3316
PHX	07L	E6-S	90	379	150	1	3316
PHX	07L	F6-B	130	410	125	11	3316
PHX	07L	F6-S	90	379	150	1	3316
PHX	07L	E7-B	135	420	125	11	4218
PHX	07L	E7-S	90	379	150	1	4218
PHX	07L	E8-B	90	668	150	19	4990
PHX	07L	E8-S	45	720	800	9	4990
PHX	07L	F8	90	330	100	14	5461
PHX	07L	E9-B	90	698	150	19	5799
PHX	07L	E9-S	45	751	800	9	5799
PHX	07L	F9-B	90	698	150	19	5799
PHX	07L	F9-S	45	751	800	9	5799
PHX	07L	E10-B	90	692	150	19	6725
PHX	07L	E10-S	45	745	800	9	6725
PHX	07L	F10-B	90	694	150	19	6725
PHX	07L	F10-S	45	747	800	9	6725
PHX	07L	E11-B	90	636	150	19	7882
PHX	07L	E11-S	45	688	800	9	7882
PHX	07L	F11-B	90	637	150	19	7882
PHX	07L	F11-S	45	689	800	9	7882
PHX	07L	E12-B	90	691	150	19	9209
PHX	07L	E12-S	45	743	800	9	9209
PHX	07L	F12-B	90	690	150	19	9209
PHX	07L	F12-S	45	742	800	9	9209
PHX	07L	E13	90	368	175	1	10104
PHX	07L	F13	90	366	175	1	10104
PHX	07L	R	45	507	250	18	10019
PHX	25R	E3	90	366	175	1	10106
PHX	25R	F3	90	372	175	1	10106
PHX	25R	E4-B	90	672	150	19	9226
PHX	25R	E4-S	45	724	800	9	9226
PHX	25R	F4-B	90	672	150	19	9226
PHX	25R	F4-S	45	724	800	9	9226
PHX	25R	E5-B	90	704	150	19	7569
PHX	25R	E5-S	45	756	800	9	7569
PHX	25R	E6-B	90	677	150	19	6277
PHX	25R	E6-S	45	730	800	9	6277
PHX	25R	F6	45	728	800	9	6277
PHX	25R	E7-B	90	653	150	19	5401

PHX	25R	E7-S	45	706	800	9	5401
PHX	25R	E8-B	135	415	125	11	4627
PHX	25R	E8-S	90	363	150	14	4627
PHX	25R	F8	90	330	100	14	4661
PHX	25R	E9-B	135	415	125	11	3777
PHX	25R	E9-S	90	376	150	1	3777
PHX	25R	F9-B	135	415	125	11	3777
PHX	25R	F9-S	90	375	150	1	3777
PHX	25R	E10-B	135	415	125	11	2857
PHX	25R	E10-S	90	375	150	1	2858
PHX	25R	F10-B	135	415	125	11	2858
PHX	25R	F10-S	90	374	150	1	2858
PHX	25R	E11	90	370	150	1	1762
PHX	25R	F11	90	369	150	1	1762
PHX	8	A4	90	345	100	14	1856
PHX	8	B4	90	378	150	1	1803
PHX	8	B5	90	385	150	1	2833
PHX	8	A5	90	351	100	14	3928
PHX	8	B6	90	368	150	14	3887
PHX	8	A6	90	353	100	14	4826
PHX	8	B7	90	381	150	1	4703
PHX	8	A7	90	346	150	14	5835
PHX	8	B8-B	90	536	250	19	5567
PHX	8	B8-S	45	594	400	8	5567
PHX	8	B9-B	90	510	250	19	6406
PHX	8	B9-S	45	567	400	8	6406
PHX	8	A8	90	372	150	1	7670
PHX	8	A9	90	341	150	14	8603
PHX	8	B10-S	45	549	400	8	7493
PHX	8	B10-B	90	490	400	19	7493
PHX	8	B11-B	90	520	250	19	8336
PHX	8	B11-S	45	578	400	8	8336
PHX	8	A10	90	362	150	14	9995
PHX	8	B12	90	363	150	14	9993
PHX	8	A11	90	370	150	1	10395
PHX	8	B13	90	369	150	1	10393
PHX	8	A12	90	374	150	1	10799
PHX	8	B14	90	374	150	1	10714
PHX	26	A1	90	367	150	14	11303
PHX	26	B1	90	365	150	14	11303
PHX	26	A2	90	370	150	1	10899
PHX	26	B2	90	370	150	1	10899
PHX	26	A3	90	368	150	14	10387

PHX	26	B3	90	368	150	14	10387
PHX	26	A4	90	342	100	14	8513
PHX	26	B4-B	90	524	200	19	8256
PHX	26	B4-S	45	582	400	8	8256
PHX	26	B5-B	90	554	200	19	7187
PHX	26	B5-S	45	612	400	8	7187
PHX	26	A5	90	347	100	14	6431
PHX	26	B6-B	90	515	200	19	6188
PHX	26	B6-S	45	573	400	8	6188
PHX	26	A6	90	380	175	1	5523
PHX	26	B7-B	90	529	200	19	5348
PHX	26	B7-S	45	587	400	8	5348
PHX	26	A7	90	354	110	14	4522
PHX	26	B8	90	501	250	19	4299
PHX	26	B9-B	135	423	125	11	3657
PHX	26	B9-S	90	382	150	1	3657
PHX	26	A8	90	360	150	14	2616
PHX	26	A9	90	343	100	14	1766
PHX	26	B10-S	90	360	150	14	2616
PHX	26	B10-B	135	360	125	11	2616
PHX	26	B11	90	367	150	14	1736
MIA	9	T2	132	368	150	11	4022
MIA	9	T3	47	1052	600	17	5277
MIA	9	U	47	1041	600	17	6876
MIA	9	T5	37	1084	800	17	7660
MIA	9	Q8	127	368	160	7	11054
MIA	27	T1	90	965	150	10	7978
MIA	27	T2	45	1012	600	17	6283
MIA	27	T3	133	372	150	11	5043
MIA	27	U	133	398	120	11	3469
MIA	27	S-1	90	380	150	1	12222
MIA	27	S-2	90	375	150	1	12532
MIA	12	T-R	111	339	110	16	7213
MIA	12	T-L	35	1064	700	17	7061
MIA	12	S-R	148	427	100	4	6774
MIA	12	S-L	33	1076	700	17	6524
MIA	12	U-R	96	343	150	14	6411
MIA	12	U-L	58	1011	500	17	5585
MIA	12	V-R	60	875	350	10	5204
MIA	12	V-L	42	927	600	17	4940
MIA	12	Y-R	58	1032	600	17	4288
MIA	12	Y-L	60	467	400	13	4599
MIA	12	JJ	90	1033	150	10	3314

MIA	12	Z-R	60	394	200	15	2813
MIA	12	Z-L	120	379	120	7	2678
MIA	12	Q8	66	426	400	13	9359
MIA	30	U-R	90	331	150	14	1706
MIA	30	U-L	84	336	100	14	1778
MIA	30	V-RB	90	323	100	14	2480
MIA	30	V-RS	60	411	200	15	2500
MIA	30	V-L	122	500	150	7	2256
MIA	30	Y-R	60	477	400	13	3120
MIA	30	Y-L	122	379	150	7	3049
MIA	30	JJ	90	566	150	19	3468
MIA	30	Z-R	45	1045	600	17	4700
MIA	30	Z-L	100	1008	150	10	4480
MIA	30	Q2	60	1000	600	17	6058
MIA	30	Q-1	140	372	150	11	7950
MIA	30	Q-2	150	425	90	4	8273
MIA	08R	M3	90	372	175	1	1917
MIA	08R	L3	90	352	175	14	1917
MIA	08R	Z-R	130	399	150	11	2461
MIA	08R	Z-L	30	1135	500	17	1961
MIA	08R	JJ	130	402	150	11	3363
MIA	08R	L4	150	411	125	4	3701
MIA	08R	M4	90	373	150	1	4166
MIA	08R	M5	130	414	150	11	4555
MIA	08R	L5	30	1094	500	17	3661
MIA	08R	M6	90	369	150	1	5148
MIA	08R	L6	90	364	150	14	5130
MIA	08R	M7	47	1081	600	17	5429
MIA	08R	L7	45	1115	600	17	5429
MIA	08R	M9	45	1080	600	17	6261
MIA	08R	L9	90	358	150	14	7035
MIA	08R	M10	45	1063	600	17	7674
MIA	08R	L10-1	90	411	250	1	8046
MIA	08R	M11	123	359	120	7	10335
MIA	08R	L11-1	90	331	100	14	10299
MIA	26L	M1	160	479	100	4	10347
MIA	26L	L1	90	397	225	1	9967
MIA	26L	M2	90	452	220	1	8990
MIA	26L	L2	90	406	220	1	8966
MIA	26L	M3	90	367	150	14	8282
MIA	26L	L3	90	357	150	14	8282
MIA	26L	Z-R	45	1047	600	17	6352
MIA	26L	Z-L	45	1092	600	17	6950

MIA	26L	JJ	45	1096	600	17	6040
MIA	26L	L4	30	1121	500	17	5690
MIA	26L	M4	90	376	150	1	6035
MIA	26L	M5	45	1067	600	17	4861
MIA	26L	L5	150	465	90	4	5942
MIA	26L	M6	90	374	150	1	5066
MIA	26L	L6	90	356	150	14	5066
MIA	26L	M7	135	417	150	11	3978
MIA	26L	L7	48	1340	500	2	2684
MIA	26L	M9	130	411	150	11	3155
MIA	26L	L9	90	361	150	14	3164
MIA	26L	M10	135	408	150	11	1757
MIA	26L	L10	90	351	150	14	1798
MIA	08L	K3	130	391	125	11	2059
MIA	08L	L3	90	367	175	1	2059
MIA	08L	Z-R	130	386	125	11	3209
MIA	08L	Z-L	130	388	135	11	3209
MIA	08L	K6	45	1037	600	17	4267
MIA	08L	L6	45	1037	600	17	4267
MIA	08L	K7	45	1100	600	17	5268
MIA	08L	L7	45	1100	600	17	5268
MIA	08L	K9	45	1075	600	17	6120
MIA	08L	L9	45	1078	600	17	6120
MIA	08L	K10-1	90	354	150	14	8138
MIA	08L	L10-1	90	354	150	14	8138
MIA	08L	K10-2	90	359	150	14	8409
MIA	08L	L10-2	90	356	150	14	8409
MIA	26R	K1-1	90	336	150	14	8157
MIA	26R	L1-1	90	345	150	14	8148
MIA	26R	K2	45	1044	600	17	6264
MIA	26R	L2	45	1043	600	17	6264
MIA	26R	K3	45	1084	600	17	5455
MIA	26R	L3	45	1084	600	17	5455
MIA	26R	Z-R	45	1043	600	17	4332
MIA	26R	Z-L	45	1043	600	17	4332
MIA	26R	K6	130	377	150	11	3279
MIA	26R	L6	130	371	150	11	3279
MIA	26R	K7	130	363	150	11	2230
MIA	26R	L7	130	358	150	11	2230
MIA	26R	K1-2	90	349	150	14	8417
MIA	26R	L1-2	90	354	150	14	8417
MIA	27	T5	142	388	120	11	2721
MIA	9	T1	90	393	250	1	2337

EWR	11	Z-L	90	340	150	14	6564
EWR	11	U-L	90	368	175	1	1830
EWR	11	U-R	90	372	175	1	1830
EWR	11	T	150	457	90	4	2543
EWR	11	S-L	90	397	175	1	3534
EWR	11	S-R	60	497	450	13	3305
EWR	11	Q-L	90	350	150	14	3948
EWR	11	Q-R	90	346	150	14	3948
EWR	11	R-L	90	375	150	1	4298
EWR	11	R-R	90	402	250	1	4221
EWR	11	P-L	70	344	200	15	5306
EWR	11	P-R	110	396	150	16	5152
EWR	11	EE	125	343	150	7	6464
EWR	29	RM	78	371	175	15	6281
EWR	29	W2	30	854	1400	12	4968
EWR	29	U-L	90	378	175	1	4305
EWR	29	U-R	90	379	175	1	4305
EWR	29	T	30	878	1800	3	3653
EWR	29	S-L	90	327	120	14	2648
EWR	29	S-R	90	381	175	1	2589
EWR	29	Q-L	90	321	120	14	2321
EWR	29	Q-R	90	331	120	14	2311
EWR	29	R-L	90	325	120	14	1926
EWR	29	R-R	90	341	130	14	1925
EWR	29	Z-R	160	476	175	4	6214
EWR	04R	P2	150	614	85	5	1816
EWR	04R	E	150	672	100	5	2611
EWR	04R	G	90	360	150	14	3462
EWR	04R	J	30	1115	1800	3	3638
EWR	04R	P3	30	973	1800	3	4791
EWR	04R	K	90	442	300	1	5675
EWR	04R	EE	60	347	120	15	5858
EWR	04R	M-L	90	416	250	1	6721
EWR	04R	M-R	90	334	150	14	6846
EWR	04R	W	90	420	250	1	7544
EWR	04R	Z-L	117	373	150	7	8679
EWR	04R	Z-R	68	384	175	15	8808
EWR	04R	P4	30	894	1800	3	5833
EWR	22L	P1	90	338	100	14	8046
EWR	22L	V	48	672	800	9	6941
EWR	22L	N	30	1321	1800	20	5393
EWR	22L	P2	30	972	1800	3	4589
EWR	22L	E	30	1345	1800	20	3437

EWR	22L	G	90	363	150	14	3260
EWR	22L	J	150	437	110	4	2386
EWR	22L	P3	150	598	85	5	1628
EWR	04L	E-L	90	340	150	14	1847
EWR	04L	E-R	90	339	150	14	1847
EWR	04L	B3	145	435	85	4	2265
EWR	04L	G-L	90	357	150	14	3452
EWR	04L	G-R	90	346	150	14	3464
EWR	04L	B2	30	1033	1800	3	3896
EWR	04L	J-L	90	359	150	14	5010
EWR	04L	J-R	90	358	150	14	5010
EWR	04L	K-L	90	337	150	14	5844
EWR	04L	K-R	90	337	150	14	5844
EWR	04L	B1	30	1045	1800	3	5188
EWR	04L	L-L	90	351	150	14	5188
EWR	04L	L-R	90	339	150	14	6349
EWR	04L	M-L	110	347	150	16	6814
EWR	04L	M-R	90	341	150	14	6839
EWR	04L	Y-L	110	348	150	16	7129
EWR	04L	Y-R	90	332	150	14	7219
EWR	04L	W-L	110	350	175	16	7416
EWR	04L	W-R	70	363	150	15	7556
EWR	04L	Z-L	111	473	150	7	8366
EWR	04L	Z-R	69	365	150	15	8407
EWR	22R	AA-L	101	347	130	16	9507
EWR	22R	AA-R	105	382	175	16	9353
EWR	22R	BB-L	90	346	130	14	8953
EWR	22R	BB-R	90	350	100	14	8949
EWR	22R	CC-L	90	346	130	14	8510
EWR	22R	CC-R	90	321	85	14	8547
EWR	22R	V-L	90	355	130	14	7565
EWR	22R	V-R	90	362	175	14	7565
EWR	22R	N-L	90	353	130	14	8269
EWR	22R	N-R	90	359	140	14	6816
EWR	22R	B4	30	946	1800	3	5739
EWR	22R	C-L	90	347	150	14	5613
EWR	22R	C-R	90	340	150	14	5613
EWR	22R	E-L	90	364	150	14	4881
EWR	22R	E-R	90	360	175	14	4881
EWR	22R	B3	35	780	1000	9	4156
EWR	22R	G-L	90	349	150	14	3274
EWR	22R	G-R	90	352	150	14	3263
EWR	22R	B2	150	469	85	4	2292

EWR	22R	J-L	90	356	150	14	1713
EWR	22R	J-R	90	362	150	14	1713
JFK	04R	J	118	818	90	5	1757
JFK	04R	H	147	526	100	4	2970
JFK	04R	F	25	1242	1000	2	4917
JFK	04R	FA	20	1271	1400	20	5872
JFK	04R	FB	20	1682	1400	20	5872
JFK	04R	E	52	694	400	8	8008
JFK	22L	Z	63	531	175	13	8159
JFK	22L	J	28	1393	1800	20	5804
JFK	22L	H	33	873	1000	9	4805
JFK	22L	F	152	832	100	5	2816
JFK	22L	FA	160	769	85	5	1785
JFK	22L	FB	160	1177	85	5	1785
JFK	04L	J-L	90	426	250	1	4276
JFK	04L	J-R	90	318	100	14	3973
JFK	04L	H-L	90	405	250	1	5150
JFK	04L	H-R	90	315	100	14	5303
JFK	04L	G-L	42	579	500	8	6460
JFK	04L	G-R	98	325	100	14	6785
JFK	04L	F-L	52	504	400	13	8285
JFK	04L	F-R	90	320	100	14	8628
JFK	04L	YA-L	90	344	120	14	9542
JFK	04L	YA-R	90	342	120	14	9542
JFK	04L	C	90	333	120	14	10350
JFK	04L	FB-L	90	372	175	1	10664
JFK	04L	FB-R	90	367	200	1	10655
JFK	22R	K1	90	342	150	14	8469
JFK	22R	K2	90	320	100	14	8185
JFK	22R	K3	90	409	250	1	6664
JFK	22R	J-L	90	326	100	14	4027
JFK	22R	J-R	90	412	250	1	3882
JFK	22R	H-L	90	320	100	14	2702
JFK	22R	H-R	90	373	220	1	2586
JFK	13L	W-L	90	326	100	14	2666
JFK	13L	W-R	90	327	100	14	2666
JFK	13L	D-L	90	333	150	14	4115
JFK	13L	D-R	98	398	150	1	4078
JFK	13L	DB-L	65	369	110	15	5540
JFK	13L	DB-R	105	381	135	16	4971
JFK	13L	ZA-R	45	749	1000	9	5417
JFK	13L	Y-R	90	360	150	14	7521
JFK	13L	Y-L	60	414	175	15	7682

JFK	13L	E-R	90	343	150	14	6172
JFK	13L	E-L	90	349	150	14	6176
JFK	13L	YA	150	412	100	4	8755
JFK	31R	U	103	393	175	16	8748
JFK	31R	C	117	390	175	7	8748
JFK	31R	UA	90	378	175	1	8336
JFK	31R	CB-L	90	341	150	14	7777
JFK	31R	CB-R	35	535	275	8	7674
JFK	31R	CD	67	394	200	15	6652
JFK	31R	V-L	90	440	350	1	6396
JFK	31R	V-R	120	348	90	7	6408
JFK	31R	W-L	90	426	275	1	5024
JFK	31R	W-R	90	425	275	1	5024
JFK	31R	D-L	80	455	300	1	3445
JFK	31R	D-R	90	351	150	14	3665
JFK	31R	DB-L	65	374	130	15	2359
JFK	31R	DB-R	115	357	100	7	2294
JFK	31R	E-L	90	336	120	14	1627
JFK	31R	E-R	90	325	120	14	1635
JFK	31R	ZA-L	140	395	85	11	2055
JFK	13R	MD	150	525	100	4	2654
JFK	13R	MC	90	355	200	14	3418
JFK	13R	MB	120	360	175	7	4606
JFK	13R	M	28	795	1000	9	4943
JFK	13R	L	30	778	1000	9	6692
JFK	13R	KE-L	90	413	250	1	8622
JFK	13R	KE-R	90	332	120	14	8761
JFK	13R	KD	90	360	200	1	9109
JFK	13R	K-L	108	361	150	16	9525
JFK	13R	K-R	90	360	200	1	9650
JFK	13R	Y	90	332	120	14	10988
JFK	13R	JB	90	333	120	14	11656
JFK	13R	JA	90	337	120	14	11978
JFK	13R	Z-L	90	323	120	14	12307
JFK	13R	Z-R	90	318	120	14	12304
JFK	31L	PF	90	330	100	14	11083
JFK	31L	PE	90	330	100	14	10753
JFK	31L	PD	90	313	110	14	10448
JFK	31L	PC	90	413	250	1	9728
JFK	31L	PA	90	477	400	1	7115
JFK	31L	MD	30	872	1000	9	5916
JFK	31L	MC	90	378	175	1	5411
JFK	31L	MB	60	529	500	13	4023

JFK	31L	M	150	433	100	4	3631
JFK	31L	L	150	472	80	4	1977
JFK	04L	K	90	380	175	1	2790
JFK	04L	GG	30	749	1000	9	5550
JFK	22R	K	90	318	100	14	5123
JFK	22R	GG	150	422	100	4	2040
JFK	04L	EE	90	331	175	14	11454
JFK	04L	E-L	90	331	110	14	11456
JFK	04L	E-R	120	355	175	7	11399
IAD	30	Q	90	527	300	19	10128
IAD	30	Q1	30	1041	1800	3	6653
IAD	30	Q2	150	573	98	5	6180
IAD	30	Q3	30	1091	1800	3	4161
IAD	30	Q4	150	487	98	4	3684
IAD	12	Q	90	386	175	1	10279
IAD	12	Q1	150	589	80	5	3108
IAD	12	Q2	30	1088	1800	3	3535
IAD	12	Q3	150	636	100	5	5601
IAD	12	Q4	30	966	1800	3	6075
IAD	12	Y	90	359	85	14	9545
IAD	12	Z	90	580	270	19	9568
IAD	01R	J1	90	375	250	1	11145
IAD	01R	K1	90	399	200	1	10816
IAD	01R	K2	30	1190	1800	20	6721
IAD	01R	K3	150	564	120	5	7264
IAD	01R	K4	30	1155	1800	3	5004
IAD	01R	K5	150	578	115	5	5519
IAD	01R	K6	30	1158	1800	3	3249
IAD	01R	K7	150	587	117	5	3768
IAD	19L	K2	150	582	120	5	3777
IAD	19L	K3	30	1118	1800	3	3291
IAD	19L	K4	150	565	120	5	5527
IAD	19L	K5	30	1107	1800	3	5053
IAD	19L	K6	150	562	115	5	7300
IAD	19L	K7	30	1076	1800	3	6834
IAD	19L	K8	90	422	200	1	10788
IAD	19L	K	90	390	200	1	11155
IAD	19R	U7	90	442	250	1	9102
IAD	19R	U6	90	436	300	1	8478
IAD	19R	U5	30	1189	1800	20	7169
IAD	19R	U4	30	1237	1800	20	5840
IAD	19R	U3	150	534	72	4	3802
IAD	19R	U2	150	536	80	4	2410

IAD	01L	U4	150	544	80	4	2615
IAD	01L	U3	30	1204	1800	20	4681
IAD	01L	U2	30	1201	1800	20	6083
IAD	01L	U1	90	385	150	1	8730
IAD	01L	U	90	419	250	1	9133
IAD	01C	W4	85	358	150	14	1860
IAD	01C	E	90	354	162	14	1841
IAD	01C	W3	90	358	150	14	2624
IAD	01C	D	90	373	185	1	2588
IAD	01C	W2	90	357	150	14	3968
IAD	01C	Y7	150	578	115	5	3755
IAD	01C	Y6	30	1086	1800	3	3322
IAD	01C	Y5	150	759	120	5	5468
IAD	01C	Y4	30	1116	1800	3	5042
IAD	01C	Y3	150	599	120	5	7234
IAD	01C	Y2	30	1149	1800	3	6762
IAD	01C	Y1	90	419	200	1	10779
IAD	01C	Z	90	415	200	1	11083
IAD	19C	Y11	49	600	200	8	11279
IAD	19C	Y9	90	335	90	14	11387
IAD	19C	Y8	90	401	200	1	10939
IAD	19C	W4	95	361	135	14	9385
IAD	19C	E	90	373	175	1	9353
IAD	19C	W3	90	360	150	14	8619
IAD	19C	D	90	366	170	1	8600
IAD	19C	W2	90	368	150	14	7272
IAD	19C	Y7	30	1110	1800	3	6803
IAD	19C	Y6	150	543	125	4	7255
IAD	19C	Y5	30	1179	1800	20	4979
IAD	19C	Y4	150	600	115	5	5486
IAD	19C	Y3	30	1121	1800	3	3288
IAD	19C	Y2	150	618	120	5	3719
ATL	26R	H	90	375	165	1	8791
ATL	26R	B1	120	386	200	7	8327
ATL	26R	B3	30	962	1800	3	6296
ATL	26R	A4	45	582	500	8	5576
ATL	26R	B5	30	955	1800	3	4734
ATL	26R	C-L	90	398	200	1	4024
ATL	26R	C-R	90	386	150	1	4091
ATL	26R	D-L	90	368	165	1	3778
ATL	26R	D-R	90	400	165	1	3778
ATL	26R	B7	150	465	85	4	3669
ATL	26R	A6	135	412	100	11	2322

ATL	26R	B11	150	474	85	4	2205
ATL	26R	A	90	380	150	1	8791
ATL	08L	B3	150	551	75	5	2032
ATL	08L	A4	135	443	80	11	2974
ATL	08L	B5	150	512	80	4	3566
ATL	08L	C-L	90	413	175	1	4584
ATL	08L	C-R	90	390	200	1	4583
ATL	08L	D-L	90	398	160	1	4910
ATL	08L	D-R	90	356	150	14	4928
ATL	08L	B7	30	937	1800	3	4612
ATL	08L	A6	45	618	550	8	6214
ATL	08L	B11	30	1047	1800	3	5976
ATL	08L	B13	115	378	200	7	8478
ATL	08L	B15	115	391	200	7	8772
ATL	08L	A	90	391	200	1	8772
ATL	08R	E3	150	464	100	4	1812
ATL	08R	B4	120	401	200	7	1955
ATL	08R	E5	63	387	175	15	2827
ATL	08R	B6	90	384	200	1	2742
ATL	08R	E7	150	474	102	4	3812
ATL	08R	C-L	90	397	175	1	4411
ATL	08R	C-R	90	340	150	14	4442
ATL	08R	D-L	90	412	200	1	4675
ATL	08R	D-R	90	362	150	14	4723
ATL	08R	E11	57	899	1800	12	6119
ATL	08R	B10-S	30	599	300	8	6437
ATL	08R	B10-B	115	451	300	7	6437
ATL	08R	E13	90	402	200	1	9027
ATL	08R	E	90	366	225	1	9773
ATL	08R	B	90	388	200	1	9773
ATL	26L	H-L	90	387	225	1	9749
ATL	26L	H-R	80	374	225	1	9777
ATL	26L	E1	30	402	250	18	9265
ATL	26L	B2	150	362	75	4	9223
ATL	26L	E3	30	606	250	8	7733
ATL	26L	B4	120	398	200	7	7684
ATL	26L	E5	117	388	100	7	6879
ATL	26L	B6	90	382	175	1	6903
ATL	26L	E7	30	751	900	9	5580
ATL	26L	C-L	90	355	150	14	5292
ATL	26L	C-R	90	383	175	1	5292
ATL	26L	D-L	90	458	150	1	4979
ATL	26L	D-R	90	406	200	1	4936

ATL	26L	E11	150	451	90	4	3179
ATL	26L	B10-B	150	441	85	4	3206
ATL	27R	L-L	90	401	200	1	11634
ATL	27R	L-R	90	404	200	1	11634
ATL	27R	M2	90	400	200	1	10740
ATL	27R	T-L	90	380	200	1	9867
ATL	27R	T-R	90	383	175	1	9867
ATL	27R	M6	110	385	150	16	8106
ATL	27R	N5	112	415	150	7	8106
ATL	27R	U-L	110	337	125	16	7253
ATL	27R	U-R	90	335	125	14	7253
ATL	27R	S-L	115	389	200	7	5769
ATL	27R	S-R	115	388	175	7	5769
ATL	27R	D-L	115	417	200	7	3883
ATL	27R	D-R	90	401	200	1	3836
ATL	27R	M14	150	512	85	4	4991
ATL	27R	K	120	376	165	7	3645
ATL	27R	J-L	120	373	135	7	3287
ATL	27R	J-R	60	399	185	15	3434
ATL	27R	M16	90	351	135	14	2539
ATL	27R	M12	30	747	900	9	6172
ATL	27R	N13	75	361	175	15	2569
ATL	27R	M18	90	386	165	1	1983
ATL	27R	M4	92	393	150	1	9331
ATL	09L	T-L	90	382	175	1	1669
ATL	09L	T-R	114	377	200	7	1669
ATL	09L	M6	94	374	175	1	3475
ATL	09L	N5	116	405	150	7	3475
ATL	09L	U-L	90	330	135	14	4426
ATL	09L	U-R	110	331	135	16	4426
ATL	09L	S-L	115	374	180	7	5770
ATL	09L	S-R	115	377	200	7	5775
ATL	09L	D-L	90	387	200	1	7607
ATL	09L	D-R	112	396	175	7	7607
ATL	09L	M14	30	1040	1800	3	6055
ATL	09L	K	60	401	250	15	7873
ATL	09L	J-L	120	382	170	7	8095
ATL	09L	J-R	60	391	200	15	8288
ATL	09L	M16	90	407	250	1	9024
ATL	09L	M12	150	490	80	4	5214
ATL	09L	N13	105	382	200	16	8985
ATL	09L	M18	115	386	200	7	9557
ATL	09L	M20	90	391	200	1	11252

ATL	09L	LB	90	394	150	1	11908
ATL	09L	LC	90	412	200	1	11629
ATL	09L	LA	90	393	175	1	12162
ATL	09L	M4	92	372	150	1	2201
ATL	27L	P	90	365	200	1	8785
ATL	27L	R	118	380	200	7	8780
ATL	27L	N2	30	954	1800	3	6376
ATL	27L	R3	98	359	215	16	6887
ATL	27L	N4	30	938	1800	3	4780
ATL	27L	SC-L	90	326	100	14	4738
ATL	27L	SC-R	90	325	100	14	4741
ATL	27L	N6	150	449	100	4	3935
ATL	27L	R7	98	369	200	16	3923
ATL	27L	N10	150	454	100	4	2080
ATL	27L	R11	90	365	215	1	2054
ATL	09R	R	118	385	200	7	8774
ATL	09R	N2	150	440	110	4	1811
ATL	09R	R3	100	358	235	16	1787
ATL	09R	N4	150	468	100	4	3423
ATL	09R	SC-L	90	338	125	14	4070
ATL	09R	SC-R	90	326	105	14	4092
ATL	09R	N6	30	954	1800	3	4254
ATL	09R	R7	98	367	200	16	4736
ATL	09R	N10	30	938	1800	3	6134
ATL	09R	R11	90	362	200	1	6618
ATL	09R	K	115	406	200	7	8219
ATL	09R	J	120	450	200	7	8611
ATL	09R	N12	74	348	150	15	8854
ATL	10	SG-L	90	393	200	1	8766
ATL	10	SG4	150	475	105	4	1821
ATL	10	SG6	150	499	105	4	3120
ATL	10	SG12	30	987	1800	3	4146
ATL	10	SG14	30	991	1800	3	6334
ATL	10	SG16	90	406	200	1	8402
ATL	28	SG2	102	441	200	16	8364
ATL	28	SG4	30	1089	1800	3	6235
ATL	28	SG6	30	983	1800	3	5042
ATL	28	SG12	150	494	100	4	3974
ATL	28	SG14	150	498	100	4	1790
ATL	28	SG-R	102	416	200	16	8740
LAS	07R	A7	150	659	80	5	2214
LAS	07R	A6	150	634	80	5	3580
LAS	07R	A5	150	646	84	5	4942

LAS	07R	A4	30	1238	1800	20	5522
LAS	07R	A3	30	1239	1800	20	6725
LAS	07R	A2	90	393	200	1	10285
LAS	25L	A8	90	388	200	1	10291
LAS	25L	A7	30	1236	1800	20	7421
LAS	25L	A6	30	1235	1800	20	6060
LAS	25L	A5	30	1243	1800	20	4683
LAS	25L	A4	150	653	75	5	4094
LAS	25L	A3	150	686	75	5	2892
LAS	07L	A6-L	115	368	115	7	3064
LAS	07L	A6-R	65	419	150	15	3177
LAS	07L	B6	90	418	250	1	3286
LAS	07L	A5-L	90	397	150	1	4677
LAS	07L	A5-R	90	397	150	1	4677
LAS	07L	A4-L	90	368	140	14	7259
LAS	07L	A4-R	90	368	150	14	7259
LAS	07L	A3-L	90	402	150	1	8426
LAS	07L	A3-R	90	401	170	1	8426
LAS	07L	A2-L	90	412	150	1	10736
LAS	07L	A2-R	90	407	150	1	10736
LAS	07L	B1	90	382	150	1	11825
LAS	07L	B	108	371	135	16	12200
LAS	25R	E	155	860	150	5	13103
LAS	25R	H	90	536	150	19	13103
LAS	25R	F	117	421	200	7	13103
LAS	25R	E-L	65	442	200	15	12405
LAS	25R	E-R	115	440	200	7	12225
LAS	25R	D-L	65	407	200	15	11176
LAS	25R	D-R	115	427	200	7	10980
LAS	25R	A8-L	90	441	170	1	10269
LAS	25R	A8-R	90	360	150	14	10343
LAS	25R	A7-L	135	417	150	11	8961
LAS	25R	A7-R	76	541	425	13	9152
LAS	25R	A6-L	115	401	160	7	7463
LAS	25R	A6-R	65	469	200	15	7560
LAS	25R	B6	90	386	150	1	7307
LAS	25R	A5-L	90	393	150	1	5945
LAS	25R	A5-R	90	401	150	1	5945
LAS	25R	A4-L	90	372	150	1	3416
LAS	25R	A4-R	90	386	150	1	3416
LAS	25R	A3-L	90	399	150	1	2128
LAS	25R	A3-R	94	407	150	1	2128
LAS	01L	W-L	90	339	200	14	1955

LAS	01L	W-R	90	350	200	14	1943
LAS	01L	T	150	466	72	4	2965
LAS	01L	U	150	435	83	4	2945
LAS	01L	S-R	90	425	200	1	4662
LAS	01L	S-L	90	425	200	1	4662
LAS	01L	N-R	90	415	200	1	6583
LAS	01L	N-L	90	415	200	1	6583
LAS	01L	M	43	923	700	17	6744
LAS	01L	J	90	356	150	14	8628
LAS	01L	E	90	353	250	1	8936
LAS	01L	F	94	358	150	14	8958
LAS	19R	E	90	385	150	1	8787
LAS	19R	H	156	857	150	5	8746
LAS	19R	B-L	115	426	200	7	7565
LAS	19R	B-R	65	450	250	15	7714
LAS	19R	Y	44	887	700	17	6463
LAS	19R	W-L	90	393	200	1	6063
LAS	19R	W-R	90	394	200	1	6063
LAS	19R	T	30	1162	1800	3	4562
LAS	19R	U	30	1178	1800	20	4553
LAS	19R	S-R	90	415	200	1	3249
LAS	19R	S-L	90	416	200	1	3249
LAS	01R	D	72	524	435	13	8811
LAS	01R	E	90	428	200	1	8995
LAS	01R	W-L	115	399	110	7	2264
LAS	01R	W-R	65	401	140	15	2395
LAS	01R	V	150	564	110	5	3341
LAS	01R	S-L	90	456	200	1	4760
LAS	01R	S-R	66	544	440	13	4580
LAS	01R	P	30	1373	1800	20	4947
LAS	01R	N-L	90	411	200	1	6720
LAS	01R	N-R	75	510	435	13	6526
LAS	01R	M-L	90	445	200	1	7679
LAS	01R	M-R	90	444	175	1	7679
LAS	01R	L	75	539	425	13	8411
LAS	19L	D	90	449	250	1	8574
LAS	19L	E	90	459	250	1	8574
LAS	19L	B-L	77	457	250	15	6976
LAS	19L	B-R	65	445	250	15	7215
LAS	19L	W-L	115	451	225	7	5563
LAS	19L	W-R	65	432	200	15	5793
LAS	19L	V	30	1388	1800	20	3876
LAS	19L	S-L	90	442	250	1	3126

LAS	19L	S-R	90	445	200	1	3144
LAS	19L	P	150	594	83	5	2396
LAS	19L	A	115	475	150	7	8285
DEN	16L	F9	150	629	85	5	3203
DEN	16L	F8	150	609	88	5	4291
DEN	16L	WD	90	372	75	14	4436
DEN	16L	F6	30	1359	1800	20	6150
DEN	16L	WC-L	90	403	175	1	7891
DEN	16L	WC-R	90	364	90	14	7960
DEN	16L	F4	30	1356	1800	20	7648
DEN	16L	F3	90	409	150	1	10346
DEN	16L	F2	90	415	170	1	11367
DEN	16L	F1	90	439	160	1	11759
DEN	34R	F3	90	439	170	1	1333
DEN	34R	F12	90	409	150	1	11812
DEN	34R	WE-L	90	660	70	19	11401
DEN	34R	WE-R	90	406	150	1	11341
DEN	34R	F10	90	427	150	1	10347
DEN	34R	F9	30	1364	1800	20	7716
DEN	34R	F8	30	1369	1800	20	6624
DEN	34R	WD	90	382	85	14	7396
DEN	34R	F6	150	585	95	5	4781
DEN	34R	WC-L	90	374	90	14	3877
DEN	34R	WC-R	90	398	150	1	3826
DEN	34R	F4	150	617	78	5	3286
DEN	8	R1	90	414	150	1	11810
DEN	8	R2	90	414	150	1	11485
DEN	8	R3	90	431	150	1	10333
DEN	8	R4	30	1329	1800	20	7755
DEN	8	R6	150	608	78	5	4722
DEN	8	R7	150	657	78	5	3209
DEN	8	R8	90	416	150	1	1353
DEN	26	R3	90	449	170	1	1314
DEN	26	R4	150	629	77	5	3206
DEN	26	R6	30	1331	1800	20	6250
DEN	26	R7	30	1351	1800	20	7729
DEN	26	R8	90	409	150	1	10351
DEN	26	R9	90	407	150	1	11481
DEN	26	M	90	449	150	1	11808
DEN	35L	M4	150	653	80	5	3206
DEN	35L	M5	150	654	80	5	4709
DEN	35L	M6	30	1375	1800	20	6205
DEN	35L	M7	30	1364	1800	20	7604

DEN	35L	EC-L	90	403	150	1	10221
DEN	35L	EC-R	90	510	100	19	10290
DEN	35L	M9	90	407	150	1	11450
DEN	35L	M10	90	432	150	1	11749
DEN	17R	A	90	420	150	1	11800
DEN	17R	M2	90	413	150	1	11484
DEN	17R	EA-L	90	369	90	14	10486
DEN	17R	EA-R	90	434	150	1	10388
DEN	17R	M4	30	1366	1800	20	7721
DEN	17R	M5	30	1389	1800	20	6191
DEN	17R	M6	150	617	77	5	4711
DEN	17R	M7	150	588	80	5	3324
DEN	16R	WD	90	417	184	1	3871
DEN	16R	D9	150	851	90	5	4638
DEN	16R	D8	30	1635	1800	20	5775
DEN	16R	WC	90	428	185	20	8400
DEN	16R	D6(1)	150	802	100	5	8208
DEN	16R	D6(2)	150	653	100	5	8208
DEN	16R	D5	30	1633	1800	20	9341
DEN	16R	WB	90	418	185	1	12734
DEN	16R	D3	90	417	185	1	14334
DEN	16R	D2	90	423	185	1	15453
DEN	16R	WA	90	438	200	1	15750
DEN	34L	WE	90	437	200	1	15751
DEN	34L	D12	90	425	185	1	15452
DEN	34L	D11	90	421	185	1	14330
DEN	34L	WD	90	423	185	1	11790
DEN	34L	D9(1)	30	1621	1800	20	10230
DEN	34L	D9(2)	30	1473	1800	20	10230
DEN	34L	D8(1)	150	827	110	5	9079
DEN	34L	D8(2)	150	678	110	5	9079
DEN	34L	WC	90	418	185	1	8272
DEN	34L	D6(1)	30	1625	1800	20	6658
DEN	34L	D6(2)	30	1475	1800	20	6658
DEN	34L	D5	150	801	105	5	5524
DEN	34L	WB	90	432	185	1	2919
DEN	35R	P4	150	578	95	5	3207
DEN	35R	P6	30	1356	1800	20	6223
DEN	35R	P7	30	1360	1800	20	7607
DEN	35R	P8	90	409	150	1	10349
DEN	35R	P9	90	411	150	1	11485
DEN	35R	ED	90	422	150	1	11802
DEN	17L	EA	90	418	150	1	11803

DEN	17L	P2	90	415	150	1	11481
DEN	17L	P3	90	420	150	1	10340
DEN	17L	P4	30	1344	1800	20	7738
DEN	17L	P6	150	575	87	5	4712
DEN	17L	P7	150	589	85	5	3321
DEN	7	B7	150	574	90	5	3198
DEN	7	B4	30	1334	1800	20	7117
DEN	7	B3	90	417	150	1	10344
DEN	7	F	90	411	150	1	11460
DEN	7	G	90	419	150	1	11776
DEN	25	B10	90	416	150	1	11808
DEN	25	B9	90	413	150	1	11486
DEN	25	B8	90	417	150	1	10347
DEN	25	B7	30	1315	1800	20	7767
DEN	25	B4	150	572	88	5	3832
LGA	4	Y	53	387	250	18	985
LGA	4	CY-L	130	348	80	11	1397
LGA	4	CY-R	50	357	200	18	1527
LGA	4	D-L	115	359	200	7	2436
LGA	4	D-R	65	369	200	15	2599
LGA	4	F-L	136	332	110	11	2999
LGA	4	F-R	25	637	200	8	2999
LGA	4	E-L	90	322	175	14	3103
LGA	4	E-R	90	339	150	14	3103
LGA	4	Q	30	678	1800	12	3506
LGA	4	G-L	60	451	450	13	3878
LGA	4	G-R	90	297	100	14	4212
LGA	4	P-L	90	276	100	14	4454
LGA	4	P-R	90	299	95	14	4454
LGA	4	U	90	291	95	14	5665
LGA	4	R	134	359	125	11	6812
LGA	22	P-L	90	313	115	14	2374
LGA	22	P-R	90	292	115	14	2374
LGA	22	G-L	90	321	120	14	2602
LGA	22	G-R	90	302	105	14	2602
LGA	22	E-L	90	294	95	14	3643
LGA	22	E-R	90	302	70	14	3643
LGA	22	F-R	45	409	150	18	3661
LGA	22	D-L	115	387	200	7	3919
LGA	22	D-R	65	454	575	13	4023
LGA	22	C	30	620	750	9	4641
LGA	22	CY-L	130	347	75	11	5218
LGA	22	CY-R	50	470	400	13	5218

LGA	22	Y-R	128	372	60	11	5725
LGA	22	Y-L	90	332	200	14	6099
LGA	22	YY	97	393	225	1	6157
LGA	22	B	149	384	96	4	6777
LGA	22	AA	149	367	105	4	6837
LGA	31	J	30	685	770	9	3043
LGA	31	T	30	919	1800	3	3757
LGA	31	S	54	400	300	18	4811
LGA	31	R-L	90	370	250	1	5194
LGA	31	AA	66	372	250	15	5820
LGA	31	P	135	334	125	11	6828
LGA	13	R-R	90	298	100	14	1481
LGA	13	L	30	663	1000	9	3627
LGA	13	M	30	855	1800	3	4439
LGA	13	V	30	834	1800	3	5623
LGA	13	W	103	294	150	16	6567
LGA	13	Z	103	338	200	16	6761
MDW	31C	Y-L	90	324	150	14	1824
MDW	31C	Y-R	90	324	150	14	1824
MDW	31C	A	68	565	300	13	3738
MDW	31C	B	30	775	1800	12	4260
MDW	31C	N	135	352	100	11	5353
MDW	31C	W	135	422	150	11	5547
MDW	31C	M	109	388	150	16	5630
MDW	13C	Y-L	90	333	150	14	3249
MDW	13C	Y-R	90	333	150	14	3249
MDW	13C	K-R	135	391	130	11	4244
MDW	13C	P-L	135	397	130	11	4244
MDW	13C	K-L	45	628	450	8	4314
MDW	13C	P-R	45	574	450	8	4359
MDW	13C	E1	135	364	150	11	5551
MDW	13C	E3	108	428	225	16	5803
MDW	13C	F	135	389	150	11	5819
MDW	04L	J	135	414	110	11	885
MDW	04L	F-L	90	297	80	14	1184
MDW	04L	F-R	90	292	80	14	1184
MDW	04L	N-R	45	451	200	18	4190
MDW	04L	N-L	135	390	150	11	3909
MDW	04L	P	90	367	75	14	3091
MDW	04L	Q	90	317	105	14	4606
MDW	22R	Z	90	393	150	1	4450
MDW	22R	V	90	333	150	14	4032
MDW	22R	J	45	441	110	18	2672

MDW	22R	F-L	90	297	65	14	2534
MDW	22R	F-R	90	297	65	14	2534
MDW	13R	Y-L	90	170	80	6	2451
MDW	13R	Y-R	90	168	80	6	2451
MDW	13R	K-L	45	242	125	18	3169
MDW	13R	K-R	135	189	75	11	3035
MDW	13R	F4	90	158	75	6	3766
MDW	31L	F1	90	148	60	6	3789
MDW	31L	A-L	90	158	75	6	3540
MDW	31L	A-R	90	156	75	6	3540
MDW	31L	Y-L	90	167	75	6	1248
MDW	31L	Y-R	90	169	75	6	1248
MDW	13L	Y-R	90	305	135	14	2556
MDW	13L	Y-L	90	260	150	6	2566
MDW	13L	P-R	45	464	200	18	3000
MDW	13L	P-L	135	274	90	11	2870
MDW	13L	T	135	315	105	11	4121
MDW	31R	M	45	598	200	8	4986
MDW	31R	N-R	135	431	65	11	4390
MDW	31R	N-L	45	420	150	18	4510
MDW	31R	Y-R	90	279	115	14	1595
MDW	31R	Y-L	90	302	150	14	1595
MDW	31R	P-R	45	335	200	18	1275
MDW	31R	P-L	135	410	103	11	1076
MDW	22L	G	90	361	110	14	2298
MDW	22L	F-L	90	303	110	14	3457
MDW	22L	F-R	90	307	110	14	3457
MDW	22L	K-L	135	400	150	11	4048
MDW	22L	Y2	30	589	200	8	4050
MDW	22L	V-L	90	298	105	14	5046
MDW	22L	V-R	90	288	108	14	5046
MDW	22L	Z	90	373	125	14	5623
MDW	22L	Y	135	418	120	11	5551
MDW	04R	Y	151	382	85	4	5801
MDW	04R	R	90	298	87	14	5801
MDW	04R	N-L	134	377	88	11	5458
MDW	04R	N-R	90	300	90	14	5458
MDW	04R	Q-L	90	287	105	14	5095
MDW	04R	Q-R	90	308	105	14	5095
MDW	04R	S	60	390	200	15	4646
MDW	04R	P-L	45	498	250	18	3890
MDW	04R	P-R	135	353	105	11	3753
MDW	04R	G	90	335	110	14	2692

MDW	04R	F-L	90	306	105	14	1625
MDW	04R	F-R	90	303	105	14	1625
STL	11	A3	30	1356	1800	20	5049
STL	11	A2	30	1249	1800	20	6456
STL	11	U	60	386	150	15	8483
STL	11	T	60	383	150	15	8801
STL	11	A4	150	479	95	4	2800
STL	29	A3	150	492	95	4	2800
STL	29	A4	30	1335	1800	20	5065
STL	29	A5	30	1251	1800	20	6447
STL	29	A6	90	366	150	14	8362
STL	29	B	90	344	150	14	8833
STL	12R	S-L	60	400	150	15	2334
STL	12R	S-R	120	375	150	7	2126
STL	12R	R-L	129	419	125	11	3215
STL	12R	R-R	51	408	175	18	3391
STL	12R	Q	72	416	250	15	4337
STL	12R	P-L	90	398	175	1	4697
STL	12R	P-R	59	425	250	15	4818
STL	12R	N-L	75	380	175	15	5846
STL	12R	N-R	105	425	135	16	5700
STL	12R	M	102	347	150	16	6721
STL	12R	L-L	88	396	150	1	6798
STL	12R	L-R	57	406	200	18	7120
STL	12R	J-L	90	356	150	14	9365
STL	12R	J-R	90	353	150	14	9365
STL	12R	H-L	90	361	150	14	10356
STL	12R	H-R	90	361	150	14	10356
STL	12R	K-L	123	408	150	7	7656
STL	12R	K-R	57	378	150	15	7869
STL	30L	C	90	364	150	14	10620
STL	30L	V-L	90	419	200	1	9990
STL	30L	V-R	136	420	130	11	9990
STL	30L	S-L	60	408	250	15	7830
STL	30L	S-R	120	419	150	7	7666
STL	30L	R-L	90	382	200	1	6473
STL	30L	R-R	51	422	150	18	6850
STL	30L	Q	72	440	250	15	5438
STL	30L	P-L	66	426	250	15	4944
STL	30L	P-R	90	401	200	1	5284
STL	30L	N-L	75	373	175	15	4256
STL	30L	N-R	105	385	150	16	4170
STL	30L	M	78	362	150	15	3318

STL	30L	L-L	123	406	200	7	2750
STL	30L	L-R	57	428	130	18	3096
STL	30L	K-L	123	377	150	7	2120
STL	30L	K-R	57	393	150	15	2365
STL	12L	P-L	90	355	150	14	1693
STL	12L	P-R	90	353	150	14	1693
STL	12L	E2	150	577	70	5	2711
STL	12L	L-L	124	381	85	7	3185
STL	12L	L-R	56	416	175	18	3256
STL	12L	K-L	90	338	150	14	4331
STL	12L	K-R	90	337	150	14	4331
STL	12L	E1	30	1253	1800	20	4787
STL	12L	J-L	90	396	150	1	6288
STL	12L	J-R	90	387	150	1	6298
STL	12L	H	90	364	150	14	7312
STL	12L	E	90	388	250	1	8752
STL	30R	S-L	60	444	250	15	8761
STL	30R	S-R	120	425	150	7	8604
STL	30R	P-L	90	349	150	14	7043
STL	30R	P-R	90	349	150	14	7043
STL	30R	E2	30	1181	1800	20	5454
STL	30R	L-L	124	422	125	7	5421
STL	30R	L-R	56	400	150	18	5630
STL	30R	K-L	90	343	150	14	4434
STL	30R	K-R	90	342	150	14	4434
STL	30R	E1	150	614	65	5	3291
STL	30R	J-L	90	360	150	14	2400
STL	30R	J-R	90	364	150	14	2400
STL	6	C-L	120	352	150	7	1819
STL	6	C-R	60	348	150	15	2030
STL	6	D-L	120	360	140	7	2229
STL	6	D-R	60	359	200	15	2365
STL	6	F-L	90	335	150	14	5022
STL	6	F-R	60	345	200	15	4987
STL	6	V	90	380	200	1	7367
STL	6	P	100	395	225	16	7209
STL	24	A	60	330	150	15	7390
STL	24	S	90	376	140	1	7364
STL	24	B-L	130	349	150	11	6711
STL	24	B-R	50	387	200	18	6962
STL	24	S1	90	359	160	14	5768
STL	24	C-L	120	345	150	7	5230
STL	24	C-R	60	349	200	15	5428

STL	24	D-L	120	329	150	7	4899
STL	24	D-R	60	425	250	15	5024
STL	24	F-L	120	338	150	7	2278
STL	24	F-R	90	316	150	14	2304
IAH	08L	FG	30	1041	1800	3	5274
IAH	08L	FH	30	1038	1800	3	6780
IAH	08L	FJ	90	425	200	1	8396
IAH	08L	FK	90	405	200	1	8761
IAH	26R	FE	30	1041	1800	3	5278
IAH	26R	FD	30	1025	1800	3	6792
IAH	26R	FC	90	427	200	1	8396
IAH	26R	NE	90	397	200	1	8768
IAH	9	SH	30	1035	1800	3	5479
IAH	9	SJ	30	959	1800	3	7557
IAH	9	SK	90	407	175	1	9776
IAH	27	SG	30	1036	1800	3	5482
IAH	27	SF	30	1043	1800	3	7491
IAH	27	SC	90	398	150	1	9780
IAH	08R	NG	30	991	1800	3	2202
IAH	08R	NK-L	90	382	175	1	4534
IAH	08R	NN	30	1004	1800	3	6346
IAH	08R	NP-L	90	386	200	1	9187
IAH	08R	NP-R	90	387	200	1	9187
IAH	08R	NK-R	30	1005	1800	3	4266
IAH	26L	NE-L	90	393	200	1	9177
IAH	26L	NE-R	90	396	200	1	9177
IAH	26L	NR-L	90	365	150	14	8571
IAH	26L	NR-R	90	365	150	14	8571
IAH	26L	NF	30	998	1800	3	6352
IAH	26L	NH	30	1050	1800	3	4222
IAH	26L	NL	30	991	1800	3	2201
IAH	26L	NK-R	90	391	200	1	4519
IAH	15L	WD-R	90	393	200	1	1792
IAH	15L	WH	30	1108	1800	3	3421
IAH	15L	WJ-R	30	577	600	8	5933
IAH	15L	WK	30	1101	1800	3	5428
IAH	15L	WL-L	90	343	200	14	8412
IAH	15L	WL-R	90	347	200	14	8412
IAH	15L	WM	30	1096	1800	3	8534
IAH	15L	WZ	90	387	200	1	11440
IAH	15L	WN	90	367	200	1	11785
IAH	33R	WW-R	90	366	200	1	11783
IAH	33R	WW-L	90	370	200	1	11783

IAH	33R	WD-R	30	1063	1800	3	9468
IAH	33R	WG	30	1096	1800	3	7437
IAH	33R	WJ-R	30	1066	1800	3	5429
IAH	33R	WL-L	90	344	200	14	3275
IAH	33R	WL-R	90	342	200	14	3275
IAH	33R	WD-L	90	374	200	1	9815
IAH	33R	WV	90	373	200	1	11508
IAH	15R	WC	90	362	150	14	9808
IAH	15R	WP	90	348	200	14	9808
IAH	15R	WL-L	90	387	200	1	8867
IAH	15R	WL-R	90	360	150	14	8915
IAH	15R	WT	30	987	1800	3	7048
IAH	15R	WU	90	352	150	14	6353
IAH	15R	WS	30	981	1800	3	5048
IAH	15R	WR-R	90	350	150	14	4392
IAH	15R	WQ-R	90	363	150	14	2342
IAH	33L	WC-R	90	369	200	1	9777
IAH	33L	WU	90	360	150	14	3343
IAH	33L	WR-L	90	362	150	14	5305
IAH	33L	WR-R	30	960	1800	3	5070
IAH	33L	WQ-L	90	356	150	14	7347
IAH	33L	WQ-R	30	986	1800	3	7045
IAH	33L	WW-L	90	391	200	1	9220
IAH	33L	WW-R	90	390	200	1	9220
IAH	33L	WC-L	90	368	200	1	9777
DCA	1	J-L	160	407	95	4	7011
DCA	1	S	60	438	300	13	6125
DCA	1	N1	90	546	280	19	4545
DCA	1	N	45	588	290	8	4545
DCA	1	M-L	90	402	250	1	3781
DCA	1	M-R	69	352	200	15	4057
DCA	1	G1	135	334	110	11	3575
DCA	1	G	90	305	110	14	3575
DCA	1	H	135	343	110	11	3454
DCA	1	F-L	90	371	215	1	2419
DCA	1	F-R	70	773	200	10	2419
DCA	1	E-4	30	752	400	8	2030
DCA	1	E-33	30	707	400	8	4901
DCA	15	E-1	150	544	60	4	2013
DCA	15	E-19	30	791	400	8	2013
DCA	15	E-22	62	495	200	13	3815
DCA	19	J-R	128	345	105	11	6905
DCA	19	N1	90	306	125	14	2094

DCA	19	N	135	337	110	11	2094
DCA	19	M-L	111	310	100	16	2865
DCA	19	M-R	90	387	250	1	2865
DCA	19	G1	45	469	350	18	3189
DCA	19	G	90	428	270	1	3189
DCA	19	H	45	412	250	18	3375
DCA	19	F-L	110	691	120	19	4412
DCA	19	F-R	90	396	250	1	4236
DCA	19	A	90	386	250	1	6044
DCA	19	E	119	315	105	7	6671
DCA	19	E1-22	30	599	300	8	4624
DCA	19	E-22	30	697	270	8	4624
DCA	15	M-L	78	431	250	1	3162
DCA	15	M-R	102	348	250	16	3162
DCA	15	J-L	148	428	65	4	1398
DCA	15	J-R	32	494	250	18	1603
DCA	15	L	106	345	150	16	1600
DCA	15	K-R1	109	440	200	16	1136
DCA	15	K-R2	32	558	200	8	1136
DCA	15	F	136	357	165	11	5054
DCA	33	M-L	78	314	150	14	1676
DCA	33	M-R	102	285	110	16	1676
DCA	33	J-L	148	349	135	11	3092
DCA	33	J-R	32	579	600	8	3412
DCA	33	L	88	406	300	1	3151
DCA	33	K-L	102	304	110	16	3673
DCA	33	K-R	98	396	250	1	3878
DCA	33	S-L1	105	375	200	16	4198
DCA	33	S-L2	60	393	250	15	4198
DCA	33	N	100	356	150	16	4993
DCA	33	E-1	33	732	400	8	2504
DCA	33	E-19	147	393	60	4	2404
DCA	4	D	106	298	130	16	2055
DCA	4	F-L	115	564	280	19	2461
DCA	4	F-R	40	443	330	18	2910
DCA	4	H-L	75	347	150	15	3434
DCA	4	H-R	115	307	100	7	3434
DCA	4	M	70	377	175	15	4639
DCA	4	E-1	30	806	400	8	2227
DCA	4	E-33	62	495	200	13	4020
DCA	4	J-L-4	30	542	225	8	1628
DCA	22	B	90	435	110	1	4848
DCA	22	A-L	118	324	115	7	3705

DCA	22	A-R	62	365	200	15	3784
DCA	22	C	145	391	132	11	3475
DCA	22	J-L	30	580	400	8	2992
DCA	22	J-R	150	403	75	4	2801
DCA	22	D	90	375	250	1	2410
DCA	22	F-L	141	405	105	11	1501
DCA	22	F-R	60	544	250	13	1752
DCA	22	H-L	75	349	150	15	1100
DCA	22	E-19	30	834	400	8	1996
DCA	22	H-R	115	294	125	7	1100
SEA	34R	N-L	30	420	85	18	4444
SEA	34C	K	30	1306	1800	20	3453
SEA	34C	H	30	1149	1800	3	4800
SEA	34C	F	30	1294	1800	20	6293
SEA	16C	P-L	30	1246	1800	20	7306
SEA	16C	N-L	30	1475	1800	20	5325
SEA	16C	M	30	1366	1800	20	4669
SEA	34L	J	30	1257	1800	20	3726
SEA	34L	E	30	1295	1800	20	5538
SEA	34L	Z	30	1188	1800	20	6697
SEA	16R	Q	30	1192	1800	20	6693
SEA	16R	P	30	1271	1800	20	5564
SEA	16R	N	30	1250	1800	20	4533
SEA	16L	H-R	39	403	125	18	2842
SEA	34R	P-L	40	377	130	18	2780
SEA	16L	K-R	42	364	90	18	4115
SEA	34R	M-L	42	355	80	18	5323
SEA	16L	K-L	45	466	200	18	3906
SEA	16L	H-L	50	370	90	18	2842
SEA	16L	Q-L	90	378	200	1	9198
SEA	16L	P-L	77	388	200	15	8842
SEA	16C	J-R	90	302	120	14	3133
SEA	16L	B	90	389	200	1	11487
SEA	16L	S	90	380	200	1	9879
SEA	16L	Q-R	90	307	90	14	9326
SEA	16L	N-L	90	393	200	1	7206
SEA	16L	L	90	385	200	1	4794
SEA	34R	Q-L	90	338	105	14	2408
SEA	34R	Q-R	90	331	115	14	2408
SEA	34R	P-R	90	374	200	1	2673
SEA	34R	N-R	90	387	200	1	4292
SEA	34R	L	90	390	200	1	6708
SEA	34R	E-L	90	338	120	14	10445

SEA	34R	E-R	90	388	200	1	10352
SEA	34R	D-L	90	317	85	14	11512
SEA	34R	C-L	90	347	175	14	11712
SEA	34C	N-L	90	324	135	14	2979
SEA	34C	J-L	90	313	100	14	6144
SEA	34C	J-R	90	529	200	19	6046
SEA	34C	E-L	90	330	75	14	8019
SEA	34C	E-R	90	328	75	14	7992
SEA	34C	D	90	388	200	1	8905
SEA	34C	C-L	90	366	200	1	9196
SEA	34C	C-R	90	362	200	1	9196
SEA	16C	Q-L	90	378	200	1	9198
SEA	16C	Q-R	90	379	200	1	9198
SEA	16C	N-R	90	309	100	14	6266
SEA	16C	J-L	90	383	200	1	2997
SEA	34L	C	90	418	200	1	8221
SEA	16R	R	90	381	200	1	8257
SEA	34R	C-R	107	474	200	16	11585
SEA	34R	D-R	110	387	200	16	11365
SEA	16C	P-R	110	333	85	16	7925
SEA	16L	M-L	90	388	200	1	6325
SEA	34R	M-R	90	379	200	1	5183
SEA	34R	K-R	135	385	150	11	7536
SEA	16L	M-R	138	360	75	11	6439
SEA	34R	K-L	138	354	75	11	7634
SEA	34R	F	138	370	77	11	10445
SEA	16L	P-R	140	354	75	11	8957
SEA	34R	H-L	141	371	67	11	8895
SEA	16L	N-R	150	400	60	4	7319
SEA	34R	H-R	150	383	85	4	8895
SEA	34C	N-R	150	449	100	4	2783
SEA	34C	M	150	439	100	4	3558
SEA	16C	K	150	452	100	4	4821
SEA	16C	H	150	493	85	4	3716
SEA	16C	F	150	457	105	4	1993
SEA	34L	N	150	441	115	4	2866
SEA	16R	J	150	460	115	4	3654
CLT	36L	W7	30	1054	1800	3	5591
CLT	36L	W8	30	992	1800	3	6852
CLT	18R	W3	30	922	1800	3	6925
CLT	18R	W4	30	1005	1800	3	5538
CLT	36C	E6	30	1051	1800	3	4651
CLT	36C	E8	30	1023	1800	3	6382

CLT	18C	E4	30	1038	1800	3	6864
CLT	18C	E5	30	1033	1800	3	4666
CLT	18C	E7	30	1059	1800	3	2742
CLT	23	M2	30	963	1800	3	4369
CLT	36R	C7	30	985	1800	3	2802
CLT	18L	C4	30	907	1800	3	6409
CLT	18L	C6-S	30	992	1800	3	4857
CLT	36R	D6	40	653	980	9	4644
CLT	18L	C6-B	90	826	150	10	4857
CLT	18L	R-L	40	644	900	9	3453
CLT	36R	R-L	42	464	350	18	4838
CLT	36R	D4	43	632	900	9	2978
CLT	36R	A-R	45	436	250	18	5999
CLT	18L	D5	45	445	250	18	4475
CLT	18L	A-R	45	438	250	18	2442
CLT	36R	M-R	51	420	200	18	7105
CLT	5	C-L	52	430	200	18	5088
CLT	5	D-L	52	449	200	18	6334
CLT	23	E-L	52	338	150	18	7302
CLT	23	F-L	52	371	150	18	6963
CLT	23	C-L	52	507	320	13	2183
CLT	5	B	75	357	280	15	2332
CLT	23	B	75	645	200	19	4369
CLT	5	R-R	83	377	150	1	4329
CLT	23	A4	85	328	200	14	4770
CLT	36L	W	90	377	150	1	8798
CLT	36L	W9	90	372	150	1	8536
CLT	18R	W	90	383	170	1	8790
CLT	18R	W2	90	374	170	1	8533
CLT	36C	E	90	391	225	1	9774
CLT	36C	E3	90	452	250	1	1230
CLT	36C	S-L	90	379	150	1	4039
CLT	36C	S-R	90	376	150	1	4039
CLT	36C	V4-L	90	374	150	1	4839
CLT	36C	V4-R	90	374	150	1	4839
CLT	36C	V5-L	90	375	150	1	6606
CLT	36C	V5-R	90	373	150	1	6606
CLT	36C	N-L	90	381	150	1	7518
CLT	36C	N-R	90	381	150	1	7518
CLT	36C	E9	90	452	270	1	8235
CLT	36C	E10	90	428	225	1	9434
CLT	18C	E	90	395	200	1	9764
CLT	18C	E2	90	424	200	1	9435

CLT	18C	E3	90	444	250	1	8239
CLT	18C	S-L	90	379	150	1	5630
CLT	18C	S-R	90	383	150	1	5630
CLT	18C	V4-L	90	376	150	1	4833
CLT	18C	V4-R	90	376	150	1	4833
CLT	18C	V5-L	90	365	150	14	3081
CLT	18C	V5-R	90	365	150	14	3081
CLT	18C	N-L	90	385	150	1	2140
CLT	18C	N-R	90	385	150	1	2140
CLT	18C	E9	90	455	250	1	1232
CLT	5	G-L	90	365	200	1	3992
CLT	5	G-R	90	388	200	1	4001
CLT	5	R-L	90	336	150	14	4312
CLT	5	A8	90	392	172	1	6874
CLT	23	G-L	90	402	200	1	3083
CLT	23	G-R	90	359	200	1	3097
CLT	23	R-R	90	343	175	14	2874
CLT	36R	C5	90	319	150	14	2364
CLT	36R	D3	90	371	150	1	2364
CLT	36R	C6-S	90	321	150	14	2957
CLT	36R	C8	90	350	150	14	3930
CLT	36R	C9	90	335	150	14	5239
CLT	36R	D7	90	290	110	14	5310
CLT	36R	D8	90	356	150	14	8289
CLT	36R	D	90	375	150	1	8647
CLT	18L	D	90	394	165	1	8455
CLT	18L	C2	90	330	150	14	8105
CLT	18L	D2	90	378	150	1	8077
CLT	18L	C3	90	340	150	14	7484
CLT	18L	C5	90	337	150	14	6021
CLT	18L	D3	90	386	150	1	6021
CLT	18L	C8	90	339	150	14	4425
CLT	18L	C9	90	338	150	14	3126
CLT	18L	D7	90	314	125	14	3166
CLT	18L	C	90	359	150	14	8455
CLT	5	M	93	325	200	14	7301
CLT	5	A4	95	331	150	14	2413
CLT	23	R-L	97	375	150	1	2874
CLT	5	A	100	358	200	16	7301
CLT	23	F-R	120	356	162	7	6686
CLT	5	C-R	128	442	150	11	4855
CLT	23	E-R	128	535	250	11	6869
CLT	23	C-R	128	389	150	11	1990

CLT	36R	M-L	129	391	160	11	6864
CLT	36R	D5	135	345	80	11	3906
CLT	36R	A-L	135	361	150	11	5770
CLT	18L	A-L	135	335	85	11	2333
CLT	18L	R-R	138	409	90	11	3425
CLT	36R	R-R	140	366	82	11	4712
CLT	18L	D6	140	378	80	11	3498
CLT	5	D-R	145	435	100	4	6107
CLT	18L	D4	147	355	80	11	5199
CLT	36L	W3	150	506	85	4	1401
CLT	36L	W4	150	502	90	4	2720
CLT	18R	W7	150	513	90	4	2599
CLT	18R	W8	150	502	90	4	1401
CLT	36C	E4	150	541	85	4	2383
CLT	36C	E5	150	536	85	4	4590
CLT	36C	E7	150	587	100	5	6501
CLT	18C	E6	150	555	85	5	4581
CLT	18C	E8	150	560	85	5	2886
CLT	5	M2	150	431	86	4	2349
CLT	36R	C6-B	150	417	95	4	2957
CLT	18L	C7	150	456	80	4	5066
MSP	30R	P8	45	494	325	18	4680
MSP	12L	P3	45	612	750	9	5969
MSP	12L	P4	45	638	750	9	5149
MSP	12R	A3	45	505	350	18	7753
MSP	4	H-L	45	511	350	18	5167
MSP	22	H-L	45	475	271	18	3015
MSP	35	Y	45	788	700	9	5008
MSP	35	K8	45	805	700	9	6403
MSP	22	K-L	55	561	235	13	9203
MSP	30R	G-R	59	400	200	15	4096
MSP	4	Q-R	67	396	200	15	6542
MSP	22	S-R	67	396	250	15	8356
MSP	30L	D-L	75	406	225	15	5689
MSP	12L	C-L	76	388	175	15	2492
MSP	30L	C-L	76	366	150	15	6071
MSP	4	P-R	76	409	235	15	6895
MSP	22	T-R	76	398	200	15	6170
MSP	30R	C-L	77	382	180	15	5229
MSP	30R	M	77	410	200	15	6171
MSP	4	W-R	77	400	250	15	3423
MSP	4	A-R	77	383	200	15	4273
MSP	22	W-R	77	359	150	15	4753

MSP	22	A-R	77	381	200	15	3888
MSP	22	B-R	77	366	150	15	3349
MSP	22	B-L	78	340	135	14	3377
MSP	12R	D-L	80	358	150	14	4008
MSP	30L	M-L	85	400	250	1	6940
MSP	12L	P1	90	410	220	1	7937
MSP	12L	P2	90	395	220	1	7518
MSP	12L	G-R	90	381	190	1	3720
MSP	30R	G-L	90	385	180	1	3920
MSP	30R	P10	90	381	200	1	7759
MSP	12R	W1	90	371	250	1	9760
MSP	12R	A1	90	371	250	1	9760
MSP	12R	W2	90	404	250	1	9324
MSP	12R	A2	90	405	250	1	9324
MSP	12R	A3	90	480	350	1	7753
MSP	12R	A4-S	45	534	350	8	6449
MSP	12R	A4-B	90	509	350	19	6449
MSP	12R	W5	90	424	235	1	5903
MSP	12R	A5	90	426	235	1	5903
MSP	12R	W7	90	413	230	1	5015
MSP	12R	A7	90	414	230	1	5015
MSP	12R	C-L	90	356	150	14	3705
MSP	12R	M-L	90	378	200	1	2679
MSP	12R	W8	90	346	150	14	1773
MSP	12R	A8	90	367	150	14	1750
MSP	30L	W5	90	379	190	1	3673
MSP	30L	A5	90	352	150	14	3716
MSP	30L	W7	90	416	225	1	4512
MSP	30L	A7	90	408	200	1	4532
MSP	30L	D-R	90	427	250	1	5590
MSP	30L	C-R	90	342	150	14	6024
MSP	30L	M-R	90	395	250	1	6925
MSP	30L	W8	90	401	250	1	7878
MSP	30L	A8	90	403	250	1	7878
MSP	30L	W9	90	421	250	1	9308
MSP	30L	A9	90	423	250	1	9308
MSP	30L	W10	90	372	250	1	9758
MSP	30L	A10	90	374	250	1	9758
MSP	4	T-R	90	337	125	14	1995
MSP	4	M6	90	416	200	1	5835
MSP	4	C6	90	414	200	1	5835
MSP	4	Q-L	90	402	200	1	6442
MSP	4	C9-R	90	399	200	1	8615

MSP	22	S-L	90	367	200	1	8249
MSP	22	M2	90	391	200	1	6991
MSP	22	T-L	90	400	200	1	6131
MSP	22	M6	90	370	150	1	2240
MSP	17	K2	90	379	165	1	7383
MSP	17	K3	90	360	150	14	6355
MSP	17	N-L	90	358	150	14	4211
MSP	17	N-R	90	369	150	1	4196
MSP	17	L6	90	375	150	1	3241
MSP	17	L7	90	381	150	1	2277
MSP	35	L7	90	410	200	1	5329
MSP	35	L9	90	414	200	1	7343
MSP	22	C2	91	414	250	1	6968
MSP	30L	W3	92	341	150	14	1823
MSP	22	C6	92	369	150	1	2240
MSP	17	L3	99	353	150	16	6355
MSP	12R	M-R	100	386	200	16	2650
MSP	35	K10	100	402	220	16	7739
MSP	4	B-R	102	365	150	16	4793
MSP	12L	C-R	103	374	150	16	2442
MSP	4	W-L	103	411	180	16	3321
MSP	4	A-L	103	362	150	16	4217
MSP	4	B-L	103	375	150	16	4769
MSP	22	W-L	103	377	170	16	4640
MSP	22	A-L	103	382	175	16	3815
MSP	17	K1	103	373	200	16	7771
MSP	30R	C-R	104	376	150	16	5163
MSP	12R	D-R	104	353	150	16	3976
MSP	12R	C-R	104	345	150	16	3646
MSP	4	P-L	104	374	150	16	6856
MSP	35	L10	104	407	220	16	7739
MSP	4	T-L	105	359	130	16	1950
MSP	12R	W3	90	398	250	1	7831
MSP	4	C10	108	405	200	16	9202
MSP	30R	R10	109	383	200	16	7759
MSP	30R	R9	111	405	200	16	7365
MSP	12L	G-L	121	369	120	7	3591
MSP	30R	P9	122	401	150	7	7283
MSP	22	K-R	125	589	150	5	9368
MSP	30R	P3	135	402	110	11	1530
MSP	30R	P4	135	413	110	11	2319
MSP	30L	A3	135	380	130	11	1823
MSP	30L	A4-B	135	406	112	11	3097

MSP	4	H-R	135	394	80	11	5145
MSP	4	C9-L	135	394	110	11	8557
MSP	22	H-R	135	398	120	11	2886
MSP	17	K6	135	397	125	11	3226
MSP	17	Y	135	388	125	11	2263
MSP	12L	P8	136	415	95	11	2950
SNA	20R	H-L	45	685	200	8	2188
SNA	20R	F	45	518	350	18	3646
SNA	20R	E-L	65	527	375	13	4500
SNA	02L	G	90	331	100	14	2381
SNA	02L	H-L	90	474	230	1	2890
SNA	02L	J-L	90	440	250	1	3786
SNA	02L	J-R	90	446	250	1	3783
SNA	02L	K-L	90	392	115	1	5166
SNA	02L	K-R	90	356	150	14	5179
SNA	02L	L-L	90	306	170	14	5547
SNA	02L	L-R	90	281	170	14	5546
SNA	20R	J-L	90	396	125	1	1410
SNA	20R	J-R	90	356	180	14	1410
SNA	20R	H-R	90	458	200	1	2188
SNA	20R	G-R	90	474	195	1	2871
SNA	20R	E-R	90	612	200	19	4499
SNA	20R	D-L	90	321	200	14	5502
SNA	20R	D-R	90	312	200	14	5501
SNA	02R	J-L	90	193	102	6	1161
SNA	02R	J-R	90	196	102	6	1157
SNA	02R	K-L	90	187	100	6	2437
SNA	02R	K-R	90	191	100	6	2435
SNA	02R	L-L	90	177	150	6	2718
SNA	02R	L-R	90	191	100	6	2740
SNA	20L	J-L	90	209	150	6	1470
SNA	20L	J-R	90	230	100	6	1471
SNA	20L	H-L	90	190	150	6	2709
SNA	20L	H-R	90	215	100	6	2708
SNA	02L	F	135	422	80	11	1677
SNA	02L	H-R	135	387	135	11	2891
PVD	34	N-L	55	372	110	18	4892
PVD	5	B-L	70	433	325	15	5112
PVD	23	B-L	70	317	225	15	1737
PVD	34	M-R	70	613	250	13	3337
PVD	34	V-R	70	363	150	15	4821
PVD	16	M-R	78	317	200	14	1913
PVD	34	M-L	80	390	220	1	3166

PVD	5	T	90	283	100	14	1650
PVD	5	C-L	90	416	300	1	4194
PVD	5	C-R	90	310	200	14	4336
PVD	5	B-R	90	384	250	1	4994
PVD	5	N	90	398	280	1	6276
PVD	5	A	90	292	200	14	7008
PVD	23	C-L	90	323	200	14	2517
PVD	23	C-R	90	317	200	14	2517
PVD	23	T	90	402	300	1	5154
PVD	23	M1	90	324	250	14	6247
PVD	23	M	90	291	175	14	7013
PVD	16	B	90	438	245	1	3017
PVD	16	C1	90	307	150	14	3202
PVD	16	C	90	279	150	14	5364
PVD	34	C1	90	322	150	14	2028
PVD	34	B	90	320	150	14	2037
PVD	23	B-R	110	497	150	7	1460
PVD	16	M-L	110	305	150	16	1811
PVD	34	V-L	110	301	90	16	4792
PVD	34	F	120	330	150	7	5789
PVD	34	N-R	125	349	124	7	4759
PVD	34	S	125	453	125	7	5815
MKE	01L	M-LS	30	1250	1400	20	4957
MKE	25R	F1	35	307	98	18	1724
MKE	19R	S-R	45	777	98	8	4897
MKE	07R	T-L	50	605	890	9	5521
MKE	13	E-R	55	485	392	13	1991
MKE	31	E-R	55	516	217	13	2212
MKE	07L	E-L	60	339	110	15	2850
MKE	13	V-L	60	321	100	15	1516
MKE	31	V-L	60	388	170	15	2959
MKE	01L	M-LB	90	1088	1400	12	4957
MKE	25R	E-L	65	282	150	15	1752
MKE	25L	T-L	65	434	260	15	1814
MKE	07R	A4	70	447	270	15	2157
MKE	25L	A2	70	678	425	13	3880
MKE	07L	D-L	75	308	200	15	741
MKE	13	G-R	75	350	200	15	1825
MKE	31	G-R	75	321	214	15	2517
MKE	01L	F-R	80	347	150	14	9506
MKE	07R	R-L	80	566	215	19	5035
MKE	25L	R-L	80	442	251	1	2422
MKE	19R	M-R	85	552	332	19	2701

MKE	01R	M-R	85	332	200	14	2787
MKE	01L	R3	90	417	250	1	1256
MKE	01L	S-L	90	385	165	1	3059
MKE	01L	S-R	90	381	165	1	3059
MKE	01L	M-R	90	395	169	1	5793
MKE	19R	R3	90	459	250	1	7117
MKE	19R	R5	90	374	250	1	8658
MKE	19R	R6	90	358	175	14	9015
MKE	01R	W-R	90	547	210	19	553
MKE	19L	W	90	371	155	1	3160
MKE	19L	S	90	334	153	14	3907
MKE	07L	H-L	90	250	100	6	4653
MKE	25R	V	90	256	110	6	4650
MKE	07R	A3-L	90	400	150	1	2840
MKE	07R	A3-R	90	366	158	14	2840
MKE	07R	A1	90	404	232	1	4279
MKE	07R	N-L	90	352	184	14	8120
MKE	07R	N-R	90	350	182	14	8127
MKE	25L	A1	90	440	250	1	3077
MKE	25L	A3-L	90	392	202	1	4720
MKE	25L	A3-R	90	415	180	1	4685
MKE	25L	A4	90	452	280	1	5711
MKE	25L	A5	90	391	190	1	7642
MKE	13	N	90	300	158	14	4580
MKE	31	C	90	441	304	1	4898
MKE	01R	M-L	95	369	250	1	2682
MKE	01L	F-L	100	329	150	16	9470
MKE	07L	H-R	100	256	85	6	4653
MKE	07R	R-R	100	327	206	16	5022
MKE	25L	R-R	100	408	192	16	2422
MKE	07L	D-R	105	270	120	16	741
MKE	25R	D-L	105	294	150	16	3720
MKE	25R	C	105	250	104	16	4630
MKE	13	G-L	105	325	160	16	1765
MKE	31	G-L	105	378	142	16	2465
MKE	01L	K-L	115	348	194	7	6596
MKE	25R	E-R	115	222	98	16	1724
MKE	07R	T-R	115	372	200	7	5516
MKE	25L	T-R	115	333	115	7	1814
MKE	01L	V	120	335	100	7	8450
MKE	07L	E-R	120	252	105	7	2757
MKE	13	V-R	120	354	110	7	1352
MKE	31	V-R	120	328	124	7	2848

MKE	13	E-L	125	340	120	7	1991
MKE	31	E-L	125	359	150	7	2118
MKE	31	D	130	383	98	11	4584
MKE	13	K	135	394	76	11	3639
MKE	31	F	135	453	104	11	4648
MKE	07L	F1	140	376	75	11	2870
MKE	19R	E-R	150	487	125	4	2702
MKE	25R	D-R	110	221	100	16	3720
CLE	06L	R-R	40	646	900	9	5975
CLE	06R	R-R	42	1053	1400	12	4766
CLE	24R	N	45	623	950	9	4800
CLE	24R	P	45	589	950	9	6246
CLE	06R	K-R	45	699	775	9	2795
CLE	28	D	45	666	902	9	4882
CLE	06L	K	50	641	705	9	4560
CLE	24L	H	52	1004	1400	12	3450
CLE	06L	B-L	55	588	890	9	7021
CLE	06L	B-R	55	587	890	9	7021
CLE	24R	T	55	583	1100	9	7649
CLE	06L	R-L	65	613	850	9	5836
CLE	06R	S-R	75	385	181	15	6787
CLE	06L	G1	90	376	205	1	8323
CLE	06L	S-R	90	383	182	1	8773
CLE	24R	K	90	385	200	1	3682
CLE	24R	G	90	380	201	1	8778
CLE	06R	N-L	90	327	102	14	1368
CLE	06R	N-R	90	330	99	14	1368
CLE	06R	L1	90	387	200	1	4251
CLE	06R	R-L	90	378	185	1	5165
CLE	06R	W	90	362	220	1	7816
CLE	24L	R-R	90	381	208	1	2492
CLE	24L	L1	90	373	210	1	3393
CLE	24L	K-R	90	418	238	1	4827
CLE	24L	N-L	90	333	100	14	6465
CLE	24L	N-R	90	329	118	14	6465
CLE	24L	P-L	90	360	205	1	7827
CLE	24L	P-R	90	349	204	14	7827
CLE	24L	T-L	90	526	170	19	9221
CLE	24L	T-R	90	485	148	1	9221
CLE	24L	L	90	470	210	1	9700
CLE	10	U	90	391	209	1	5082
CLE	28	B	90	383	169	1	5811
CLE	06R	S-L	125	373	102	7	6766

CLE	06L	S-L	135	456	200	11	8438
CLE	24L	K-L	135	457	92	11	4645
CLE	10	J	135	449	165	11	5776
CLE	24L	R-L	140	421	101	11	2305
BDL	19	C-R	45	522	250	18	737
BDL	6	H	65	625	1400	12	6515
BDL	24	S-L	70	505	374	13	6181
BDL	24	V	75	476	334	13	6964
BDL	6	V	90	401	201	1	2014
BDL	6	S-L	90	396	156	1	2725
BDL	6	S-R	90	400	205	1	2725
BDL	6	K	90	386	200	1	4014
BDL	6	C	90	361	215	1	9266
BDL	24	H	90	346	158	14	2327
BDL	24	K	90	396	210	1	5111
BDL	24	S-R	90	449	274	1	6346
BDL	24	R-L	90	488	299	19	9093
BDL	24	R-R	90	487	300	19	9095
BDL	15	J	90	379	144	1	1250
BDL	15	C-L	90	375	149	1	2371
BDL	15	C-R	90	338	146	14	2373
BDL	15	P	90	362	140	14	4090
BDL	15	E-L	90	361	160	14	5108
BDL	15	E-R	90	371	162	1	5111
BDL	15	L	90	315	203	14	6629
BDL	15	S	90	337	220	14	6628
BDL	33	E-L	90	353	171	14	1378
BDL	33	E-R	90	351	158	14	1378
BDL	33	P	90	352	151	14	2380
BDL	33	C-L	90	358	150	14	4116
BDL	33	C-R	90	389	168	1	4116
BDL	33	J	90	392	155	1	5223
BDL	33	U-L	90	325	204	14	6707
BDL	33	U-R	90	289	120	14	6712
BDL	1	F	90	315	150	14	786
BDL	19	F	90	315	150	14	2745
BDL	19	T	90	240	150	6	4109
BDL	1	C-R	45	437	250	18	2844
BDL	1	C-L	135	356	75	11	2718
BDL	19	C-L	135	341	60	11	737
BWI	33R	M-R	30	546	1800	12	1348
BWI	10	V1	55	393	220	18	9248
BWI	15L	M-R	65	644	1400	12	3400

BWI	33L	F-L	65	332	212	15	5606
BWI	15R	Y2	70	357	130	15	5688
BWI	15R	Y1	70	364	208	15	6253
BWI	10	G-L	90	327	157	14	1557
BWI	10	G-R	90	326	120	14	1557
BWI	10	R1-L	90	366	174	1	2902
BWI	10	R1-R	90	364	161	14	2902
BWI	10	D-L	90	346	166	14	6009
BWI	10	D-R	90	342	160	14	6009
BWI	10	U2	90	328	164	14	7989
BWI	10	U1	90	387	166	1	9010
BWI	28	U2	90	337	180	14	773
BWI	28	D-L	90	325	120	14	2968
BWI	28	D-R	90	331	155	14	2968
BWI	28	R1-L	90	424	246	1	5920
BWI	28	R1-R	90	405	253	1	5921
BWI	28	G-L	90	435	250	1	7325
BWI	28	G-R	90	425	252	1	7322
BWI	15L	K-L	90	307	121	14	1388
BWI	15L	K-R	90	386	120	1	1399
BWI	15L	L	90	294	106	14	1988
BWI	15L	Q	90	298	109	14	4858
BWI	15L	S	90	303	110	14	4858
BWI	33R	L	90	326	100	14	2785
BWI	33R	K-R	90	384	116	1	3380
BWI	33R	Q	90	308	109	14	4865
BWI	15R	F-L	90	337	130	14	2886
BWI	15R	R-L	90	347	167	14	3836
BWI	15R	R-R	90	317	155	14	3905
BWI	15R	D3	90	328	180	14	6666
BWI	15R	D2	90	345	180	14	7911
BWI	15R	D1	90	350	165	14	9005
BWI	33L	D3	90	336	185	14	1760
BWI	33L	R-L	90	342	159	14	4570
BWI	33L	R-R	90	337	175	14	4570
BWI	33L	F-R	90	328	187	14	5554
BWI	33L	H	90	334	183	14	6956
BWI	10	V2	105	341	161	16	9790
BWI	33L	P	105	343	200	16	8814
BWI	33L	Y1	109	329	108	16	2203
BWI	33L	Y2	109	341	141	16	2750
BWI	28	F2	110	419	201	16	9530
BWI	15R	F-R	115	330	85	7	2886

BWI	15L	M-L	120	391	95	7	3209
BWI	33R	J	125	315	150	7	4892
BWI	33R	M-L	145	473	46	4	1172
BWI	33R	K-L	160	370	138	4	3380
MEM	27	V3	35	1272	1800	20	6697
MEM	36R	S3	35	977	1800	3	5385
MEM	36R	Y1	35	1071	1800	3	6292
MEM	36R	S4	35	977	1800	3	5390
MEM	18C	C2	35	997	1800	3	4941
MEM	18C	C1	35	1014	1800	3	7254
MEM	36C	C4	35	1041	1800	3	5378
MEM	36C	C5	35	1012	1800	3	7008
MEM	18R	M4	35	1107	1800	3	5601
MEM	18R	M3	35	993	1800	3	7236
MEM	36L	M7	35	981	1800	3	7209
MEM	18L	S2	38	1107	1400	12	4987
MEM	18L	S	38	984	1400	12	6924
MEM	36C	S5	45	917	900	17	7124
MEM	36C	B1	50	397	200	18	10889
MEM	9	V1	70	377	200	15	8726
MEM	9	V2	70	417	195	15	8925
MEM	27	S-R	75	402	172	15	5557
MEM	18L	H-L	75	460	310	13	8120
MEM	27	N-L	88	385	200	1	8557
MEM	9	C-L	90	359	150	14	2205
MEM	9	C-R	90	385	150	1	2211
MEM	9	S-R	90	392	173	1	3093
MEM	9	B-L	90	387	162	1	3978
MEM	9	B-R	90	370	150	1	3990
MEM	9	Y-L	90	412	170	1	4790
MEM	9	Y-R	90	370	135	14	4790
MEM	9	A2	90	368	162	1	6414
MEM	9	A1-R	90	394	201	1	8652
MEM	27	A2	90	380	152	1	2225
MEM	27	Y-L	90	411	165	1	3818
MEM	27	Y-R	90	388	158	1	3818
MEM	27	B-L	90	398	150	1	4633
MEM	27	B-R	90	399	151	1	4633
MEM	27	S-L	90	390	150	1	5513
MEM	27	C-L	90	374	150	1	6430
MEM	27	C-R	90	388	150	1	6430
MEM	18L	P-L	90	366	150	14	3757
MEM	18L	P-R	90	365	150	14	3757

MEM	18L	E	90	373	150	1	6081
MEM	18L	H-R	90	361	150	14	8302
MEM	18L	Q	90	329	117	14	8576
MEM	18L	R-L	90	358	214	1	8795
MEM	18L	R-R	90	346	195	14	8794
MEM	36R	E	90	346	150	14	2630
MEM	36R	P-L	90	347	148	14	4940
MEM	36R	P-R	90	345	150	14	4940
MEM	36R	S6	90	385	163	1	8287
MEM	36R	Y2	90	376	162	1	8287
MEM	36R	D-L	90	356	200	14	8782
MEM	36R	D-R	90	355	200	14	8782
MEM	18C	D-L	90	365	150	14	1994
MEM	18C	D-R	90	363	151	14	1995
MEM	18C	K-L	90	362	152	14	2843
MEM	18C	K-R	90	362	154	14	2843
MEM	18C	L-L	90	352	150	14	4442
MEM	18C	L-R	90	352	150	14	4442
MEM	18C	P-L	90	349	158	14	5895
MEM	18C	P-R	90	350	160	14	5895
MEM	18C	E-L	90	358	150	14	8202
MEM	18C	E-R	90	363	150	14	8202
MEM	18C	H-L	90	365	148	14	10412
MEM	18C	H-R	90	374	150	1	10412
MEM	18C	R-L	90	345	200	14	10914
MEM	18C	R-R	90	347	200	14	10914
MEM	36C	E-L	90	360	168	14	2602
MEM	36C	E-R	90	356	155	14	2602
MEM	36C	P-L	90	347	150	14	4941
MEM	36C	P-R	90	352	150	14	4941
MEM	36C	L-L	90	353	150	14	6372
MEM	36C	L-R	90	354	150	14	6372
MEM	36C	K-L	90	353	150	14	7966
MEM	36C	K-R	90	357	150	14	7966
MEM	36C	D-L	90	358	150	14	8812
MEM	36C	D-R	90	362	150	14	8812
MEM	36C	C6	90	323	150	14	10376
MEM	36C	S7	90	343	110	14	10446
MEM	36C	C7	90	328	133	14	10670
MEM	36C	C8	90	354	210	14	10908
MEM	18R	M6	90	350	200	14	2613
MEM	18R	M5	90	381	201	1	4503
MEM	18R	M2	90	382	216	1	8660

MEM	18R	M1	90	366	224	1	9090
MEM	36L	M5	90	366	200	1	4394
MEM	36L	M6	90	370	202	1	6363
MEM	36L	M8	90	373	200	1	8680
MEM	36L	M9	90	350	200	14	9106
MEM	27	N-R	92	410	201	1	8557
MEM	9	S-L	105	364	125	16	3093
MEM	36C	B	110	351	200	16	10889
MEM	9	V3	135	410	132	11	1256
MEM	18L	S3	142	461	65	4	2836
MEM	18L	S4	145	434	82	4	1178
MEM	18L	Y1	145	442	55	4	1822
MEM	36R	S2	145	407	99	4	3042
MEM	36L	M4	145	418	95	4	2764
SDF	29	M	30	984	1800	3	4531
SDF	17L	D3	45	1044	1400	12	4666
SDF	17L	D2	45	1025	1400	12	5678
SDF	35R	D4	45	1086	1400	12	4761
SDF	35R	D5	45	956	1400	12	5900
SDF	17R	B4	45	1072	1400	12	5116
SDF	17R	B3	45	1025	1400	12	6170
SDF	35L	B5	45	942	1400	12	4975
SDF	35L	B6	45	1015	1400	12	5907
SDF	11	C-R	55	371	112	18	1105
SDF	11	E-R	55	402	200	18	6816
SDF	29	D-R	55	345	200	15	1371
SDF	29	C-RS	55	385	160	18	6031
SDF	29	C-RB	90	364	150	14	6031
SDF	29	B-RS	55	422	150	18	6337
SDF	17L	G-L	55	435	200	18	4105
SDF	17L	F-L	55	402	200	18	5114
SDF	35R	F-L	55	432	201	18	2500
SDF	35R	G-L	55	421	150	18	3500
SDF	17R	F-L	55	414	200	18	2215
SDF	35L	F-L	55	429	200	18	7610
SDF	11	G2	60	373	135	15	4817
SDF	35R	D6	65	361	150	15	7620
SDF	29	B-RB	90	391	150	1	6337
SDF	29	P	80	414	150	1	2858
SDF	29	N	80	348	155	14	3700
SDF	11	E-L	90	343	150	14	6608
SDF	11	G1	90	346	150	14	7080
SDF	11	F1	90	347	150	14	7080

SDF	17L	E4	90	357	150	14	1355
SDF	17L	E3	90	361	152	14	3099
SDF	17L	E2	90	342	152	14	6162
SDF	17L	D1	90	365	150	14	7613
SDF	17L	D	90	354	150	14	8025
SDF	35R	E2	90	339	150	14	1383
SDF	35R	E3	90	363	160	14	4394
SDF	35R	E4	90	358	150	14	6175
SDF	35R	E	90	358	150	14	7602
SDF	35R	D	90	348	150	14	7955
SDF	17R	A6	90	338	150	14	3205
SDF	17R	A5	90	374	150	1	4186
SDF	17R	A4	90	364	150	14	5774
SDF	17R	A3	90	364	150	14	6781
SDF	17R	B2	90	387	150	1	7923
SDF	17R	A2	90	387	150	1	7923
SDF	17R	B1	90	375	150	1	9500
SDF	17R	B	90	369	165	1	9803
SDF	17R	A	90	369	150	1	9803
SDF	35L	A2	90	364	150	14	1748
SDF	35L	B2	90	364	150	14	1746
SDF	35L	A3	90	358	150	14	2918
SDF	35L	A4	90	358	150	14	3914
SDF	35L	A5	90	354	150	14	5519
SDF	35L	A6	90	369	150	1	6504
SDF	35L	B7	90	384	150	1	9500
SDF	35L	A8	90	351	150	14	9832
SDF	35L	B8	90	358	150	14	9832
SDF	11	N	100	373	160	16	3239
SDF	11	P	100	348	110	16	4101
SDF	29	G2	120	363	83	7	2205
SDF	11	D-L	125	357	65	7	5682
SDF	11	C-L	125	336	40	7	1093
SDF	11	D-RS	55	397	150	18	5682
SDF	29	D-L	125	431	52	7	1371
SDF	29	C-L	125	370	151	7	5810
SDF	29	B-L	125	384	150	7	6132
SDF	17L	G-R	125	377	150	7	3911
SDF	17L	F-R	125	423	150	7	4837
SDF	35R	F-R	125	355	65	7	2466
SDF	35R	G-R	125	364	65	7	3464
SDF	17R	F-R	125	358	50	7	2193
SDF	35L	F-R	125	373	60	7	7575

SDF	35L	G	125	393	150	7	8401
SDF	17L	D5	135	361	150	11	956
SDF	17L	D4	135	399	118	11	2109
SDF	35R	D2	135	384	100	11	1235
SDF	35R	D3	135	383	100	11	2230
SDF	17R	B6	135	454	150	11	3111
SDF	17R	B5-B	135	443	150	11	4134
SDF	35L	B3	135	438	150	11	2864
SDF	35L	B4	135	424	150	11	3869
SDF	11	D-RB	90	374	150	1	5682
SDF	11	M	145	440	125	4	1866
SDF	17R	B5-RC	135	437	150	11	4134
SDF	35L	29	125	376	85	7	8047
SDF	17L	11	125	362	85	7	4533
SDF	35R	11	55	436	200	18	3003
SDF	29	17R	55	432	200	18	6883
SDF	11	35R	55	435	200	18	6232
SDF	11	17L	125	360	85	7	6162
SFO	28R	C1	40	663	550	8	11186
SFO	28L	S	40	598	400	8	10564
SFO	28R	K-R1	50	607	550	8	8028
SFO	28L	N-L	50	321	150	18	1983
SFO	19L	G-R1	55	496	450	13	5660
SFO	19L	G-R2	90	326	150	14	5982
SFO	19L	F1-R	60	526	450	13	4193
SFO	10L	P-R	60	544	590	13	8132
SFO	28R	K-R2	90	386	150	1	8422
SFO	28R	D-L1	60	467	440	13	7362
SFO	28R	D-L2	90	333	150	14	7642
SFO	28R	D-R	65	534	450	13	7362
SFO	01L	F1-R	70	380	200	15	2792
SFO	19R	F1-R	70	398	250	15	3876
SFO	01R	F1-R	70	365	200	15	3439
SFO	10L	E-L	70	432	200	15	5400
SFO	28R	E-L	70	359	250	15	5925
SFO	10R	E-L	70	316	150	15	4676
SFO	28L	E-L	70	338	300	15	6141
SFO	28L	U	70	561	350	13	9660
SFO	28R	R-R	75	518	385	13	9925
SFO	10R	D-R	80	339	175	14	3192
SFO	28L	D-R	80	353	250	1	7576
SFO	28L	Q-L	80	373	250	1	9413
SFO	01L	F-R	85	345	200	14	3193

SFO	19R	F-R	85	339	150	14	3494
SFO	28L	S1	85	367	250	1	10008
SFO	01L	C-L	90	295	150	14	5034
SFO	01L	C-R	90	294	150	14	5034
SFO	01L	V-L	90	283	116	14	6178
SFO	01L	V-R	90	278	115	14	6178
SFO	01L	E-L	90	321	150	14	6829
SFO	01L	E-R	90	302	150	14	6829
SFO	19R	C-L	90	301	150	14	1729
SFO	19R	C-R	90	307	140	14	1729
SFO	19R	G-L	90	302	150	14	5264
SFO	19R	G-R	90	308	150	14	5264
SFO	19R	H-R	90	312	200	14	6517
SFO	19R	M-L	90	305	160	14	7112
SFO	19R	M-R	90	321	150	14	7205
SFO	19R	A2	90	418	150	1	7461
SFO	19R	M1	90	311	150	14	7461
SFO	01R	G-L	90	308	121	14	1833
SFO	01R	F-L	90	292	105	14	3643
SFO	01R	F-R	90	315	125	14	3643
SFO	01R	C-L	90	298	140	14	5380
SFO	01R	C-R	90	288	140	14	5380
SFO	01R	V-L	90	303	140	14	6481
SFO	01R	V-R	90	304	140	14	6481
SFO	01R	E-L	90	304	125	14	7179
SFO	01R	E-R	90	339	125	14	7179
SFO	01R	L	90	326	125	14	7939
SFO	19L	V-L	90	303	115	14	1382
SFO	19L	V-R	90	301	112	14	1382
SFO	19L	C-L	90	291	115	14	2496
SFO	19L	C-R	90	297	115	14	2496
SFO	19L	F-L	90	342	135	14	4222
SFO	19L	F-R	90	290	115	14	4258
SFO	19L	M-L	90	333	135	14	7862
SFO	19L	M-R	90	302	135	14	7862
SFO	19L	L2	90	364	140	14	8438
SFO	19L	A1	90	327	135	14	8438
SFO	10L	K-L	90	361	150	14	2852
SFO	10L	K-R	90	323	150	14	2852
SFO	10L	D-L	90	362	150	14	3634
SFO	10L	D-R	90	314	150	14	3634
SFO	10L	L-L	90	360	150	14	7350
SFO	10L	L-R	90	319	135	14	7350

SFO	10L	P-L	90	353	150	14	8540
SFO	10L	N-L	90	340	135	14	9343
SFO	10L	N-R	90	308	150	14	9343
SFO	10L	W	90	389	280	1	11072
SFO	10L	C-L	90	404	280	1	11580
SFO	10L	C-R	90	351	250	1	11580
SFO	28R	N-L	90	298	150	14	1979
SFO	28R	N-R	90	342	150	14	2004
SFO	28R	P-L	90	287	105	14	2814
SFO	28R	P-R	90	331	130	14	2814
SFO	28R	L-L	90	285	115	14	4008
SFO	28R	L-R	90	326	115	14	4008
SFO	28R	K-L	90	299	150	14	8456
SFO	28R	R-L	90	308	150	14	10364
SFO	28R	S4	90	360	250	1	10982
SFO	28R	S3	90	385	250	1	11265
SFO	10R	K-L	90	323	160	14	2334
SFO	10R	K-R	90	323	160	14	2334
SFO	10R	L-L	90	297	130	14	6862
SFO	10R	L-R	90	299	135	14	6862
SFO	10R	P-L	90	306	150	14	8041
SFO	10R	P-R	90	301	150	14	8041
SFO	10R	N-L	90	306	150	14	8842
SFO	10R	F-L	90	379	300	1	11054
SFO	10R	F-R	90	381	300	1	11054
SFO	28L	N-R	90	329	150	14	1947
SFO	28L	P-L	90	318	150	14	2756
SFO	28L	P-R	90	319	145	14	2756
SFO	28L	L-L	90	319	150	14	3949
SFO	28L	L-R	90	315	145	14	3949
SFO	28L	K-L	90	345	200	14	8368
SFO	28L	K-R	90	351	200	14	8368
SFO	28L	Z	90	299	115	14	10410
SFO	28L	R	90	289	112	14	10410
SFO	28L	Z1	90	327	200	14	10837
SFO	01L	F-L	95	291	150	14	3230
SFO	19R	F-L	95	319	150	14	3494
SFO	28L	D-L	95	349	200	14	7494
SFO	10R	D-L	100	290	90	16	3228
SFO	01L	F1-L	110	301	150	16	2758
SFO	19R	F1-L	110	316	100	16	3938
SFO	01R	F1-L	110	304	90	16	3439
SFO	19L	F1-L	110	323	100	16	4430

SFO	10L	E-R	110	326	112	16	5400
SFO	28R	E-R	110	340	115	16	5925
SFO	10R	E-R	110	308	125	16	4601
SFO	28L	E-R	110	328	115	16	6141
SFO	01R	G-R	120	383	110	7	1784
SFO	19L	G-L	120	361	125	7	5999
SFO	10R	N-R	135	325	135	11	8842
SFO	28R	U-L	140	408	120	11	10364
SFO	28L	Q-R	145	382	110	11	9540
SFO	19R	H-L	150	439	95	4	6517
SFO	10R	T-R	150	442	70	4	2906
SFO	10R	J	150	459	105	4	5282
SFO	28L	T-R	150	490	100	4	7505
SFO	01R	H	155	552	90	5	1547
HOU	4	B	40	820	1400	12	5710
HOU	22	H2	40	878	1400	12	4956
HOU	31L	M1	40	908	1400	12	5706
HOU	4	C-L	45	444	250	18	4564
HOU	4	R	45	456	200	18	4568
HOU	4	K2	45	470	200	18	6222
HOU	22	C-L	45	461	250	18	2862
HOU	13R	M3	45	681	1000	9	4754
HOU	13R	Q	45	461	260	18	4994
HOU	31L	F	45	433	250	18	6028
HOU	31L	G-R	45	351	150	18	7603
HOU	17	H-R	45	330	125	18	3406
HOU	17	K1	45	428	260	18	4560
HOU	35	H-R	45	411	200	18	2438
HOU	31R	D-L	62	219	142	15	4555
HOU	35	D	70	326	150	15	5418
HOU	13R	K-R	80	295	105	14	2462
HOU	4	J	90	295	115	14	2204
HOU	4	M-L	90	292	115	14	3466
HOU	4	M-R	90	293	115	14	3466
HOU	4	Y	90	323	200	14	7391
HOU	4	K	90	316	200	14	7391
HOU	22	M-L	90	298	110	14	3944
HOU	22	M-R	90	281	110	14	3944
HOU	22	J	90	290	110	14	5200
HOU	22	K1	90	550	200	19	7070
HOU	22	G-2	90	378	200	1	7400
HOU	13L	H-L	90	169	80	6	2272
HOU	13L	H-R	90	170	80	6	2272

HOU	13L	K-L	90	186	105	6	3535
HOU	13L	K-R	90	177	105	6	3535
HOU	13L	L-L	90	192	105	6	4733
HOU	13L	L-R	90	189	105	6	4733
HOU	13L	P-L	90	195	105	6	5020
HOU	13L	P-R	90	192	105	6	5020
HOU	31R	K-L	90	185	110	6	1443
HOU	31R	K-R	90	191	110	6	1443
HOU	31R	H-L	90	154	75	6	2764
HOU	31R	H-R	90	155	75	6	2764
HOU	31R	E	90	173	80	6	5036
HOU	13R	H-L	90	285	150	14	1153
HOU	13R	H-R	90	292	125	14	1153
HOU	13R	K-L	90	277	90	14	2463
HOU	13R	L-L	90	286	90	14	3660
HOU	13R	L-R	90	287	90	14	3660
HOU	13R	M	90	288	85	14	6458
HOU	13R	N	90	300	130	14	6423
HOU	31L	L-L	90	279	85	14	2750
HOU	31L	L-R	90	280	85	14	2750
HOU	31L	K-R	90	291	90	14	3940
HOU	31L	H-L	90	291	115	14	5212
HOU	31L	H-R	90	290	115	14	5212
HOU	17	F-L	90	266	60	6	1508
HOU	17	F-R	90	217	60	6	1508
HOU	17	G2	90	224	60	6	2595
HOU	17	G3	90	217	60	6	4004
HOU	17	K	90	311	200	14	5807
HOU	17	G-2	90	257	110	6	5847
HOU	35	G3	90	217	60	6	1884
HOU	35	G2	90	221	58	6	3290
HOU	35	F-L	90	213	60	6	4394
HOU	35	F-R	90	265	60	6	4394
HOU	35	E	90	261	150	6	5818
HOU	22	G-1	95	344	200	14	7155
HOU	31L	K-L	100	284	80	16	3940
HOU	31R	D-R	118	206	65	7	4535
HOU	4	C-R	135	382	55	11	4508
HOU	22	C-R	135	355	105	11	2726
HOU	22	R	135	396	105	11	2758
HOU	31L	G-L	135	332	80	11	7460
HOU	17	H-L	135	342	35	11	3406
HOU	35	H-L	135	275	35	11	2438

HOU	17	G	140	307	200	11	4528
BDL	6	33-R	90	345	120	14	3214
BDL	6	33-L	90	332	120	14	3214
BDL	6	1-R	110	463	75	7	6325
BDL	24	15	90	334	120	14	6043
BDL	24	33	90	345	120	14	6043
BDL	24	1	105	545	200	19	2930
BDL	33	24	90	354	120	14	4691
BDL	33	6	90	354	120	14	4691
BDL	15	6-R	90	331	120	14	1870
BDL	15	6-L	90	341	120	14	1870
BDL	1	24	65	412	175	15	3452
DEN	17R	EC-L	90	527	100	19	1535
DEN	17R	EC-R	90	405	150	1	1485
ATL	26L	B10-S	90	319	85	14	3206
LGA	4	31	90	318	100	14	4755
LGA	22	31	90	303	100	14	2015
LGA	22	F-L	110	450	75	7	3610
LGA	22	Q	150	401	75	4	3011
LGA	13	4	90	294	100	14	1132
LGA	13	S	130	302	70	11	1935
LGA	13	J	150	436	70	4	3550
LGA	31	M	150	420	75	4	1911
LGA	31	L	150	398	75	4	2913
LGA	31	4	90	335	120	14	5725
EWR	11	22R	110	325	90	16	4870
EWR	11	22L	110	330	80	16	5900
EWR	04R	11	110	351	90	16	8307
EWR	04L	11	110	435	90	7	7948
EWR	29	22R	70	374	150	15	1406
SNA	20R	F-S	45	518	250	18	3644
SNA	20R	F-B	90	472	250	1	3644
SNA	20R	G-L	135	424	80	11	3000
STL	6	30L	60	384	175	15	2841
STL	24	30L	120	327	100	7	4493
SFO	28L	1R	90	354	150	14	4451
SFO	28L	1L	90	360	150	14	5200
CLT	36R	C10	30	730	500	8	6895
CLT	36R	C11	90	376	150	1	8273
CLT	36R	C	90	377	150	1	8649
CLT	36R	5	130	360	75	11	6550
SFO	10R	1L	90	368	150	14	5562
SFO	10R	19R	90	336	150	14	5562

SFO	10R	1R	90	359	150	14	6328
SFO	10R	19L	90	322	150	14	6328
SFO	10L	Q	150	455	100	4	2487
SFO	10L	1L	90	334	150	14	6063
SFO	10L	19R	90	359	150	14	6063
SFO	10L	1R	90	331	150	14	6814
SFO	10L	19L	90	364	150	14	6814
SFO	28L	19L	90	329	150	14	4450
SFO	28L	19R	90	330	150	14	5206
SFO	28R	1R	90	326	150	14	4453
SFO	28R	1L	90	318	150	14	5214
SFO	28R	19R	90	360	150	14	5201
SFO	28R	19L	90	357	150	14	4456
HNL	08L	22R	35	504	175	18	10063
HNL	08L	22L	35	504	175	18	10897
HNL	22R	8L	35	606	350	8	2492
HNL	04R	8L	145	421	75	4	6617
HNL	22L	8L	35	595	350	8	2044
MSP	17	22	125	364	85	7	5560
MSP	35	22	55	419	175	18	2187
MSP	35	N-R	90	380	200	1	3463
MSP	35	N-L	90	379	200	1	3463
MSP	35	K6	45	789	700	9	4041
MSP	35	L6	90	416	200	1	4370
MSP	4	30L	75	383	175	15	3855
MSP	4	30R	75	375	175	15	7350
MSP	22	30L	105	350	110	16	4295
MSP	22	35	55	423	200	18	9872
MSP	12R	4	105	344	110	16	3195
MSP	12R	22	75	388	175	15	3182
MSP	30L	A4-RC	90	381	112	1	3097
MSP	30L	22	105	338	110	16	6534
MSP	30L	4	75	369	150	15	6546
MSP	30R	4	75	389	175	15	5632
MKE	07R	19R	65	417	150	15	6230
MKE	07L	31	60	310	175	15	1940
MKE	07L	19R	65	312	175	15	3245
MKE	13	1L	55	367	200	18	2580
MKE	31	7L	60	351	150	15	3285
MKE	19L	7R	65	501	200	13	1802
MKE	19R	7R	65	425	200	15	3914
MKE	01L	7R	115	366	100	7	4710
MKE	01L	13	55	478	250	18	7413

MKE	01R	7R	115	332	85	7	2100
MIA	9	Q	90	313	75	14	11529
MIA	12	27	31	698	500	8	8526
SFO	19L	10R	90	333	150	14	3696
SFO	19L	10L	90	343	150	14	2947
SFO	19R	10L	90	334	150	14	2184
SFO	19R	10R	90	362	150	14	2952
SFO	01R	10L	90	333	150	14	4836
SFO	01R	10R	90	344	150	14	4079
SFO	01L	10R	90	364	150	14	3734
SFO	01L	10L	90	458	150	1	4488
SFO	10L	T-R	150	622	90	5	4844
LAS	19R	25R	115	365	85	7	8433
LAS	19R	D	90	524	400	19	8801
LAS	25R	1R	115	365	105	7	11783
LAS	25R	1L	115	384	105	7	12821
LAS	19L	25R	115	367	100	7	7877
JFK	04L	13R	90	353	150	14	3226
JFK	04L	13L	90	359	150	14	9915
JFK	13R	22R	90	357	150	14	10139
JFK	13L	4L	90	352	150	14	6720
HOU	31L	22	90	350	120	14	4450
HOU	13R	22	90	320	125	14	1862
HOU	4	31L	90	351	125	14	2923
HOU	4	13R	90	328	125	14	2923
HOU	4	31R	90	291	110	14	3750
HOU	4	13L	90	313	110	14	3740
HOU	22	13L	90	312	105	14	3636
HOU	22	31R	90	303	105	14	3636
HOU	22	13R	90	310	105	14	4445
HOU	22	31L	90	330	105	14	4445
HOU	35	31L	135	356	85	11	5000
HOU	31R	22	90	208	120	6	1935
HOU	31R	4	90	211	90	6	1935
HOU	13L	4	90	205	115	6	2958
HOU	13L	22	90	205	115	6	2958
MDW	31C	22L	90	334	120	14	2251
MDW	31C	4R	90	319	120	14	2251
MDW	31C	4L	90	320	120	14	3166
MDW	31C	22R	90	339	120	14	3166
MDW	13C	4L	90	341	130	14	1940
MDW	13C	22R	90	322	120	14	1940
MDW	13C	4R	90	318	120	14	2881

MDW	13C	22L	90	315	120	14	2881
MDW	04L	31L	90	294	85	14	1369
MDW	04L	31C	90	315	120	14	1831
MDW	04L	31R	90	326	120	14	2618
MDW	22R	31C	90	315	120	14	1784
MDW	22R	31L	90	312	90	14	2309
MDW	13R	4R	90	140	90	6	2048
MDW	31L	4R	90	148	90	6	1641
MDW	31L	4L	90	149	90	6	2559
MDW	13L	22L	90	310	120	14	2147
MDW	31R	22L	90	312	150	14	1965
MDW	31R	22R	90	359	130	14	2912
MDW	22L	31R	90	317	110	14	1952
MDW	22L	13L	90	316	110	14	1952
MDW	22L	31C	90	290	100	14	2759
MDW	22L	13C	90	318	100	14	2759
MDW	22L	31L	90	284	80	14	3275
MDW	22L	13R	90	290	80	14	3275
MDW	04R	31L	90	297	85	14	1840
MDW	04R	13R	90	298	85	14	1840
MDW	04R	13C	90	335	110	14	2313
MDW	04R	31C	90	318	110	14	2313
MDW	04R	31R	90	304	100	14	3107
MDW	04R	13L	90	311	100	14	3107
BOS	04R	15R	65	444	200	15	4038
BOS	04R	15L	65	366	130	15	5731
BOS	22L	9	55	391	200	18	6638
BOS	33L	4L	115	330	100	7	6715
BOS	04L	15R	65	355	175	15	3769
BOS	04L	15L	65	350	150	15	5445
BOS	22R	15R	115	305	90	7	3018
BOS	9	15R	120	351	85	7	4305
BOS	27	15R	60	406	200	15	2442
BOS	27	22L	120	257	95	7	5802
BOS	15L	4R	65	320	150	15	2027
BOS	33R	4L	115	310	80	7	1982
BOS	22L	15R	115	372	75	7	3377
BOS	15R	4L	65	417	125	15	2260
BOS	15R	4R	65	358	125	15	3925
BOS	15R	9	120	346	90	7	7020
BOS	33L	4R	115	317	85	7	5072
BDL	6	33	90	355	125	14	3200
BDL	6	15	90	337	125	14	3200

JFK	22R	13R	90	367	150	14	4663
DTW	03R	W4	30	954	1800	3	5158
DTW	03R	W5	30	1067	1800	3	6345
DTW	21L	W2	30	1026	1800	3	5010
DTW	27R	V2	30	1042	1800	3	4706
DTW	04L	A7	45	967	1400	12	5551
DTW	04L	A8	45	902	1400	12	7266
DTW	22R	A3	45	973	1400	12	7195
DTW	09R	T3	45	1187	900	2	4672
DTW	09R	T2	45	999	900	17	5858
DTW	27L	T6	45	1161	700	17	5714
DTW	27L	T5	45	1216	900	2	4684
DTW	09L	G-L	45	472	225	18	3838
DTW	27R	G-L	45	562	250	8	4675
DTW	09L	F-R	50	535	250	18	2554
DTW	04R	V-R	60	812	700	9	5498
DTW	04R	Y5	60	509	550	13	7511
DTW	22L	V-R	60	386	150	15	5362
DTW	09R	W-L	60	397	95	15	2650
DTW	27L	W-L	60	383	125	15	5733
DTW	03R	T-R	60	381	150	15	2121
DTW	03R	V-R	60	399	150	15	9448
DTW	21L	T-R	60	492	250	13	7636
DTW	21L	J	60	451	250	13	7266
DTW	03L	V-R	60	367	200	15	4290
DTW	21R	V-R	60	457	250	13	3950
DTW	09L	M-L	60	399	150	15	4572
DTW	09L	W-L	60	400	150	15	6646
DTW	27R	Y-L	60	383	175	15	7431
DTW	27R	K-L	60	383	150	15	7157
DTW	27R	M-L	60	403	150	15	3987
DTW	27R	W-L	60	416	200	15	1874
DTW	04L	A9	90	408	200	1	9333
DTW	04L	A10	90	344	150	14	9831
DTW	22R	A1	90	367	175	1	9819
DTW	04R	R-L	90	401	200	1	1467
DTW	04R	R-R	90	392	200	1	1467
DTW	04R	Y3	90	344	120	14	3519
DTW	04R	Z5	90	363	150	14	7971
DTW	04R	Z7	90	357	150	14	9258
DTW	04R	Y7	90	360	150	14	9258
DTW	04R	Y9	90	388	200	1	10872
DTW	04R	Z10	90	382	200	1	11247

DTW	04R	Y10	90	378	200	1	11247
DTW	22L	Y1	90	393	200	1	11739
DTW	22L	Y2	90	364	200	1	11412
DTW	22L	R-L	90	402	150	1	9616
DTW	22L	R-R	90	413	150	1	9616
DTW	22L	Y3	90	427	150	1	7658
DTW	22L	Z5	90	360	150	14	3570
DTW	22L	Z7	90	404	150	1	1898
DTW	22L	Y7	90	386	200	1	1898
DTW	09R	T1	90	380	200	1	7862
DTW	09R	T	90	378	200	1	8265
DTW	27L	T8	90	376	200	1	8265
DTW	27L	T7	90	370	200	1	7872
DTW	03R	S1-R	90	403	200	1	5493
DTW	03R	W6	90	338	140	14	7901
DTW	03R	S6	90	345	130	14	7901
DTW	03R	W7	90	330	150	14	9855
DTW	21L	S6	90	355	90	14	1872
DTW	21L	W6	90	351	90	14	1872
DTW	21L	W1	90	392	200	1	9744
DTW	21L	S1	90	409	200	1	4087
DTW	03L	M5	90	303	150	14	7101
DTW	03L	P5	90	309	150	14	7101
DTW	03L	M6	90	394	160	1	8232
DTW	03L	P	90	400	160	1	8232
DTW	21R	PP1	90	359	200	1	8260
DTW	21R	F-L	90	332	115	14	6650
DTW	09L	F-L	90	360	120	14	2554
DTW	09L	S7	90	379	150	1	8519
DTW	09L	V1	90	367	150	14	8519
DTW	27R	V4	90	396	150	1	8467
DTW	27R	F-R	90	434	250	1	5773
DTW	21R	F-R	93	420	250	1	6387
DTW	03R	V-L	96	442	250	1	9111
DTW	21R	M	113	391	200	7	8260
DTW	04R	V-L	120	396	150	7	5778
DTW	22L	V-L	120	372	125	7	5230
DTW	22L	Y5	120	373	125	7	3512
DTW	09R	W-R	120	394	95	7	2536
DTW	27L	W-R	120	364	125	7	5589
DTW	03R	T-L	120	398	105	7	2009
DTW	03R	J	120	393	115	7	2401
DTW	21L	T-L	120	370	110	7	7623

DTW	03L	V-L	120	416	150	7	4105
DTW	21R	V-L	120	345	115	7	3912
DTW	09L	M-R	120	393	1225	16	4464
DTW	09L	W-R	120	378	160	7	6465
DTW	27R	Y-R	120	408	150	7	7230
DTW	27R	K-R	120	361	140	7	6991
DTW	27R	M-R	120	364	90	7	3891
DTW	27R	W-R	120	351	120	7	1792
DTW	04L	A3	135	546	75	4	2171
DTW	04L	A4	135	544	115	4	3803
DTW	22R	A7	135	550	115	4	3796
DTW	22R	A8	135	541	115	4	2144
DTW	09R	T6	135	411	105	11	1733
DTW	09R	T5	135	427	140	11	2674
DTW	27L	T3	135	426	105	11	2737
DTW	27L	T2	135	423	105	11	1738
DTW	09L	G-R	135	455	100	11	3650
DTW	27R	F-L	135	427	90	11	5871
DTW	27R	G	135	400	160	11	4409
DTW	09L	V2	140	589	60	5	3308
DTW	04R	Y4	150	479	90	4	4650
DTW	03R	W2	150	539	88	4	4178
DTW	21L	W3	150	537	85	4	5130
DTW	21L	W5	150	538	85	4	2788
DTW	22L	27R	120	344	100	7	5721
DTW	21L	W4	150	479	90	4	4119
DTW	21L	9R	60	393	150	15	8409
DTW	27L	21L	120	353	90	7	4928
DTW	09R	21L	60	386	150	15	3330
DTW	22R	A4	45	995	1400	12	5523
DTW	09L	3L	120	395	100	7	4951
DTW	09L	21R	60	377	150	15	5039
DTW	09L	3R	120	349	90	7	7277
DTW	09L	21L	60	388	150	15	7350
DTW	27R	B-R	90	331	110	14	6423
DTW	27R	B-L	90	328	110	14	6423
DTW	27R	22L	120	359	100	7	7800
DTW	27R	4R	60	386	150	15	7885
DTW	03L	27R	60	409	200	15	3821
DTW	03L	9L	120	322	90	7	3773
DTW	21R	9L	60	392	200	15	4450
DTW	21R	27R	120	348	90	7	4420
DTW	04R	27R	60	411	200	15	5475

DTW	03R	9L	122	391	80	7	8922
DTW	09L	B-R	90	338	125	14	2057
DTW	09L	B-L	90	341	120	14	2057
DTW	27R	21R	120	361	100	7	3412
DTW	27R	3L	60	455	200	15	3467
DTW	22L	Y4	30	919	1800	3	6107
DTW	03R	W3	30	1003	1800	3	4068
FLL	10L	B6	30	678	700	9	6327
FLL	10L	A4	30	1258	1800	20	5112
FLL	10L	B5	30	1259	1800	20	5112
FLL	10L	B4	30	627	900	9	4619
FLL	10L	D-R	45	489	250	18	2610
FLL	10L	A5	90	347	150	14	7243
FLL	10L	B7	90	335	150	14	7243
FLL	10L	Q-R	90	345	150	14	4312
FLL	10L	Q-L	90	346	150	14	4312
FLL	10L	E-R	90	370	150	1	1618
FLL	10L	A-2	90	381	150	1	7985
FLL	10L	A-1	90	391	130	1	8239
FLL	10L	B-2	90	398	150	1	8239
FLL	10L	B-1	90	384	150	1	7985
FLL	10L	D-L	135	410	75	11	2552
FLL	10R	J9	45	735	820	9	6224
FLL	10R	J8	80	584	200	19	4775
FLL	10R	J7	90	328	150	14	3636
FLL	10R	J10	90	396	150	1	7217
FLL	10R	J11	90	359	150	14	7524
FLL	10R	J12	90	365	150	14	7798
FLL	10R	J5-1	150	446	88	4	1970
FLL	28L	J5-1	30	1390	1800	20	4787
FLL	28L	J4	80	540	175	19	6390
FLL	28L	J8	90	339	150	14	2564
FLL	28L	J7	90	324	150	14	4051
FLL	28L	J3	90	351	150	14	7262
FLL	28L	J2	90	353	150	14	7531
FLL	28L	J1	90	361	150	14	7785
FLL	28R	B2	30	1170	1800	3	5774
FLL	28R	D-R	45	436	150	18	5038
FLL	28R	E-R	45	444	150	18	6166
FLL	28R	Q-L	90	339	150	14	3231
FLL	28R	Q-R	90	339	150	14	3231
FLL	28R	E-L	90	348	150	14	5909
FLL	28R	B1	90	347	150	14	7088

FLL	28R	A1	90	356	150	14	7088
FLL	28R	B-1	90	388	150	1	7948
FLL	28R	B-2	90	377	150	1	8209
FLL	28R	A	120	395	150	7	8210
FLL	28R	D-L	135	366	150	11	4736
FLL	28R	B6	150	490	76	4	1044
FLL	28R	A4	150	512	90	4	1612
FLL	28R	B5	150	504	90	4	1612
FLL	28R	B4	150	469	75	4	2800
PVD	23	16	110	301	80	16	2142
PVD	23	34	70	333	150	15	2149
PVD	5	16	70	347	150	15	4802
PVD	5	34	110	292	100	16	4777
PVD	16	5	70	343	130	15	2321
PVD	16	23	110	282	80	16	2300
PVD	34	23	70	349	150	15	2982
PVD	34	5	110	294	85	16	2967
BWI	33L	28	130	385	75	11	3587
BWI	28	15R	50	470	200	18	4448
BWI	10	15R	135	366	75	11	4529
BWI	15R	28	50	435	200	18	4838
PHL	17	9L	97	297	110	14	5222
PHL	09L	17	95	322	110	14	7533
BDL	6	1	135	465	75	11	6315
FLL	10R	J5-2	90	331	150	14	1907
FLL	28L	J5-2	90	1221	150	10	4787
MIA	08R	L10-2	90	358	150	14	8412
MIA	08R	L11-2	90	362	150	14	10103
SDF	17L	29	53	427	150	18	4609
SFO	28R	Q	30	915	1200	12	8340

Appendix B – Runway Geometry Database and Runway Clusters

Airport_Name	rw_name	rw_length	rw_name1	rw_name2	Number_Exits	AverageTHRdist	STDthrDists	Ratio_Avg_Len	Num_exits_2k	AverageTHRdist_2k	STDthrDists_2k	Ratio_Avg_Len_2k	Cluster_idx
ORD	04L_22R	7497.639475	04L	22R	6	4748.333333	1838.543735	0.633310437	6	4748.333333	1838.543735	0.633310437	3
ORD	04R_22L	8070.582869	04R	22L	6	5196.166667	2505.226889	0.643840321	5	5918.2	1983.736676	0.733305152	9
ORD	09L_27R	7480.301161	09L	27R	2	6521.5	1030.25458	0.871823187	2	6521.5	1030.25458	0.871823187	7
ORD	09R_27L	7945.756479	09R	27L	10	5326.5	1741.621419	0.670357821	10	5326.5	1741.621419	0.670357821	9
ORD	10C_28C	10771.83976	10C	28C	15	6584.866667	2699.789433	0.611303808	15	6584.866667	2699.789433	0.611303808	11
ORD	10L_28R	12966.0065	10L	28R	16	8090.375	3121.28155	0.623968143	16	8090.375	3121.28155	0.623968143	16
ORD	10R_28L	7480.441081	10R	28L	3	5987.666667	1219.707069	0.800442996	3	5987.666667	1219.707069	0.800442996	7
DEN	35L_17R	12014.59113	35L	17R	8	8179.25	3230.863562	0.680776392	8	8179.25	3230.863562	0.680776392	4
DEN	08_26	11967.35275	8	26	7	7238.142857	4202.83295	0.604824058	6	8219	3621.475887	0.686785137	5
DEN	35R_17L	12014.8439	35R	17L	6	8445.5	3382.674548	0.702922158	6	8445.5	3382.674548	0.702922158	4
DEN	34L_16R	16019.59314	34L	16R	13	9690.153846	3881.629551	0.604893888	13	9690.153846	3881.629551	0.604893888	10
DEN	07_25	11966.88712	7	25	5	8779	3623.837745	0.733607655	5	8779	3623.837745	0.733607655	4
DEN	34R_16L	12014.54798	34R	16L	12	6978.333333	3618.589638	0.580823627	11	7491.545455	3305.587069	0.623539518	5
CLT	18L_36R	8695.787404	18L	36R	21	5207.095238	2008.424679	0.598806644	21	5207.095238	2008.424679	0.598806644	17
CLT	05_23	7500.737045	5	23	14	4827.714286	1764.948089	0.643631987	14	4827.714286	1764.948089	0.643631987	3
CLT	18C_36C	10022.21258	18C	36C	17	4810.411765	2553.745975	0.479975028	16	5034.0625	2459.546719	0.502290533	15

CLT	18R_36L	9018.931379	18R	36L	6	5631	3071.478276	0.6243533348	5	6477	2534.680157	0.718156035	1
LGA	04_22	7003.753297	4	22	17	3463.764706	1522.355269	0.4945583555	14	3926.785714	1237.639265	0.560668765	13
LGA	13_31	6994.745684	13	31	9	3901.666667	2125.11982	0.5577996446	6	5094.5	1427.831047	0.728332413	13
IAD	01R_19L	11525.70053	01R	19L	8	6685.75	2971.137241	0.5800732011	8	6685.75	2971.137241	0.580073201	5
IAD	01C_19C	11526.66642	01C	19C	13	5102	3099.911289	0.4426258055	11	5693.181818	3005.399468	0.493913991	11
IAD	01L_19R	9421.743546	01L	19R	5	6248.4	2746.131424	0.6631893352	5	6248.4	2746.131424	0.663189352	12
IAD	12_30	10475.62682	12	30	7	6815.857143	2987.553203	0.6506395552	7	6815.857143	2987.553203	0.650639552	11
MCO	18R_36L	12047.24861	18R	36L	8	7334.25	3065.721018	0.6087904058	8	7334.25	3065.721018	0.608790458	5
MCO	18L_36R	12048.9616	18L	36R	11	7525.090909	3153.450474	0.6245426922	11	7525.090909	3153.450474	0.624542692	5
MCO	17R_35L	10038.25709	17R	35L	11	5348.636364	2351.56094	0.5328252022	11	5348.636364	2351.56094	0.532825202	15
MCO	17L_35R	9031.986544	17L	35R	6	5782.166667	2889.114841	0.6401876975	5	6587.8	2359.214424	0.729385498	1
SAN	09_27	6878.959622	9	27	13	4813.230769	2352.896129	0.6993033011	11	5444.363636	1932.275616	0.791451605	3
SEA	16R_34L	8501.30157	16R	34L	5	5740.2	1808.502006	0.6752142154	5	5740.2	1808.502006	0.675214254	9
SEA	16C_34C	9427.879839	16C	34C	12	5545.583333	2441.797418	0.5882110755	11	5868.545455	2276.355041	0.622467146	1
SEA	16L_34R	11902.6617	16L	34R	15	6898.466667	2725.362829	0.5795734477	15	6898.466667	2725.362829	0.579573447	5
FLL	10L_28R	7803.732011	10L	28R	15	5567.2	2237.020442	0.7134022533	14	5849.285714	2025.784802	0.749549793	9
FLL	10R_28L	7984.951493	10R	28L	8	5131.375	2424.082739	0.6423070634	6	6195.666667	1670.093011	0.775917884	9
FLL	10R_28L	7984.951493	10R	28L	8	5131.375	2424.082739	0.6423070634	6	6195.666667	1670.093011	0.775917884	9
BDL	01_19	3796.165355	1	19	4	2450	1154.694765	0.6453881134	3	3004.666667	392.4911889	0.791500471	19

BDL	06_24	9502.708558	6	24	12	4393.916667	2188.191884	0.46238571	12	4393.916667	2188.191884	0.462385712	17
BDL	15_33	6841.610849	15	33	10	3730	2041.137482	0.545193242	7	4615.714286	1776.473634	0.674653146	13
BOS	04L_22R	7049.542113	04L	22R	10	5036.5	2171.771589	0.714443565	10	5036.5	2171.771589	0.714443565	3
BOS	04R_22L	7656.954735	04R	22L	13	4385.153846	2209.906101	0.572702073	13	4385.153846	2209.906101	0.572702073	14
BOS	09_27	6983.532237	9	27	7	4725.571429	1713.923263	0.676673533	7	4725.571429	1713.923263	0.676673533	3
BOS	14_32	4993.246448	14	32	2	3047	687.3077913	0.610224236	2	3047	687.3077913	0.610224236	2
BOS	15L_33R	2554.99332	15L	33R	2	1603.5	598.9194437	0.627594596	1	2027	0	0.793348454	8
BOS	15R_33L	9194.283556	15R	33L	11	4812.636364	2079.589107	0.523437888	11	4812.636364	2079.589107	0.523437888	17
BWI	10_28	9230.923049	10	28	11	5591.090909	3113.362506	0.605691422	9	6487.555556	2672.771086	0.702806807	1
BWI	15L_33R	5000.915155	15L	33R	7	3014.285714	1488.425887	0.602746821	4	4081.25	900.2967566	0.816100628	2
BWI	15R_33L	8702.576535	15R	33L	10	5387.4	2090.991907	0.619058043	10	5387.4	2090.991907	0.619058043	17
CLE	06L_24R	8990.552256	06L	24R	8	6993.375	1479.447478	0.777858223	8	6993.375	1479.447478	0.777858223	20
CLE	06R_24L	8021.136093	06R	24L	9	4564.666667	2356.485731	0.569079818	7	5478	1739.137717	0.682945645	14
CLE	10_28	6001.817872	10	28	2	5429	490.7321061	0.904559271	2	5429	490.7321061	0.904559271	3
DFW	13L_31R	8375.121306	13L	31R	3	6663.333333	2287.216941	0.795610367	3	6663.333333	2287.216941	0.795610367	12
DFW	13R_31L	9305.827399	13R	31L	6	5944.333333	2657.727576	0.638775369	6	5944.333333	2657.727576	0.638775369	1
DFW	17C_35C	13435.99262	17C	35C	24	7290.5	3671.524361	0.542609706	22	7784	3420.853013	0.579339407	16
DFW	17L_35R	8522.524149	17L	35R	8	5056.125	2584.889743	0.593266139	7	5572.857143	2302.857169	0.653897489	17
DFW	17R_35L	13435.58263	17R	35L	29	7724.517241	3638.226595	0.57492983	27	8158.703704	3378.794992	0.607245992	16

DFW	18L_36R	13435.26868	18L	36R	28	7543.821429	3569.619464	0.56149390 1	26	7980.730769	3313.940658	0.594013485	16
DFW	18R_36L	13435.67573	18R	36L	23	7339.086957	3422.047406	0.54623876 8	21	7860.714286	3097.725184	0.585062817	16
DTW	03L_21R	8502.177628	03L	21R	8	5831.875	2013.689467	0.68592721 2	8	5831.875	2013.689467	0.685927212	9
DTW	03R_21L	10002.50597	03R	21L	14	6065.071429	2831.136289	0.60635519 2	14	6065.071429	2831.136289	0.606355192	15
DTW	04L_22R	10002.02538	04L	22R	6	6325.833333	3047.650007	0.63245523 7	6	6325.833333	3047.650007	0.632455237	11
DTW	04R_22L	11496.03927	04R	22L	14	6801.285714	3361.062342	0.59161991	12	7690.333333	2704.601208	0.668955034	5
DTW	09L_27R	8684.764199	09L	27R	17	4930.588235	2180.107883	0.56772851	17	4930.588235	2180.107883	0.567728511	17
DTW	09R_27L	8477.424751	09R	27L	9	4397.777778	2421.188591	0.51876341 1	8	4730.875	2357.618746	0.558055676	14
EWR	04L_22R	7023.899724	04L	22R	22	5586.272727	2061.191222	0.79532353 1	20	5960.2	1754.062071	0.848559955	7
EWR	04R_22L	7021.050142	04R	22L	14	5756.357143	2249.779566	0.81987124 8	13	6059.461538	2022.351174	0.863042054	7
EWR	11_29	6485.713936	11	29	15	4247.533333	1500.23388	0.65490605 6	13	4619.461538	1225.51321	0.712251817	13
HOU	04_22	7607.331123	4	22	14	4487.571429	1633.204811	0.58990089 4	14	4487.571429	1633.204811	0.589900894	3
HOU	17_35	6018.640004	17	35	10	3716.9	1548.024795	0.61756476 5	8	4269.125	1156.925042	0.709317221	13
LAS	01L_19R	8410.763134	01L	19R	12	5463.666667	2645.81537	0.64960415 4	10	6166.6	2293.874461	0.733179606	9
LAS	01R_19L	8411.804939	01R	19L	13	5931.384615	2375.981044	0.70512626 7	13	5931.384615	2375.981044	0.705126267	9
LAS	07L_25R	10950.30941	07L	25R	13	7365.230769	3359.028807	0.67260480 9	13	7365.230769	3359.028807	0.672604809	5
LAS	07R_25L	10499.91104	07R	25L	6	5544.666667	2799.318608	0.52806796 6	6	5544.666667	2799.318608	0.528067966	15
LAX	06L_24R	8906.903159	06L	24R	5	4688.4	2781.735483	0.52637823 9	4	5499.75	2434.914971	0.617470506	17
LAX	06R_24L	8710.017426	06R	24L	15	6100.266667	3000.701501	0.70037364 7	13	6818.769231	2511.790734	0.782865165	12

LAX	07L_25R	11110.53687	07L	25R	19	6513.210526	3143.430832	0.58621924	17	7056	2853.497372	0.635072822	11
LAX	07R_25L	11071.56621	07R	25L	16	5736.125	2873.910712	0.51809517	14	6285.285714	2632.836477	0.567696168	11
MDW	04L_22R	3868.894434	04L	22R	10	2486.7	1391.909643	0.64274175	5	3682.8	813.1332609	0.951899842	19
MDW	04R_22L	5289.492026	04R	22L	18	3636.611111	1550.340158	0.68751613	14	4180.642857	1305.846593	0.790367551	2
MDW	13C_31C	5358.936035	13C	31C	13	3882.615385	1330.792843	0.72451235	11	4235.818182	1110.510317	0.790421486	2
MDW	13L_31R	4384.93334	13L	31R	6	2876.666667	677.5507853	0.65603429	6	2876.666667	677.5507853	0.656034298	19
MDW	13R_31L	3856.09019	13R	31L	6	2820	621.4898229	0.73131069	6	2820	621.4898229	0.731310696	19
MEM	09_27	8926.418519	9	27	13	4778.692308	2630.314664	0.53534262	12	5072.25	2515.030964	0.568229015	17
MEM	18C_36C	11144.54307	18C	36C	16	6350	3209.943115	0.56978558	14	6972.214286	2924.632158	0.625616882	11
MEM	18L_36R	9020.460473	18L	36R	13	5686.846154	2790.457843	0.63043856	11	6448.090909	2275.932796	0.714829462	1
MEM	18R_36L	9342.252489	18R	36L	6	6283.833333	2511.573484	0.67262508	6	6283.833333	2511.573484	0.672625081	12
MIA	08L_26R	8585.176495	08L	26R	14	5352.857143	2297.739453	0.62349995	14	5352.857143	2297.739453	0.623499953	9
MIA	08R_26L	10487.63258	08R	26L	21	5571.571429	2753.865675	0.53125158	18	6178.222222	2488.834586	0.589095983	15
MIA	09_27	11377.11591	9	27	7	6965	3439.232957	0.61219381	7	6965	3439.232957	0.612193815	5
MIA	12_30	8411.853559	12	30	15	5685.933333	1983.036757	0.67594297	15	5685.933333	1983.036757	0.675942977	9
MKE	01L_19R	8912.779803	01L	19R	12	5768.833333	2623.895606	0.64725410	11	6179.090909	2313.352997	0.693284368	1
MKE	01R_19L	4185.119997	01R	19L	4	2030.5	1030.304324	0.48517127	3	2523	370.0716147	0.602850098	19
MKE	07L_25R	4788.857715	07L	25R	9	2716.666667	1424.366263	0.56728907	6	3504.666667	905.0040147	0.731837711	18
MKE	07R_25L	7848.68738	07R	25L	11	5062.454545	1986.343846	0.64500652	11	5062.454545	1986.343846	0.645006522	9

MKE	13_31	4588.066807	13	31	9	2359.888889	1075.500633	0.5143536436	3	3599.666667	1000.579998	0.784571546	18
MSP	04_22	8446.723309	4	22	21	5477.952381	2039.928564	0.6485298871	19	5846.947368	1764.806835	0.692214857	9
MSP	12L_30R	7984.869598	12L	30R	9	4640.888889	2104.353134	0.5812103541	9	4640.888889	2104.353134	0.581210354	14
MSP	12R_30L	9981.049011	12R	30L	23	5513.173913	2608.089769	0.5523641766	21	5870.47619	2437.371199	0.588162245	15
MSP	17_35	8003.903833	17	35	11	4803.454545	1983.276096	0.6001389633	11	4803.454545	1983.276096	0.600138963	14
PHL	08_26	4989.100436	8	26	2	1897	985.706853	0.3802288626	1	2594	0	0.519933341	18
PHL	09L_27R	9478.532834	09L	27R	19	5919.105263	2214.99152	0.6247483479	18	6138.611111	2055.592805	0.647633048	12
PHL	09R_27L	10482.59512	09R	27L	15	6224.4	2572.808243	0.5937842622	15	6224.4	2572.808243	0.593784262	11
PHL	17_35	6506.893668	17	35	14	4263.5	1547.686351	0.6552281655	13	4465.153846	1406.485866	0.686218966	13
PHX	07L_25R	10276.98475	07L	25R	29	6475.931034	2349.753679	0.6301392028	28	6636.714286	2224.496345	0.645784191	11
PHX	07R_25L	7782.667941	07R	25L	9	5084	1507.104177	0.6532464424	9	5084	1507.104177	0.653246424	3
PHX	08_26	10567.45293	8	26	24	6826.541667	2810.529766	0.6459968844	22	7280.818182	2461.092008	0.688985154	11
PVD	05_23	7166.370169	5	23	9	4794.333333	1487.199381	0.6690044422	8	5187.375	968.902905	0.723849714	3
PVD	16_34	5514.864465	16	34	7	2846.857143	1225.544155	0.5162152151	5	3240.8	1254.064073	0.587648168	2
SDF	11_29	7236.402764	11	29	15	4883	2117.863917	0.6747827844	12	5765.083333	1195.382819	0.796678062	3
SDF	17L_35R	7812.144279	17L	35R	15	4451.466667	2024.769294	0.5698136778	13	4958.538462	1639.275583	0.634721823	14
SDF	17R_35L	10014.76088	17R	35L	16	5748.1875	2636.419851	0.5739715178	16	5748.1875	2636.419851	0.573971518	15
SFO	01L_19R	7016.582924	01L	19R	12	4689.75	1551.479594	0.6683808899	12	4689.75	1551.479594	0.668380899	3
SFO	01R_19L	8097.609143	01R	19L	16	4641.375	2040.894669	0.5731784433	13	5315.230769	1605.952114	0.656395076	14

SFO	10L_28R	11553.1901	10L	28R	21	6721.285714	2835.598229	0.5817688765	21	6721.285714	2835.598229	0.581768815	5
SFO	10R_28L	11065.18837	10R	28L	20	6096.55	2652.864638	0.5509666671	20	6096.55	2652.864638	0.550966671	11
SLC	14_32	4893.622803	14	32	4	3747.25	766.5534888	0.7657414787	4	3747.25	766.5534888	0.765741487	2
SLC	16L_34R	12016.42941	16L	34R	14	7003.5	3142.468622	0.5828270413	13	7392.461538	2898.871062	0.615196186	5
SLC	16R_34L	12013.0842	16R	34L	9	6671.222222	3346.448893	0.5553296815	9	6671.222222	3346.448893	0.555329681	5
SLC	17_35	9283.167504	17	35	10	5551.6	2570.197104	0.5980286361	10	5551.6	2570.197104	0.598028636	1
SNA	02L_20R	5709.338789	02L	20R	10	3884.6	1413.117373	0.6803940259	9	4129.888889	1252.852197	0.723356774	2
SNA	02R_20L	2890.417448	02R	20L	6	2108	746.7133319	0.7293064204	4	2582.5	169.4038567	0.893469558	8
JFK	04L_22R	8197.116059	04L	22R	20	7770.15	2975.373754	0.9479126491	20	7770.15	2975.373754	0.947912649	6
JFK	04R_22L	8402.665789	04R	22L	6	4899.333333	2242.893994	0.5830689285	5	5527.8	1823.715767	0.657862652	17
JFK	13L_31R	8053.821147	13L	31R	13	5575.307692	1872.066033	0.6925620913	13	5575.307692	1872.066033	0.692256209	9
JFK	13R_31L	9190.3693	13R	31L	16	8584.5	3201.005113	0.9340756311	16	8584.5	3201.005113	0.934075631	6
IAH	08L_26R	8982.262836	08L	26R	4	7302.75	1603.203333	0.8130189161	4	7302.75	1603.203333	0.813018961	20
IAH	08R_26L	9383.711471	08R	26L	6	5953.666667	2828.479785	0.6344682151	6	5953.666667	2828.479785	0.634468215	1
IAH	09_27	9980.153523	9	27	3	7604	2148.885525	0.7619121277	3	7604	2148.885525	0.761912127	20
IAH	15L_33R	12025.15071	15L	33R	9	7239.666667	3390.716849	0.6020437336	8	7920.625	2893.070042	0.658671578	5
IAH	15R_33L	10019.57343	15R	33L	9	6953.444444	2637.067031	0.6939860759	9	6953.444444	2637.067031	0.693986075	20
ATL	08L_26R	8980.507664	08L	26R	13	5415.461538	2164.404176	0.6030239873	13	5415.461538	2164.404176	0.603023987	17
ATL	08R_26L	9977.421136	08R	26L	15	5264.333333	2640.639118	0.5276246513	13	5784.461538	2436.432215	0.579755175	15

ATL	09L_27R	11863.48892	09L	27R	23	6875.73913	3260.555115	0.57957142 1	21	7371.619048	2953.834228	0.621370248	5
ATL	09R_27L	8980.297581	09R	27L	13	5491	2558.695892	0.61144967 1	11	6162.272727	2152.775004	0.686199168	1
ATL	10_28	8980.471489	10	28	6	5431.5	2856.169445	0.60481234 3	5	6153.6	2507.272781	0.685220148	1
STL	06_24	7594.736137	6	24	9	3985.444444	2220.408865	0.52476404 3	8	4256.25	2209.122563	0.560421005	14
STL	11_29	8988.676576	11	29	5	6317.8	2492.902064	0.70286208 9	5	6317.8	2492.902064	0.702862089	12
STL	11_29	8988.676576	11	29	5	6317.8	2492.902064	0.70286208 9	5	6317.8	2492.902064	0.702862089	12
STL	12R_30L	10337.35534	12R	30L	18	6226.111111	2626.8629	0.60229245 4	18	6226.111111	2626.8629	0.602292454	11
STL	12L_30R	8991.269469	12L	30R	12	4553.083333	2231.144283	0.50638937 6	10	5125.1	1975.569367	0.570008497	17
STL	12R_30L	10337.35534	12R	30L	18	6226.111111	2626.8629	0.60229245 4	18	6226.111111	2626.8629	0.602292454	11
ORD	04L_22R	7497.639475	22R	04L	9	5974.555556	1747.772018	0.79685820 8	9	5974.555556	1747.772018	0.796858208	7
ORD	04R_22L	8070.582869	22L	04R	4	5057.75	2253.05206	0.62668955 7	4	5057.75	2253.05206	0.626689557	9
ORD	09L_27R	7480.301161	27R	09L	2	6438	1134.199277	0.86066053 5	2	6438	1134.199277	0.860660535	7
ORD	09R_27L	7945.756479	27L	09R	10	4667.4	2101.363959	0.58740788 4	9	4971.222222	1982.229162	0.625644926	14
ORD	10C_28C	10771.83976	28C	10C	17	6432.352941	2881.111416	0.59714525	17	6432.352941	2881.111416	0.597145225	11
ORD	10L_28R	12966.0065	28R	10L	18	7743.111111	3613.326264	0.59718550 3	18	7743.111111	3613.326264	0.597185503	16
ORD	10R_28L	7480.441081	28L	10R	3	6000.333333	1197.969254	0.8021363	3	6000.333333	1197.969254	0.8021363	7
DEN	35L_17R	12014.59113	17R	35L	10	6912.5	4040.196674	0.57534209 3	8	8263.125	3250.053557	0.687757487	5
DEN	08_26	11967.35275	26	8	7	7448.428571	4099.528056	0.62239567 3	6	8470.833333	3374.424361	0.707828499	5
DEN	35R_17L	12014.8439	17L	35R	6	8232.5	3591.770079	0.68519408 7	6	8232.5	3591.770079	0.685194087	4

DEN	34L_16R	16019.59314	16R	34L	11	9608.636364	4303.986623	0.59980526	11	9608.636364	4303.986623	0.599805269	10
DEN	07_25	11966.88712	25	7	5	9048	3320.258348	0.75608635	5	9048	3320.258348	0.756086355	4
DEN	34R_16L	12014.54798	16L	34R	10	7505.1	3010.188198	0.62466769	10	7505.1	3010.188198	0.624667695	5
CLT	18L_36R	8695.787404	36R	18L	23	5306.173913	2082.120743	0.61020051	23	5306.173913	2082.120743	0.610200511	17
CLT	05_23	7500.737045	23	5	13	4417.615385	1942.077004	0.58895750	12	4619.916667	1879.93063	0.615928336	14
CLT	18C_36C	10022.21258	36C	18C	17	5834.352941	2322.910538	0.58214220	16	6122.125	2062.515353	0.610855632	15
CLT	18R_36L	9018.931379	36L	18R	6	5649.666667	3043.881907	0.62642306	5	6499.4	2483.177561	0.7206397	1
LGA	04_22	7003.753297	22	4	20	4207.45	1538.206525	0.60074217	20	4207.45	1538.206525	0.600742177	13
LGA	13_31	6994.745684	31	13	9	4444.666667	1624.415202	0.63542934	8	4761.375	1408.54017	0.680707379	3
IAD	01R_19L	11525.70053	19L	01R	8	6715.625	2956.554942	0.58266523	8	6715.625	2956.554942	0.582665234	5
IAD	01C_19C	11526.66642	19C	01C	14	7740.285714	2673.277517	0.67151121	14	7740.285714	2673.277517	0.671511214	4
IAD	01L_19R	9421.743546	19R	01L	6	6133.5	2636.945942	0.65099415	6	6133.5	2636.945942	0.650994157	12
IAD	12_30	10475.62682	30	12	5	6161.2	2555.143969	0.58814619	5	6161.2	2555.143969	0.588146119	11
MCO	18R_36L	12047.24861	36L	18R	10	7813.3	3465.423913	0.64855472	10	7813.3	3465.423913	0.648554724	4
MCO	18L_36R	12048.9616	36R	18L	12	7439.833333	3505.274619	0.61746676	12	7439.833333	3505.274619	0.617466764	5
MCO	17R_35L	10038.25709	35L	17R	12	6069.333333	2426.800787	0.60462023	12	6069.333333	2426.800787	0.604620232	15
MCO	17L_35R	9031.986544	35R	17L	5	6219.6	2662.900918	0.68861927	5	6219.6	2662.900918	0.688619272	12
SAN	09_27	6878.959622	27	9	11	3292.363636	2323.677614	0.47861360	8	4252.625	1947.094901	0.618207583	13
SEA	16R_34L	8501.301577	34L	16R	5	5409.6	2172.686425	0.63632609	5	5409.6	2172.686425	0.636326091	9

SEA	16C_34C	9427.879839	34C	16C	13	6104.923077	2419.434695	0.64753933	13	6104.923077	2419.434695	0.647539339	12
SEA	16L_34R	11902.6617	34R	16L	20	7329.75	3418.793506	0.615807639	20	7329.75	3418.793506	0.615807639	5
FLL	10L_28R	7803.732011	28R	10L	16	4981	2457.207032	0.638284348	13	5802.153846	1906.171724	0.743510136	14
FLL	10R_28L	7984.951493	28L	10R	8	5644.625	1882.704509	0.706907864	8	5644.625	1882.704509	0.706907864	9
FLL	10R_28L	7984.951493	28L	10R	8	5644.625	1882.704509	0.706907864	8	5644.625	1882.704509	0.706907864	9
BDL	01_19	3796.165355	19	1	4	2082	1649.883632	0.548448185	2	3427	964.4936495	0.902753089	19
BDL	06_24	9502.708558	24	6	10	6013.3	2209.462632	0.632798529	10	6013.3	2209.462632	0.632798529	12
BDL	15_33	6841.610849	33	15	10	4139.2	1924.71636	0.605003718	8	4829.5	1428.297388	0.705901009	13
BOS	04L_22R	7049.542113	22R	04L	11	5086.272727	1499.738655	0.721503985	11	5086.272727	1499.738655	0.721503985	3
BOS	04R_22L	7656.954735	22L	04R	14	5208.285714	1751.661121	0.680203279	14	5208.285714	1751.661121	0.680203279	3
BOS	09_27	6983.532237	27	9	8	4781.625	1837.859231	0.684700068	8	4781.625	1837.859231	0.684700068	3
BOS	14_32	4993.246448	32	14	3	3574.666667	1383.940148	0.715900307	3	3574.666667	1383.940148	0.715900307	2
BOS	15L_33R	2554.99332	33R	15L	5	1933.2	559.1356723	0.756636029	2	2475	101.8233765	0.968691378	8
BOS	15R_33L	9194.283556	33L	15R	14	5953.071429	2248.782114	0.647475292	14	5953.071429	2248.782114	0.647475292	12
BWI	10_28	9230.923049	28	10	9	5241.666667	2713.795912	0.56783776	8	5800.25	2281.991658	0.628349946	1
BWI	15L_33R	5000.915155	33R	15L	7	3117.428571	1492.597055	0.623371618	5	3860.4	960.6603458	0.771938711	2
BWI	15R_33L	8702.576535	33L	15R	10	4637	2197.945303	0.532830706	9	4956.666667	2070.080373	0.569563123	17
CLE	06L_24R	8990.552256	24R	06L	5	6231	2064.177802	0.693060874	5	6231	2064.177802	0.693060874	12
CLE	06R_24L	8021.136093	24L	06R	13	5987.538462	2646.002696	0.746470125	13	5987.538462	2646.002696	0.746470125	9

CLE	10_28	6001.817872	28	10	2	5346.5	656.902199	0.8908134363	2	5346.5	656.902199	0.890813436	3
DFW	13L_31R	8375.121306	31R	13L	7	6579.428571	2802.697977	0.7855920333	6	7392.666667	1967.421426	0.882693682	12
DFW	13R_31L	9305.827399	31L	13R	5	5286	2525.772654	0.5680311677	5	5286	2525.772654	0.568031167	1
DFW	17C_35C	13435.99262	35C	17C	23	6967.826087	3564.501197	0.5185940699	23	6967.826087	3564.501197	0.518594069	16
DFW	17L_35R	8522.524149	35R	17L	8	5620.75	2248.773618	0.6595170527	7	6149.571429	1813.760445	0.721566911	9
DFW	17R_35L	13435.58263	35L	17R	29	7470.724138	3739.429319	0.5560402066	29	7470.724138	3739.429319	0.556040206	16
DFW	18L_36R	13435.26868	36R	18L	29	7474.862069	3741.293586	0.5563611936	29	7474.862069	3741.293586	0.556361193	16
DFW	18R_36L	13435.67573	36L	18R	24	6986.333333	3693.199587	0.5199837161	24	6986.333333	3693.199587	0.519983716	16
DTW	03L_21R	8502.177628	21R	03L	8	5786.125	1847.108662	0.6805462388	8	5786.125	1847.108662	0.680546238	9
DTW	03R_21L	10002.50597	21L	03R	12	5463	2638.977281	0.5461631333	10	6181.2	2252.345385	0.617965114	15
DTW	04L_22R	10002.02538	22R	04L	5	5695.4	2979.209677	0.569424675	5	5695.4	2979.209677	0.569424675	15
DTW	04R_22L	11496.03927	22L	04R	13	6410.692308	3363.655511	0.5576435644	11	7231.181818	2960.339907	0.629015059	5
DTW	09L_27R	8684.764199	27R	09L	20	5483.2	2001.991813	0.6313585335	18	5888.777778	1654.571053	0.678058453	9
DTW	09R_27L	8477.424751	27L	09R	9	5251.111111	2109.560289	0.619422918	8	5690.25	1761.381905	0.671223888	9
EWR	04L_22R	7023.899724	22R	04L	21	6055.809524	2608.578149	0.8621719979	19	6512.947368	2290.112624	0.927255175	7
EWR	04R_22L	7021.050142	22L	04R	8	4460	2226.788719	0.6352326099	7	4864.571429	2063.336526	0.692855247	3
EWR	11_29	6485.713936	29	11	13	3450.153846	1639.218912	0.5319620755	10	3959.5	1521.053162	0.610495628	13
HOU	04_22	7607.331123	22	4	14	4584.071429	1608.747887	0.6025860266	14	4584.071429	1608.747887	0.602586026	3
HOU	17_35	6018.640004	35	17	9	3897.111111	1431.445462	0.6475069308	8	4148.75	1300.170071	0.689316855	13

LAS	01L_19R	8410.763134	19R	01L	13	6480.615385	2061.089378	0.7705145512	13	6480.615385	2061.089378	0.770514552	12
LAS	01R_19L	8411.804939	19L	01R	12	5949.916667	2306.997831	0.7073293677	12	5949.916667	2306.997831	0.707329367	9
LAS	07L_25R	10950.30941	25R	07L	22	8851.454545	3711.188485	0.8083291733	22	8851.454545	3711.188485	0.808329173	4
LAS	07R_25L	10499.91104	25L	07R	6	5906.833333	2661.218925	0.5625603222	6	5906.833333	2661.218925	0.562560322	15
LAX	06L_24R	8906.903159	24R	06L	5	5373.8	2335.003362	0.6033297899	5	5373.8	2335.003362	0.603329789	17
LAX	06R_24L	8710.017426	24L	06R	14	5975	2660.970766	0.6859917399	14	5975	2660.970766	0.685991739	12
LAX	07L_25R	11110.53687	25R	07L	15	6473.933333	2826.858111	0.5826841144	14	6794.5	2635.490722	0.6115366052	11
LAX	07R_25L	11071.56621	25L	07R	16	6089.4375	2810.806266	0.5500068722	16	6089.4375	2810.806266	0.550006872	11
MDW	04L_22R	3868.894434	22R	04L	7	2902.142857	965.9645315	0.7501220007	6	3088.5	909.9348878	0.798290068	19
MDW	04R_22L	5289.492026	22L	04R	15	3636.533333	1232.235707	0.6875014313	13	3895.692308	1107.144931	0.736496489	2
MDW	13C_31C	5358.936035	31C	13C	11	3546.363636	1474.190712	0.6617663688	9	3929.111111	1345.401840	0.733188656	2
MDW	13L_31R	4384.933334	31R	13L	9	2700.444444	1543.260113	0.6158461779	4	4199.5	896.0913272	0.957711252	18
MDW	13R_31L	3856.090199	31L	13R	7	2509.285714	1132.878886	0.6507331504	4	3357	544.7953744	0.870570924	19
MEM	09_27	8926.418519	27	9	12	5572.333333	1899.305887	0.6242518577	12	5572.333333	1899.305887	0.624251857	17
MEM	18C_36C	11144.54307	36C	18C	19	7635.473684	2724.594269	0.6851311357	19	7635.473684	2724.594269	0.685131135	5
MEM	18L_36R	9020.460473	36R	18L	11	6068.818182	2215.336174	0.6727836344	11	6068.818182	2215.336174	0.672783634	12
MEM	18R_36L	9342.252489	36L	18R	6	6419.333333	2466.535033	0.6871290777	6	6419.333333	2466.535033	0.687129077	12
MIA	08L_26R	8585.176495	26R	08L	14	5447.071429	2256.639485	0.6344740178	14	5447.071429	2256.639485	0.634474018	9
MIA	08R_26L	10487.63258	26L	08R	21	5874.857143	2583.686964	0.5601719	19	6306.157895	2314.169740	0.601294701	15

MIA	09_27	11377.11591	27	9	7	7178.285714	3952.38391	0.6309407021	7	7178.285714	3952.38391	0.630940721	5
MIA	12_30	8411.853559	30	12	13	3986	2209.406519	0.47385513	11	4394	2160.392511	0.522358119	14
MKE	01L_19R	8912.779803	19R	01L	7	5572	2690.997337	0.625169714	7	5572	2690.997337	0.625169714	1
MKE	01R_19L	4185.119997	19L	01R	3	2956.333333	1067.176805	0.706391534	2	3533.5	528.2087655	0.844300761	19
MKE	07L_25R	4788.857715	25R	07L	7	3131.428571	1360.707029	0.653898854	4	4180	531.2249994	0.87285951	2
MKE	07R_25L	7848.68738	25L	07R	10	3818.7	1893.095704	0.486539954	8	4319.875	1781.141162	0.550394581	14
MKE	13_31	4588.066807	31	13	10	3253.4	1065.084264	0.709100398	10	3253.4	1065.084264	0.709100398	2
MSP	04_22	8446.723309	22	4	20	5490.3	2516.365301	0.649991695	20	5490.3	2516.365301	0.649991695	9
MSP	12L_30R	7984.869598	30R	12L	13	5300.461538	2000.421315	0.663813162	12	5614.666667	1722.026994	0.703163226	9
MSP	12R_30L	9981.049011	30L	12R	22	5930.909091	2453.595708	0.594217009	20	6341.7	2167.923481	0.635374097	15
MSP	17_35	8003.903833	35	17	11	5189.545455	1900.781174	0.648376788	11	5189.545455	1900.781174	0.648376788	9
PHL	08_26	4989.100436	26	8	5	3932	1198.550374	0.788118029	5	3932	1198.550374	0.788118029	2
PHL	09L_27R	9478.532834	27R	09L	17	5335	2413.666868	0.562850822	17	5335	2413.666868	0.562850822	1
PHL	09R_27L	10482.59512	27L	09R	14	5454.5	2554.743424	0.520338708	13	5741.615385	2412.537859	0.547728432	15
PHL	17_35	6506.893668	35	17	13	3796.230769	1760.403566	0.583416752	11	4227	1546.627169	0.64961873	13
PHX	07L_25R	10276.98475	25R	07L	26	5610.192308	2668.435572	0.545898674	24	5930.875	2518.871768	0.577102637	15
PHX	07R_25L	7782.667941	25L	07R	15	4861.4	1983.848489	0.624644407	14	5080.357143	1861.167938	0.652778351	14
PHX	08_26	10567.45293	26	8	26	6426.461538	3131.602277	0.608137229	24	6816.083333	2932.647311	0.64500721	11
PVD	05_23	7166.370169	23	5	9	3437.333333	2105.328419	0.479647751	7	3962.714286	2110.533322	0.552959754	13

PVD	16_34	5514.864465	34	16	12	3948.75	1352.336976	0.71601941	12	3948.75	1352.336976	0.71601941	2
SDF	11_29	7236.402764	29	11	13	4584.384615	2032.816912	0.633517062	11	5168.636364	1586.871215	0.714254932	3
SDF	17L_35R	7812.144279	35R	17L	15	4279.2	2289.538263	0.547762541	13	4736.153846	2101.947107	0.606255297	14
SDF	17R_35L	10014.76088	35L	17R	17	5927.117647	2767.019265	0.59183816	15	6484.466667	2433.339735	0.647490913	15
SFO	01L_19R	7016.582924	19R	01L	16	4762.3125	2093.227005	0.678722471	14	5195.642857	1854.167182	0.740480504	3
SFO	01R_19L	8097.609143	19L	01R	17	4808.411765	2352.695264	0.593806354	15	5265.266667	2103.593166	0.650224847	14
SFO	10L_28R	11553.1901	28R	10L	25	6739.96	2982.953423	0.583385194	24	6938.333333	2873.727161	0.600555628	5
SFO	10R_28L	11065.18837	28L	10R	25	6763.28	2947.661114	0.611221407	23	7180.521739	2683.935626	0.648929011	11
SLC	14_32	4893.622803	32	14	5	2483.4	1919.323396	0.507476792	2	4584	118.7939392	0.936729328	18
SLC	16L_34R	12016.42941	34R	16L	14	6508.928571	2913.660359	0.541669105	14	6508.928571	2913.660359	0.541669105	5
SLC	16R_34L	12013.0842	34L	16R	9	6652.444444	3384.472046	0.553766571	9	6652.444444	3384.472046	0.553766571	5
SLC	17_35	9283.167504	35	17	10	5822.5	2377.258377	0.627210486	10	5822.5	2377.258377	0.627210486	1
SNA	02L_20R	5709.338789	20R	02L	13	3384.846154	1376.134008	0.592861324	11	3743.909091	1162.183932	0.655751783	2
SNA	02R_20L	2890.417448	20L	02R	4	2089.5	714.7598664	0.722905961	2	2708.5	0.707106781	0.937061877	8
JFK	04L_22R	8197.116059	22R	04L	10	4834.1	2281.982688	0.589731799	10	4834.1	2281.982688	0.589731799	14
JFK	04R_22L	8402.665789	22L	04R	6	4192.333333	2537.403213	0.498928964	4	5396	2221.584577	0.642177154	14
JFK	13L_31R	8053.821147	31R	13L	17	5168.647059	2623.629164	0.641763328	15	5640.333333	2416.722032	0.700330096	9
JFK	13R_31L	9190.3693	31L	13R	10	7008.5	3320.680728	0.762591771	9	7567.555556	2981.472048	0.823422358	12
IAH	08L_26R	8982.262836	26R	08L	4	7308.5	1602.341932	0.813659112	4	7308.5	1602.341932	0.813659112	20

IAH	08R_26L	9383.711471	26L	08R	8	6598.75	2684.603655	0.70321322	8	6598.75	2684.603655	0.703213224	12
IAH	09_27	9980.153523	27	9	3	7584.333333	2150.51955	0.75994155	3	7584.333333	2150.51955	0.75994155	20
IAH	15L_33R	12025.15071	33R	15L	9	8197	3492.96561	0.681654658	9	8197	3492.96561	0.681654658	4
IAH	15R_33L	10019.57343	33L	15R	9	7344.888889	2353.288414	0.73305405	9	7344.888889	2353.288414	0.73305405	20
ATL	08L_26R	8980.507664	26R	08L	13	5106.307692	2296.160142	0.56859900 2	13	5106.307692	2296.160142	0.568599002	17
ATL	08R_26L	9977.421136	26L	08R	16	6430.1875	2320.334407	0.64447389 9	16	6430.1875	2320.334407	0.644473899	15
ATL	09L_27R	11863.48892	27R	09L	22	6439.454545	3119.925117	0.54279601 8	21	6651.666667	3029.908304	0.560683852	5
ATL	09R_27L	8980.297581	27L	09R	11	5189	2309.966104	0.57782049 6	11	5189	2309.966104	0.577820496	17
ATL	10_28	8980.471489	28	10	6	5690.833333	2657.982575	0.63368981 7	5	6471	2065.463386	0.720563504	1
STL	06_24	7594.736137	24	6	12	5320.916667	1721.868565	0.70060586 3	12	5320.916667	1721.868565	0.700605863	3
STL	11_29	8988.676576	29	11	5	6301.4	2473.093063	0.70103757 2	5	6301.4	2473.093063	0.701037572	12
STL	11_29	8988.676576	29	11	5	6301.4	2473.093063	0.70103757 2	5	6301.4	2473.093063	0.701037572	12
STL	12R_30L	10337.35534	30L	12R	17	5715.294118	2757.578711	0.55287778 4	17	5715.294118	2757.578711	0.552877784	15
STL	12L_30R	8991.269469	30R	12L	12	5409.583333	2160.180609	0.60164844 9	12	5409.583333	2160.180609	0.601648449	17
STL	12R_30L	10337.35534	30L	12R	17	5715.294118	2757.578711	0.55287778 4	17	5715.294118	2757.578711	0.552877784	15

Appendix C – Individual Aircraft ROT Statistics and Aircraft Groupings

Aircraft Type	Average ROT	Standard Deviation	Median ROT	90th Percentile	Minimum ROT	Maximum ROT
A124	87.6	23.8	83.6	119.5	41.4	174.0
A306	60.8	14.9	58.0	77.5	25.9	171.0
A30B	62.6	11.5	61.1	74.7	35.8	152.9
A310	62.5	12.3	61.7	77.0	32.2	158.6
A318	48.1	13.2	45.3	61.0	26.4	163.9
A319	51.8	10.5	50.4	63.4	21.0	175.4
A320	51.9	10.4	50.6	63.9	22.0	174.7
A321	53.5	9.6	52.4	64.7	26.0	170.4
A332	65.5	13.1	63.8	81.6	28.6	176.7
A333	62.0	11.9	60.6	76.3	29.2	175.0
A342	76.0	18.9	70.5	99.3	47.6	142.9
A343	66.0	13.4	64.5	81.8	31.9	174.4
A346	63.5	12.5	61.8	79.0	32.1	152.3
A359	62.2	13.4	59.8	78.3	34.1	149.1
A388	76.7	16.7	72.2	99.4	39.0	176.7
A400	67.8	16.7	66.9	85.0	36.0	111.9
AA1	47.2	15.3	45.0	58.8	27.0	81.4
AA5	53.2	18.1	50.0	75.7	24.1	144.4
AC11	49.3	11.2	47.4	63.7	29.8	83.8
AC50	54.8	20.0	50.5	75.3	20.1	167.0
AC80	53.9	16.1	52.2	73.6	28.2	98.1
AC90	54.5	14.5	52.3	71.6	18.9	134.4
AC95	54.5	16.0	52.0	70.0	22.7	138.6
AEST	55.3	19.1	51.0	80.0	24.6	153.4
ASTR	53.6	13.2	51.3	69.3	24.8	157.0
AT42	51.3	10.7	52.0	65.0	34.4	68.8
AT43	51.5	13.1	49.0	66.0	27.0	147.7
AT45	52.7	9.8	51.0	64.5	28.9	137.3
AT46	47.7	8.0	46.8	58.3	30.6	71.0
AT72	57.5	13.2	54.3	75.1	23.8	173.0
AT73	53.1	10.1	51.0	65.2	31.0	144.2
AT75	53.4	11.2	50.9	67.6	35.6	142.5
AT76	46.9	7.8	45.9	56.8	28.0	97.7
B190	50.0	13.3	48.0	65.7	17.0	163.0
B350	52.0	14.7	49.8	70.3	21.3	168.0
B36T	53.1	17.9	52.4	69.3	24.2	100.6
B712	49.5	8.5	48.7	59.3	24.2	174.5
B721	59.4	15.9	56.3	85.6	36.9	105.4

B722	55.9	14.3	54.1	74.9	26.8	120.0
B732	51.7	13.8	48.2	68.7	29.0	159.5
B733	48.5	10.0	46.8	59.4	21.6	168.5
B734	50.3	12.4	48.0	64.3	24.3	158.6
B735	46.8	8.1	45.4	56.4	22.0	123.2
B736	52.4	10.3	52.7	65.4	28.2	122.1
B737	48.4	10.2	46.8	59.9	23.0	168.1
B738	50.6	9.9	49.1	62.2	20.0	176.9
B739	51.3	10.2	49.7	63.8	23.4	174.3
B73Q	53.9	7.3	52.8	63.9	45.8	68.2
B742	88.5	23.0	82.4	125.9	43.2	167.5
B744	71.0	16.3	67.8	92.6	29.7	178.0
B748	76.4	18.8	72.9	101.6	36.0	174.1
B752	54.7	11.6	53.0	68.0	21.0	174.9
B753	57.6	12.0	55.4	73.1	27.0	169.6
B757	58.0	13.0	56.7	74.1	31.9	114.0
B762	62.4	16.9	58.8	85.2	22.7	169.1
B763	58.2	13.2	55.9	73.6	17.0	174.0
B764	54.8	12.0	52.6	69.8	26.9	154.3
B767	59.6	13.9	57.8	76.0	39.0	129.2
B772	62.4	13.3	60.7	78.9	25.7	179.0
B773	66.1	10.2	64.8	79.4	37.3	119.0
B77L	69.2	15.7	66.3	89.3	32.4	179.6
B77W	65.7	12.9	63.9	81.4	30.9	177.8
B788	67.9	14.9	65.2	87.1	29.8	173.9
B789	66.8	14.7	64.4	85.1	33.0	173.0
BE10	54.6	16.5	51.6	77.3	23.2	146.2
BE20	51.4	15.4	48.7	70.1	17.0	173.0
BE23	51.2	16.2	49.6	69.2	31.1	116.5
BE24	58.5	18.0	52.3	86.9	33.0	113.9
BE30	52.4	15.6	49.4	71.9	17.2	161.4
BE33	48.0	17.1	43.9	72.0	19.0	159.0
BE35	46.9	16.4	42.8	67.1	18.2	161.1
BE36	49.7	18.0	45.4	71.3	16.2	168.0
BE40	51.7	14.2	49.0	67.5	20.0	170.0
BE50	49.7	15.5	48.8	61.8	27.9	106.0
BE55	50.3	15.8	46.5	71.0	21.6	143.0
BE58	49.7	14.9	46.9	67.7	21.8	152.6
BE60	50.2	11.1	48.7	63.1	32.8	103.7
BE65	49.8	15.3	47.0	67.7	23.3	165.1
BE70	59.6		59.6	59.6	59.6	59.6
BE90	47.7	13.8	45.0	62.6	21.6	112.0
BE95	58.0	15.2	56.7	81.1	20.4	96.7

BE99	52.7	17.9	49.9	74.0	15.8	173.0
BE9L	57.8	17.3	55.8	78.0	19.0	165.5
BE9T	50.2	16.1	47.0	71.0	16.0	130.6
BL17	57.3	19.8	55.9	79.4	25.5	133.0
C150	53.5	18.4	49.8	76.9	21.0	125.9
C152	54.9	15.6	51.0	76.2	28.9	98.7
C160	48.9	8.2	47.0	59.4	37.9	66.0
C162	84.0		84.0	84.0	84.0	84.0
C172	55.8	17.8	51.7	78.1	19.0	161.7
C175	53.0	16.4	49.8	75.3	30.8	88.9
C177	54.3	16.6	50.0	76.9	26.5	124.0
C180	57.7	18.2	52.7	82.1	26.4	99.4
C182	54.4	17.7	50.6	76.3	19.0	160.8
C185	62.3	20.1	56.6	92.0	23.5	128.0
C195	58.8	18.0	56.2	68.7	34.5	107.9
C206	51.0	16.5	48.0	72.0	21.7	169.0
C208	51.9	16.7	49.2	72.0	15.5	174.6
C210	53.9	18.5	49.3	76.4	20.5	167.0
C240	52.7	15.2	48.0	75.9	32.2	93.1
C25A	51.8	14.1	49.1	68.8	24.0	167.7
C25B	51.8	13.5	49.5	67.8	21.1	161.1
C25C	50.9	12.9	48.5	66.0	20.9	132.0
C303	45.6	14.9	41.2	64.5	26.5	121.0
C310	52.8	19.6	48.0	77.0	20.1	169.1
C320	39.8	14.3	36.0	53.5	27.4	131.1
C335	50.7	19.1	43.6	80.0	32.0	96.0
C340	52.4	16.1	49.2	74.0	24.0	138.0
C402	48.1	14.5	45.3	68.0	15.8	155.0
C404	57.3	20.8	53.4	73.4	30.3	152.0
C414	52.1	15.2	49.2	69.7	19.7	173.9
C421	52.3	15.8	50.1	71.0	10.1	166.1
C425	50.4	15.5	48.9	70.2	16.3	130.9
C441	52.0	14.9	49.9	69.7	17.2	155.0
C500	52.5	12.7	50.1	67.0	28.6	145.5
C501	53.4	14.8	51.2	70.7	20.2	160.5
C510	50.7	13.8	48.5	66.5	20.8	165.0
C525	52.0	14.6	49.3	69.4	20.9	167.0
C526	54.3	19.4	52.0	65.9	31.3	154.9
C550	53.0	14.0	50.5	70.1	22.0	165.0
C551	54.2	13.1	51.6	68.8	34.0	127.2
C560	52.5	14.1	50.1	69.7	23.0	165.1
C56X	50.7	13.4	48.1	66.8	21.0	170.0
C650	52.9	12.5	50.8	67.9	23.1	145.8

C65X	57.8	8.7	57.8	62.8	51.6	64.0
C680	51.3	13.6	48.8	67.0	18.6	164.0
C68A	53.2	11.6	51.5	70.0	30.0	92.0
C72R	60.7	21.3	56.8	84.3	26.1	120.3
C750	51.8	13.2	49.4	67.2	22.7	165.2
C77R	48.7	15.6	45.9	60.4	31.2	102.3
C82R	53.1	19.9	47.0	74.4	31.4	152.9
CL30	50.0	13.0	47.7	65.3	14.7	172.0
CL35	50.6	13.4	48.0	66.3	22.0	133.2
CL41	62.9	13.2	67.7	71.9	47.9	73.0
CL60	52.8	12.6	50.4	68.0	19.0	157.0
COL3	51.7	17.2	48.0	72.5	17.8	145.8
COL4	51.0	15.1	48.1	69.8	29.2	141.5
CRJ1	49.8	10.0	48.0	62.3	28.9	121.0
CRJ2	47.5	9.2	46.3	58.7	21.0	153.7
CRJ7	48.2	9.6	46.9	59.8	20.0	161.8
CRJ9	47.6	8.7	46.5	58.0	23.1	170.0
CVLP	52.4	10.6	51.8	61.6	34.9	108.0
CVLT	48.0	10.8	46.7	57.5	25.4	169.0
D328	55.5	15.7	54.0	75.6	20.0	142.7
DA20	56.4	23.2	45.0	81.2	39.9	110.0
DA40	54.2	18.0	50.8	77.2	19.8	163.1
DA42	50.3	18.0	44.5	73.0	27.5	145.0
DC10	64.0	15.6	61.7	82.6	28.7	173.3
DC3	59.8	12.1	60.0	74.3	40.3	101.0
DC87	54.0	8.0	51.6	62.8	42.0	70.0
DC91	56.8	15.0	53.8	77.2	28.9	168.0
DC93	60.1	15.7	56.1	81.9	35.9	124.4
DH6	47.7	6.2	45.0	53.5	43.8	57.0
DH8A	45.9	8.8	44.4	57.2	19.3	151.0
DH8B	38.9	8.9	36.3	51.0	20.8	141.0
DH8C	44.8	9.2	44.0	55.5	20.9	132.3
DH8D	45.5	10.3	43.6	58.5	22.8	136.0
DHC2	45.0		45.0	45.0	45.0	45.0
DHC8	46.3	11.1	45.0	59.2	28.0	71.6
DV20	62.9	17.2	63.2	84.6	29.0	105.6
E110	50.0	16.3	48.0	67.3	28.1	115.9
E120	48.2	12.0	46.0	63.0	20.0	153.0
E135	46.4	9.2	45.1	57.0	18.1	164.2
E145	45.6	8.7	44.5	55.7	17.2	163.9
E170	46.8	8.8	45.7	57.3	20.9	170.0
E175	47.7	8.7	46.8	60.0	31.9	74.0
E190	46.3	8.5	45.2	56.8	20.3	165.4

E35L	52.5	14.3	50.0	69.5	22.5	127.9
E45X	46.4	9.8	45.2	57.2	18.2	165.9
E50P	51.4	13.9	49.1	68.6	18.4	161.0
E545	53.2	14.8	49.2	72.1	27.3	108.0
E550	52.5	11.7	51.2	66.3	24.0	140.7
E55P	49.5	13.7	47.2	65.9	22.0	169.3
E75L	48.6	9.6	47.5	60.5	14.0	167.1
E75S	47.3	9.2	46.3	57.7	25.1	172.0
EA50	53.2	19.0	50.3	72.5	22.6	155.3
ERCO	52.4	21.2	57.6	67.9	29.0	70.5
F2TH	52.2	13.1	49.8	68.0	20.9	170.0
F900	53.4	13.8	51.0	69.0	25.6	155.0
FA10	54.9	13.5	52.6	70.5	26.0	130.0
FA20	56.2	14.2	53.6	73.4	19.6	152.5
FA50	53.8	13.1	51.4	69.0	27.5	149.5
FA7X	55.3	14.6	52.3	73.1	26.3	162.9
G150	50.9	10.8	49.1	65.0	26.3	130.4
G280	52.9	12.9	50.7	67.3	27.2	142.3
GA7	69.1	21.7	65.0	90.4	38.8	120.0
GALX	52.3	13.7	49.9	68.2	24.5	169.1
GL5T	55.1	14.2	52.0	72.4	25.9	137.0
GLEX	56.0	14.5	53.4	72.7	21.5	159.2
GLF2	55.7	11.7	54.2	68.8	31.3	115.7
GLF3	57.8	14.3	55.7	75.0	31.3	153.0
GLF4	54.9	13.8	52.6	70.9	25.3	171.8
GLF5	56.1	14.4	53.3	72.9	20.7	171.9
GLF6	57.1	14.6	54.3	74.0	28.0	165.3
H25A	52.7	12.7	50.1	68.8	29.0	133.0
H25B	52.6	13.2	50.2	67.8	23.4	169.0
H25C	55.8	14.7	53.2	71.6	29.0	151.0
HA4T	53.1	14.1	50.5	69.9	28.6	147.9
HDJT	54.5	15.3	51.7	69.7	31.8	144.0
J328	49.7	13.0	47.7	66.0	20.2	170.6
JS31	48.7	13.5	46.0	63.0	22.0	135.0
JS32	44.4	10.6	42.8	57.0	22.1	118.0
JS41	44.1	9.4	42.8	53.3	29.5	131.6
L29B	52.7	11.7	50.4	69.0	31.7	87.1
L5	86.2	13.7	78.7	97.3	77.9	102.0
LJ24	56.4	17.4	54.3	84.3	36.0	96.0
LJ25	58.6	15.1	55.1	78.8	31.0	116.5
LJ31	52.8	14.8	50.0	69.4	20.8	158.0
LJ35	55.7	15.9	52.6	73.7	26.0	168.8
LJ40	49.7	12.8	47.1	64.0	23.4	171.0

LJ45	50.1	12.6	47.9	64.2	22.7	169.5
LJ55	54.4	14.5	51.7	71.6	28.3	148.0
LJ60	52.6	13.8	50.1	68.8	23.6	164.3
LJ70	49.6	10.9	48.0	62.5	27.5	119.0
LJ75	49.7	12.9	47.6	63.1	22.7	156.2
LNC4	45.5	17.2	42.2	62.6	21.0	156.8
LNP4	50.9	20.0	43.7	70.6	36.6	79.6
LR35	47.7	10.3	44.0	61.5	36.4	72.2
M20C	57.0		57.0	57.0	57.0	57.0
M20F	45.4	4.8	45.4	48.1	42.0	48.7
M20P	52.9	17.5	48.8	73.6	21.0	156.6
M20R	56.1	18.1	47.6	71.0	43.8	76.9
M20T	54.7	20.1	49.7	79.9	25.0	171.8
MD11	63.9	15.9	61.0	84.0	24.9	175.9
MD80	55.8	13.8	53.7	73.1	33.6	109.0
MD82	52.0	8.9	51.0	62.3	26.4	157.0
MD83	51.7	8.9	50.9	62.0	25.6	168.3
MD88	48.2	8.2	46.9	58.0	23.9	162.9
MD90	48.2	8.8	46.8	58.2	25.6	176.7
MO20	53.4	19.4	47.1	77.7	27.4	160.0
MO21	56.5	18.0	50.0	85.1	35.2	93.9
MU2	51.0	15.0	48.0	68.0	25.2	155.0
MU20	47.9	18.5	41.1	70.8	25.0	75.8
MU30	54.2	15.2	51.2	71.8	30.8	141.0
P180	54.9	15.3	51.8	71.9	28.0	152.0
P210	53.9	19.2	50.5	76.3	25.6	143.9
P28A	53.2	15.4	49.8	72.1	21.5	158.0
P28B	51.1	17.0	46.7	73.0	28.9	110.6
P28T	64.9	20.8	62.5	81.3	38.1	128.0
P32A	52.3	12.3	48.5	65.3	36.9	78.9
P32R	48.3	17.4	44.1	69.8	17.0	163.0
P32T	54.2	18.4	52.9	76.5	20.7	91.6
P46T	51.3	16.2	48.4	70.8	17.3	160.4
P51	60.3	20.0	59.1	75.8	35.5	167.5
P68	49.0	17.8	44.1	66.0	25.6	168.6
P750	37.9		37.9	37.9	37.9	37.9
PA12	65.1	16.8	71.9	79.1	43.4	81.2
PA18	68.9	30.2	57.0	116.7	38.0	131.7
PA22	56.8	6.5	57.0	62.9	45.0	65.0
PA23	53.8	18.5	50.1	78.1	27.5	153.3
PA24	51.3	16.2	47.0	73.8	21.3	118.7
PA27	50.6	15.4	48.9	67.5	23.9	161.9
PA28	52.6	18.1	48.4	73.5	20.5	163.1

PA30	53.9	16.1	50.2	79.3	24.9	107.2
PA31	50.2	14.7	48.0	67.2	19.5	173.9
PA32	49.3	16.4	46.0	69.3	17.9	157.0
PA36	61.1	10.6	56.0	73.2	53.5	81.0
PA38	54.3	12.4	48.9	69.1	43.0	75.2
PA44	52.7	15.8	49.0	70.8	20.9	162.2
PA46	51.3	15.9	48.7	70.1	19.5	166.6
PA60	53.8	11.7	51.7	71.2	38.6	77.8
PAT4	67.7	24.5	61.0	104.4	23.7	136.4
PAY1	51.0	14.7	48.6	68.1	18.0	143.0
PAY2	55.3	18.7	51.0	80.4	23.0	161.9
PAY3	55.8	15.1	53.8	71.0	25.6	148.8
PAY4	50.4	12.3	47.9	65.6	25.1	88.0
PC12	51.9	15.4	49.3	69.3	13.1	170.0
PRM1	51.0	12.8	48.6	66.0	25.0	158.0
S22T	49.9	15.6	46.0	71.0	28.5	95.0
SBR1	54.8	13.3	52.9	69.1	28.3	165.0
SBR2	57.3	10.2	55.5	68.8	45.3	77.5
SC7	46.6	17.3	44.3	67.5	21.6	128.3
SF34	47.1	9.6	46.0	58.3	22.0	153.3
SH36	55.1	17.9	51.8	72.5	13.7	162.2
SR20	50.3	15.4	46.1	70.0	25.7	145.0
SR22	48.9	15.1	45.6	67.2	15.3	159.0
SU95	58.6	8.6	58.1	69.0	33.8	120.2
SW3	57.1	15.5	54.2	77.4	23.2	138.0
SW4	53.9	15.3	51.7	70.8	16.8	170.0
T210	59.0	18.4	55.2	81.6	33.5	88.0
T28	76.5	23.2	65.8	101.6	55.0	102.0
T6	58.0	14.4	57.0	72.0	34.0	94.0
TB20	49.1	15.5	47.5	61.0	29.4	105.5
TBM	49.4	16.7	46.3	60.6	30.5	113.9
TBM7	50.9	13.6	48.7	67.6	22.9	156.9
TBM8	51.5	15.8	48.8	70.4	20.6	165.9
TBM9	53.9	17.6	50.0	76.8	29.0	128.4
TOBA	50.9	21.3	43.3	75.6	31.0	87.7
WW24	55.7	12.8	53.9	71.6	25.3	127.6